SELF-HEALING PAINT

Functionalizing an Acrylic Coating with a Quadruple Hydrogen Bonding Network

By

Maximilian Arthur Beach

ORCID: 0009-0004-4556-7403

A Thesis Submitted to the School of Chemistry
University of Melbourne

In Total Fulfilment of the Requirements for the Degree of
Doctor of Philosophy

December 2023

ABSTRACT

Paints are coatings which serve to both protect surfaces from damage and impart a variety of aesthetic qualities. They are composed of a matrix of interlocking hydrophobic acrylic polymers which constitute the body of the coating, while binding together a myriad of other additives including pigment particles. Paints represent the majority fraction of a vast global coatings market, and, like all coatings, are exposed to a variety of stresses that can lead to long term damage in the form of microcracks. To date, the only method to repair such damage is to simply replace the paint with a new coat, which is expensive and time consuming. Self-healing technology is perhaps the most promising solution to this problem, as it offers the ability to heal damage spontaneously and without external diagnosis. However, neither a self-healing paint, nor any viable self-healing acrylic coating currently exists. The work presented herein represents a 3-and-a-half-year research effort to successfully design both a self-healing acrylic coating and a feasible self-healing paint.

The strong quadruple hydrogen bonding unit 2-ureido-4[1H]-pyrimidinone (UPy) was incorporated into an acrylic coating to form a hydrogen bonding network. Upon damage to the coating, the strong attractive forces between the broken UPy units in the network prompted self-healing through polymer rearrangement and the reformation of UPy–UPy bonds. This was achieved first through the design of an UPy functionalized acrylic monomer with a long amphiphilic spacer. This monomer, at a concentration of only 2.5 wt%, was able to successfully imbue a typical acrylic coating with efficient self-healing (~25%) at room temperature. Then, in order to enhance self-healing efficiency, a UPy functionalized crosslinker system with exotic architecture was designed. One crosslinker design in particular successfully enhanced self-healing efficiency by over 10%. Finally, in collaboration with the international paint company DuluxGroup, this self-healing acrylic coating design was incorporated into a paint formulation according to the product range Weathershield™. The resulting UPy-Paint was subjected to range of industry specific paint tests, and its optical and mechanical self-healing performance was evaluated.

This work represents the first design of a strong acrylic coating which is able to self-heal efficiently at room temperature without diminishing its optical and material properties. Furthermore, such research yields important information into the mechanisms governing self-healing, clarifying both the challenges associated with self-healing, as well as potential directions worthy of greater research. Finally, this work presents a viable strategy for the design of commercially viable self-healing paint, which, for the last 20 years, has remained essentially out of reach.

DECLARATION OF AUTHORSHIP

I, Maximilian Beach, declare that this thesis entitled “Self-Healing Paint” and the work presented herein are my own.

I confirm that:

i) This thesis comprises my original work towards the Doctor of Philosophy except where indicated in the preface;

ii) due acknowledgment has been made in the text to all other materials used; and

iii) the thesis is fewer than 100,000 words in length, exclusive of table, maps, bibliographies, and appendices.

Signed 

December 2023

PREFACE

This thesis is comprised of both published and unpublished work, and the publication status of each chapter is as follows:

Chapter 1: Published by *Progress in Organic Coatings*, Elsevier, October 2023.

Chapter 2: Submitted for publication by *Progress in Organic Coatings*, Elsevier, November 2023.

Chapter 3: Unpublished work in preparation for publication.

Chapter 4: Unpublished material not submitted for publication.

The following individuals directly contributed to the research described in this thesis:

Dr Hamish Brown and Geoff Wang, for their assistance with TEM and Cryo-TEM

Dr Sunalee Jayasundara, Dr Axel-Laurenz Buckinx and Dr Matthias Hilder, for their assistance regarding paint testing, latex formulation and differential scanning calorimetry respectively

The Department of Chemical Engineering, for their assistance regarding strain recovery measurements

and

Dr Tim Davey, for his invaluable contribution to latex and paint formulation

ACKNOWLEDGEMENTS

My PhD has led me to explore cutting edge areas of science previously unknown to me. Its successful accomplishment has demanded creativity, extensive problem solving and a high degree of resilience, resulting in an incredibly rewarding, challenging and transformative experience. To all the exceptional colleagues, friends and family who supported me along the way, thank you.

First and foremost, I would like to express my heartfelt gratitude to Associate Professor Georgina Such. Thank you for your supportive, passionate, and encouraging nature, as well as your valuable insight and measured critiques. You have created an environment in which I was able to flourish, for which I am eternally grateful. You are the perfect supervisor, and I am confident that the extensive knowledge that I have learned from you will serve me well in the future.

I would also like to express my gratitude to Dr Tim Davey. I deeply appreciate your support, enthusiasm, and composure. Thank you for generously guiding me through a completely new environment, and teaching me a diverse set of skills. I will remember how selfless you were with your valuable time.

I would like to thank the members of my advisory panel, Dr Bradley Clarke and Professor Muthupandian Ashokkumar. Ashok, thank you for your support and your steadiness.

I am humbled by my association with The University of Melbourne, a great institution. To Dulux, thank you for your willingness to support cutting-edge research.

Over the past four years, a number of individuals have made important contributions to my research, for which I am grateful. I would like to thank Dr Hamish Brown, Geoff Wang and the staff at Dulux in particular, who were welcoming and helpful. Sunalee, I appreciate your enthusiasm and support.

To my friends and colleagues, in particular Sarah Kermaniyan, as well as Umeka Nayanathara, Sam Smith and Yanting Gao, thank you for your camaraderie and assistance. I enjoyed our in-lab conversations.

Finally, thank you Mum, Daria McGauran, and Dad, Jonathan Beach, for your unconditional support.

TABLE OF CONTENTS

TABLE OF FIGURES

GLOSSARY

AA	Acrylic acid
AIBN	Azobisisobutyronitrile
BA	Butyl acrylate
CDI	Carbonyl diimidazole
$CDCl_3$	Deuterated chloroform
$CHCl_3$	Chloroform
D_2O	Deuterated water
DBTDL	Dibutyl tin dilaurate
DCM	Dichloromethane
DLS	Dynamic light scattering
DMF	Dimethyl formamide
DMSO	Dimethyl sulfoxide
DSC	Differential scanning calorimetry
FTIR	Fourier-transform infrared spectroscopy
^{1}H NMR	Proton nuclear magnetic resonance
MMA	Methyl methacrylate
MW	Molecular weight
MWCO	Molecular weight cut-off
PEG	Poly(ethylene glycol)
PEGMA	Poly(ethylene glycol) methacrylate
RAFT	Reversible addition–fragmentation chain–transfer polymerization
SDS	Sodium dodecyl sulfate

TEA	Triethanolamine
TEM	Transmission electron microscopy
***T*g**	Glass transition temperature
UPy	2-ureido-4[1H]-pyrimidinone (a self-complementary quadruple hydrogen bonding moiety)
UPy-NCO	2(6-isocyanatohexylaminocarbonylamino)-6-methyl-4[1H] pyrimidinone (Isocyanate functionalized UPy precursor)
UPy-1	A UPy functionalized methacrylate monomer with a PEG spacer ($n = 0$)
UPy-2	A UPy functionalized methacrylate monomer with a PEG spacer ($n = 11$)
UPy-3	A UPy functionalized methacrylate monomer with a PEG spacer ($n = 8$)
UPy-4	A UPy functionalized methacrylate monomer with a PEG spacer ($n \sim 52$)
UPy-Linear	A crosslinker comprised of a linear PEG chain end capped with UPy
UPy-XL-1	The crosslinker comprised of linear PEG ($n = 0$) end capped with UPy
UPy-XL-2	The crosslinker comprised of linear PEG ($n = 4$) end capped with UPy
UPy-XL-3	The crosslinker comprised of linear PEG ($n \sim 130$) end capped with UPy
UPy-XL-4	The crosslinker comprised of linear PEG ($n \sim 220$) end capped with UPy
UPy-Brush	A crosslinker comprised of a Brush PEG polymer with approximately two UPy moieties per polymer chain

UPy-Brush-5	The crosslinker comprised of a Brush PEG polymer (*MW ~ 5 kDa*) with approximately two UPy moieties per polymer chain
UPy-Brush-10	The crosslinker comprised of a Brush PEG polymer (*MW ~ 10 kDa*) with approximately two UPy moieties per polymer chain
UPy-Brush-20	The crosslinker comprised of a Brush PEG polymer (*MW ~ 20 kDa*) with approximately two UPy moieties per polymer chain
UTM	A universal testing machine for stress–strain measurements

Chapter 1. Self-Healing Organic Coatings

Coatings are ubiquitous and touch practically all aspects of daily life. They play a vital role in protecting surfaces from external damage and are also able to impart a variety of functional and aesthetic qualities. However, coatings are not permanent, and are susceptible to mechanical stress, corrosion, and solvent damage. It is impossible to accurately quantify the cost of coating degradation to the global economy, but estimates suggest it probably reaches into the trillions of US dollars.[1] This enormous cost is largely due to the fact that, until recently, the only solution to healing a damaged coating was simply to replace it. Replacement is energy intensive, expensive and time consuming. Therefore, there exists a strong incentive in materials science to develop new healing methods that increase the service lifetime of a coating, while maintaining its desired functionality.

For this reason, intense research has centered around the creation of self-healing materials over the past 20 years. Self-healing materials are synthetically designed materials that have the built-in ability to repair damage to their structure without either diagnosis or external (human) intervention. These materials are inspired by nature and the ability of wood, bone and organic tissue to heal damage autonomically and almost flawlessly.[2] The early work into self-healing materials came in 1993, when Dry and Sottos designed a self-healing concrete matrix.[3] However, it was only in 2001, after a seminal paper by White *et al.*, that the interest in self-healing materials increased markedly. Presently, the Web of Science lists over 5400 papers whose primary focus falls under the classification "self-healing materials". There are also a growing number of reviews that focus on the different applications of self-healing materials, as well as multiple books that cover the general field.[4-7] Despite being a relatively new concept in materials science, self-healing has the potential to radically enhance the functional and aesthetic performance of coatings by providing outstanding durability. This review aims to outline the self-healing strategies applicable to organic coatings in particular, and to give a clear appraisal of the future prospects of self-healing technology by balancing its significant potential with its inevitable limitations.

1.1 FUNDAMENTAL UNDERSTANDING OF ORGANIC COATINGS

Before examining the various self-healing techniques currently being investigated by researchers, a general overview of organic coatings is necessary. Organic coatings are composite mixtures that include a matrix (binder), and a number of other diverse, function-specific elements. The binder, as the name suggests, holds the other elements together to form the coating. Coatings can be applied to a surface (substrate) in the form of a liquid or a powder, ultimately forming a thin, solid film via drying or curing. An organic coating is simply a coating whose binder is comprised of organic polymers. For the purpose of this review, *coatings* and *organic coatings* are used interchangeably.

The global coatings market is vast, and is projected to grow beyond $250 billion USD by 2026.[8] Architectural coatings are paints used to decorate the interior and exteriors of buildings, and represent the primary fraction of this market by consumption and price.[8] Waterborne latex-based acrylic paints comprise the majority of these architectural coatings. Industrial protective coatings and anti-corrosion coatings also represent a significant fraction of the coatings market. The size of the coatings industry reflects the important role coatings play in every level of society. As well as architectural paints and varnishes, coatings are vital to the protection of cars, aircraft, household appliances, furniture, electronic components, wires, metal containers, cans, chewing gum wrappers -the list is endless [9]. To suit these varying applications, organic coatings must have a diverse range of operative capabilities. These include, but are not limited to, mechanical strength, corrosion protection, solvent resistance, abrasion resistance, and oxidation resistance. Architectural coatings must also maintain their aesthetic features, including colour, gloss and opacity. More precise coatings may have important inbuilt functionality such as thermal or electrical conductivity, optical or antimicrobial behavior, or perhaps the ability to self-heal.

All organic coatings contain a polymeric binder. The most common polymers used in organic coatings are acrylics and vinyls, which make up the majority of architectural paints; polyurethanes, a tough and highly resistant coating which is used for a variety of industrial applications; and epoxy, a general-purpose protective resin. A breakdown of the major polymers used in organic coatings are shown in Figure 1.1.[9] The mechanical and rheological properties of an organic coating are governed almost completely by the kind of polymer that

makes up the binder. Most organic coatings are mechanically strong, high modulus materials at room temperature, but above a certain temperature known as the glass transition temperature (*T*g), they become rubbery and plastic. Epoxies and polyurethanes are tough, highly crosslinked thermoset materials that form hard films following a curing (crosslinking) process. Latex paints form hard thermoplastic films as they dry, during which the acrylic polymers coalesce and interlock with each other.[10]

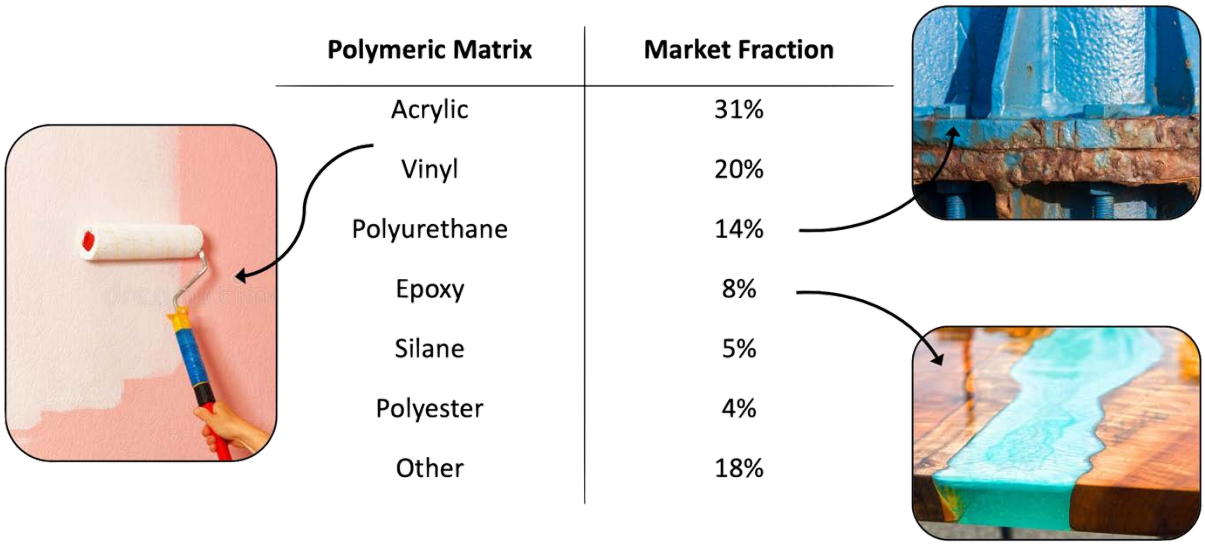

Figure 1.1 A breakdown of the different resins according to US market share in 2014 [9].

As well as the binder, most organic coatings also contain finely dispersed inorganic particles (pigments) ranging from dozens of nanometers to hundreds of microns in size. These particles are primarily responsible for giving the coating its colour and opacity. Pigments which add colour to the coating are also known as colourants. Organic coatings may be either solvent-borne or waterborne (meaning that water is the continuous phase of the binder), and the coatings may also include a small amount of volatile organic compounds (VOCs). VOCs primarily act as *coalescents* to temporarily lower the *T*g of the binder, allowing for easy application of the paint at room temperature.[9] They can also neutralize acidic groups from the binder or other additives, as well as slow down the drying of paint. Organic coatings can contain other additives to give the coating specific properties. These can include *extenders*, which control the gloss of the coating by altering its light scattering properties, *surfactants*, which provide colloidal stability, and *dispersants*, which disperse and stabilize pigment particles. *Thickeners* (rheology modifiers) are used to control the viscosity of the coating, while

plasticizers lower the coating's *T*g, resulting in a softer, more rubbery material. Anti-oxidants and biocides protect the long term stability of coatings in both their wet and dry state by preventing coating decomposition, and the growth of mold and fungi. Most organic coatings are complex chemical mixtures containing different combinations of the substances mentioned above.[9]

A perfectly designed organic coating should maintain both its desired functionality, as well as its visual façade, for the entire lifetime of the substrate. Unfortunately, all organic coatings fall victim to damage over time. Coating damage is observed by the formation of cracks, which arise due to physical forces such as tension, compression, shear and heat related fatigue, as well as chemical factors such as oxidation, UV degradation and corrosion. For organic coatings, Van Bentham *et al.* clearly defined three different kinds of cracking damage according to scale: micro, where the bonds between polymers are broken; meso, where larger networks of polymers are pushed apart (colloquially known as *crazing* or *alligatoring*); and macro, where the cracks are clearly visible to the naked eye.[11] In reality, cracking is a continuous process. Invisible microcracks within the polymer matrix generally arise due to interfacial pressure, temperature differences, and low level mechanical stress such as scratching.[12] These microcracks will lead to the formation of larger cracks that at first appear aesthetically displeasing, but if left unchecked will eventually result in delamination, the exposure of the substrate, and the complete failure of the coating as a protective material. It is estimated that the maintenance cost of coating degradation in developed countries is roughly 2-3% of their GDP.[1] Furthermore, the initial microcracks contained in the bulk of the coating are practically impossible to detect without complex instrumentation.[13] Thus, discovering methods that can heal cracks in a polymer matrix spontaneously, represents a significant opportunity to radically enhance the performance and durability of organic coatings.

1.2 SELF-HEALING STRATEGIES FOR ORGANIC COATINGS

Given the diverse spectrum of organic coatings, there is no single 'catch-all' self-healing strategy. Any successful self-healing strategy must take into account:

i) The nature of the polymers that make up the binder.
ii) The rheological and viscoelastic properties of the coating.
iii) The additives within the coating, such as nanoparticles and VOCs.

iv) The size and type of cracking damage needing to be healed.
v) The timescale and external conditions in which the self-healing occurs.
vi) The impact of the self-healing mechanism on the coating performance.

Thus, designing a self-healing strategy that can optimize all these parameters is no trivial task.

Self-healing strategies in the literature are traditionally classified into autonomic (passive) and non-autonomic (active). Autonomic systems are able to self-heal spontaneously without any intervention, whereas non-autonomic systems require external triggers to initiate the healing process.[14] However, expressing self-healing according to these two categories is somewhat flawed. Certain self-healing principles conventionally thought of as autonomic do in fact require external triggers. Microcapsules which break autonomically but require moisture from an external humid environment for their self-healing agents to react, would fall into this category. Likewise, there are some supramolecular polymeric matrixes, conventionally considered non-autonomic, that do not require external stimuli and have been shown to self-heal under ambient conditions.

Dividing self-healing materials into either extrinsic or intrinsic is a more precise categorization. *Extrinsic* self-healing materials use a healing agent that is distinct and separate from the polymeric matrix. The healing agent is typically a liquid that flows into cracks, healing them via physical or chemical interactions with the matrix. *Intrinsic* self-healing materials, on the other hand, have their self-healing functionality as part of the polymer matrix itself. In the case of a mechanical damage event, the polymers are first ripped apart, causing a crack, but are ultimately able to reform, allowing the matrix to self-heal. Figure 1.2 illustrates the difference between extrinsic and intrinsic self-healing strategies.

This review presents a detailed description of both extrinsic and intrinsic self-healing materials, with a focus on how these healing strategies are applicable to organic coatings. Furthermore, determining the potential of self-healing organic coatings requires not just a discussion of the benefits of self-healing strategies, but also a critical analysis of their limitations. Thus, the benefits and limitations of both these approaches are comprehensively evaluated.

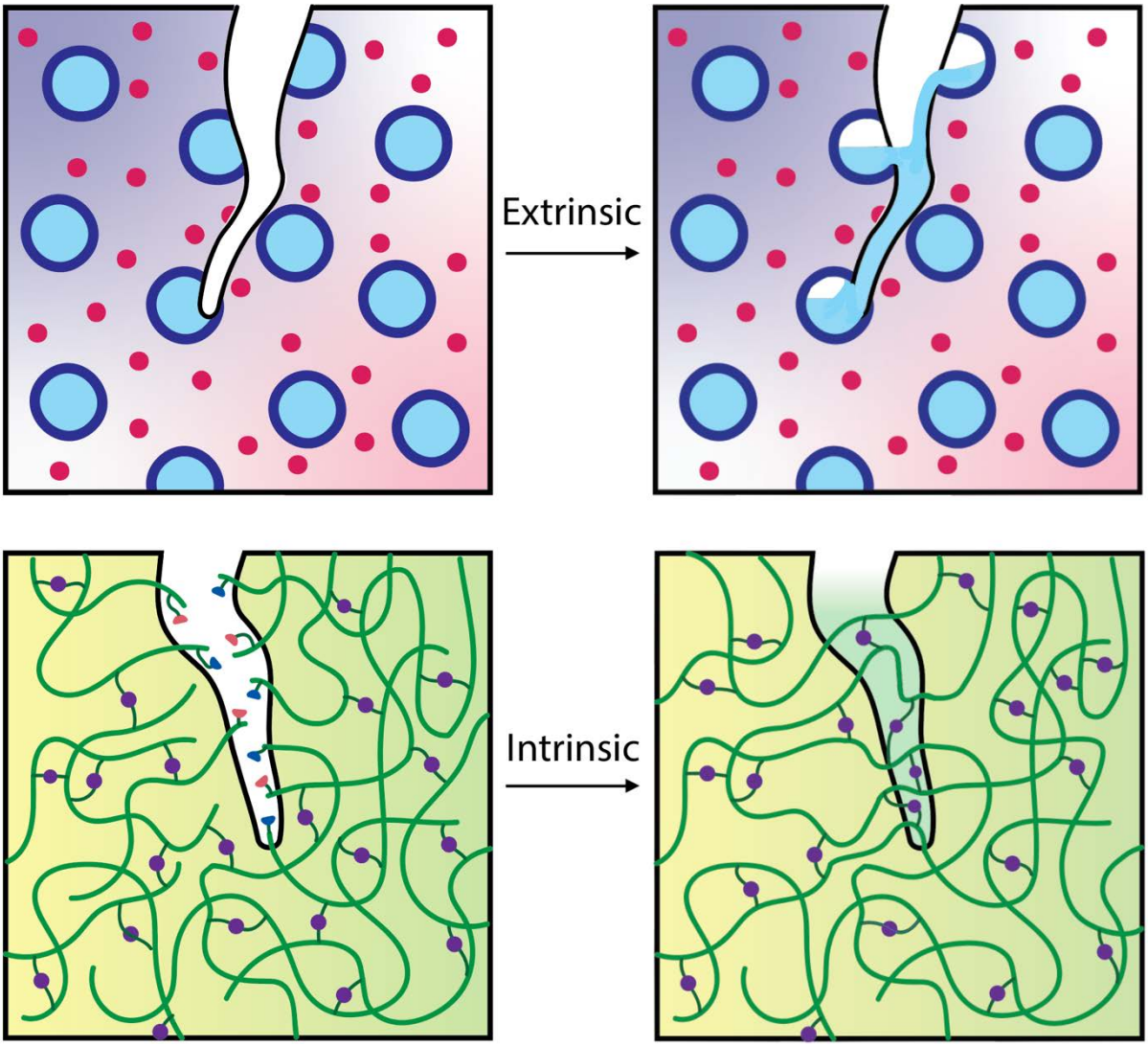

Figure 1.2 Extrinsic healing systems contain separated healing agents (in this case within microcapsules). Intrinsic systems have self-healing functionality as part of the polymeric material itself.

1.2.1 Extrinsic self-healing strategies

The majority of extrinsic self-healing strategies make use of microcapsules to separate and protect the liquid healing agent from the polymer matrix. The healing agents are encapsulated in the microcapsules which are dispersed amongst the matrix and rupture upon mechanical damage (cracking). Once the microcapsules are ruptured, the liquid healing agent can flow through the matrix via capillary forces, reach the crack, and initiate self-healing.[15] Most healing agents heal cracks via crosslinking or polymerization. A similar strategy involves the use of

hollow microvascular networks, rather than capsules, to protect the healing agent.[16] The microvascular network, like the capsules, can be ruptured by mechanical damage. Some have suggested that a microvascular network may be preferable to dispersed microcapsules because its hollow channels could, in principle, be refilled with healing agent upon depletion.[2] Another kind of extrinsic technique makes use of what are known as "phase separated additives". These additives are unencapsulated, but nevertheless distinct from the polymeric matrix. They are normally lower molecular weight (MW) thermoplastic polymers which, at temperatures above their *T*g, can flow through the matrix into cracks, healing them via crosslinking.[17]

Extrinsic self-healing techniques, in particular microcapsules, have shown promising self-healing potential across a number of different polymer matrixes. Their benefits include:

i) Extrinsic self-healing materials have demonstrated high healing efficiency, in some cases restoring the mechanical strength of the polymer coating to over 100% of its original value.
ii) Given that the extrinsic healing agent is a separate, flowable liquid to the polymeric matrix, the viscoelastic properties of the matrix are less important, and healing can take place even in tough, high modulus materials.
iii) Extrinsic materials, and microvascular networks in particular, store larger amounts of healing agent, which allows them to self-heal cracks of large dimensions.

There are also a number of drawbacks one needs to consider when assessing the applicability of extrinsic self-healing materials for organic coatings:

i) Once a damage event occurs, the capsules are fractured and the healing agent is consumed, meaning that a crack in a specific area can only be healed once.
ii) Healing agents normally require a catalyst or curing agent to react. Catalysts are expensive, add complexity to the material, and may not necessarily be present at the crack site, resulting in low self-healing efficiency.
iii) Encapsulated healing agents are susceptible both to evaporation and decomposition, threatening the long-term stability of extrinsic healing systems.
iv) Dispersed microcapsules in the polymeric matrix may change the material and functional properties of the coating, including its colour, viscosity, and opacity. In some cases, the larger microcapsules may have a diameter greater than the desired coating thickness itself. Furthermore, the presence of microcapsules, due to their

higher refractive index and light scattering/absorption properties, inevitably opacifies transparent polymer coatings.

Nevertheless, extrinsic techniques are extremely useful for designing self-healing materials. Many different kinds of microcapsules have been synthesized in an attempt to overcome some of the inherent limitations of extrinsic self-healing. These systems are reviewed in the sections below.

1.2.1.1 Microcapsules

The first successful extrinsic self-healing technology, and the pioneering work that sparked the high levels of interest in self-healing materials seen today, was described by White and coworkers in 2001.[18] They designed poly(urea-formaldehyde) (PUF) microcapsules encapsulating a healing agent, endo-dicyclopentadiene (DCPD), and dispersed them throughout an epoxy matrix. These capsules ruptured during crack formation, allowing DCPD to flow into the crack and, in the presence of Grubbs catalyst, complete the healing process via ring opening metathesis polymerization (ROMP). Since 2001, this microencapsulation approach to self-healing has advanced significantly, leading to roughly four distinct system designs[19] (Figure 1.3):

i) Single capsule system: where a single healing component is microencapsulated.[20]
ii) Capsule/dispersed system: where one healing component is microencapsulated, and the other healing agent (normally a catalyst or crosslinker) is dispersed throughout the matrix.[18]
iii) Dual capsule system: where both healing components are separately microencapsulated.[21]
iv) All-in-one system: where all the necessary healing components are contained in a single microcapsule.[22]

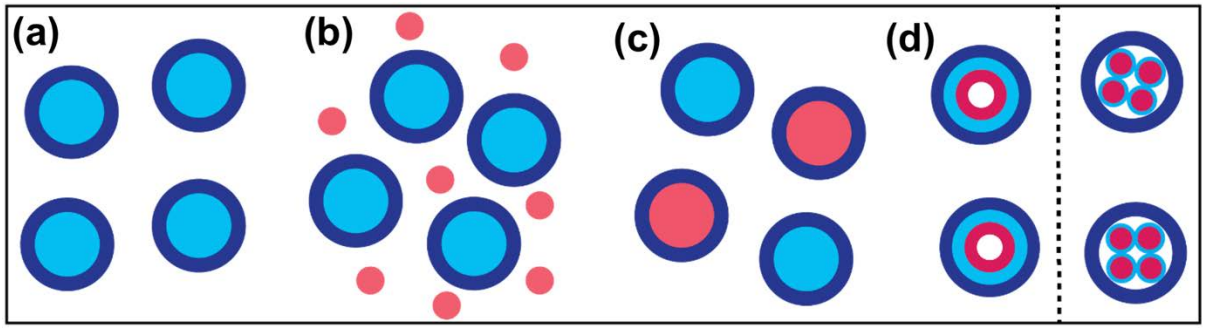

Figure 1.3 Different strategies to encapsulate active components for extrinsic self-healing using microcapsules. (a) A single capsule system with a blue healing agent.[20] (b) A capsule system with a dispersed red healing component.[18] (c) A double capsule system, with two self-healing agents localized in each capsule.[21] (d) All-in-one systems containing multiple healing agents within a multilayered capsule.[22]

Presently, the vast majority of capsule based self-healing technology falls under categories two and three. This is due to their simpler design, and the available self-healing chemistry.

Whereas the initial microencapsulation designs were based on emulsion polymerization, the present diversity of self-healing chemistry necessitates a larger number of microencapsulation techniques. These principally include:

i) In-situ polymerization: A technique based on an oil-in-water (O/W) emulsion, where the healing agent forms the oil droplets (dispersed phase), and polymerization of the shell monomers occurs in the aqueous phase. The polymers, insoluble in the aqueous phase, accumulate on the droplet surface, forming the polymeric shell. In-situ polymerization is simple, cost effective and easier to scale.[15]

ii) Interfacial polymerization: Similar to in-situ polymerization, this technique is an O/W emulsion, however one shell component is dissolved in the aqueous phase, and the other is dissolved in the dispersed (oil droplet) phase. Polymerization occurs at the interface of the oil droplet and water, forming the polymeric shell. Interfacial polymerization is simple, offers a fast shell forming reaction and occurs under mild conditions.[15] However, some unreacted monomer may remain in the encapsulated oil droplet.

iii) Pickering emulsion: A more complex technique, based on a two-stage emulsion. First, a stable "Pickering" emulsion of inorganic nanoparticles in water is formed. This becomes the new aqueous phase. Then, in the O/W emulsion, the oil droplets are

stabilized by these nanoparticles, which act like a surfactant. The nanoparticles are then immobilized in place, normally via crosslinking, to form a hard-compact shell.[23] Pickering emulsions are generally non-toxic, highly stable, and able to encapsulate materials that are difficult to encapsulate via traditional emulsion techniques. Pickering emulsions can also create more complex capsule designs.

iv) Miniemulsion: An O/W emulsion whereby energy is added, normally via sonication, to shear the droplets down to the nano scale. Polymerization can happen in both phases, or at the droplet interface to form the capsule shell. Miniemulsion is useful for applications requiring narrowly dispersed nanocapsules (50-1000 nm).[24]

v) Solvent evaporation: This technique involves dissolving the healing agent and the polymeric shell in a volatile organic solvent (normally chloroform), and then adding this solution dropwise into water to form an emulsion. As the organic solvent evaporates under high temperature or low pressure the droplets harden, and the polymer eventually forms the shell of a microcapsule.[25] Solvent evaporation offers many advantages, namely simplicity, mild reaction conditions, the ability to encapsulate hydrophilic material, and a wide variety of polymeric shells, including poly(vinyl alcohol) (PVA), poly(styrene) (PS), poly(butyl acrylate) (PBA) and poly(methyl methacrylate) (PMMA).[26]

vi) Sol-gel: This technique involves first forming a suspension of inorganic shell material in water (sol) which then agglomerates and forms a gel. During the drying process of the gel, microcapsules can be formed.[13] The sol-gel method is non-toxic, preformed under mild conditions, and is used for synthesizing capsules with an inorganic shell (normally silica). The sol gel process is time consuming however, and cracks and pores may form in the capsules.

The vast majority of self-healing studies based on the microencapsulation of healing agents are tailored for epoxy resins.[27] However, some other organic binders have been tested, including polyurethane resins and vinyl-ester resins. The most well-known microencapsulation/healing agent system is the DCPD-Grubbs catalyst system, designed to spontaneously heal epoxy resins via ROMP at mechanical damage sites (cracks).

DCPD/Grubbs catalyst

The pioneering design reported by White *et al.* encapsulated DCPD in 220 µm PUF microcapsules via in-situ polymerization, and dispersed Grubbs catalyst (Figure 1.4a) throughout an epoxy matrix (EPON 828).[18] They postulated that mechanical damage would rupture the capsules, allowing DCPD to flow into cracks via capillary action and polymerize in the presence of Grubbs catalyst, thus spontaneously healing the crack. The self-healing ability of this modified epoxy coating was tested by cracking the film with a razor blade, and determining the critical load required to fracture the film. After film fracture, the load was removed, and the crack allowed to self-heal at room temperature for 48 hours. The fracture load was then measured a second time, and determined to be roughly 75% of the original epoxy film, indicating that substantial self-healing had taken place.

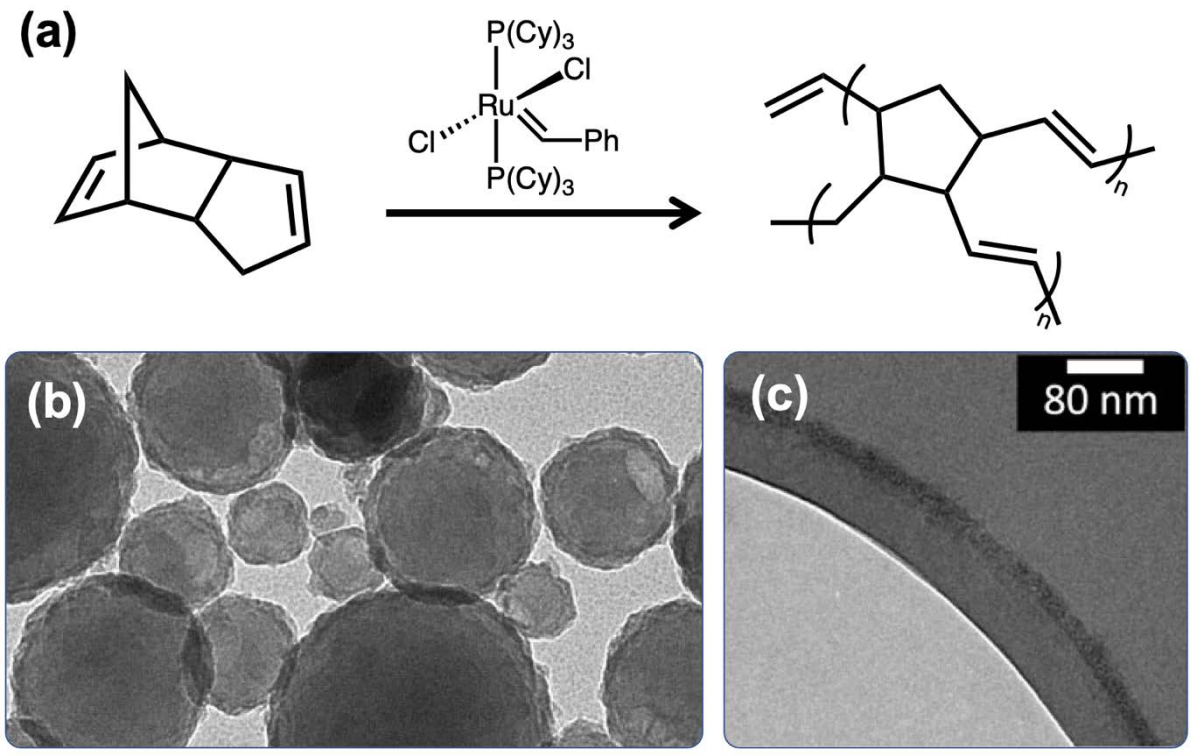

Figure 1.4 Initial self-healing strategies involved encapsulating liquid DCPD in PUF microcapsules. (a) The self-healing mechanism is based on the ROMP of DCPD initiated by Grubbs catalyst. (b/c): SEM images of 1.5 µm microcapsules encapsulating DCPD and Grubbs catalyst. This represents a double capsule system.[28]

In the years following this report, the DCPD-Grubbs catalyst system became the healing chemistry of choice for researchers designing microcapsules. Caruso[29] advanced this PUF capsule design by synthesizing a PUF-Polyurethane (PU) double shelled microcapsule via a combined in-situ polymerization (PUF shell) and interfacial polymerization (PU shell). Their design retained a similar capsule diameter to previous designs, but increased the shell thickness by over 200%, allowing capsules to survive the high temperatures (>120˚C) associated with certain epoxy resin curing, while maintaining self-healing functionality.[30] These initial capsule designs were mechanically strong, however their bulky size prevented the self-healing of small-scale microcracks. In some cases, the larger capsules exceeded the layer thickness required of many commercial organic coatings. In 2007, Bialsik[31] employed sonication during the in-situ polymerization process to reduce the diameters of PUF microcapsules to as low as 200 nm, with an average of about 1.5 μm. However, these capsules had lower mechanical stability, and were prone to aggregation within the polymer matrix. Jackson[28] sought to design tiny nanocapsules which maintained mechanical integrity and were more evenly dispersed throughout an epoxy matrix (Figure 1.4b–c). This was achieved via a dual capsule system, where DCPD and Grubbs catalyst were encased in separate micro/nanocapsules. DCPD was encapsulated in a 1.5 μm PUF capsule protected by a thin layer of silica, and Grubbs catalyst was encapsulated in a 1.5 μm microcapsule with a PS-PMMA shell, synthesized via solvent evaporation. The resulting epoxy film contained 15 wt% of the DCPD capsules and 7 wt% of the capsules containing Grubbs catalyst. The self-healing ability of this epoxy was tested according to White *et al's* method. The cracked epoxy showed modest self-healing efficiency, recovering above 20% of fracture toughness after 24 hours.

The DCPD-Grubbs catalyst design can imbue epoxy resins with strong self-healing capability; however, the high cost of Grubbs catalyst is a significant commercial obstacle, and its dull purple-brown colour limits its attractiveness for architectural organic coatings. Grubbs catalyst can also react slowly with air, limiting its use in organic coatings with longer lifetimes. Moreover, DCPD is known to solidify below 15˚C, which would significantly harm its ability to flow into damage sites at temperatures well within the performance specifications of most commercial organic coatings.

To reduce the amount of Grubbs catalyst and find alternatives to DCPD, Lee[32] compared the ROMP performance of DCDP with a new healing agent, 5-ethylidene-2-norbornene (ENB). They found that the polymerization of ENB was faster than DCPD, and required lower amounts

of Grubbs catalyst. In 2014, Wolfgang Binder[33] sought to use this idea to design self-healing epoxies that could withstand harsh, high temperature curing cycles. ENB was encapsulated in 760 nm UF microcapsules synthesized via in-situ polymerization, and Hoveyda-Grubbs first-generation catalyst was dispersed throughout various epoxy resins. To gauge the self-healing potential of this design, each epoxy resin was cut with a razor blade and subjected to two curing cycles (125˚C and 175˚C). The healing efficiency was tested via White *et al's* fracture toughness method. For epoxy resins with 10 wt% microcapsules, load-displacement curves yielded a healing efficiency of up to 98%.

PDMS-catalyst

Recently, Cho[34] proposed a new healing mechanism based on the tin-catalyzed polycondensation of hydroxy-functionalized polydimethylsiloxane (PDMS) and polydiethylsiloxane (PDES). They designed a single capsule system, where the catalyst was contained within PU microcapsules (1-20 μm), formed via interfacial polymerization. PDMS and PDES, which do not react without the catalyst present, were dispersed within a vinyl-ester matrix as phase separated droplets. This siloxane-based healing approach offers significant advantages over the older DCPD-Grubbs catalyst system, including a comparatively low cost, thermal stability above 100˚C and the complete lack of Grubbs catalyst. However, the healing efficiency was low compared to this traditional healing chemistry, maxing out at 24% fracture recovery for vinyl resins with 15 wt% of PDMS.

Magnun[35] transferred this PDMS healing mechanism to self-healing epoxy resins. They designed a dual capsule system with both PDMS and the tin catalyst encapsulated in separate PUF/PU microcapsules with an average diameter of 30-60 μm. These microcapsules were dispersed in an epoxy resin (EPON 828), which was first cracked, then allowed to heal at room temperature for 24 hours. White *et al's* fracture toughness method yielded a healing efficiency of 25-35%. A similar platinum catalyzed PDMS self-healing mechanism was applied to a polyurethane coating by Koh.[36] They designed a dual microcapsule system where one capsule contained PDMS and the platinum catalyst together, while the other capsule contained a siloxane-based crosslinker (TSF 848). The PUF microcapsules were prepared by in-situ polymerization and had an average diameter of 80 μm. The polyurethane coating containing 10 wt% microcapsules was cut with a razor, and the resulting scratch was observed to self-heal.

Epoxy resin healing agents

The majority of extrinsic microcapsule-based self-healing technology is tailored to spontaneously heal epoxy resins. Epoxy resins are first applied in liquid form before reacting with a hardener to form a highly crosslinked solid coating. This process is known as "curing". Thus separating (microencapsulating) a fraction of liquid epoxy to flow into cracks and crosslink in the presence of a hardener, represents a useful way to develop highly compatible self-healing epoxy resins. This method was first developed by Yin[37] for a commercial resin (bisphenol-A type epoxy resin E-51). They encapsulated the uncured epoxy in PUF microcapsules (30-70 μm) and dispersed a copper-based curing agent throughout the matrix. The resulting coating contained 10 wt% of the microencapsulated epoxy, and 2 wt% of the dispersed hardener. The coating had very similar mechanical properties to the commercial epoxy, with a slight reduction in its Young's modulus. The self-healing ability of this resin was assessed by fracturing a sample, pressing the two fractured edges together for 1 hour at 120 ˚C (curing temperature), and then refracturing the self-healed sample. Comparison of the fracture toughness of the epoxy before and after self-healing showed that the healed sample recovered 111% of its fracture toughness.

Later, Jin[38] applied this new technique to a commercial epoxy resin EPON 828, which cures under ambient conditions. They designed a dual capsule system, encapsulating an epoxy monomer (EPON 815C) in 110 μm PUF microcapsules, and a curing agent (EPIKURE™ 3274) in 117 μm hollow polymeric microcapsules. To evaluate the ambient self-healing ability of this epoxy, a sample was cut with a razorblade, and left to heal at room temperature for 48 hours. Comparing the fracture toughness of the undamaged sample and the self-healed sample yielded a self-healing efficiency of up to 91%.

In 2018, Zhang[39] designed a self-healing system for EPON 828 epoxy resin which only required the microencapsulation of a single epoxy-ester healing agent. This single capsule design rests on the fact that their epoxy ester can undergo curing via auto-oxidation at room temperature, precluding the need for any encapsulated curing agent. PUF microcapsules were synthesized via in-situ polymerization and had an average diameter of 101 μm (Figure 1.5a). They were incorporated into EPON 828 at a concentration of 1 wt%. The resulting epoxy coating was scratched with a razor blade, resulting in a crack approximately 100 μm wide, and left to self-heal at room temperature. After 72 hours, the coating's self-healing performance

was evaluated by scanning electron microscopy (SEM), which yielded detailed images of how the resin healed over this timespan (Figure 1.5b–c).

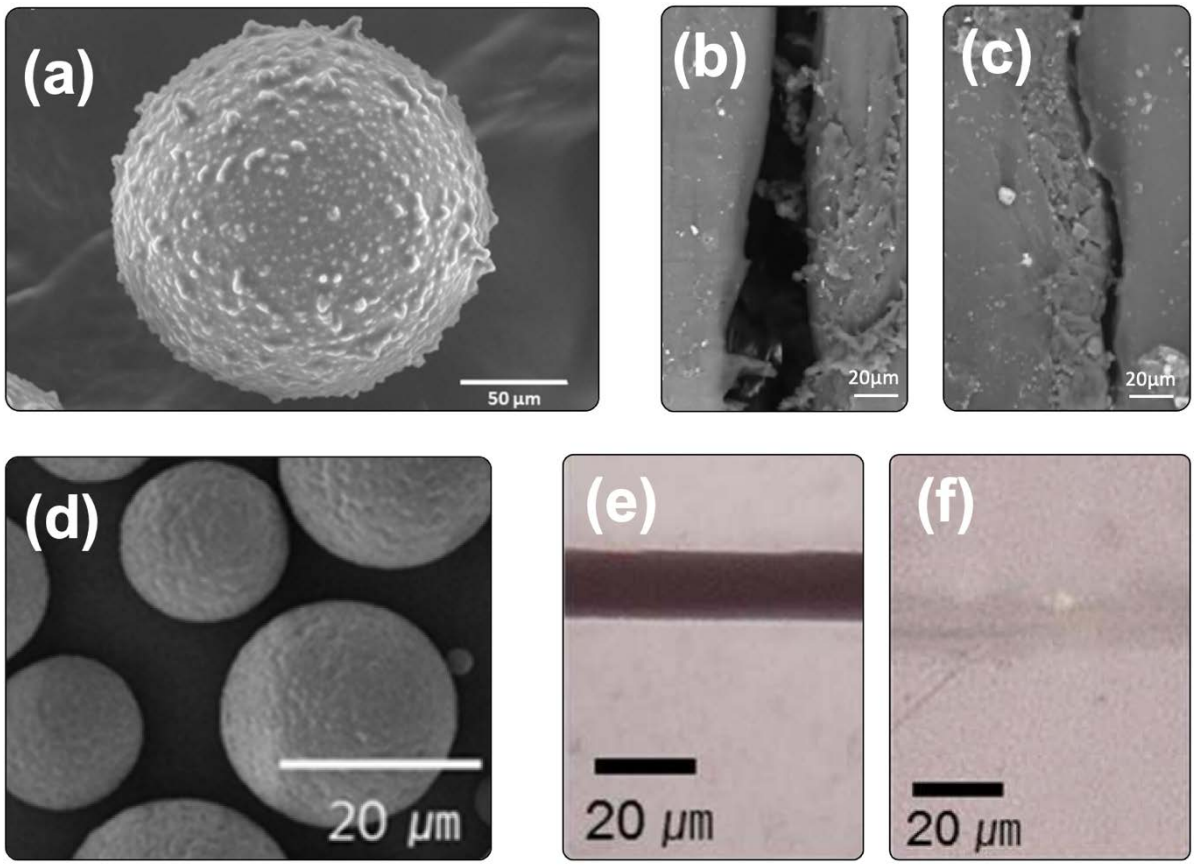

Figure 1.5 Liquid polymer resins as healing agents allowed for the absence of costly and potentially toxic catalysts. (a) A PUF microcapsule encapsulating liquid epoxy resin as a healing agent. (b/c) The self-healing of a crack through the release of liquid epoxy.[39] (d) SEM images of a typical PU capsule encapsulating acrylic healing agent. (e/f) Self-healing images of a scratched PU car paint initially, and after 3-5 hours, following the release of acrylic healing agent.[40]

Polymeric and inorganic shell microcapsules

Early research into extrinsic microcapsule-based self-healing centered heavily around the synthesis of capsules based on formaldehyde shells, specifically urea-formaldehyde, melamine-formaldehyde and polyurethane/urea-formaldehyde. However, for the majority of organic coatings, these kinds of microcapsules are commercially problematic, given the toxicity and carcinogenicity of formaldehyde. Formaldehyde is also a highly regulated compound in industry. Thus, research has begun to shift toward designing microcapsules with polymeric, inorganic or even biodegradable shells.

PMMA, a non-hazardous polymer ubiquitous in the coatings industry, has been extensively explored as a biocompatible shell material for the next generation of microcapsules. Li[41] synthesized PMMA microcapsules through a simple solvent evaporation technique. Briefly, PMMA and a given healing agent were dissolved in dichloromethane to make up the dispersed phase of an O/W emulsion, then DCM was allowed to evaporate, leaving the healing agent encapsulated by PMMA microcapsules. The diameter of these microcapsules could be tuned between 20 and 160 μm depending on the agitation rate. To study self-healing in a bisphenol-A epoxy resin (DGEBA), PMMA microcapsules were employed in the design of a dual component capsule system, encapsulating both the epoxy healing agent and a polyether-amine hardener.[42] The self-healing efficiency of this resin, containing 15 wt% microcapsules, was evaluated via the familiar fracture toughness procedure outlined by White *et al's* load displacement curves and yielded a self-healing efficiency of up to 85% over 24 hours at room temperature. In a similar study, Ahangaran[43] developed a dual component PMMA microcapsule system to imbue the epoxy resin Epikote™ 828 with self-healing ability. They encapsulated an epoxy prepolymer and mercaptan (as a hardener) in 20 μm PMMA microcapsules. The resulting epoxy had a capsule concentration of 10 wt%. Fracture toughness tests yielded a self-healing efficiency of 80% after 24 hours at room temperature.

Polyurethane (PU) microcapsules are another capsule design based on a polymer common in the coatings industry. Polyurethane capsules can be simply synthesized via interfacial polymerization, but normally require the use of isocyanate prepolymers, including toluene-diisocyanate. In 2014, Koh[40] imbued an acrylic polyurethane car paint (DHDC-2740) with self-healing capability by encapsulating some of the paint (in waterborne form) into PU microcapsules (44-57 wt%) (Figure 1.5d). The microcapsules had an average diameter anywhere between 20 and 80 μm, and were dispersed in a 150 μm thick layer of paint coating

at concentrations between 0 and 35 wt%. To evaluate the self-healing efficiency of this system, the automotive coating was scratched with a razor, yielding a crack between 20 and 40 μm deep. The coatings were allowed to heal for 3-5 hours at ambient conditions. The cracks were observed to have self-healed via an optical microscope (Figure 1.5e–f).

For applications requiring very thin coatings, Zhou[44] designed mechanically strong PU nanocapsules by incorporating silica nanoparticles onto their shell surface. Synthetically, this was achieved via interfacial polymerization using a Pickering emulsion template stabilized by silica nanoparticles. The nanocapsules had diameters ranging from 400-1000 nm, high mechanical strength (E = 2.39 GPa) and a resistance to common industrial solvents such as xylene and acetone. The self-healing ability of these nanocapsules was tested by dispersing them in a silicone anticorrosion coating. The coating was scratched and immersed in saltwater for 48 hours. SEM images of the scratched coating revealed the cracks had partially healed, as opposed to the unmodified resin.

PMMA and PU are perhaps the most common non-toxic capsule shell materials, but there are other important examples. For synthesizing microcapsules with different polymeric shells, the solvent evaporation method is robust. Crespy and Landfester[45] illustrated this by utilizing a combination of solvent evaporation and miniemulsion to synthesize micro/nanocapsules with shells made of: PMMA, poly(vinyl acetate) (PVAc), poly(vinyl formal) (PVF), poly(l-lactide) (PLLA), poly(2,6-dimethyl-1,4-phenylene oxide) (PPO), and poly(vinyl cinnamate) (PVCi). All of the resulting nanocapsules were able to encapsulate hexadecane, a model self-healing agent, and DLS results showed that the nanocapsules had average diameters between 230-330 nm.

Recently, researchers looking to create formaldehyde-free extrinsic self-healing systems have explored designing microcapsules with inorganic shells. This idea, though still in its infancy, presents a useful way to synthesize capsules that are both non-toxic and mechanically strong. Furthermore, many organic coatings already use inorganic nanoparticles dispersed in the binder as colour and opacity controls. In 2019, Hettiarachchi[46] designed a self-healing epoxy resin (EPIKOTE 828) containing calcium carbonate (CC) microcapsules (Figure 1.6a). The CC-capsules were synthesized via in-situ polymerization. These inorganic capsules had a mean diameter of 3.4 μm and thickness of about 800 nm and were able to encapsulate the epoxy healing agent ARALDITE 506 (36 wt%). The CC-capsule containing epoxy resin was

scratched in an "X" shape and left to heal over 24 hours. SEM images showed that the microcapsules, at concentrations above 20 wt%, were broken along the axis of the crack, and released healing agent into the damage site. This self-healing epoxy showed significantly superior anti-corrosion properties to the unmodified epoxy (Figure 1.6b–c).

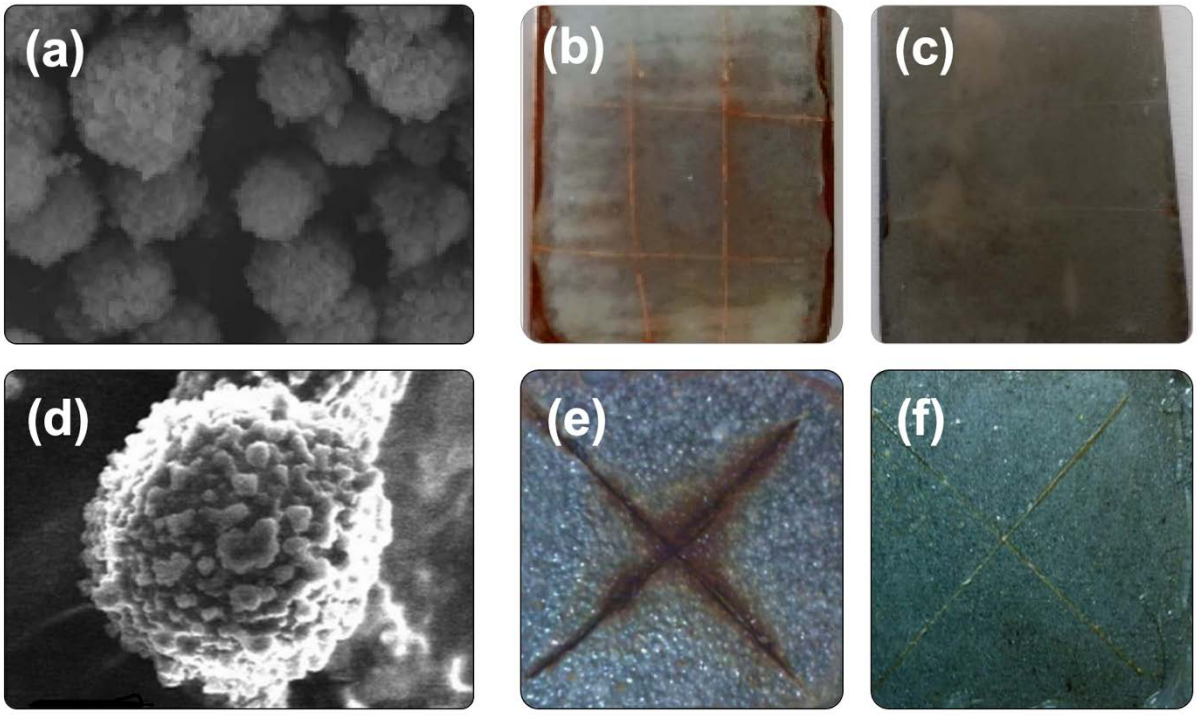

Figure 1.6 Recent research has centered on utilizing non-synthetic, non-toxic microcapsules and healing agents. (a) An SEM image of inorganic calcium carbonate (CC) microcapsules encapsulating liquid epoxy resin. (b/c) The resultant self-healing of CC capsules over 48h in a saltwater environment.[46] (d) An SEM image of PUF capsules containing tung oil. (e/f) The resultant self-healing of tung oil after 14 days in a saltwater environment.[47]

Pickering emulsions are emulsions which utilize solid particles as stabilizers. They have received extensive recent study as a template to design non-toxic microcapsules. Yi[48] used a Pickering emulsion to synthesize a 5 μm thick lignin microcapsule containing a mixture of diisocyanates, which were subsequently dispersed within an epoxy coating. This coating showed noticeable anti-corrosive and self-healing activity following 120 hours of immersion in salt water. In 2021, Wu[49] designed a dual chamber microcapsule (all-in-one) system

comprising a diisocyanate healing agent encapsulated by a SiO_2 shell containing an epoxy curing agent. They showed that their all-in-one design was able to heal an epoxy resin to 85% of its original tensile stress after 1 hour, following 2.5% induced strain. This was a 20% increase in efficiency when compared to a double capsule system containing the same healing agent-curing agent pair. Graphene oxide and TiO_2 have also received significant attention as microcapsule shell components chiefly for self-healing epoxy resins.[50, 51]

The range and diversity of microcapsules formed from various polymeric shells, as well as the burgeoning research into inorganic capsules, presents a promising method for designing non-toxic, formaldehyde-free, extrinsic self-healing systems. Already these capsules have displayed high healing efficiency for epoxy resin applications, but they also have the necessary scope to enhance the self-healing of other polymer matrixes.

Drying oils

In an alternative approach to the classic two component (healing agent and catalyst/hardener/curing agent) system, some recent attention has been devoted to using drying oils as self-healing materials for corrosion-protective coatings. Drying oils, such as linseed, tung, rapeseed, and other vegetable oils, are cheap, renewable and non-toxic, and thus attractive for organic coating applications. As self-healing agents, drying oils can flow through a polymeric matrix into cracks and crosslink via air exposure, forming a hard film. Suryanarayana[52] first encapsulated linseed oil into PUF microcapsules (80 wt%). The microcapsules had a diameter of between 40-100 μm and an average thickness of 200 nm, and were dispersed in an epoxy resin (XR-87). Their design showed that the linseed oil was able to flow into cracks quickly and form a protective film in minutes, resulting in superior anti-corrosion properties to the naked epoxy. A similar method was employed by Samadzedeh[47], who encapsulated Tung oil in PUF microcapsules (40-100 μm) (Figure 1.6d). Unlike the unmodified epoxy, their design was able to heal macro-sized cracks (400 μm-1 mm) by forming a hard film that protected the substrate from corrosion in a saltwater environment (Figure 1.6e–f).

More recently, Mirabedini[53] synthesized a biodegradable microcapsule whose shell comprised of ethyl cellulose. These microcapsules had a diameter between 10 and 50 μm, depending on the agitation rate, and were shown to successfully encapsulate both linseed and rapeseed oil. Seeking to expand the scope of microencapsulated drying oils, they employed this design as a

first step to examining the self-healing potential of waterborne acrylic paints.[54, 55] Ethyl cellulose microcapsules (5-50 μm) containing rapeseed and a small amount of red dye were dispersed (1-3 wt%) in a colourless, transparent styrene/butadiene latex film. The mechanical properties of the latex were unaffected by the addition of microcapsules, and the rapeseed oil was shown, via the red dye, to be released into the matrix by physically elongating the latex film (100-150%). From this, the researchers indirectly inferred that the rapeseed oil, released during a damage event, could flow into cracks and heal the latex film. Drying oils as self-healing materials are cheap, non-toxic and synthetically simple. They no doubt offer a valid path for researchers looking to design self-healing coatings, in particular anti-corrosion coatings. However, given that drying oils form a hard film that is easily distinguishable from the original matrix, their applicability in architectural coatings is less clear.

Microcapsule systems are the most well studied self-healing technique and represent a promising strategy for imbuing coatings with self-healing functionality. They have shown the ability to yield highly efficient self-healing epoxy resins, and present a viable pathway toward developing a wider array of self-healing organic coatings. However, preserving both the optical and mechanical functionality of certain organic coatings remains a significant challenge. The development of cheaper, non-toxic and synthetically accessible microcapsule systems is the next logical step for researchers looking to design such extrinsic self-healing systems.

Solvent swelling

In 2015, White[56] attempted to design an ambient self-healing system for thermoplastic PMMA matrixes. Their idea was to encapsulate a solvent (anisole) that, when released, promotes reptation between polymer chains and thus the intrinsic self-healing of cracks. PMMA dissolved in anisole was encapsulated within double-walled PU/UF microcapsules (250-350 μm). These microcapsules were dispersed within a linear PMMA mold (2.5-10 wt%), resulting in a PMMA film that had a storage modulus (E') of between 0.8 and 1.1 GPa, and a *T*g around 90˚C. Self-healing was evaluated via fracture toughness comparisons between the virgin and self-healed sample. The PMMA coating was cracked with a razor blade, and then allowed to heal at ambient conditions for between 1 and 7 days. For the PMMA films containing 5 wt% of the anisole-containing microcapsules, the healing efficiency was 89%. Control PMMA films containing the same capsules with DCPD healing agent displayed no fracture toughness recovery.

Self-reporting extrinsic self-healing coatings.

One of the major benefits of self-healing coatings is the ability to heal damage without external intervention. However, for coatings that require external intervention in the form of applied light or heat to initiate self-healing, the ability to detect and report the exact position of damage allows for healing capability.[57] These coatings, which can autonomically detect and report the presence of damage, are known as self-reporting coatings. Recent research has focused on designing coatings which combine self-healing functionality and self-reporting capability, and generally involves the microencapsulation of a healing and a reporting agent, which are both released in the presence of mechanical damage.[58]

In 2020, Chen[59] developed double PU-PUF microcapsules containing hexamethylene diisocyanate, a healing agent which can polymerize in the presence of water to form polyurea, and a tetraphenylene based fluorescent compound (luminogen). Upon damage, the healing agent was released, along with the luminogen, which, in the presence of PU, yields a distinct blue fluorescence via aggregated induced emission (AIE), revealing the exact location of damage. In 2022, Wang [60] imbued an anticorrosive epoxy resin with silica microcapsules containing an ammonium corrosion inhibitor and 1,10-phenanthroline-5-amine (Phen-NH_2), which functioned as both a corrosion inhibitor and a reporting agent. Upon damage, Phen-NH_2 was released from the capsule and formed a complex with Fe^{2+} ions, yielding a distinctive red colour at the crack sites. Zhang[61] designed a pH responsive self-healing, self-reporting epoxy coating. A dual capsule system was synthesized, with one capsule containing a polyamine, and the other containing an epoxy monomer (healing agent) and a pH responsive dye (reporting agent). Upon damage, all three agents were released, resulting in self-healing via the epoxy healing agent, and self-reporting via the dye, which in the presence of basic polyamine, yielded a conspicuous red colour at the damage site.

1.2.1.2 Microvascular systems

Microvascular systems take their inspiration from nature and the human body, attempting to mimic how capillary networks supply blood to cuts on the skin, promoting biological self-healing.[27] Synthetic microvascular self-healing systems involve dispersing the healing agent across a polymeric matrix within hollow vessels. Once damage occurs, these hollow vessels will be ruptured, resulting in the release of healing agent at the crack site (Figure 1.7). The self-healing chemistry utilized by vascular systems is not remarkably different from microcapsule systems; rather, it is the method of encapsulation that sets these two techniques apart.

Vascular designs have two key theoretical advantages over their microcapsule counterparts. First, vascular networks can, in principle, be externally refilled with healing agent upon depletion, allowing for repeatable crack healing at the same site within a matrix.[5] This can be achieved first by injecting fresh healing agent into open vessels at the coating edge with a syringe, and then, once healing agent begins to seep out, covering the edges with adhesive.[62] Coope[63], for example, achieved this in an epoxy resin system by injecting healing agent by hand into 0.45 mm wide vessels, allowing for repeated healing cycles. Secondly, microvascular systems are able to both store and release a larger amount of healing agent, increasing the self-healing efficiency of a given material.[64] Nevertheless, these systems include a number of drawbacks. Foremost amongst them is the production cost and complex synthesis necessary to introduce vascular systems into coatings. The fabrication of stable synthetic capillaries within a polymeric matrix is a multistep process.

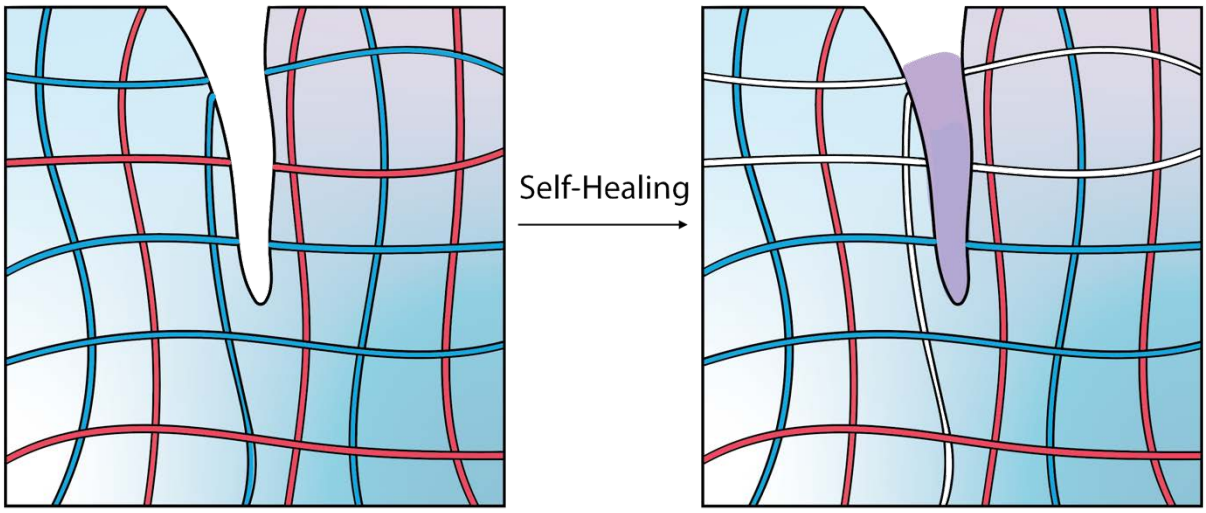

Figure 1.7 A schematic of the microvascular healing system, whereby a crack breaks open the vessels, releasing healing agent (blue) and catalyst (red) into the polymeric matrix.

The first microvascular self-healing materials were synthesized via direct wire assembly. Direct wire assembly involves the robotic deposition of fugitive organic inks into a scaffold. The scaffold is then mixed with an epoxy resin, and the fugitive ink is evaporated by heating the epoxy up to 75˚C, leaving behind a hollow microvascular system. Frequently the hollow vessels must be filled with wax during this process, to prevent the epoxy resin from infiltrating the scaffold. In 2007, Toohey[65] used this synthetic route to design a self-healing epoxy resin embedded with a microvascular network. EPON 828 containing dispersed Grubbs catalyst was infiltrated with a microvascular network filled with DCPD. This design is similar to the single capsule/dispersed catalyst system used for microcapsule based self-healing. The hollow channels had an average diameter of 300 μm. The self-healing potential of this new epoxy design was tested via the ability to recover fracture toughness after a damage event. Coatings with different amounts of catalyst were put under a load until a crack formed, and were then allowed to heal at room temperature for 12 hours. After two cycles, the epoxy coating, containing 10 wt% of the catalyst, recovered 70 % of its fracture toughness. However, some of the liquid DCPD was released from the epoxy and formed droplets on its surface.

White[66] adapted this design by using direct wire assembly to form two distinct microvascular networks within an EPON 828 epoxy matrix. The procedure for synthesizing two separate microchannels is significantly more complicated, given that both inks must be removed independently of each other to maintain network separation. Once this was achieved, the

separate hollow channels, with diameters ranging from 100-300 μm, were filled with either a low-viscosity epoxy resin, or an epoxy hardener. Their design proposed that upon mechanical damage, the vascular structure would rupture, and both the epoxy and the hardener would be released to self-heal the resulting microcrack. The fracture toughness of this microvascular epoxy resin was tested to evaluate its self-healing capability. It is generally asserted that microvascular networks can hold a higher volume of healing agent relative to microcapsules, thus the researchers subjected their epoxy resin to 30 healing cycles. Even after such a large number of cycles, the healing efficiency remained steady at around 50%. Direct wire assembly is a complex synthetic procedure that offers the ability to form microvascular epoxy resins containing large amounts of healing agent based on fugitive ink scaffolds. These scaffolds, however, have limitingly large diameters, and are far too fragile to survive the basic manufacturing and transport processes relevant to the majority of organic coatings.

In the past decade, most new microvascular self-healing strategies have been based on the electrospinning method, which allows the formation of tiny fibers based on threads of polymer solutions.[67] These fibers can have diameters raging from 10 nm to 10 μm. As well as permitting the synthesis of fibers with size ranges more beneficial to a wide range of coating applications, the electrospinning method is simpler, and allows for the random deposition of fibers throughout a polymer matrix. In 2016, White[68] used electrospinning to design a self-healing silicone coating. Poly(vinyl alcohol) (PVA) shelled nanofibers, with diameters between 300 and 400 nm, contained a mixture of either PDMS and PDES, or a tin catalyst (DBTL). Upon a mechanical damage event, PDMS, PDES and the tin catalyst would be released into a crack, self-healing it via the polycondensation of PDMS and PDES. The self-healing ability of this silicone coating was tested by scratching the coating's surface with a razor blade, forming a 2.5 cm long crack. The coating was allowed to heal at room temperature for 24 hours. SEM images showed that a degree of self-healing had taken place over this time, but the crack had only been partially filled. This material also showed strong anti-corrosive performance over a 4-month period relative to the unaltered silicone coating.

In 2019, Li[69] designed a self-healing waterborne polyurethane coating by embedding poly(acrylonitrile) (PAN) fibers containing linseed oil. In the event of mechanical damage, linseed oil would be released into the crack, allowing it to react with oxygen and form a hard film, thus healing the polyurethane coating. The PAN fibers encapsulating linseed oil were synthesized via coaxial electrospinning and were then embedded into waterborne coating

NeoRez R-9679 (40 wt%) (Figure 1.8a–b). The fibers had a diameter of about 400 nm, with PAN shell thickness ranging from 30-50 nm. The self-healing behavior of this modified polyurethane coating was tested by scratching the surface to form a crack with a width of 13 µm and leaving the coating to self-heal over 7 days. SEM images show that after 7 days, the crack was significantly filled with released linseed oil (Figure 1.8c–d).

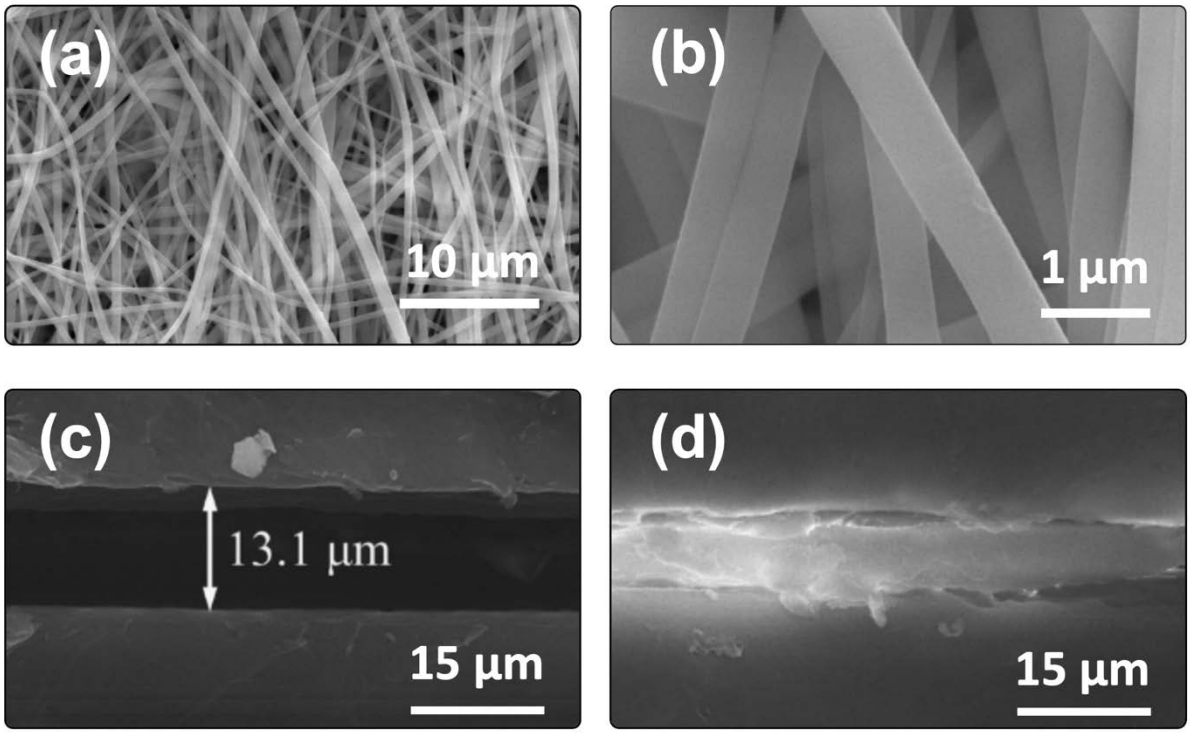

Figure 1.8 Microvascular systems can promote self-healing across a wide variety of organic coatings. (a/b) SEM images of a typical microvascular system, electrospun PAN fibers. (c/d) The self-healing of a polyurethane coating via the release of linseed oil from PAN fibers.[69]

Recently, researchers have attempted to translate these fiber designs to self-healing epoxy resins. In 2015, Zanjani[70] synthesized three distinct PMMA shelled fibers, encapsulating DCPD, an epoxy healing agent and a hardener respectively. The fibers had an average diameter between 200 nm and 1 µm. A year later, Neisiany[71] was able to encapsulate both an epoxy resin precursor (EPIKOTE 240) and a hardener (EPIKURE 3370) into PAN nanofibers. The fibers had an average diameter of about 400 nm. In 2021, Wang[72] designed a self-healing anti-corrosion epoxy resin based on core (polyacrylonitrile)-shell (tannic acid) nanofibers encapsulating tung oil. The combination of tannic acid and tung oil, which both act as acidic

and alkaline self-healing agents respectively, resulted in strong self-healing efficiency across a wide range of pH conditions. Interestingly, in 2022, the same research group imbued an epoxy resin coated on a steel substrate with phenanthroline-chitosan core-shell fibers.[73] Upon mechanical damage, phenanthroline was released and formed metal-ligand complexes with the iron of the steel substrate, thus providing the attractive force necessary to generate crack self-healing. This supramolecular attractive healing mechanism is atypical of extrinsic self-healing strategies, which normally rely on the dispersion of liquid healing agents.

In summary, the primary benefit of microvascular self-healing materials is their potential to repeatedly heal damage even after many cycles — a rarity for extrinsic systems. This is due mainly to the size of the scaffold and the higher total volume of healing agent able to be encapsulated. However, large microvascular networks are a double-edged sword, especially for applications which require only a thin coating layer. Vascular systems with significant size control have only recently become research hotspots. Furthermore, vascular systems are difficult both to synthesize and to incorporate into various coating binders, which, for the moment at least, limits their commercial viability.

1.2.2 Intrinsic self-healing strategies

Intrinsic self-healing relies on the coating material to generate a spontaneous response to mechanical damage. In the absence of a distinct healing agent, this is normally achieved via the addition of latent self-healing functionality to the matrix's polymeric structure. Unlike extrinsic self-healing strategies, this kind of healing generally relies on contact between the edges of the crack. For low modulus, thermoplastic coatings, this can be achieved through the inherent mobility and even flowability of polymer segments and the coating itself. However, for stronger, glassier coatings, this crack closure is a significant challenge.[74] One potential solution to this problem are shape memory polymers. These polymers are generally highly entangled three dimensional matrixes where damage results in polymer deformation and conformational change, rather than slippage/flowing.[75] Upon damage, these polymers, due to their conformational entropy, spontaneously attempt to recover their original (undamaged) shape.[76] One can think of shape memory polymers like springs, which upon damage become 'coiled up' and wish to return to their original 'uncoiled' shape. The vast majority of highly entangled polymers have inherent shape memory properties, however shape memory alone is

not normally enough to provide self-healing, and must be coupled with intrinsic healing functionality.[77] In addition to shape memory effects, phase separation, whereby thermoplastic, softer polymeric domains are embedded within a stiffer polymeric matrix (Figure 1.9), allows for crack closure and subsequent intrinsic self-healing, without needing to heat the material significantly above its *T*g.[78]

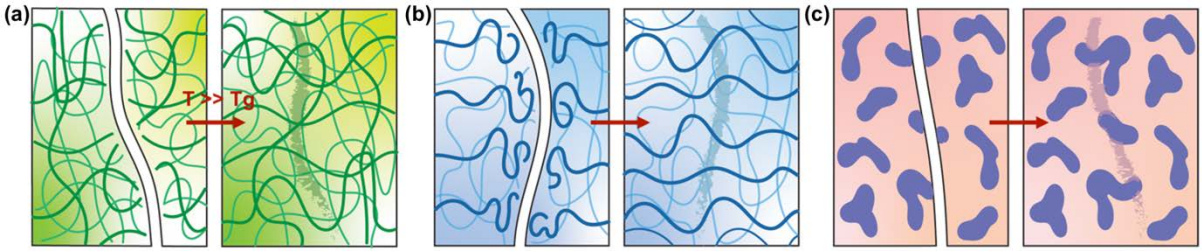

Figure 1.9 Physical processes which can promote crack closure. (a) Polymer flow or chain interdiffusion through high temperatures. (b) The shape memory effect. (c) Phase separated morphologies

Intrinsic self-healing functionality can be split into two categories: dynamic covalent bonding, and supramolecular networks (aka reversible non-covalent bonding).[12] These connections will be broken when a crack is produced via mechanical damage, but can reform due to their reversible nature, thus healing the crack. Dynamic covalent bonding includes the Diels–Alder and retro Diels–Alder reactions, other cycloaddition reactions, disulfide linkages, and certain radical fission/recombination reactions.[12] These bonds are stronger than their supramolecular counterparts, and thus offer the ability to maintain a material's mechanical strength following the self-healing process. However, they normally require some external stimuli such as heat or light to initiate the bond reforming reaction.[79] Supramolecular bonds, on the other hand, are more suited to healing under ambient conditions -an attractive proposition for many organic coating applications. Supramolecular self-healing networks mainly focus on the hydrogen bond, but also include π-π stacking, metal-ligand complexation,[80] host-guest interactions, and ionic interactions, including ionomers, polyampholytes and polyelectrolytes.[81]

Intrinsic self-healing technology has been tested across a range of polymeric coatings and offers benefits distinctly different from extrinsic healing technology. They include:

i) Repeatable self-healing. Given the reversibility of covalent and supramolecular bonds, and the lack of a depletable healing agent, the intrinsic healing process can be repeated

a theoretically infinite number of times in the same place. This is perhaps the primary benefit of intrinsic self-healing materials.

ii) Superior material properties for organic coatings. Intrinsic self-healing materials lack the need for microcapsules or other larger structures within the polymeric matrix. This means that many coating properties, in particular optics and tensile strength, are likely to remain unaffected.

iii) A generally simpler design method. Intrinsic techniques rarely require coating- specific capsules, or the incorporation of expensive catalysts and healing agents into the polymeric matrix.

As well as the benefits, there are also a number of drawbacks one needs to consider when assessing the applicability of intrinsic self-healing materials for organic coatings:

i) For intrinsic healing systems to work, there must be a level of viscoelastic flow in the matrix. This is to allow functionalized sections of polymer, following a damage event, to come into close enough steric contact to initiate the healing process. Thus, designing intrinsic self-healing systems is rather simple for soft materials, but a challenging proposition for stiff, rigid materials.

ii) Due to the importance of polymer chain dynamics in intrinsically self-healing materials, the scale of damage that can be healed is small, and usually limited to microcracks.

iii) Many intrinsic self-healing materials require external stimulus, including heat and light, to initiate healing. This limits their applicability to certain kinds of organic coatings.

Continuous research is being done to overcome these drawbacks, and already a number of groups have begun the process of designing intrinsically self-healing systems for more rigid, high modulus polymeric matrixes. Intrinsic self-healing materials offset many of the problems associated with the microencapsulation of healing agents, and offer a more optimistic picture of how a highly dynamic self-healing coating could be designed.

1.2.2.1 Reversible covalent bonds

Reversible covalent bonds offer a promising and attractive route to designing intrinsic self-healing coatings. These bonds, when incorporated into polymeric coatings, form covalent networks whose reversibility allows for self-healing under a range of conditions. In many cases, their covalent bonds provide the necessary mechanical strength required for organic coating applications, and certain designs can achieve very high healing efficiencies. Reversible covalent bonds can be divided into two categories: *dissociative*, where bond breakage and reformation are two separate steps, and normally occur at two different temperatures, and *associative*, where bond breakage and reformation occur simultaneously.[82, 83] Covalent networks based on the associative mechanism are sometimes known as vitrimers.[84] Both associative and dissociative covalent networks frequently require high temperatures to initiate reversibility, however dissociative reactions may require two separate stages of temperature treatment to initiate the different reaction/retro-reaction. For a coating that does not require high temperature curing, the primary practical concern is whether the base coating can withstand these necessary thermal cycles (90–150˚C), and if it can, whether such a high energy input is a worthwhile investment. Figure 1.10 displays the four most well studied self-healing reversible covalent bond chemistries.

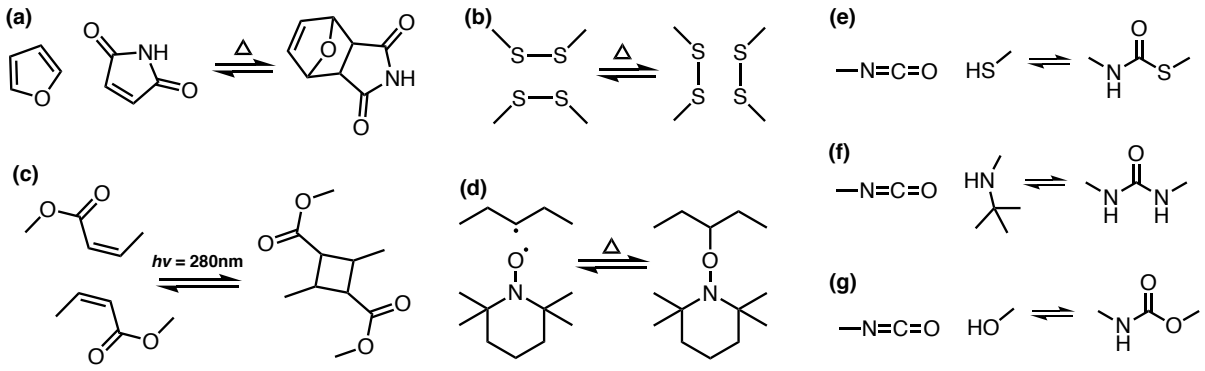

Figure 1.10 A selection of the most common self-healing covalent bond chemistries. (a) Diels–Alder (retro) reaction. (b) Dynamic disulfide bonds. (c) Light-induced cycloaddition. (d) Alkoxyamine radical fission/recombination. (e) Thiourethane exchange. (f) Hindered urea exchange. (g) Carbamate exchange.

Some new covalent designs, which are currently limited to lower modulus materials, have shown promise by achieving significant self-healing under ambient conditions.

Diels–Alder reaction

Of all the reversible covalent bonds potentially pertinent to self-healing technology, the Diels–Alder reaction (Figure 1.10a) has received the most attention. The Diels–Alder reaction (DA) is a [4+2] cycloaddition reaction between a conjugated diene and a dienophile that results in the formation of two new carbon-carbon sigma bonds. It is a thermally reversible dissociative reaction, meaning that the bond formation and bond breaking process occurs separately and is controlled by temperature.[85] Most self-healing designs center on utilizing the DA reaction to synthesize thermally reversible crosslinked polymer matrixes. The self-healing mechanism involves first heating a crosslinked polymer matrix to initiate the retro Diels–Alder reaction (RDA), which causes the crosslinks to debond (break). The resulting high chain mobility allows network reconnection at the mechanical damage site, and reformation of the crosslinks as the material cools. Importantly, the DA/RDA reaction is tolerant to oxygen and moisture, and its "click" characteristics make it a convenient reaction for polymer synthesis and design.[86] In 2002 Wudl,[87] building on a patent submitted by Craven in 1969,[88] designed a self-healing macromolecular structure held together by thermally reversible Diels–Alder adducts of furan and maleimide. Their matrix was first cracked with a razor, then heated to between 120˚C and 150˚C to initiate the RDA reaction, and finally, after two hours, allowed to cool to room temperature. Fracture recovery tests showed the self-healed material recovered between 41–57% of the original fracture toughness. This furan-maleimide system has been investigated and improved upon in the ensuing two decades. In 2009, Tian[89] designed a novel epoxy with a furan pendant group. When this epoxy was cured with a bis-maleimide compound, an epoxy resin crosslinked with reversible Diel-Alder bonds was formed. The epoxy resin had a high Young's modulus (2.5 GPa) and a *T*g of around 130˚C. The self-healing potential of this new epoxy was evaluated by first generating cracks in its matrix, then thermally treating the matrix at 125˚C for 20 minutes and annealing at 80˚C for 72 hours. A visual inspection of the cracks showed significant self-healing.

Bai,[90] preferring to simply modify a commercial epoxy rather than design a novel one, synthesized a crosslinker containing Diels–Alder adducts to be used as a curing agent for the epoxy resin constituent DGEBA (Figure 1.11a). Thus, following the curing process, their epoxy resin was imbued with thermally reversible, Diels–Alder based crosslinks. The epoxy resin had a *T*g of about 61˚C, and was stable up to 200˚C. To gauge its self-healing ability, the

epoxy was scratched with a blade and heated to 140˚C for 30 minutes to initiate the RDA reaction. Figures 1.11b–c show that over this time the crack completely healed. The healed sample was kept at 75˚C for 5 hours to reinitiate crosslinking via the DA reaction.

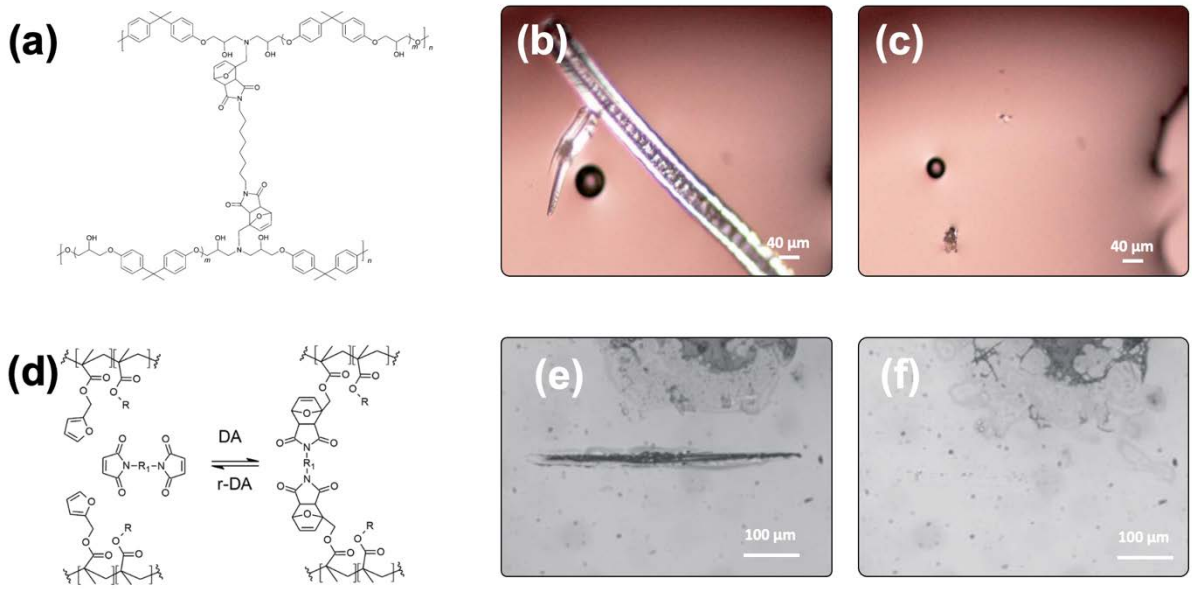

Figure 1.11 The Diels–Alder reaction allows for significant self-healing capability at high temperatures. (a) A Diels–Alder crosslinked epoxy design which was able to self-heal a microcrack after 30 minutes at 140˚C (b/c).[90] (d) A Diels–Alder acrylate coating design which was able to self-heal a microcrack after 90 minutes at 150˚C (e/f).[91]

In 2013, Kötteritzsch[92] utilized Diels–Alder chemistry in an attempt to design a self-healing acrylate coating. Using atom transfer radical polymerization (ATRP), they synthesized a terpolymer consisting of maleimide methacrylate (MIMA), furan methacrylate (FMA) and one of MMA, butyl methacrylate (BMA) or lauryl methacrylate (LMA). Diels–Alder reactions between MIMA and FMA would form thermally reversible crosslinks, resulting in a self-healing material. The *T*g of these three polymers was –16˚C for the LMA copolymer, 40–60˚C for the BMA copolymer and 120˚C for the MMA copolymer. Of these three designs, the LMA copolymer showed the best self-healing properties, which the researchers assert is due to its chain flexibility. Nevertheless, the LMA copolymer still formed a mechanically strong film (E = 5 GPa). Its self-healing ability was tested by inducing a crack, and then heating the damaged material to 80˚C, 110˚C and 160˚C. At 160˚C, SEM images showed that self-healing took place in under 3 minutes, while at 110˚C, the scratch was only partially healed after 4 hours.

In 2020, Fortunato[91] slightly altered this design, and was able to form colourless and transparent Diels–Alder functionalized acrylate coatings. Instead of attaching both the furan and maleimide functionality to one single polymer, they synthesized a copolymer containing FMA and one of BMA, LMA and 2-ethylhexyl methacrylate (EHMA) (Figure 1.11d). Blending this copolymer with a bis-maleimide crosslinker resulted in the formation of clear acrylate coatings with a *T*g between 7˚C (LMA copolymer) and 50–60˚C (BMA/EHMA copolymer). In order to assess the self-healing potential of these acrylate coatings, each was scratched with a scalpel to form a crack 30–40 μm deep. The films were then heated to 150˚C for 90 minutes and slowly cooled to room temperature. The EHMA film showed near-complete self-healing (Figure 1.11e–f), and the LMA and BMA films showed strong self-healing, according to optical microscope images.

Diels–Alder chemistry has also been used to design self-healing polyurethane matrixes for application as automotive clear coats. In 2019, Sung[93] compared a commercial polyurethane automotive coating with a Diels–Alder crosslinked polyurethane coating. The coatings were formed by crosslinking an acrylic polyol resin with either Desmodur N3300 or a furan-maleimide adduct. The latter formed polyurethane networks with Diels–Alder crosslinks and was expected to have superior self-healing properties to the commercial coating at elevated temperature. To evaluate the self-healing properties of both coatings, each was scratched to form a 0.8 mm long crack, and subsequently heated to 150˚C for 1 hour to initiate the retro-Diels–Alder reaction. After cooling, the crack on the DA crosslinked coating had completely disappeared. Interestingly, the commercial coating also underwent incomplete self-healing, which the authors assert was due to elastic recovery. In 2022, Tortelli[94] introduced self-healing Diels–Alder chemistry to a typical transparent acrylic coating. They synthesised terpolymers of methacrylic acid (MAA), 2-ethylhexyl methacrylate (EHMA) and furfuryl methacrylate blended with a bismaleimide crosslinker to form coatings which displayed near perfect optical self-healing at 150˚C for 30 minutes.

Diels–Alder chemistry is a promising approach for designing self-healing coatings due to its reversible crosslinking capability, its relatively simple synthetic incorporation, and its applicability to a variety of different polymer matrixes. Furthermore, Diels–Alder crosslinks are covalent bonds, and hence maintain the mechanical strength required for most organic coating applications at ambient conditions. However, Diels–Alder based self-healing requires

a significant energy input in the form of high thermal cycles (120–160˚C), limiting its application for a variety of organic coatings.

Disulfide bridges

Many research groups have focused on the dynamic and relatively weak disulfide bond for designing materials whose intrinsic self-healing can take place at more moderate temperatures. Disulfide exchange is reversible and can occur through a radical mediated pathway via UV irradiation, or at modest temperatures (Figure 1.10b).[95]

In 2011, Canadell[96] first investigated the self-healing capability of an epoxy resins crosslinked with disulfide bonds. Their idea involved healing broken crosslinks at mechanical damage sites through disulfide exchange. The resulting rubbery material had a low *T*g of –35˚C and displayed almost complete self-healing at 60˚C after 1 hour. In 2016, Odriozola[97] designed a repairable "vitrimer" system by imbuing a commercial epoxy resin (DGEBA) with disulfide crosslinks via curing with 4-aminophenyl disulfide. The resin had strong mechanical properties (storage modulus = 2.5 GPa) below its *T*g of 130˚C. Despite disulfide exchange requiring more modest temperatures than the RDA reaction, the self-healing potential of disulfide-crosslinked epoxy was only tested at 200˚C for 5 minutes. A crack on the matrix surface was completely healed under these conditions.

Disulfide exchange has also been employed to instill polyurethane coatings with self-healing capability. Lai[98] synthesized self-healing polyurethane elastomers with disulfide bonds contained in their backbones. The crosslinked polymer films had a Young's modulus of between 30 and 50 MPa and *T*gs between 30 and 50˚C. Their self-healing potential was investigated by cutting the films in half, and then pressing them together at 70˚C for 6 hours. The polyurethane films were able to regain up to 86% of the tensile strain of the uncut samples, indicating a strong self-healing effect. The films were also able to spontaneously heal cracks on their surface within 60 seconds at 70˚C (Figure 1.12a–b). In 2020, Liu[99] developed a stronger polyurethane coating by incorporating disulfide bonds into the polyurethane backbones (Figure 1.12c). Both the *T*g and Young's modulus of the resulting polyurethane matrixes were highly variable depending on the wt% of added disulfides, and varied from 10–80˚C and 3.5–182 MPa respectively. The researchers were able to form an optimized polyurethane matrix that self-healed a crack at 90˚C after 12 hours (Figure 1.12d–e), while maintaining relatively high mechanical strength (Young's modulus = 111 MPa).

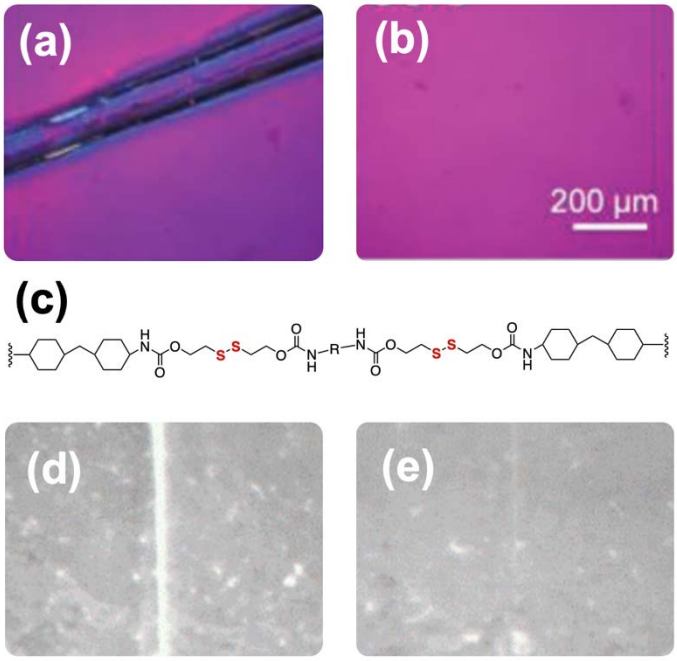

Figure 1.12 Reversible disulfide bonds have yielded coatings which can self-heal at more moderate temperatures. (a/b) The self-healing of a disulfide functionalized polyurethane elastomer at 70˚C after 60 seconds.[98] (c) The structure of a high modulus, disulfide functionalized polyurethane matrix. (d/e) The self-healing of a crack in the polyurethane matrix at 90˚C after 12 hours.[99]

Recent research has focused on enhancing self-healing efficiency by designing coatings which combine both Diels–Alder and disulfide functionality. In 2021, Behera[100] imbued a polyurethane coating with dual self-healing functionality via a disulfide-furfuryl chain extender with maleimide crosslinkers. Their coating had a self-healing efficiency >90% in terms of tensile strength recovery, achieved through healing temperatures of 135˚C for 10 minutes and 70˚C for 24h. This dual system was also shown to have a superior self-healing efficiency when compared to the PU coating with either Diels–Alder or disulfide functionality alone. Chen[101] designed a high modulus (209 MPa) coating which blended disulfide functionalized polyurethane with Diels–Alder functionalized epoxy oligomers. Their coating was damaged and subjected to 30 minutes at 130˚C and 12 hours at 60˚C, resulting in noticeable optical self-healing and significant strain recovery. Xu[102] was able to reduce the healing temperature of a disulfide functionalized polyurethane material via the addition of dynamic boronic ester bonds as crosslinking points. This polyurethane had a tensile strength of 27 MPa,

and displayed noticeable optical self-healing along with very strong stress and strain recovery at a healing temperature of 60˚C for 12 hours.

Disulfide bonding provides a useful way to design thermally reversible crosslinked materials whose self-healing can take place at more moderate temperatures than materials based on Diels–Alder chemistry. However, these coatings generally lack high mechanical strength, and many of the studied disulfide moieties contain benzene substituents, whose toxicity may limit the industrial applicability of coating synthesis.

Photochemical cycloaddition

Photochemical reactions initiated by the absorption of energy in the form of light are generally fast and simple (Figure 1.10c). Thus, many research groups have investigated these reactions as possible candidates for imbuing materials, including coatings, with self-healing functionality. Chung[103] first developed this concept in 2004, by synthesizing a polymeric matrix containing cinnamoyl groups as crosslinkers. These groups can undergo photochemical [2+2] cycloaddition to form cyclobutane crosslinks, and then revert back to two separate cinnamoyl groups. Self-healing involves mechanical damage rupturing all of the cyclobutane structures to form a crack, which can then be healed via irradiation (>280 nm) to reform the cyclobutane crosslinks. In this initial study the polymer matrixes were cracked, and showed significant self-healing capability after being irradiated for 10 minutes at a temperature of 100˚C. Saito[104] designed a self-healing acrylate matrix imbued with coumarin crosslinkers. Coumarin groups can undergo [2+2] cycloaddition via irradiation (>300nm) to form cyclobutanes (Figure 1.13a). They synthesized copolymers containing the coumarin crosslinker (7-methacryloyloxy coumarin) and one of MMA, BA, hexyl methacrylate (HMA) or ethyl acrylate (EA). The resulting films had a *T*g raging from 30–70˚C, and their hardness was between 50 and 60 MPa. The self-healing potential of each acrylate matrix was assessed by inducing a crack and irradiating the sample with light (254 nm) at room temperature for the EA film (Figure 1.13b–c), and 60˚C for the other three films. Optical microscopy showed near-complete self-healing of the crack for all four samples.

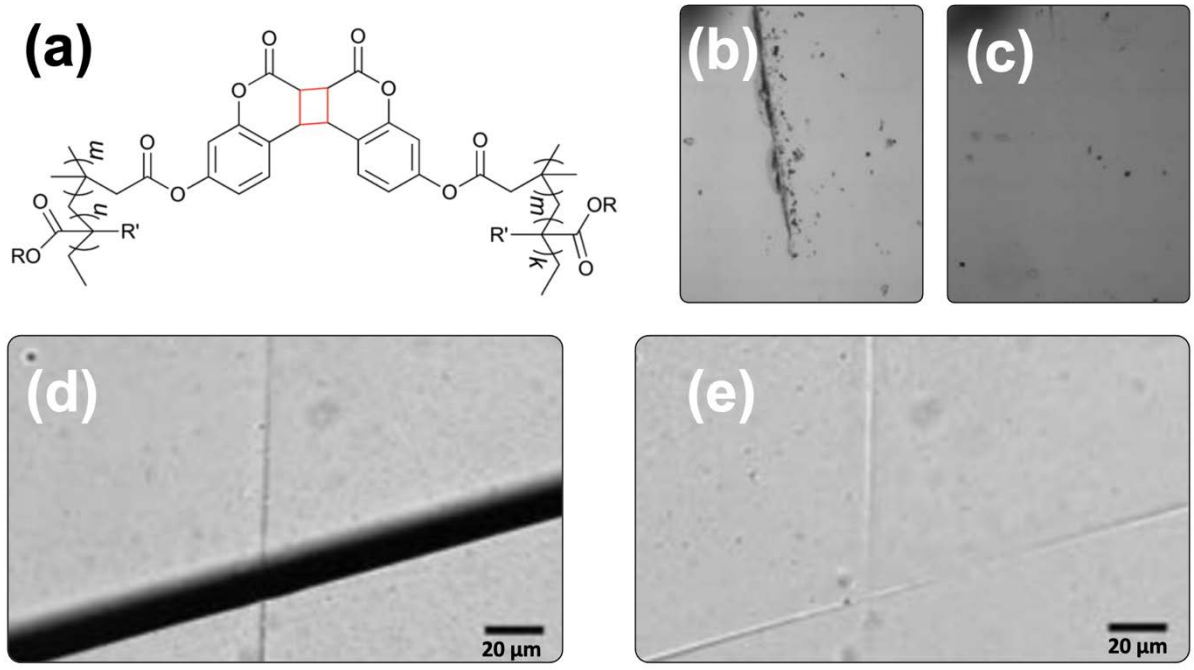

Figure 1.13 The introduction of reversible coumarin groups allows for light induced self-healing via 2+2 cycloaddition. (a) The structure of a coumarin functionalised acrylate matrix, and its subsequent self-healing at room temperature following 254 nm irradiation (b/c).[104] (d/e) A polyurethane coating with coumarin pendant groups showed strong self-healing following bisection with a horizontal crack. Adapted with permission.[105]

This coumarin design has also been used to design self-healing polyurethane polymeric matrixes. Ling[105] synthesized a polyurethane with a coumarin pendant group (7-hydroxyethoxy-4-methylcoumarin) to form photo reversible cyclobutane crosslinks. The coumarin imbued polyurethane films were cut with a razor, and then irradiated with 254 nm UV light for 1 minute, then 350 nm light for 90 minutes under ambient conditions. Optical microscopy showed that over this short time period the cracks were almost completely healed, even after three healing cycles (Figure 1.13d–e). The polyurethane films had a Young's modulus between 5 and 10 MPa. Such reversible photochemical reactions present a useful mechanism for designing outdoor self-healing coatings that are exposed to sunlight for extended periods of time. This light exposure mechanism however, is a double-edged sword, as cycloaddition reactions often require extended UV irradiation, potentially resulting in unwanted side-reactions and coating decomposition.[83] Presently, more research is required to apply photochemical chemistry to high mechanical strength materials.

Radical fission/recombination via alkoxyamine chemistry

Another thermally reversible reaction that has been tested as potential self-healing technology involves the reversible reactions of alkoxyamine (C–O–N) moieties (Figure 1.10d). At high temperatures above 120˚C, alkoxyamine groups can undergo covalent bond fission and radical recombination simultaneously, thus providing a possible mechanism for thermally induced self-healing.[106] This one step simultaneous fission-recombination reaction is potentially advantageous relative to Diels–Alder chemistry, which requires a heating (RDA)–cooling (DA) cycle.

Yuan[107] first explored this idea in 2011. They synthesized polystyrene with a methacrylate alkoxyamine pendant group via nitroxide-mediated radical polymerization, forming a reversibly crosslinked polystyrene matrix. The matrix had a *T*g of around 120˚C, and the researchers reported a flexural strength and a modulus of 100 MPa and 5 GPa respectively. To test their design's self-healing performance, each polystyrene film was first fractured, then heated to 130˚C for 2.5 hours. The healed film was able to retain up to 75% of the critical stress load required to fracture the virgin polystyrene film, indicating significant self-healing had taken place.

Alkoxyamine chemistry has also been investigated for imbuing both polyurethane coatings and epoxy resins with self-healing ability. Zhang[108] synthesized a polyurethane coating crosslinked by an alkoxyamine bond containing a nitrile group. It was hypothesized that the nitrile's electron withdrawing capabilities would stabilize the carbon radicals, allowing radical fission/recombination at ambient conditions. Their polyurethane design did display the ability to heal scratches at temperatures between 15˚C and 25˚C over 48 hours. However the material had a very low *T*g (as low as –60˚C) and more importantly, a melting point of just 37˚C. These properties severely limit its application as a coating binder in non-polar regions.

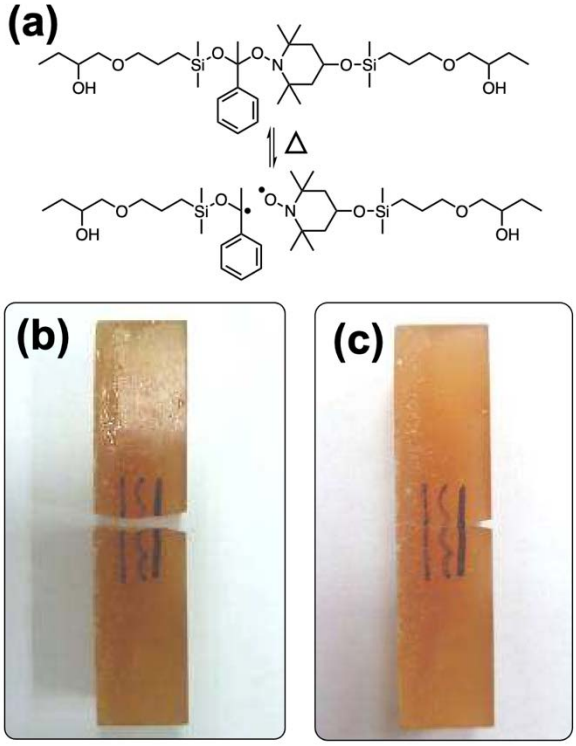

Figure 1.14 (a) An alkoxyamine functionalized epoxy design which was able to undergo 3 cycles of self-healing at 90˚C (b/c).[109]

Zhang[109] synthesized a novel alkoxyamine-containing epoxy (Figure 1.14a), and blended it with the commercial epoxy EPIKOTE 828. They hoped that the incorporated alkoxyamine bonds would help heal mechanical damage via fission/recombination reactions at modest temperatures. The resulting epoxy resin had a high Young's modulus between 0.9 and 1.3 GPa. The self-healing efficiency of these new epoxy-alkoxyamine blends was evaluated by first fracturing the epoxy films, and then pressing them together for 1.5 hours at 90˚C (above their *T*g). To test whether the self-healing was repeatable, 3 fracture-healing cycles were performed. The films were able to retain 62% of their fracture toughness after the first healing cycle, then 59% and 55% after the second and third cycles (Figure 1.14b–c).

Isocyanate mediated and other exchange reactions

Thiourethane (Figure 1.10e), carbamate (Figure 1.10g) and hindered urea bonds (Figure 1.10f) are all examples of reversible covalent bonds which can form self-healing covalent networks. They are associative exchange reactions based on an isocyanate intermediary, and have endowed a variety of organic coatings with self-healing capability. In 2023, Qian[110] designed

a self-healing waterborne thiourethane-urethane coating which was able to self-heal after 6h at 90˚C via reversible thiourethane exchange. Nguyen[111] coupled thiourethane exchange with the Diels–Alder reaction to design a strong, thermoset polyurethane which was able to heal at the comparatively mild temperature of 60˚C over 1–3 days. The difunctional polyurethane recovered up to 80% of its mechanical strength, along with the near complete disappearance of micron-sized scratches.

Hindered urea bonds offer a possible mechanism for designing self-healing coatings based on covalent bonds which can heal at temperatures well below 100˚C. This is due to the presence of a bulky substituent hindering the Urea's nitrogen, which in turn weakens its stability and promotes reversible dissociation.[112] Ying, for example, synthesised a polyurethane-urea coating with a variety of bulky substituents attached to the urea group. Their coating was soft, with a Young's modulus of ~ 1 MPa, but showed strong self-healing capability, recovering up to 80% of its strain after 12 hours at only 37˚C.

Carbamate exchange reactions have been effectively employed in the design of self-healing coatings when coupled with oximes, yielding a blocked isocyanate group. This results in reversibility under relatively mild conditions, a feature which was employed by Fu,[113] who synthesized a urethane coating functionalized with an oxime-carbamate polymer backbone. The coating was able to undergo complete self-healing in 30 minutes at 110˚C. Furthermore, their coating was able to be synthesized without a catalyst, and using low-cost, commercially available reagents. In 2021, Liu[114] designed a waterborne polyurethane coating using a phenol-carbamate system as opposed to an oxime-carbamate system. The self-healing coating combined phenol-carbamate bonds in the urethane backbone and Fe^{3+}–catechol coordination bonds, a supramolecular self-healing bond. Their coating was cut in half, but was able to recover >90% of its strain-at-break following 90 minutes at 120˚C and 30 minutes at 85˚C.

Dynamic imine bonds have been extensively studied as a self-healing moiety, and are another kind of covalent bond whose reversibility comes in the form of exchange reactions. They have been mainly utilized to imbue low modulus gel-like materials with self-healing capability, and are most relevant to self-healing coatings when coupled with other forms of healing functionality. For example, Lee[115] designed a polyurethane coating comprising of two different dynamic covalent bonds moieties: disulfide bonds in the polymer backbone, and imine bonds as crosslinkers. This polyurethane coating showed superior self-healing capability when dual-

functionalized, as compared to imine or disulfide functionalization alone. The coating also displayed strong optical self-healing capability at only 65˚C. In 2020, Chen[116] developed an anticorrosive silicone-based coating based on a PDMS polymer whose backbone was functionalized with both imine groups and urea moieties. The imine groups represent dynamic reversible covalent bonds, and the urea moieties provide a self-complementary hydrogen bonding network, which is an example of supramolecular self-healing. These two self-healing technologies allowed the coating to display strong anticorrosive performance when cut and immersed in salt water for >10 days. Interestingly, the self-healing performance reached a maximum based on the amount of urea groups (hydrogen bonding). It was theorized that the extra hydrogen bonding limits the overall movement of polymer chains, degrading the ability of the imine linkages to self-heal.

1.2.2.2 Supramolecular bonds

Hydrogen bonds

The hydrogen bond is a dipole-dipole bonding interaction between a hydrogen atom, which is covalently bonded to an electronegative atom (donor), and another electronegative atom (acceptor).[117] The donor and acceptor atoms are normally oxygen, nitrogen or fluorine. The bond energy for a hydrogen bond can vary between 5 and 40 kJ/mol.[118] This makes them somewhat weak compared to covalent bonds. Though single hydrogen bonds are not sufficient to induce supramolecular assemblies of polymers, multiple hydrogen bonding arrays offer significantly enhanced binding efficiency.[119] The primary examples of multivalent hydrogen bonding motifs that have been used for designing self-healing polymer matrixes are shown in Figure 1.15. They include amides, urea groups, Meijer's 2-ureido-4[1H]-pyrimidinone (UPy) dimers, and Hamilton wedge-barbiturate receptors (Figure 1.15a–d respectively). Hydrogen bonding has been used extensively in the design of self-healing polymeric composites such as hydrogels, organogels, rubbers, and low *T*g, low modulus thermoplastic elastomers.[120] These materials are soft, and their polymeric matrixes generally lack the mechanical strength necessary to perform as organic coating binders. Thus, successfully synthesizing high-modulus materials is the perhaps most significant challenge facing the design of hydrogen bond induced self-healing organic coatings.[74]

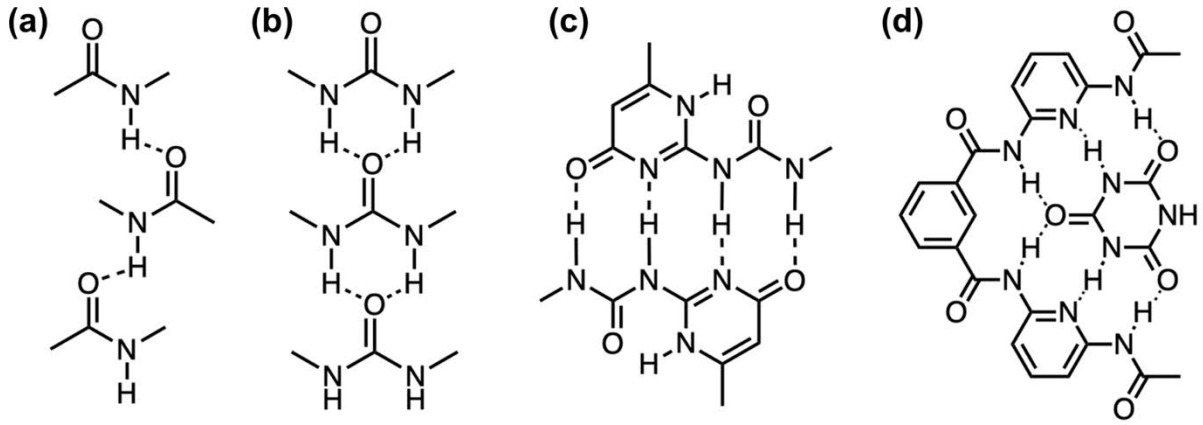

Figure 1.15 A selection of hydrogen bonding units. (a) Amide groups. (b) Urea groups. (c) Ureidopyrimidinone (UPy) groups. (d) Barbiturate-Hamilton wedge association.

Amides

To address this mechanical strength conundrum, Zhibin Guan's research group first introduced the concept of multiphasic self-healing materials. These materials contain both a hard phase, which provides the material's high mechanical strength, and a soft phase, which allows for favorable polymer chain dynamics and hence more efficient self-healing.[121] In 2012, they designed a graft copolymer consisting of a hard-polystyrene backbone, and soft polyacrylate amide brushes (PA–amide). These polymers form a phase separated matrix, where the amides of the soft phase form hydrogen bonds with each other. Termed a 'molecular velcro', these soft sections can reversibly break and reform allowing spontaneous self-healing upon mechanical damage. The tensile strength of the polymer film was up to 35 MPa depending on the weight fraction of polystyrene, which is notably higher than soft polymeric composites. To assess the self-healing potential of this new polymeric matrix, a section of film was cut in half, and the two pieces were brought gently back into contact and allowed to self-heal for 24 hours at ambient conditions. The healed film was able to recover 92% of its original extensibility. Guan[122] enhanced this design in 2014, by synthesizing a phase separated, ABA triblock copolymer with a hard PMMA middle block, and soft PA-amide outer blocks which were connected via hydrogen bonds. This material had superior tensile strength (up to 77 MPa), and was able to self-heal at room temperature, recovering 70–90% of its original strength. Both these self-healing systems utilized simple hydrogen bonding amide units, which are significantly weaker than other multivalent hydrogen bonding units. Their synthesis is less laborious however, and embedding a higher number of weaker binding motifs, as opposed to a

single, powerful multivalent hydrogen bonding moiety, may result in a more sensitive self-healing coating.

Villani[123] also used amide motifs to design a self-healing thermoset epoxy resin with the ability to pre-emptively relax mechanical stress, and self-heal cracks on the matrix surface. Mechanical stress can build up within thermoset coatings due to the thermal differences between the coating and substrate, shrinkage following solvent evaporation, the high temperatures that sometimes accompany curing, or simply the forces associated with coating application. Ultimately this kind of stress can morph into physical damage, reducing the protective qualities of the coating and leading eventually to delamination. Villani's new design incorporated hydrogen bonding amide motifs to replace the covalent crosslinks of a typical thermoset epoxy resin (Eponex 1510). Their material maintained almost identical mechanical strength to the unmodified epoxy (>2 GPa), but displayed higher stress relaxation and creep compliance due to the reversibility of the hydrogen bonded crosslinks. Their new epoxy was also able to self-heal a 200 μm wide, 60 μm deep scratch in less than 10 minutes at 45˚C.

2-Ureido-4[1H]-Pyrimidinone -UPy

UPy units are strongly dimerizing due to their quadruple hydrogen bonds, and exhibit solvent and temperature dependent mechanical strength, as well as the ability to self-heal under ambient conditions. For organic coatings, utilizing reversible UPy units as crosslinkers in place of irreversible covalent bonds has been proposed as a method for designing pre-emptive self-healing materials. Wietor[124] incorporated UPy units as crosslinkers into a thermoset polyurethane-polyester coating. Commercial polyurethane-polyester coatings are tough and durable below their *T*g, but are susceptible to mechanical stress during the high-temperature curing stages of the coating. The researchers found that when the percentage of UPy crosslinks is between 10 and 40%, the thermoset matrix had slight thermoplastic elastomeric properties. The reversibility of the UPy crosslinks represents an additional relaxation mechanism, which allows the material to pre-emptively relax local stresses that if left unchecked would lead to coating damage.

Many of the self-healing supramolecular materials that make use of UPy hydrogen bonding units are soft polymeric composites, including hydrogels, rubbers and thermoplastic elastomers, including even low *T*g, low modulus epoxy resins.[125] These materials are at odds with the necessary mechanical strength required for certain organic coating applications. To

address this dilemma, many research groups have explored Guan's multiphasic material concept to design self-healing coatings that make use of UPy functionality. In 2012, Henschel[126] synthesized an ABA block copolymer containing a hard polystyrene block (A, *T*g = 100˚C), and a soft poly(butyl-acrylate) block (B, *T*g = –40˚C) (Figure 1.16a). They reasoned that substituting a UPy supramolecular linkage for the covalent linkage at the center of the PBA soft block would allow the material to self-heal following mechanical damage. The material showed two distinct *T*g values (roughly –40˚C and 80˚C) with elastic modulus values between 20 and 40 MPa. The self-healing ability of this material was tested at 45˚C. Two sections of the polymeric film were bisected and pressed together for one minute, and then left to sit over 18 hours. The resultant, self-healed film showed a strong recovery of its tensile strength (up to 90%).

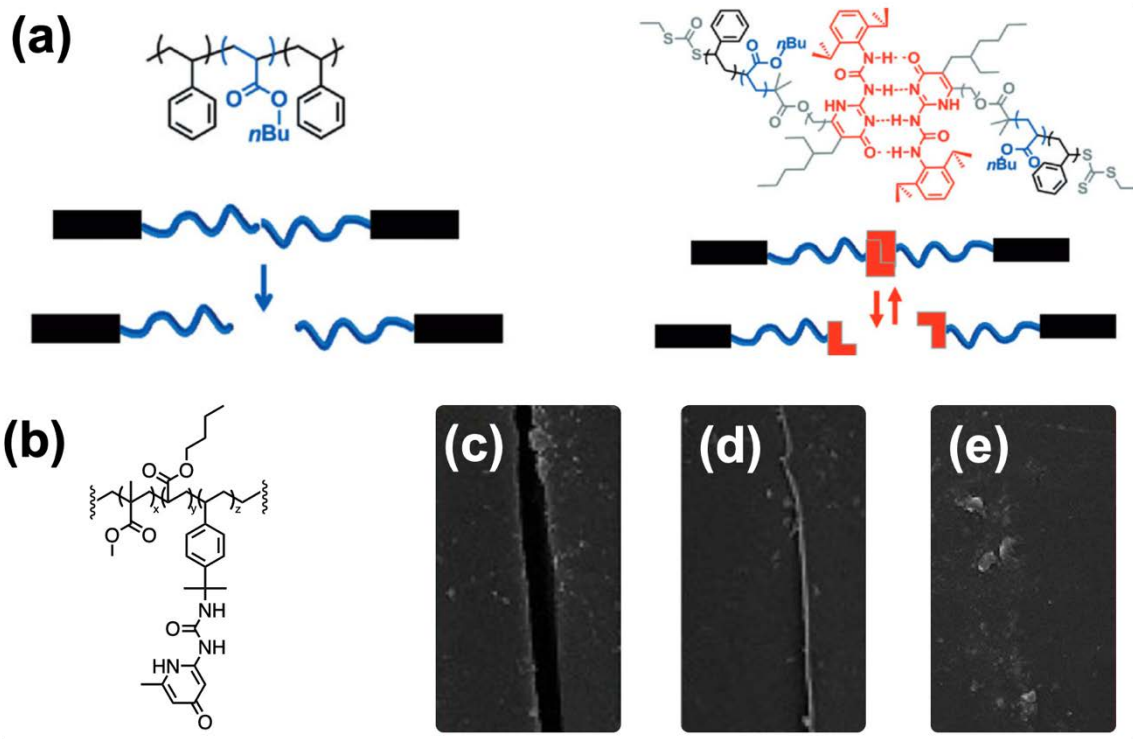

Figure 1.16 (a) Henschel's hard-soft multiphase material. The addition of UPy units provides the attractive force necessary for self-healing.[126] (b) The structure of a UPy functionalized PMMA-PBA waterborne latex. (c) The self-healing of a scratch within this latex coating at 100˚C after 10 minutes (d) and 30 minutes (e).[127]

This design was built upon by Naoko Yoshie's group, who synthesized an ABA block copolymer with UPy functionality connected to both the hard polyurethane block, and the soft dodecyl-norbornene block.[128] This material displayed slightly less tensile strength than Guan's design, but far more significant toughness (62 MJ/m3). The polymer film was able to self-heal a scratch 150 μm deep after 3 hours at 50˚C.

In 2019, Hu[129] sought to create a strong, tough polyurethane coating with UPy induced self-healing potential. Rather than design a distinct multiphasic material, they attached dangly chains with UPy end groups to the harder polyurethane segments. It was hoped that these dangly chains would allow greater mobility for the UPy groups to rebond following a cracking event. Their design yielded tough (100 MJ/m3) polymeric films with a tensile strength of up to 25 MPa, and a *T*g that increased from 1˚C to 18˚C as the amount of polymers containing UPy chains increased from 20% to 50%. These films were cut clean in half and gently pressed together for 10 seconds at room temperature, then left for 2 hours at either 100, 80 or 40˚C. The resulting self-healing efficiency was extremely high at 100˚C, with >95% of tensile strength recovered for all the films. But perhaps more significantly, the material showed noticeable self-healing at 40˚C, with between 15 and 50% of tensile strength recovered for the films containing 20% and 50% UPy functionalized polymers respectively.

Waterborne acrylic latexes comprise a large and vital section of the organic coatings market. Several groups have attempted to imbue latex coatings with self-healing and mechanical functionality via the UPy group. In 2012, Stefan Bon[130] synthesized 'soft' poly(methyl methacrylate-co-butyl acrylate) latexes via emulsion polymerization with a UPy functionalized methacrylate comonomer. Their initial design showed superior mechanical strength and solvent resistance, but the self-healing potential of the material was not tested. Qiu[127] utilized a similar design to create waterborne acrylic latexes with the capacity to self-heal (Figure 1.16b). In 2016, they synthesized a latex consisting of MMA, BA and a small amount of a UPy functionalized acrylate monomer (0, 1, 2, 3, 4 and 5 wt%) via emulsion polymerization. Their dried coatings had a tensile strength of up to 41 MPa, and *T*g that increased from 18˚C to 40˚C as the UPy content increased from 1 to 5 wt%. The self-healing potential of the coating was demonstrated by first cutting a part of the coating film in half, then placing the two sections together at 100˚C over the course of half an hour (Figure 1.16c–e). As opposed to the film without UPy functionality, which displayed no self-healing, the film containing 2% UPy displayed significant self-healing, recovering over 94% of its tensile strength. The coating was

then subjected to multiple self-healing cycles by recutting the films in the same place and repeating the heating process. The 2% UPy film was able to recover over 70% of its tensile strength after the second cycle, and 66% of its tensile strength after the third cycle. Though this UPy functionalized coating lacks the mechanical strength typically required for acrylic latex coating applications, Qiu's research represents a step forward in the design of intrinsic self-healing architectural paints. It should be noted, however, that for an MMA BA latex, temperatures of 100˚C are well above *T*g, and likely high enough to induce the flowing of the polymer matrix, no doubt contributing significantly to the self-healing efficiency.

Other hydrogen bonding functionality

There are a number of other multivalent hydrogen bonding motifs that have been investigated as potential vectors for self-healing. Wolfgang Binder's research group created a self-healing epoxy resin by utilizing either barbiturate or thyamine hydrogen bonding moieties connected to carbon nanotubes.[131] These hydrogen bonding groups act as reversible crosslinks, and the carbon nanotubes allowed for easier dispersion throughout the epoxy matrix. The new epoxy had a high storage modulus (>2 GPa) and maintained stability and functionality above the high temperature curing cycles (70–120˚C) normally employed in industry. To evaluate the self-healing potential of this enhanced epoxy, the barbiturate and thyamine films were cracked, and the cracked faces were allowed back into contact for 24 hours. Load-displacement curves yielded a healing efficiency of between 50 and 57% for both epoxy films.

Barbiturate units were again employed by Binder,[132] who adopted Guan's concept of phase separated materials and synthesized a V shaped ABA triblock copolymer with soft poly(butyl acrylate) sections (A), and a hard PS domain (B). The barbiturate group was attached to the PS section, and the whole triblock polymer was blended with a small Hamilton Wedge-functionalized poly(isoprene). The Hamilton wedge and barbiturate units connect to form a strong reversible linkage consisting of 6 hydrogen bonds. The resulting phase separated material had weaker tensile strength (4 MPa) but was able to almost completely self-heal over 24 hours at ambient conditions after being cut in half, recovering 91–95% of its strain-at-break.

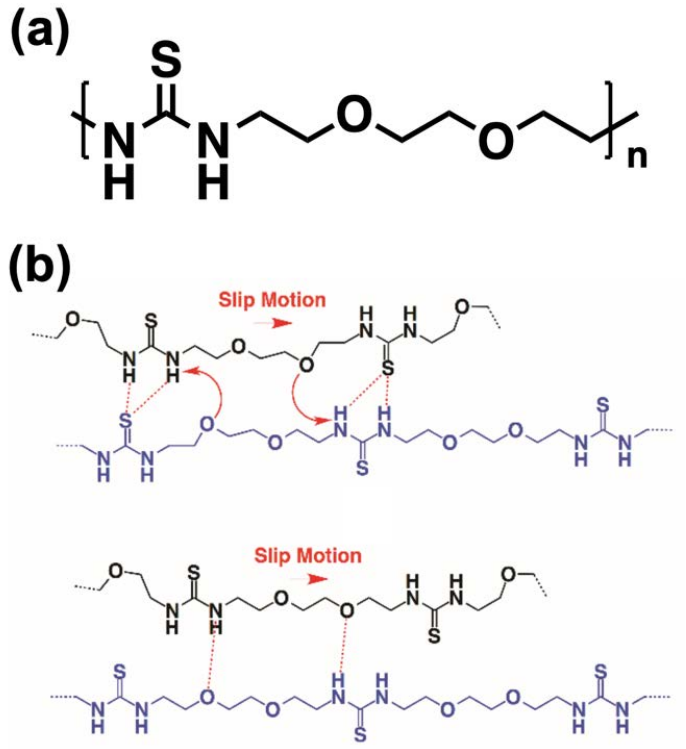

Figure 1.17 Thiourea groups allow for the self-healing of higher modulus materials. (a) A thiourea based self-healing polymer design. (b) Its theorized self-healing mechanism.[133]

Urea groups have also been utilized as self-healing functionality and have shown strong performance for lower modulus materials. For example, Zhang[134] designed a urea functionalized polymeric matrix which displayed almost perfect optical self-healing and strain recovery after only a couple of hours at room temperature. However, the material in question had a low Young's modulus of only ~0.04 MPa. Seeking to design a tough, high modulus self-healing polymeric coating, Aida and co-workers designed a poly(ether-thiourea) (Figure 1.17a) which formed a tough, high modulus (1.4 GPa) glassy coating.[133, 135, 136] After being sliced through, this coating was able recover 85% of its mechanical strength at ambient conditions after a short compression of the two sliced edges. The posited mechanism for this high modulus self-healing was that the thiourea moieties formed an amorphous, zig-zag array of hydrogen bonds (as opposed to linear urea hydrogen bonding), which upon compression were able to slide across the ethylene glycol units, resulting in strong self-healing (Figure 1.17b). This work is amongst the first that displays strong intrinsic self-healing for glassy polymeric coatings without highly energetic external intervention.

π–π stacking

π–π stacking is a type of attractive non-covalent bond between π-electron rich aromatic groups with π-electron deficient groups. π–π stacking is thermo-reversible. The self-healing mechanism involves first heating the material above 100˚C, where the π–π crosslinks become disrupted, and then cooling the material to allow the π–π crosslinks to reform.[137] Burattini and Hayes [138, 139] were the first to explore how polymers functionalized with π-electron functionality could be used as self-healing materials. In 2014, Hayes[140] developed a polymer blend consisting of a chain folding electron-deficient diimide copolymer and a pyrenyl-terminated electron-rich PEG crosslinker (Figure 1.18a). These polymers assembled to form a π–π crosslinked film with a Young's modulus of up to 49 MPa, with a *T*g between 80 and 105˚C. Self-healing was demonstrated by cutting the films to form a crack 75 μm wide, and slowly heating the material. Self-healing was observed at 100˚C, and the film completely healed at 200˚C (Figure 1.18b–c). Even after three healing cycles, where the films were cut in the same place, the healed material retained 95% of its tensile strength.

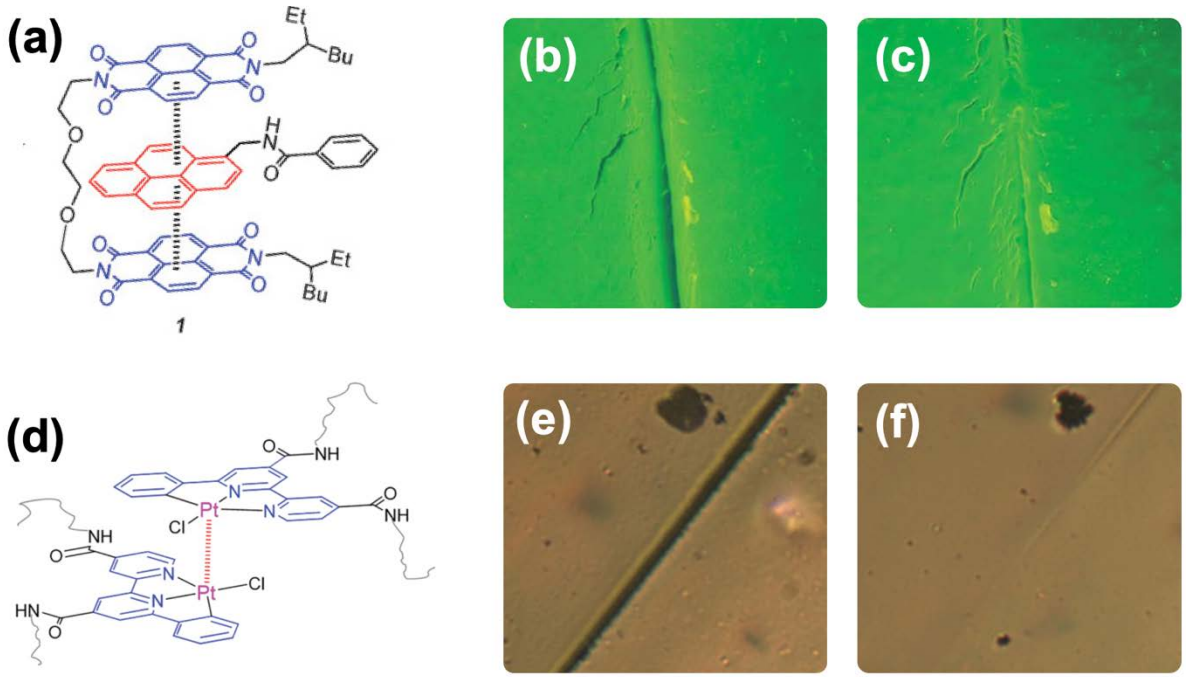

Figure 1.18 π–π stacking has shown the ability to imbue polymeric composites with self-healing capability, especially when coupled with other reversible bonds. (a) A self-healing polymer blend utilizing π–π stacking, which was able to self-heal a crack at 100˚C and 200˚C (b/c).[140] (d) The combination of π–π and Pt–Pt interactions allows for a material which can heal a microcrack at room temperature after 12 hours (e/f).[141]

In related work, Mei[141] attempted to design π–π crosslinked materials that could self-heal under ambient conditions by attaching a π-electron platinum complex to PDMS to form a material which combines π-π stacking and Pt–Pt 'metallophilic' interactions (Figure 1.18d). The material was highly stretchable but mechanically weak (elastic modulus = 0.19 MPa), and had a *T*g of around –50˚C. It did however display complete self-healing at room temperature after being cut in half, recovering all its mechanical strength after 12 hours (Figure 1.18e–f).

π–π stacking has been shown to imbue materials with very high self-healing efficiency, however these materials generally lack the kind of mechanical strength most coating applications demand and require elevated temperatures to initiate self-healing.

Host Guest interaction

Host-Guest interactions are spatially directional associations between macromolecular segments held together by some combination of electrostatic interactions, hydrogen bonding, van der Waals forces or hydrophobic interactions.[142] These interactions are highly reversible, and involve a larger 'host' molecule encompassing a 'guest' molecule to form a complex.[143] In biological systems, enzyme-substrate interactions are a well-known subcategory of host-guest chemistry. In 2012, Zhang[144] designed a self-healing gel by synthesizing PMMA with a crown ether pendant group (dibenzo-24-crown-8), and blending it with a bis-ammonium crosslinker (Figure 1.19a). The resulting polymeric matrix was reversibly crosslinked by host-guest chemistry, and formed a low modulus gel. The gel was able to heal a scratch completely in under 10 seconds at room temperature. Most self-healing materials based on host-guest chemistry are low modulus gels, meaning that their application in organic coatings is limited. Recently, Hu[145] attempted to form a self-healing epoxy resin by copolymerizing azobenzene 'guest' moieties into the epoxy polymers, and blending the matrix with graphene-cyclodextrin 'host' segments. This epoxy coating had a higher tensile strength (between 10 and 20 MPa), and a *T*g between 80 and 89˚C depending on the amount of cyclodextrin/azobenzene in the matrix. It was found that scratched epoxy coatings with 10 wt% cyclodextrin/azobenzene compositions were able to self-heal 80% of their mechanical strength after 30 minutes at 120˚C (Figure 1.19b–c).

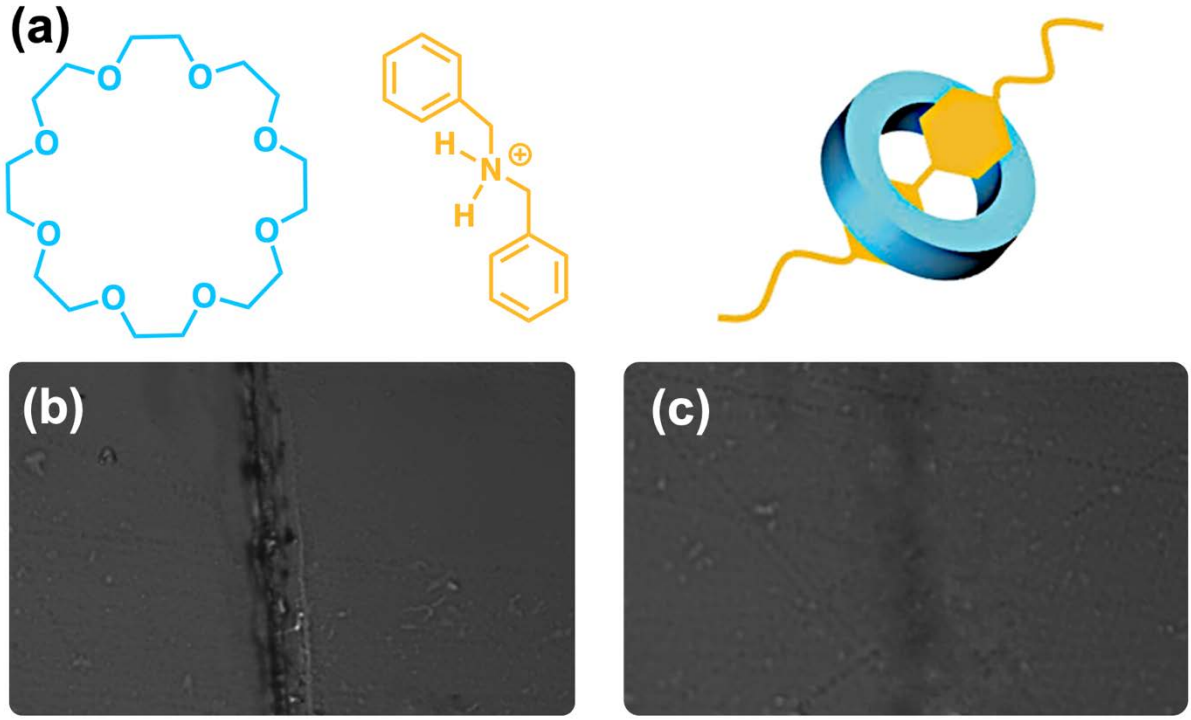

Figure 1.19 (a) Typical crown ether/bis-ammonium host-guest complex. (b/c) The self-healing of an epoxy resin blend which utilizes this crown ether/bis-ammonium complex (30 minutes/120˚C).[145]

This initial research shows how host-guest chemistry can be applied to imbue highly crosslinked thermoset coatings with self-healing capability. However, their high healing temperatures, cost, and synthetic complexity currently limit their applicability to more general kinds of organic coatings.

Ionomers and ionic interactions:

Ionomers are an interesting class of materials which contain ionizable pendant groups (and their counterions) attached to the backbone of polymeric materials to form physical crosslinks in the form of ionic clusters. These ionic clusters are thermally reversible (Figure 1.20a). The self-healing mechanism of ionomeric materials involves raising the temperature above what is known as the 'order–disorder temperature', whereby the ionic crosslinks will first rapidly break down, and then slowly reform as the material cools. In practice, the addition of ionic groups to a polymer matrix drastically changes its mechanical properties, and rarely will an ionic species make up more than 15 mol% of the material.[146] This distinguishes ionomers from polyelectrolytes, which can have larger fractions of ionic groups. The strong interaction of

ionic moieties frequently leads to a separation of the polar and non-polar phases of the material, akin to the phase separation of hard-soft block copolymers. Generally, ionomers are comprised of carboxylate or sulfonate pendant groups in a larger polymeric matrix, blended with alkaline metal counterions.

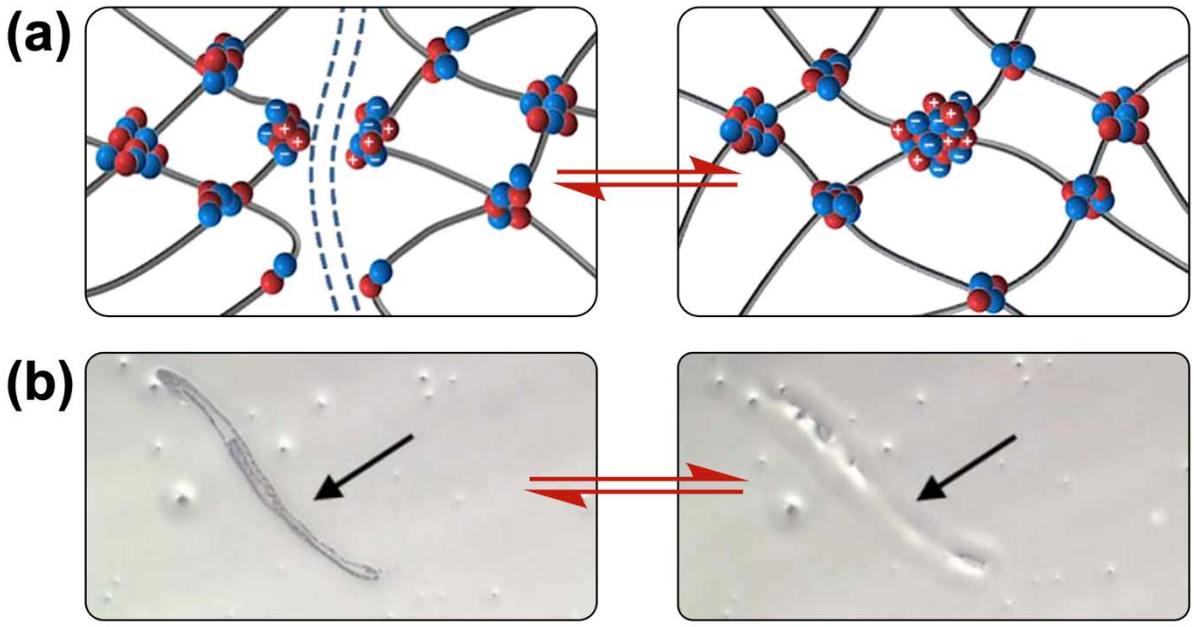

Figure 1.20 (a) Schematic of the damage/healing cycle of ionomers via reversible electrostatic attraction, usually accompanied by the addition of heat. (b) The self-healing capacity of a butyl acrylate ionomer blend after 3.5 hours at 100˚C.[147]

Ionomers were first utilized for self-healing applications as anti-ballistics. It was discovered that poly(ethylene-co-methacrylic acid) (PEMAA)/Na+ ionomers were able to reseal fracture damage caused by ballistic impacts. Ward[148,] and Kalista[149] published extensive studies detailing the mechanism of this self-sealing ability, concluding that the local heating (> 90˚C) caused by a bullet impact melted the material and separated the ionic clusters, which then recombined to self-seal the wound as the material cooled. This discovery immediately opened the door for utilizing ionomers in police, military and aerospace applications, for example, as coatings for self-sealing meteorite impacts in space.[150] Currently, commercial PEMAA ionomers include Iotek from Exxon, and Surlyn from Dupont.

Looking to design ionomers with the mechanical strength suitable for coating applications, Dahlke[147] synthesized a butyl acrylate copolymer containing an anionic orthophosphate pendant group. To enhance the mechanical strength, this copolymer was blended with a bis-bidentate halogen compound to imbue the material with reversible 'halogen bonding'. The synthesis of the halogen bonding compound was complex. The ionomeric copolymer without the halogen bonding crosslinker had a *T*g of 33˚C and a hardness of 7 MPa and was able to self-heal a scratch after 3.5 hours at 100˚C (Figure 1.20b). The mechanical properties of the film after self-healing were not tested. The addition of the halogen bonding crosslinker maintained a similar *T*g (35˚C) and self-healing performance to the ionomer but yielded a much harder material (54 MPa).

Recently, polyampholytes and polyelectrolytes have gained increasing interest as self-healing materials because they are generally synthetically simpler materials and allow for higher fractions of ionizable units. Polyampholytes are polymers that contain both anionic and cationic pendant groups. In 2018, Peng[151] synthesized a polyampholyte in an attempt to design a material that could self-heal at relatively lower temperatures. Their design involved the reversible addition-fragmentation chain-transfer (RAFT) polymerization of a triblock copolymer containing a BA, acrylic acid (anionic species) and dimethylamino ethyl methacrylate (cationic species). Their design relies on charge monomers that do not precipitate quickly. The *T*g of the resulting polymer was between –30˚C and 15˚C for ionic monomer fractions between 0 and 60%. For ionic monomer fractions between 27 and 60%, the material showed a tensile strength between 14 and 30 MPa. The self-healing ability of this polyampholyte material was demonstrated by cutting each film in half and then bringing the cut surfaces into contact for 24 hours at 60˚C. Self-healing efficiency was calculated by comparing the tensile strength of the healed film with the pristine film. It was found that for samples with between 10–27% ionic fractions, the healing efficiency was over 75%.

These two examples show how the appeal of ionomers and polyampholytes for self-healing coating design varies significantly. Ionomers are already commercialized, and have proven self-healing potential, but so far lack the ability to heal under ambient conditions, limiting their general applicability to coatings. Polyampholytes have shown potential as efficient self-healing materials at lower temperatures, but their use as self-healing materials has only recently been explored, and none have yet been applied to the types of polymeric matrixes used as common organic coating binders.

In 2018, Zacharia[152] attempted to design a self-healing paint by incorporating polyelectrolyte multilayers (PEMs) into a BA/MMA latex with varying amounts of hydroxyethyl methacrylate (HEMA). The PEMs contained branched polyethyleneimine (BPEI) (cationic) and poly acrylic acid (PAA) (anionic), which formed a film via ion-pairing. This ion paring can be "dissolved" by water. Their healing mechanism involves an aqueous environment, in which the PEMs become plasticized and mobile, flowing through the latex into the crack, reforming it after water evaporates. The resulting latexes had a *T*g of between 12 and 50˚C for HEMA content between 0 and 60%. To test the hardness of the PEM latex, the researchers conducted a "pencil hardness test", which yielded hardness between 2H and 3H, depending on the HEMA content. The self-healing performance of the latex was assessed by scratching the films with razorblade to form a 90 μm cut, and then dipping the films into either cold (15˚C) or hot (60˚C) water for 10 minutes. The films showed modest self-healing under cold water, with the efficiency increasing as the % of HEMA in the latex increased. Under hot water, the latex films showed stronger self-healing, and the cracks were completely healed for all latex samples within 10 minutes. The mechanical properties of the films after self-healing were not assessed. Nevertheless, this is one of the few designs that attempts to create self-healing acrylic latexes, and it successfully displays noteworthy self-healing efficiency under moderate conditions.

1.2.2.3 Photothermal self-healing

One of the most significant drawbacks to intrinsic self-healing is the fact that many of the reversible reactions, chiefly reversible covalent bonds, require significant temperatures >100˚C to initiate self-healing. Recently, efforts have been made to induce this temperature locally at the damage site via irradiation, without subjecting the entire coating to harsh conditions. Ideally, this irradiation comes in the form of IR or visible light, as opposed to UV, which has the potential to damage the coating structure through chemical decomposition. Photothermal self-healing can be induced by adding an additive into the coating, which, when irradiated, releases enough heat to initiate self-healing. For example, Lin[153] designed a polyurethane with furan pendant groups and a maleimide crosslinker, a common motif in Diels–Alder healing systems. They also introduced graphene oxide-based nanowires, which have the ability to undergo photothermal conversion. This additive allowed light induced self-healing of the

Diels–Alder functionality only at the damage site, thus avoiding temperatures >100˚C across the entire coating.

Photothermally active nanoparticles are a common additive in the design of these self-healing coatings, however, given that the nanoparticles provide a stimulus, and do not themselves represent a healing agent, these systems can be considered intrinsic. Polypyrrole nanoparticles have received significant attention due to the high photothermal conversion rates of polypyrrole, including by Wu[154], who introduced them to a polyurethane coating. IR irradiation allowed the temperature locally to reach up to 150˚C, allowing the polymers to rearrange and spontaneously heal. A sample cut in half was able to recover 80% of its stress-at-break after only 30 seconds of irradiation. Dong[155] introduced core-shell polydopamine-polypyrrole nanoparticles into an epoxy resin at 5 wt%. Ten minutes of irradiation was enough to allow a ~50 μm crack to significantly self-heal, as the local heating allowed for polymer rearrangement and an enhanced shape-memory effect. In 2022, Cao[156] designed a self-healing acrylic coating, by utilizing cuprous oxide nanoparticles, which are photothermally active via the surface plasmon resonance effect. Their coating was able to heal a ~30 μm razor cut with only 200 seconds of irradiation (808 nm), and also showed the ability to self-heal repeatedly, with high strain recovery after five healing cycles.

1.3 PERSPECTIVES ON COMMERCIALIZATION

Given the considerable advances in both polymer engineering and particle design over the last two decades, self-healing technology has now become a reality in materials science. One industry amongst many that stands to benefit substantially from the rapid development of self-healing materials is the organic coatings industry. An organic coating able to spontaneously heal would have a radically longer lifetime, as well as enhanced protective functionality and reduced maintenance costs. However, given the diversity of coatings, there is no one-size-fits-all approach to designing a self-healing strategy. A coating's mechanical properties, desired function, and the chemical nature of its binder all dictate the choice of self-healing strategy.

Before evaluating the commercial potential of self-healing organic coatings, it is necessary to mention the automotive industry, which currently includes multiple self-healing commercial products. These products are ceramic coatings whose body is comprised of inorganic materials such as silicon dioxide rather than a polymeric binder. These upmarket car paints are able to

heal small cracks visible to the naked eye, such as key scratches, either by heating, or exposure to sunlight over a period of days. FEYNLAB™, for example, has a range of self-healing ceramic coatings which involve the introduction of shape memory polymers to the ceramic system. These polymers first deform when exposed to mechanical damage in the form of scratches, and reform when heated, thus healing the coating.

For designing a commercial self-healing organic coating, extrinsic microcapsules are perhaps the most promising approach. Microcapsule designs have shown the ability to efficiently self-heal tough, high modulus epoxy and polyurethane coatings through the release of liquid healing agent at mechanical damage sites. The research surrounding this self-healing strategy is vast and diverse, reporting many possible permutations regarding the design of the capsule and the nature of the healing chemistry. Carefully tailored microcapsule/healing-agent designs have resulted in very high self-healing efficiencies (90–100%) for a variety of commercial coatings. The microcapsule design also allows for the healing of micro *and* macro cracks, including those easily visible to the naked eye.

The commercial potential of microcapsule-based extrinsic systems is underlined by the significant number of patents detailing a variety of self-healing organic coatings. Several early patents in the area focused on White's 2001 healing agent-catalyst microcapsule design, including a DCPD-Grubb's catalyst system in 2001,[157] and a PDMS-tin catalyst system in 2007.[158] A patent application submitted in 2006 describes a self-healing gloss acrylic latex based on 60–150 μm PUF microcapsules (20 wt% of the coating) encapsulating either $Ca(OH)_2$, polybutene, or a combination of both.[159] The same researchers submitted a similar application where PUF microcapsules encapsulated phenolic varnish and a variety of other healing agents to imbue an epoxy resin with self-healing capability.[160] Rok Protective Systems patented a self-healing anti-corrosive polyurethane coating.[161] Their polyurethane topcoat was comprised of paraffin wax microcapsules containing a liquid diisocyanate healing agent. In 2016, Worcester Polytechnic Institute applied for a patent which details a self-healing organic coating designed to protect steel embedded in concrete.[162] Their design employed large PUF microcapsules (650 μm) to encapsulate tung oil as a healing agent. A more recent patent application submitted in 2020 describes a self-healing epoxy resin based on an epoxy-solvent-alkoxysilane healing agent, encapsulated within < 25 μm polymeric microcapsules.[163] This abundance of patent literature implies a significant interest across a broad range of microcapsule-based healing systems for application beyond research laboratories. There are

even several specific commercial self-healing coatings currently available, including AmpArmor 1000™ and AmpArmor 3000™. These coatings, offered by Autonomic Materials Inc., utilize single and dual component capsule systems with PDMS additives. The AmpArmor™ range represents an early step into commercial extrinsic self-healing organic coatings, but there still remains a notable lack of widespread commercial products based on microencapsulated healing agents.

Such an absence is due to a combination of many significant challenges. Most extrinsic healing systems are high cost, mainly due to the presence of a separate healing agent and the possible presence of a catalyst. This cost, coupled with synthetic and design complexity, which is energy intensive and cannot easily be scaled, are the two primary challenges preventing rapid commercialization. Furthermore, toxicity, in the form of monomeric healing agent, catalysts, and the process by which microcapsules are often synthesized, is a further issue that needs to be carefully considered. Researchers should focus on synthesizing extrinsic healing systems based on low-toxicity, low-cost renewable reagents, with as simple a design as possible. Furthermore, extrinsic self-healing systems, particularly microcapsules, inevitably alter both the mechanical and optical properties of the coating. This is a particular challenge both for architectural coatings whose colour and opacity are derived from inorganic nanoparticles (pigments), and for transparent coatings. Interestingly, the long-term effects of empty microcapsules on the nature of the healed coating remains poorly studied, and may, counterintuitively, provide a new avenue for mechanical damage and corrosion.[164] To avoid the complexities and challenges of microcapsule-based extrinsic healing, some research has focused on un-microencapsulated flowable healing agents. General Motors obtained a patent describing a self-healing acrylic coating imbued with a flowable cyclic ether healing agent and a UV-sensitive Lewis acid initiator.[165] Upon damage and UV irradiation, the cyclic ether flows into the crack and polymerizes via a cationic ring opening process, initiating self-healing. Designs such as these have the potential to avoid some of the practical drawbacks associated with microcapsules.

Intrinsic strategies offer the possibility to imbue organic coatings with repeatable self-healing, while having the healing functionality as part of the coating itself, rather than completely separate, as in extrinsic designs. Repeatable self-healing is a significant upside that would enhance any commercial self-healing product. Dynamic reversible covalent networks, for example, offer the ability to repeatedly heal damage to very high efficiencies, given the strength

of covalent bonds. In 2020, Hentschel, Williams and Satpute obtained a patent which detailed the design of a self-healing acrylic resin via the Diels–Alder reaction.[166] Their design involves the synthesis of a latex emulsion polymer containing MMA and BA as well as the Diels–Alder active pendant group, furfuryl methacrylate (FFMA). Blending the resulting latex with a bismaleimide crosslinker results in an acrylic coating that the inventors assert shows self-healing capacity at 60˚C after 10 minutes. This 60˚C healing temperature represents a significant improvement on the healing temperatures typically associated with Diels–Alder based self-healing. A patent published in 2022 reported a self-healing laminate coating whose polymeric structure included hindered urea bonds in its backbone.[167] The coating was able to self-heal cuts at modest temperatures (30–40˚C) over 20 hours. In 2021, Covestro obtained a patent describing a self-healing waterborne polyurethane functionalized with blocked polyisocyanates.[168] Self-healing was tested by scrubbing the coating with steel wool, and then heating it to 60˚C for two hours, leading to a gloss recovery of 90%. As opposed to dynamic covalent bonds, supramolecular chemistry, in particular hydrogen bonding networks, has been used to design certain materials which can self-heal under ambient conditions. However, the patent literature regarding supramolecular self-healing organic coatings is relatively sparse. In 2022, Covestro also obtained a patent reporting a self-healing coating for optical fibers.[169] The coating was an acrylic resin containing self-healing oligomers (30–80 wt%) based on a multiple hydrogen bonding network comprised of barbiturate and various pyrimidone-based moieties.

Intrinsic self-healing strategies have garnered less overall commercial interest than extrinsic designs, principally due to the fact that intrinsic self-healing coatings are often mechanically ‘soft’. Intrinsic self-healing relies on the inherent mobility of polymer chains to rearrange, directly contradicting the mechanical strength required for organic coating performance. Designing an intrinsic self-healing coating which contains high self-healing efficiency, while maintaining sufficient mechanical strength, would represent a significant breakthrough in the field, and yield significant commercial benefit. Dynamic covalent networks, given the strength of covalent bonds, can imbue tougher coatings with self-healing capability. However, these coatings generally require high healing temperatures, which limits their commercial applicability. Recent research has focused on self-healing coatings whose reversible covalent bonds can heal at more moderate temperatures (~60˚C). Such research, which further lowers the self-healing temperature of coatings either by functional modification or blending with other healing moieties such as hydrogen bonds, will no doubt enhance commercial viability. Supramolecular chemistry has shown the ability to self-heal material under ambient conditions,

and thus can potentially negate the challenges of high healing temperatures associated with reversible covalent bonds. These materials, however, are almost always very soft gel-like materials, with a Young's modulus normally below 1 MPa. To design an intrinsic self-healing coating with sufficient mechanical strength, recent research has focused on separate phases or soft domains, whose enhanced polymer mobility allows for ambient self-healing without drastically weakening the coating's overall mechanical performance. Multiphasic self-healing coatings are promising, but have yet to express themselves in a commercially viable design. Furthermore, the cost, synthetic complexity, and effect on mechanical performance associated with introducing additional functional groups to coatings must also be carefully monitored.

Commercializing self-healing organic coatings is subject to significant challenges, some of which are common to all self-healing strategies, such as cost, scalability, and complexity, while others are more specific, such as stability, healing efficiency and repeatability, and impact optical and mechanical performance. However, given the pace of research, the presence of self-healing ceramic coatings in the automotive industry, and the obvious potential benefits of imbuing coatings with self-healing properties, there is scope to develop more commercially viable self-healing organic coatings in the future. Before creating such a coating however, one must thoroughly consider all the distinctly different self-healing designs and examine how each design fits with the coating's functional, chemical and mechanical properties.

1.4 SCOPE AND OBJECTIVES OF THIS RESEARCH

The review above outlines in great detail the fundamental theories, present designs and commercial prospects of a wide variety of self-healing coatings. In evaluating this review, one quickly concludes that research into self-healing acrylic coatings, from which paints are derived, is severely lacking. Given that these coatings, which are composed of waterborne hydrophobic acrylic latex particles, represent the most commercially important and widespread form of organic coating, the absence of any effective self-healing design is highly undesirable. Thus, the research undertaken over the last 3-and-a-half years endeavours to solve this problem by designing a self-healing acrylic coating, and ultimately, a self-healing paint.

In designing a self-healing paint, it is crucial to select an appropriate self-healing chemistry out of the myriad that have been studied over the past two decades (detailed in the review above). Any effective self-healing paint must be able to spontaneously heal undiagnosed damage

without exposure to hostile or impractical conditions, while maintaining sufficient mechanical strength. Given the paint-specific weaknesses of extrinsic self-healing strategies — namely their cost, production and material complexity, undesirable optical properties and ability to heal a given damage site only once — an intrinsic self-healing strategy was investigated. Reversible covalent bonds, which are a widely utilized and highly efficient intrinsic self-healing system, frequently require very high temperatures (>100˚C) to initiate their retro-reactions and stimulate self-healing. Alternatively, supramolecular reversible bonds are an intrinsic system which has been shown to yield room temperature self-healing for a variety of different materials. These materials, however, rely on polymer rearrangement and hence are normally soft materials with a low Young's modulus, such as hydrogels and elastomers. Paints, on the other hand, are a much stronger, stiffer material. This has led some to characterize the intrinsic self-healing of strong materials as a 'contradiction in terms'. Supramolecular self-healing systems have other clear benefits apart from ambient self-healing, including the ability to heal damage in the same area repeatedly, and the fact that they have a far smaller impact on the material's optical and mechanical properties compared to extrinsic strategies.

The hydrogen bond is the most well-studied and perhaps the most promising supramolecular bond utilized in self-healing technology. Hydrogen bonds have been widely employed for room temperature self-healing gels and elastomers, but have also been used to imbue stronger polymeric matrixes with self-healing capacity. The self-complementary hydrogen bonding unit 2-Ureido-4[1H]-Pyrimidinone (UPy) was selected as the basis for a self-healing paint design. UPy is a common self-healing moiety which is synthetically accessible and forms the basis for ambient intrinsic self-healing in stronger thermoplastic coatings, as opposed to gels and elastomers. Perhaps most importantly, UPy, as a quadruple hydrogen bonding unit, forms extremely strong self-complementary hydrogen bonds, which are somewhat analogous to reversible covalent bonds.

The body of a paint, known as a binder, is a composed of a suspension of hydrophobic nanoparticles composed of acrylic polymers (latex), which, upon the evaporation of water, coalesce to form a coating. This latex is formed from the emulsion polymerization of a variety of acrylic monomers. Chapter 2 details the synthesis, characterization, and self-healing performance of a UPy-functionalized acrylic monomer. The UPy-monomer was introduced into an acrylic coating to form a hydrogen bonding network, whose attractive forces provide a mechanism for self-healing. The UPy-monomer had its UPy unit separated from its acrylic

backbone via a long amphiphilic spacer comprised of a hexyl chain and a variable PEG unit. The hydrophilicity of the PEG chain was necessary to allow monomer transport through the aqueous phase of an emulsion polymerization. A library of monomers with varying spacer lengths were studied, as it was hypothesized that the self-healing efficiency of the UPy unit was dependent on polymer chain flexibility. The resultant self-healing capacity of this UPy-functionalized acrylic coating was investigated.

Chapter 3 seeks to enhance the self-healing efficiency of this UPy-monomer based acrylic coating via the introduction of a UPy-functionalized crosslinker. Such a crosslinker is designed to increase the total amount of UPy units/UPy–UPy connections in the coating, thus increasing the strength of the hydrogen bonding network and increasing self-healing efficiency. The crosslinker was also designed with the theory of preventing undesirable UPy–UPy interactions in the latex particles before coalescence, ideally leading to a more evenly distributed hydrogen bonding network. The UPy-crosslinkers were intended to exist in the aqueous phase of the latex, and were based on the hydrophilic polymer PEG. Specifically, two architectures of PEG, linear and brush PEG, were grafted with UPy functionality to form a library of crosslinkers. The crosslinkers based on brush PEG were added to the latex, and the self-healing capacity of the resulting coating was examined.

Having created a self-healing acrylic coating through the introduction of a UPy functionalized monomer, Chapter 4 seeks to design a self-healing paint, which includes pigments and other additives. In partnership with DuluxGroup, a leading designer, manufacturer, and supplier of paints, the UPy monomer design was successfully incorporated into a scaled-up synthesis of a latex. This latex was then added to a paint formulation based on one of Dulux's exterior paint ranges, Weathershield™. The resulting UPy functionalized paint was subjected to a range of industry-specific paint tests. The self-healing properties of this paint, compared to Weathershield™, were investigated both through optical self-healing of damage in the form of a crack, and through the recovery of mechanical properties.

1.5 REFERENCES

1. Zhang, F.; Ju, P.; Pan, M.; Zhang, D.; Huang, Y.; Li, G.; Li, X., Self-healing mechanisms in smart protective coatings: A review. *Corrosion Science* **2018,** *144*, 74-88.

2. Yang, Y.; Urban, M. W., Self-healing polymeric materials. *Chem Soc Rev* **2013,** *42* (17), 7446-7467.

3. Dry, C. M.; Sottos, N. R. In *Passive smart self-repair in polymer matrix composite materials*, Smart Structures and Materials 1993: Smart Materials, International Society for Optics and Photonics: 1993; pp 438-444.

4. Binder, W. H., *Self-healing polymers: from principles to applications*. John Wiley & Sons: 2013.

5. Li, G.; Meng, H., *Recent advances in smart self-healing polymers and composites*. Elsevier: 2015.

6. Zwaag, S., *Self healing materials: an alternative approach to 20 centuries of materials science*. Springer Science+ Business Media BV Dordrecht, The Netherlands: 2008; Vol. 30.

7. Ghosh, S. K., *Self-healing materials: fundamentals, design strategies, and applications*. Wiley Online Library: 2009.

8. Verma, J.; Khanna, S. A., *Digital advancements in smart materials design and multifunctional coating manufacturing*. Physics Open, **2023**, 14, 100133.

9. Wicks, Z. W.; Jones, F. N.; Pappas, S. P.; Wicks, D. A., *Organic Coatings: Science and Technology*. Wiley: 2007.

10. Eckersley, S. T.; Rudin, A., The film formation of acrylic latexes: A comprehensive model of film coalescence. *Journal of applied polymer science* **1994,** *53* (9), 1139-1147.

11. van der Zwaag, S., Self-healing materials: an alternative approach to 20 Centuries of Material Science. *Virginia: Springer* **2007**.

12. García, S.; Fischer, H.; Van Der Zwaag, S., A critical appraisal of the potential of self healing polymeric coatings. *Progress in Organic Coatings* **2011,** *72* (3), 211-221.

13. Ullah, H.; M Azizli, K. A.; Man, Z. B.; Ismail, M. B. C.; Khan, M. I., The potential of microencapsulated self-healing materials for microcracks recovery in self-healing composite systems: a review. *Polymer Reviews* **2016,** *56* (3), 429-485.

14. Wu, D. Y.; Meure, S.; Solomon, D., Self-healing polymeric materials: a review of recent developments. *Progress in polymer science* **2008,** *33* (5), 479-522.

15. Zhu, D. Y.; Rong, M. Z.; Zhang, M. Q., Self-healing polymeric materials based on microencapsulated healing agents: From design to preparation. *Progress in Polymer Science* **2015,** *49*, 175-220.

16. Bekas, D. G.; Tsirka, K.; Baltzis, D.; Paipetis, A. S., Self-healing materials: A review of advances in materials, evaluation, characterization and monitoring techniques. *Compos Part B-Eng* **2016,** *87*, 92-119.

17. Urdl, K.; Kandelbauer, A.; Kern, W.; Müller, U.; Thebault, M.; Zikulnig-Rusch, E., Self-healing of densely crosslinked thermoset polymers—a critical review. *Progress in Organic Coatings* **2017,** *104*, 232-249.

18. White, S. R.; Sottos, N. R.; Geubelle, P. H.; Moore, J. S.; Kessler, M. R.; Sriram, S. R.; Brown, E. N.; Viswanathan, S., Autonomic healing of polymer composites. *Nature* **2001,** *409* (6822), 794-7.

19. Utrera-Barrios, S.; Verdejo, R.; López-Manchado, M. A.; Santana, M. H., Evolution of self-healing elastomers, from extrinsic to combined intrinsic mechanisms: A review. *Materials Horizons* **2020,** *7* (11), 2882-2902.

20. Caruso, M. M.; Blaiszik, B. J.; White, S. R.; Sottos, N. R.; Moore, J. S., Full recovery of fracture toughness using a nontoxic solvent-based self-healing system. *Advanced Functional Materials* **2008,** *18* (13), 1898-1904.

21. Keller, M. W.; White, S. R.; Sottos, N. R., A self-healing poly (dimethyl siloxane) elastomer. *Advanced Functional Materials* **2007,** *17* (14), 2399-2404.

22. Zhu, D. Y.; Wetzel, B.; Noll, A.; Rong, M. Z.; Zhang, M. Q., Thermo-molded self-healing thermoplastics containing multilayer microreactors. *Journal of Materials Chemistry A* **2013,** *1* (24), 7191-7198.

23. Chevalier, Y.; Bolzinger, M.-A., Emulsions stabilized with solid nanoparticles: Pickering emulsions. *Colloids and Surfaces A: Physicochemical and Engineering Aspects* **2013,** *439*, 23-34.

24. Asua, J. M., Challenges for industrialization of miniemulsion polymerization. *Progress in Polymer Science* **2014,** *39* (10), 1797-1826.

25. Lensen, D.; Vriezema, D. M.; van Hest, J. C. M., Polymeric Microcapsules for Synthetic Applications. *Macromolecular Bioscience* **2008,** *8* (11), 991-1005.

26. Ahangaran, F.; Navarchian, A. H.; Picchioni, F., Material encapsulation in poly(methyl methacrylate) shell: A review. *Journal of Applied Polymer Science* **2019,** *136* (41), 48039.

27. An, S.; Lee, M. W.; Yarin, A. L.; Yoon, S. S., A review on corrosion-protective extrinsic self-healing: Comparison of microcapsule-based systems and those based on core-shell vascular networks. *Chemical Engineering Journal* **2018,** *344*, 206-220.

28. Jackson, A. C.; Bartelt, J. A.; Marczewski, K.; Sottos, N. R.; Braun, P. V., Silica-protected micron and sub-micron capsules and particles for self-healing at the microscale. *Macromol Rapid Commun* **2011,** *32* (1), 82-7.

29. Caruso, M. M.; Blaiszik, B. J.; Jin, H.; Schelkopf, S. R.; Stradley, D. S.; Sottos, N. R.; White, S. R.; Moore, J. S., Robust, double-walled microcapsules for self-healing polymeric materials. *ACS Appl Mater Interfaces* **2010,** *2* (4), 1195-9.

30. Jin, H.; Mangun, C. L.; Griffin, A. S.; Moore, J. S.; Sottos, N. R.; White, S. R., Thermally stable autonomic healing in epoxy using a dual-microcapsule system. *Adv Mater* **2014,** *26* (2), 282-7.

31. Blaiszik, B.; Sottos, N. R.; White, S. R., Nanocapsules for self-healing materials. *Compos Sci Technol* **2008,** *68* (3-4), 978-986.

32. Lee, J. K.; Hong, S. J.; Liu, X.; Yoon, S. H., Characterization of dicyclopentadiene and 5-ethylidene-2-norbornene as self-healing agents for polymer composite and its microcapsules. *Macromolecular Research* **2004,** *12* (5), 478-483.

33. Guadagno, L.; Raimondo, M.; Naddeo, C.; Longo, P.; Mariconda, A.; Binder, W. H., Healing efficiency and dynamic mechanical properties of self-healing epoxy systems. *Smart Mater Struct* **2014,** *23* (4), 045001.

34. Cho, S. H.; Andersson, H. M.; White, S. R.; Sottos, N. R.; Braun, P. V., Polydimethylsiloxane-based self-healing materials. *Advanced Materials* **2006,** *18* (8), 997-1000.

35. Mangun, C.; Mader, A.; Sottos, N. R.; White, S. R., Self-healing of a high temperature cured epoxy using poly (dimethylsiloxane) chemistry. *Polymer* **2010,** *51* (18), 4063-4068.

36. Chung, U. S.; Min, J. H.; Lee, P.-C.; Koh, W.-G., Polyurethane matrix incorporating Pdms-based self-healing microcapsules with enhanced mechanical and thermal stability. *Colloids and Surfaces A: Physicochemical and Engineering Aspects* **2017,** *518*, 173-180.

37. Yin, T.; Rong, M. Z.; Zhang, M. Q.; Yang, G. C., Self-healing epoxy composites–preparation and effect of the healant consisting of microencapsulated epoxy and latent curing agent. *Compos Sci Technol* **2007,** *67* (2), 201-212.

38. Jin, H.; Mangun, C. L.; Stradley, D. S.; Moore, J. S.; Sottos, N. R.; White, S. R., Self-healing thermoset using encapsulated epoxy-amine healing chemistry. *Polymer* **2012,** *53* (2), 581-587.

39. Zhang, C.; Wang, H.; Zhou, Q., Preparation and characterization of microcapsules based self-healing coatings containing epoxy ester as healing agent. *Progress in Organic Coatings* **2018,** *125*, 403-410.

40. Koh, E.; Kim, N.-K.; Shin, J.; Kim, Y.-W., Polyurethane microcapsules for self-healing paint coatings. *RSC advances* **2014,** *4* (31), 16214-16223.

41. Li, Q.; Mishra, A. K.; Kim, N. H.; Kuila, T.; Lau, K.-t.; Lee, J. H., Effects of processing conditions of poly (methylmethacrylate) encapsulated liquid curing agent on the properties of self-healing composites. *Composites Part B: Engineering* **2013,** *49*, 6-15.

42. Li, Q.; Siddaramaiah; Kim, N. H.; Hui, D.; Lee, J. H., Effects of dual component microcapsules of resin and curing agent on the self-healing efficiency of epoxy. *Compos Part B-Eng* **2013,** *55*, 79-85.

43. Ahangaran, F.; Hayaty, M.; Navarchian, A. H.; Pei, Y.; Picchioni, F., Development of self-healing epoxy composites via incorporation of microencapsulated epoxy and mercaptan in poly (methyl methacrylate) shell. *Polymer Testing* **2019,** *73*, 395-403.

44. Zhou, X.; Li, W.; Zhu, L.; Ye, H.; Liu, H., Polymer–silica hybrid self-healing nano/microcapsules with enhanced thermal and mechanical stability. *RSC advances* **2019,** *9* (4), 1782-1791.

45. Zhao, Y.; Fickert, J.; Landfester, K.; Crespy, D., Encapsulation of self-healing agents in polymer nanocapsules. *Small* **2012,** *8* (19), 2954-2958.

46. Hettiarachchi, N. M.; De Silva, R. T.; Mantilaka, M. P. G.; Pasbakhsh, P.; De Silva, K. N.; Amaratunga, G. A., Synthesis of calcium carbonate microcapsules as self-healing containers. *RSC advances* **2019,** *9* (41), 23666-23677.

47. Samadzadeh, M.; Boura, S. H.; Peikari, M.; Ashrafi, A.; Kasiriha, M., Tung oil: An autonomous repairing agent for self-healing epoxy coatings. *Progress in Organic Coatings* **2011,** *70* (4), 383-387.

48. Yi, H.; Yang, Y.; Gu, X.; Huang, J.; Wang, C., Multilayer composite microcapsules synthesized by Pickering emulsion templates and their application in self-healing coating. *Journal of materials chemistry A* **2015,** *3* (26), 13749-13757.

49. Wu, K.; Chen, Y.; Luo, J.; Liu, R.; Sun, G.; Liu, X., Preparation of dual-chamber microcapsule by Pickering emulsion for self-healing application with ultra-high healing efficiency. *J Colloid Interface Sci* **2021,** *600*, 660-669.

50. Li, J.; Feng, Q.; Cui, J.; Yuan, Q.; Qiu, H.; Gao, S.; Yang, J., Self-assembled graphene oxide microcapsules in Pickering emulsions for self-healing waterborne polyurethane coatings. *Compos Sci Technol* **2017,** *151*, 282-290.

51. Xu, C.; Chen, Z.; Wang, C.; Chen, K., Fabrication of Dual Self-Healing Multifunctional Coating Based on Multicompartment Microcapsules. *ACS Appl Mater Interfaces* **2021,** *13* (49), 59298-59309.

52. Suryanarayana, C.; Rao, K. C.; Kumar, D., Preparation and characterization of microcapsules containing linseed oil and its use in self-healing coatings. *Progress in organic coatings* **2008,** *63* (1), 72-78.

53. Mirabedini, S.; Dutil, I.; Farnood, R., Preparation and characterization of ethyl cellulose-based core–shell microcapsules containing plant oils. *Colloids and Surfaces A: Physicochemical and Engineering Aspects* **2012,** *394*, 74-84.

54. Mirabedini, S.; Dutil, I.; Gauquelin, L.; Yan, N.; Farnood, R. R., Preparation of self-healing acrylic latex coatings using novel oil-filled ethyl cellulose microcapsules. *Progress in Organic Coatings* **2015,** *85*, 168-177.

55. Es-Haghi, H.; Mirabedini, S.; Imani, M.; Farnood, R., Mechanical and self-healing properties of a water-based acrylic latex containing linseed oil filled microcapsules: Effect of pre-silanization of microcapsules' shell compound. *Composites Part B: Engineering* **2016,** *85*, 305-314.

56. Celestine, A.-D. N.; Sottos, N. R.; White, S. R., Autonomic healing of PMMA via microencapsulated solvent. *Polymer* **2015,** *69*, 241-248.

57. Geiselhart, C. M.; Mutlu, H.; Barner-Kowollik, C., Prevent or Cure—The Unprecedented Need for Self-Reporting Materials. *Angewandte Chemie International Edition* **2021,** *60* (32), 17290-17313.

58. Ma, L.; Ren, C.; Wang, J.; Liu, T.; Yang, H.; Wang, Y.; Huang, Y.; Zhang, D., Self-reporting coatings for autonomous detection of coating damage and metal corrosion: A review. *Chemical Engineering Journal* **2021,** *421*, 127854.

59. Chen, S.; Han, T.; Zhao, Y.; Luo, W.; Zhang, Z.; Su, H.; Tang, B. Z.; Yang, J., A facile strategy to prepare smart coatings with autonomous self-healing and self-reporting functions. *Acs Appl Mater Inter* **2019,** *12* (4), 4870-4877.

60. Wang, J.; Ma, L.; Guo, X.; Wu, S.; Liu, T.; Yang, J.; Ren, C.; Li, S.; Zhang, D., Two birds with one stone: Nanocontainers with synergetic inhibition and corrosion sensing abilities towards intelligent self-healing and self-reporting coating. *Chemical Engineering Journal* **2022,** *433*, 134515.

61. Zhang, H.; Zhang, X.; Bao, C.; Li, X.; Duan, F.; Friedrich, K.; Yang, J., Skin-inspired, fully autonomous self-warning and self-repairing polymeric material under damaging events. *Chemistry of Materials* **2019,** *31* (7), 2611-2618.

62. Mohammadi, M. A.; Eslami-Farsani, R.; Ebrahimnezhad-Khaljiri, H., Experimental investigation of the healing properties of the microvascular channels-based self-healing glass fibers/epoxy composites containing the three-part healant. *Polymer Testing* **2020,** *91*, 106862.

63. Coope, T. S.; Wass, D. F.; Trask, R. S.; Bond, I. P., Repeated self-healing of microvascular carbon fibre reinforced polymer composites. *Smart Mater Struct* **2014,** *23* (11), 115002.

64. Blaiszik, B. J.; Kramer, S. L.; Olugebefola, S. C.; Moore, J. S.; Sottos, N. R.; White, S. R., Self-healing polymers and composites. *Annual review of materials research* **2010,** *40*, 179-211.

65. Toohey, K. S.; Sottos, N. R.; Lewis, J. A.; Moore, J. S.; White, S. R., Self-healing materials with microvascular networks. *Nat Mater* **2007,** *6* (8), 581-5.

66. Hansen, C. J.; Wu, W.; Toohey, K. S.; Sottos, N. R.; White, S. R.; Lewis, J. A., Self-healing materials with interpenetrating microvascular networks. *Advanced Materials* **2009,** *21* (41), 4143-4147.

67. Bhardwaj, N.; Kundu, S. C., Electrospinning: a fascinating fiber fabrication technique. *Biotechnology advances* **2010,** *28* (3), 325-347.

68. Doan, T. Q.; Leslie, L. S.; Kim, S. Y.; Bhargava, R.; White, S. R.; Sottos, N. R., Characterization of core-shell microstructure and self-healing performance of electrospun fiber coatings. *Polymer* **2016,** *107*, 263-272.

69. Li, J.; Hu, Y.; Qiu, H.; Yang, G.; Zheng, S.; Yang, J., Coaxial electrospun fibres with graphene oxide/PAN shells for self-healing waterborne polyurethane coatings. *Progress in Organic Coatings* **2019,** *131*, 227-231.

70. Zanjani, J. S. M.; Okan, B. S.; Letofsky-Papst, I.; Menceloglu, Y.; Yildiz, M., Repeated self-healing of nano and micro scale cracks in epoxy based composites by tri-axial electrospun fibers including different healing agents. *RSC advances* **2015,** *5* (89), 73133-73145.

71. Neisiany, R. E.; Khorasani, S. N.; Lee, J. K. Y.; Ramakrishna, S., Encapsulation of epoxy and amine curing agent in PAN nanofibers by coaxial electrospinning for self-healing purposes. *RSC advances* **2016,** *6* (74), 70056-70063.

72. Wang, Q.; Wang, W.; Ji, X.; Hao, X.; Ma, C.; Hao, W.; Li, X.; Chen, S., Self-Healing Coatings Containing Core-Shell Nanofibers with pH-Responsive Performance. *ACS Appl Mater Interfaces* **2021,** *13* (2), 3139-3152.

73. Cao, L.; Wang, Q.; Wang, W.; Li, Q.; Chen, S., Synthesis of Smart Nanofiber Coatings with Autonomous Self-Warning and Self-Healing Functions. *ACS Appl Mater Interfaces* **2022**.

74. Hoogenboom, R., Hard Autonomous Self-Healing Supramolecular Materials—A Contradiction in Terms? *Angewandte Chemie International Edition* **2012,** *51* (48), 11942-11944.

75. Hornat, C. C.; Urban, M. W., Shape memory effects in self-healing polymers. *Progress in Polymer Science* **2020,** *102*, 101208.

76. Ji, G.; Zhang, P.; Nji, J.; John, M.; Li, G., 11 - Shape memory polymer-based self-healing composites. In *Recent Advances in Smart Self-healing Polymers and Composites*, Li, G.; Meng, H., Eds. Woodhead Publishing: 2015; pp 293-363.

77. Wang, S.; Urban, M. W., Self-healing polymers. *Nature Reviews Materials* **2020,** *5* (8), 562-583.

78. Cheng, M.; Fu, Q.; Tan, B.; Ma, Y.; Fang, L.; Lu, C.; Xu, Z., Build a bridge from polymeric structure design to engineering application of self-healing coatings: A review. *Progress in Organic Coatings* **2022,** *167*, 106790.

79. Yang, Y.; Ding, X.; Urban, M. W., Chemical and physical aspects of self-healing materials. *Progress in Polymer Science* **2015,** *49*, 34-59.

80. Sheng, Y.; Wang, M.; Zhang, K.; Wu, Z.; Chen, Y.; Lu, X., An "inner soft external hard", scratch-resistant, self-healing waterborne poly(urethane-urea) coating based on gradient metal coordination structure. *Chemical Engineering Journal* **2021,** *426*, 131883.

81. Campanella, A.; Döhler, D.; Binder, W. H., Self-healing in supramolecular polymers. *Macromol Rapid Comm* **2018,** *39* (17), 1700739.

82. Khan, A.; Ahmed, N.; Rabnawaz, M., Covalent Adaptable Network and Self-Healing Materials: Current Trends and Future Prospects in Sustainability. *Polymers* **2020,** *12* (9), 2027.

83. Zheng, N.; Xu, Y.; Zhao, Q.; Xie, T., Dynamic Covalent Polymer Networks: A Molecular Platform for Designing Functions beyond Chemical Recycling and Self-Healing. *Chemical Reviews* **2021,** *121* (3), 1716-1745.

84. Montarnal, D.; Capelot, M.; Tournilhac, F.; Leibler, L., Silica-Like Malleable Materials from Permanent Organic Networks. *Science* **2011,** *334* (6058), 965-968.

85. Park, J. S.; Darlington, T.; Starr, A. F.; Takahashi, K.; Riendeau, J.; Hahn, H. T., Multiple healing effect of thermally activated self-healing composites based on Diels–Alder reaction. *Compos Sci Technol* **2010,** *70* (15), 2154-2159.

86. Liu, Y.-L.; Chuo, T.-W., Self-healing polymers based on thermally reversible Diels–Alder chemistry. *Polymer Chemistry* **2013,** *4* (7), 2194-2205.

87. Chen, X.; Dam, M. A.; Ono, K.; Mal, A.; Shen, H.; Nutt, S. R.; Sheran, K.; Wudl, F., A thermally re-mendable cross-linked polymeric material. *Science* **2002,** *295* (5560), 1698-1702.

88. Craven, J. M., Cross-linked thermally reversible polymers produced from condensation polymers with pendant furan groups cross-linked with maleimides. 1969.

89. Tian, Q.; Yuan, Y. C.; Rong, M. Z.; Zhang, M. Q., A thermally remendable epoxy resin. *Journal of Materials Chemistry* **2009,** *19* (9), 1289-1296.

90. Bai, N.; Saito, K.; Simon, G. P., Synthesis of a diamine cross-linker containing Diels–Alder adducts to produce self-healing thermosetting epoxy polymer from a widely used epoxy monomer. *Polymer Chemistry* **2013,** *4* (3), 724-730.

91. Fortunato, G.; Tatsi, E.; Rigatelli, B.; Turri, S.; Griffini, G., Highly Transparent and Colourless Self-Healing Polyacrylate Coatings Based on Diels–Alder Chemistry. *Macromolecular Materials and Engineering* **2020**, 1900652.

92. Kötteritzsch, J.; Stumpf, S.; Hoeppener, S.; Vitz, J.; Hager, M. D.; Schubert, U. S., One-Component Intrinsic Self-Healing Coatings Based on Reversible Crosslinking by Diels–Alder Cycloadditions. *Macromol Chem Phys* **2013,** *214* (14), 1636-1649.

93. Sung, S.; Kim, S. Y.; Lee, T. H.; Favaro, G.; Park, Y. I.; Lee, S.-H.; Ahn, J. B.; Noh, S. M.; Kim, J. C., Thermally reversible polymer networks for scratch resistance and scratch healing in automotive clear coats. *Progress in Organic Coatings* **2019,** *127*, 37-44.

94. Tortelli, A.; Manarin, E.; Corsini, F.; Griffini, G.; Turri, S., Water-reducible and self-healing acrylic coatings based on Diels-Alder reversible reaction. *Progress in Organic Coatings* **2022,** *171*, 107012.

95. Azcune, I.; Odriozola, I., Aromatic disulfide crosslinks in polymer systems: Self-healing, reprocessability, recyclability and more. *European Polymer Journal* **2016,** *84*, 147-160.

96. Canadell, J.; Goossens, H.; Klumperman, B., Self-healing materials based on disulfide links. *Macromolecules* **2011,** *44* (8), 2536-2541.

97. de Luzuriaga, A. R.; Martin, R.; Markaide, N.; Rekondo, A.; Cabanero, G.; Rodriguez, J.; Odriozola, I., Epoxy resin with exchangeable disulfide crosslinks to obtain reprocessable, repairable and recyclable fiber-reinforced thermoset composites. *Materials Horizons* **2016,** *3* (3), 241-247.

98. Lai, Y.; Kuang, X.; Zhu, P.; Huang, M.; Dong, X.; Wang, D., Colourless, Transparent, Robust, and Fast Scratch-Self-Healing Elastomers via a Phase-Locked Dynamic Bonds Design. *Advanced Materials* **2018,** *30* (38), 1802556.

99. Liu, M.; Zhong, J.; Li, Z.; Rong, J.; Yang, K.; Zhou, J.; Shen, L.; Gao, F.; Huang, X.; He, H., A high stiffness and self-healable polyurethane based on disulfide bonds and hydrogen bonding. *European Polymer Journal* **2020**, 109475.

100. Behera, P. K.; Raut, S. K.; Mondal, P.; Sarkar, S.; Singha, N. K., Self-Healable Polyurethane Elastomer Based on Dual Dynamic Covalent Chemistry Using Diels–Alder "Click" and Disulfide Metathesis Reactions. *ACS Applied Polymer Materials* **2021,** *3* (2), 847-856.

101. Chen, T.; Fang, L.; Li, X.; Gao, D.; Lu, C.; Xu, Z., Self-healing polymer coatings of polyurea-urethane/epoxy blends with reversible and dynamic bonds. *Progress in Organic Coatings* **2020,** *147*, 105876.

102. Xu, M.; Cheng, B.; Sheng, Y.; Zhou, J.; Wang, M.; Jiang, X.; Lu, X., High-Performance Cross-Linked Self-Healing Material Based on Multiple Dynamic Bonds. *ACS Applied Polymer Materials* **2020,** *2* (6), 2228-2237.

103. Chung, C.-M.; Roh, Y.-S.; Cho, S.-Y.; Kim, J.-G., Crack healing in polymeric materials via photochemical [2+ 2] cycloaddition. *Chemistry of Materials* **2004,** *16* (21), 3982-3984.

104. Abdallh, M.; Hearn, M. T.; Simon, G. P.; Saito, K., Light triggered self-healing of polyacrylate polymers crosslinked with 7-methacryloyoxycoumarin crosslinker. *Polymer Chemistry* **2017,** *8* (38), 5875-5883.

105. Ling, J.; Rong, M. Z.; Zhang, M. Q., Coumarin imparts repeated photochemical remendability to polyurethane. *Journal of Materials Chemistry* **2011,** *21* (45), 18373-18380.

106. Otsuka, H.; Aotani, K.; Higaki, Y.; Takahara, A., Polymer scrambling: Macromolecular radical crossover reaction between the main chains of alkoxyamine-based dynamic covalent polymers. *J Am Chem Soc* **2003,** *125* (14), 4064-4065.

107. Yuan, C. e.; Rong, M. Z.; Zhang, M. Q.; Zhang, Z. P.; Yuan, Y. C., Self-healing of polymers via synchronous covalent bond fission/radical recombination. *Chemistry of Materials* **2011,** *23* (22), 5076-5081.

108. Zhang, Z. P.; Rong, M. Z.; Zhang, M. Q., Alkoxyamine with reduced homolysis temperature and its application in repeated autonomous self-healing of stiff polymers. *Polymer Chemistry* **2013,** *4* (17), 4648-4654.

109. Zhang, M. Q.; Rong, M. Z., Application of alkoxyamine in self-healing of epoxy. *Journal of Materials Chemistry A* **2014,** *2* (18), 6558-6566.

110. Qian, Y.; Dong, F.; Guo, L.; Lu, S.; Xu, X.; Liu, H., Self-Healing and Reprocessable Terpene Polysiloxane-Based Poly (thiourethane-urethane) Material with Reversible Thiourethane Bonds. *Biomacromolecules* **2023,** *24* (3), 1184-1193.

111. Nguyen, L.-T. T.; Truong, T. T.; Nguyen, H. T.; Le, L.; Nguyen, V. Q.; Van Le, T.; Luu, A. T., Healable shape memory (thio) urethane thermosets. *Polymer Chemistry* **2015,** *6* (16), 3143-3154.

112. Zhang, Q.; Wang, S.; Rao, B.; Chen, X.; Ma, L.; Cui, C.; Zhong, Q.; Li, Z.; Cheng, Y.; Zhang, Y., Hindered urea bonds for dynamic polymers: An overview. *Reactive and Functional Polymers* **2021,** *159*, 104807.

113. Fu, D.; Pu, W.; Wang, Z.; Lu, X.; Sun, S.; Yu, C.; Xia, H., A facile dynamic crosslinked healable poly (oxime-urethane) elastomer with high elastic recovery and recyclability. *Journal of Materials Chemistry A* **2018,** *6* (37), 18154-18164.

114. Liu, Y.; Li, Z.; Zhang, Z.; Wang, J.; Sun, L.; Xie, T., Thermal-driven self-healing waterborne polyurethane with robust mechanical properties based on reversible phenol-carbamate network and Fe3+-catechol coordination bond. *Progress in Organic Coatings* **2021,** *153*, 106153.

115. Lee, S.-H.; Shin, S.-R.; Lee, D.-S., Self-healing of cross-linked PU via dual-dynamic covalent bonds of a Schiff base from cystine and vanillin. *Mater Design* **2019,** *172*, 107774.

116. Chen, G.; Sun, Z.; Wang, Y.; Zheng, J.; Wen, S.; Zhang, J.; Wang, L.; Hou, J.; Lin, C.; Yue, Z., Designed preparation of silicone protective materials with controlled self-healing and toughness properties. *Progress in Organic Coatings* **2020,** *140*, 105483.

117. Thangavel, G.; Tan, M. W. M.; Lee, P. S., Advances in self-healing supramolecular soft materials and nanocomposites. *Nano convergence* **2019,** *6* (1), 29.

118. Li, Z.-T.; Wu, L.-Z., *Hydrogen Bonded Supramolecular Structures*. Springer: 2015.

119. Yang, Y.; Urban, M. W., Self-Healing of Polymers via Supramolecular Chemistry. *Advanced Materials Interfaces* **2018,** *5* (17), 1800384.

120. Lin, C.; Xiao, T.; Wang, L., Hydrogen-Bonded Supramolecular Polymers. In *Hydrogen Bonded Supramolecular Structures*, Springer: 2015; pp 321-350.

121. Chen, Y.; Kushner, A. M.; Williams, G. A.; Guan, Z., Multiphase design of autonomic self-healing thermoplastic elastomers. *Nature chemistry* **2012,** *4* (6), 467.

122. Chen, Y.; Guan, Z., Multivalent hydrogen bonding block copolymers self-assemble into strong and tough self-healing materials. *Chem Commun* **2014,** *50* (74), 10868-10870.

123. Villani, M.; Deshmukh, Y. S.; Camlibel, C.; Esteves, A. C. C., Superior relaxation of stresses and self-healing behavior of epoxy-amine coatings. *RSC advances* **2016,** *6* (1), 245-259.

124. Wietor, J.-L.; Dimopoulos, A.; Govaert, L. E.; van Benthem, R. A.; de With, G.; Sijbesma, R. P., Preemptive healing through supramolecular cross-links. *Macromolecules* **2009,** *42* (17), 6640-6646.

125. Liu, T.; Zhao, H.; Zhang, D.; Lou, Y.; Huang, L.; Ma, L.; Hao, X.; Dong, L.; Rosei, F.; Lau, W. M., Ultrafast and high-efficient self-healing epoxy coatings with active multiple hydrogen bonds for corrosion protection. *Corrosion Science* **2021,** *187*, 109485.

126. Hentschel, J.; Kushner, A. M.; Ziller, J.; Guan, Z., Self-healing supramolecular block copolymers. *Angew Chem Int Ed Engl* **2012,** *51* (42), 10561-5.

127. Qiu, T.; Wang, X. J.; Lin, X. Y.; Zhu, Z. Q.; Li, X. Y.; Guo, L. H., Emulsion polymerization to synthesize self-healing films toward healing on fractures: A feasible strategy. *Journal of Polymer Science Part a-Polymer Chemistry* **2016,** *54* (19), 3071-3078.

128. Yoshida, S.; Ejima, H.; Yoshie, N., Tough Elastomers with Superior Self-Recoverability Induced by Bioinspired Multiphase Design. *Advanced Functional Materials* **2017,** *27* (30).

129. Hu, J.; Mo, R. B.; Jiang, X.; Sheng, X. X.; Zhang, X. Y., Towards mechanical robust yet self-healing polyurethane elastomers via combination of dynamic main chain and dangling quadruple. *Polymer* **2019,** *183*.

130. Chen, Y.; Jones, S. T.; Hancox, I.; Beanland, R.; Tunnah, E. J.; Bon, S. A. F., Multiple Hydrogen-Bond Array Reinforced Cellular Polymer Films from Colloidal Crystalline Assemblies of Soft Latex Particles. *Acs Macro Letters* **2012,** *1* (5), 603-608.

131. Guadagno, L.; Vertuccio, L.; Naddeo, C.; Calabrese, E.; Barra, G.; Raimondo, M.; Sorrentino, A.; Binder, W. H.; Michael, P.; Rana, S., Self-healing epoxy nanocomposites via reversible hydrogen bonding. *Compos Part B-Eng* **2019,** *157*, 1-13.

132. Chen, S.; Mahmood, N.; Beiner, M.; Binder, W. H., Self-Healing Materials from V- and H-Shaped Supramolecular Architectures. *Angew Chem Int Ed Engl* **2015,** *54* (35), 10188-92.

133. Yanagisawa, Y.; Nan, Y.; Okuro, K.; Aida, T., Mechanically robust, readily repairable polymers via tailored noncovalent cross-linking. *Science* **2018,** *359* (6371), 72-76.

134. Zhang, L.; Wang, D.; Xu, L.; Zhang, X.; Zhang, A.; Xu, Y., A highly stretchable, transparent, notch-insensitive self-healing elastomer for coating. *J Mater Chem C* **2020,** *8* (6), 2043-2053.

135. Fujisawa, Y.; Asano, A.; Itoh, Y.; Aida, T., Mechanically Robust, Self-Healable Polymers Usable under High Humidity: Humidity-Tolerant Noncovalent Cross-Linking Strategy. *J Am Chem Soc* **2021,** *143* (37), 15279-15285.

136. Fujisawa, Y.; Nan, Y.; Asano, A.; Yanagisawa, Y.; Yano, K.; Itoh, Y.; Aida, T., Blending to Make Nonhealable Polymers Healable: Nanophase Separation Observed by CP/MAS (13) C NMR Analysis. *Angew Chem Int Ed Engl* **2023,** *62* (5), e202214444.

137. Zhong, N.; Post, W., Self-repair of structural and functional composites with intrinsically self-healing polymer matrices: A review. *Composites Part A: Applied Science and Manufacturing* **2015,** *69*, 226-239.

138. Burattini, S.; Colquhoun, H. M.; Fox, J. D.; Friedmann, D.; Greenland, B. W.; Harris, P. J. F.; Hayes, W.; Mackay, M. E.; Rowan, S. J., A self-repairing, supramolecular polymer system: healability as a consequence of donor-acceptor pi-pi stacking interactions. *Chem Commun* **2009,** (44), 6717-6719.

139. Burattini, S.; Colquhoun, H. M.; Greenland, B. W.; Hayes, W., A novel self-healing supramolecular polymer system. *Faraday Discuss.* **2009,** *143*, 251-264.

140. Hart, L. R.; Hunter, J. H.; Nguyen, N. A.; Harries, J. L.; Greenland, B. W.; Mackay, M. E.; Colquhoun, H. M.; Hayes, W., Multivalency in healable supramolecular polymers: the effect of supramolecular cross-link density on the mechanical properties and healing of non-covalent polymer networks. *Polymer Chemistry* **2014,** *5* (11), 3680-3688.

141. Mei, J. F.; Jia, X. Y.; Lai, J. C.; Sun, Y.; Li, C. H.; Wu, J. H.; Cao, Y.; You, X. Z.; Bao, Z. N., A Highly Stretchable and Autonomous Self-Healing Polymer Based on Combination of Pt center dot center dot center dot Pt and pi-pi Interactions. *Macromol Rapid Comm* **2016,** *37* (20), 1667-1675.

142. Schmidt, B.; Barner-Kowollik, C., Dynamic Macromolecular Material Design-The Versatility of Cyclodextrin-Based Host-Guest Chemistry. *Angew Chem Int Edit* **2017,** *56* (29), 8350-8369.

143. Qin, B.; Yin, Z.; Tang, X.; Zhang, S.; Wu, Y.; Xu, J.-F.; Zhang, X., Supramolecular polymer chemistry: From structural control to functional assembly. *Progress in Polymer Science* **2020,** *100*, 101167.

144. Zhang, M. M.; Xu, D. H.; Yan, X. Z.; Chen, J. Z.; Dong, S. Y.; Zheng, B.; Huang, F. H., Self-Healing Supramolecular Gels Formed by Crown Ether Based Host-Guest Interactions. *Angew Chem Int Edit* **2012,** *51* (28), 7011-7015.

145. Hu, Z.; Zhang, D. Y.; Lu, F.; Yuan, W. H.; Xu, X. R.; Zhang, Q.; Liu, H.; Shao, Q.; Guo, Z. H.; Huang, Y. D., Multistimuli-Responsive Intrinsic Self-Healing Epoxy Resin Constructed by Host-Guest Interactions. *Macromolecules* **2018,** *51* (14), 5294-5303.

146. Dahlke, J.; Bose, R. K.; Zechel, S.; Garcia, S. J.; van der Zwaag, S.; Hager, M. D.; Schubert, U. S., A New Approach Toward Metal-Free Self-Healing Ionomers Based on Phosphate and Methacrylate Containing Copolymers. *Macromol Chem Phys* **2017,** *218* (23).

147. Dahlke, J.; Tepper, R.; Geitner, R.; Zechel, S.; Vitz, J.; Kampes, R.; Popp, J.; Hager, M. D.; Schubert, U. S., A healing ionomer crosslinked by a bis-bidentate halogen bond linker: a route to hard and healable coatings. *Polymer Chemistry* **2018,** *9* (16), 2193-2197.

148. Kalista, S. J.; Ward, T. C., Thermal characteristics of the self-healing response in poly (ethylene-co-methacrylic acid) copolymers. *Journal of the Royal Society Interface* **2007,** *4* (13), 405-411.

149. Kalista, S. J., Self-healing of poly(ethylene-co-methacrylic acid) copolymers following projectile puncture. *Mech. Adv. Mater. Struct.* **2007,** *14* (5), 391-397.

150. Francesconi, A.; Giacomuzzo, C.; Grande, A. M.; Mudric, T.; Zaccariotto, M.; Etemadi, E.; Di Landro, L.; Galvanetto, U., Comparison of self-healing ionomer to aluminium-alloy bumpers for protecting spacecraft equipment from space debris impacts. *Advances in Space Research* **2013,** *51* (5), 930-940.

151. Peng, Y.; Zhao, L. J.; Yang, C. Y.; Yang, Y.; Song, C.; Wu, Q.; Huang, G. S.; Wu, J. R., Super tough and strong self-healing elastomers based on polyampholytes. *Journal of Materials Chemistry A* **2018,** *6* (39), 19066-19074.

152. Cui, X. Y.; Zhang, C.; Camilo, R. P.; Zhang, H.; Cobaj, A.; Soucek, M. D.; Zacharia, N. S., Self-Healing Latex Containing Polyelectrolyte Multilayers. *Macromolecular Materials and Engineering* **2018,** *303* (8).

153. Lin, C.; Sheng, D.; Liu, X.; Xu, S.; Ji, F.; Dong, L.; Zhou, Y.; Yang, Y., NIR induced self-healing electrical conductivity polyurethane/graphene nanocomposites based on Diels– Alder reaction. *Polymer* **2018,** *140*, 150-157.

154. Wu, H.; Sheng, D.; Liu, X.; Zhou, Y.; Dong, L.; Ji, F.; Xu, S.; Yang, Y., NIR induced self-healing polyurethane/polypyrrole nanocomposites. *Polymer* **2020,** *189*, 122181.

155. Dong, Y.; Gong, M.; Huang, D.; Gao, J.; Zhou, Q., Shape memory, self-healing property, and NIR photothermal effect of epoxy resin coating with polydopamine@ polypyrrole nanoparticles. *Progress in Organic Coatings* **2019,** *136*, 105232.

156. Cao, L.; Wang, W.; Li, Q.; Feng, C.; Wang, T.; Qin, X.; Piao, J.; Chen, S., Three-dimensional nanofibers network multifunctional material for photothermal self-healing protective coating. *Chemical Engineering Journal* **2022,** *440*, 134943.

157. White, S. R.; Sottos, N. R.; Geubelle, P. H.; Moore, J. S.; Sriram, S. R.; Kessler, M. R.; Brown, E. N., Multifunctional autonomically healing composite material. US6518330B2: 2003.

158. Braun, P. V.; Cho, S. H.; White, S. R., Self-healing coating system. US7723405: 2010.

159. Kumar, A.; Stephenson, L., Self healing coatings using microcapsules. **2006**, 2006042504-A1.

160. Sarangapani, S.; Kumar, A.; Thies, C.; Stephenson, L. D., Self-healing coating and microcapsules to make same. US7192993B1: 2007.

161. Henry, J. J. M., Nano-based self-healing anti-corrosion coating. US20140134426A1: 2014.

162. Peterson, A. M.; Sakulich, A. R.; Chen, Y.; Xia, C. T., Self-healing coating for reinforcement steel. US20170044379A1: 2017.

163. Dayton, C. R.; Wilson, G. O.; Kasisomayajula, S. V.; Shukla, S.; Navarro, A. G. R.; Rodriguez, D., One-component waterborne self-healing epoxy formulation. US11613668B2: 2023.

164. Wang, L.; Li, S.; Fu, J., Self-healing anti-corrosion coatings based on micron-nano containers with different structural morphologies. *Progress in Organic Coatings* **2023,** *175*, 107381.

165. Fang, D.; Abd Elhamid, M.; Dailly, A. M.; Cai, M., Self-healing, UV-absorbing polymer coating. US11084947B2 2021.

166. Williams, G. A.; Hentschel, J.; Satpute, A., Self-healing resin. US10800866: 2020.

167. Rabnawaz, M.; Khan, A., Self-healing laminate composition, related articles and related methods. US11529648B2: 2022.

168. Nakao, M. One-component waterborne polyurethane self-healing coatings using hydrophobic blocked polyisocyanates. WO2022039927A1, 2022.

169. He, M.; Fauvell, T.; Urruti, E., Self-healing optical fibers and the compositions used to create the same. US11358899B2: 2022.

Chapter 2. A Self-Healing Monomer

ABSTRACT

Acrylic coatings suffer damage in the form of cracking, which degrades both their protective and aesthetic performance over time. Self-healing technology offers the ability to solve this problem by allowing cracks to spontaneously heal without external diagnosis or intervention, offsetting the enormous costs associated with coating damage and repair. However, there is currently no efficient self-healing acrylic coating design, and research in the area remains noticeably sparse. In this research a mechanically tough methyl methacrylate (MMA)/butyl acrylate (BA)/acrylic acid (AA) acrylic coating was imbued with self-healing functionality by incorporating self-healing monomers within the formulation. A library of four acrylic monomers containing both a long amphiphilic spacer of variable length, and the 2-ureido-4[1H]-pyrimidinone (UPy) unit, which forms strong self-complementary quadruple hydrogen bonds, was synthesized. These UPy-monomers were able to participate in the emulsion polymerization of MMA, BA and AA, forming intrinsic hydrogen bonding networks within the subsequent acrylic coatings. These UPy functionalized coatings displayed both optical self-healing and strain recovery over 24 hours both at room temperature (~28%), and at elevated temperatures up to 50˚C (~80%). The coatings also displayed repeatable self-healing after four healing cycles, relative to an MMA/BA/AA coating.

2.1 INTRODUCTION

Coatings play a vital role in society by protecting surfaces from damage while at the same time imparting a variety of functional and aesthetic qualities. The coatings market is vast, and primarily composed of epoxy and polyurethane based coatings as well as latex coatings, which are based on a suspension of polymer particles in water (latex). These coatings are commonly referred to as paints.[1] All coatings fall victim to a variety of stresses over time, leading first to the formation of cracks, and subsequently the total failure of the coating.[2] Replacement of the failed coating is expensive, time consuming and energy intensive. Thus, with the rapid development of self-healing technology since 2001, there exists a strong incentive to develop self-healing coatings.[3]

Self-healing coatings can be defined as coatings which are able to heal damage spontaneously and without intervention. Based on their healing mechanisms, self-healing coatings can be divided into two categories: extrinsic and intrinsic.[4] Extrinsic self-healing is based on a healing agent which is added as a distinct component separate from the coating itself. Normally this involves encapsulating the healing agent within microcapsules, or occasionally microfibers, dispersed throughout the coating.[5] Following cracking, the microcapsules are ruptured, allowing the healing material to flow into the crack and initiate self-healing.[6] This healing normally occurs via auto-polymerization in the presence of a catalyst. Extrinsic self-healing strategies have been shown to yield high self-healing efficiencies for coatings, mainly epoxy resins.[7-10] However, the applicability of extrinsic self-healing strategies is limited by cost, the presence of microcapsules, which can alter the mechanical and optical properties of the coating, and the fact that a given damage area can heal only once.[11, 12] Intrinsic self-healing coatings, on the other hand, have their healing functionality as part of the material itself. In the case of polymeric coatings, this normally involves the presence of reversible covalent or supramolecular bonds, which can reform following a damage event via attractive forces.[13] Dynamic covalent bonds, such as the disulfide bond, and reversible covalent reactions, such as the Diels–Alder reaction/retro reaction, have been used to synthesize healable epoxy resins and polyurethane coatings. However, these coatings require high temperatures (>100˚C) to initiate the self-healing process, limiting their real-world applicability.[14-16] Supramolecular interactions such as hydrogen bonding, π-π stacking, electrostatic interactions and metal-ligand coordination bonds have shown the ability to impart polymer matrixes with robust self-healing at ambient temperatures.[17-19] Yet supramolecular self-healing is normally limited to softer low-modulus materials such as hydrogels, given that this healing relies on the rearrangement of polymer chains. Thus, imbuing stronger stiffer coatings with intrinsic self-healing functionality to allow for ambient self-healing represents a fundamental dilemma in materials science.[20]

Nevertheless, recent efforts have been made to resolve this seeming contradiction. Stiffer polymeric materials have shown self-healing capability by combining a hard block, which utilizes higher *T*g polymers to provide mechanical strength, with a soft block that provides the flexibility necessary for intrinsic self-healing. For example, copolymers containing a hard block such as poly(methyl methacrylate) (PMMA) or polystyrene (PS) and a soft polyacrylate amide block have shown the ability to heal materials with tensile strengths between 30 and 80 MPa.[21, 22] A polymeric film containing a hard PS block and a soft poly(butyl acrylate) (PBA)

block functionalized with the hydrogen bonding unit 2-ureido-4[1H]-pyrimidinone (UPy) was able to self-heal at only 45˚C and recover 90% of its original tensile strength (up to 40 MPa).[23] First developed by Meijer, the UPy unit forms strong, self-complementary quadruple hydrogen bonds, and thus has been extensively employed for the development of intrinsic self-healing materials.[24] UPy-based intrinsic self-healing materials such as hydrogels have shown strong self-healing at ambient conditions. The UPy unit has also been introduced to stronger materials such as epoxy and polyurethane coatings, allowing self-healing under more moderate conditions.[25, 26]

Despite the myriad of self-healing strategies presently available, research regarding self-healing acrylic coatings, as opposed to epoxy resins, polyurethane coatings and specialized anti-corrosive coatings, is lacking. In 2018, Cui *et al.* designed a self-healing acrylic coating based on the electrostatic attraction between poly(ethylene imine) (PEI) and poly(acrylic acid) (PAA).[27] This design was able to self-heal when immersed in salt water, which helped plasticize the coating. UPy-based hydrogen bonding was used by Qiu *et al.* to imbue an MMA/BA acrylic coating with self-healing capability.[28] Their design incorporated a UPy functionalized monomer, dissolved in chloroform, to form coatings that displayed self-healing at 100˚C. Despite these limited studies, acrylic coatings which can heal under moderate conditions relevant to real-world applications remains a serious challenge.

Herein, a waterborne MMA/BA/AA acrylic coating which exhibits self-healing capability under ambient conditions, and across a range of temperatures up to 60˚C (Figure 2.1), is presented. This was achieved through the incorporation of an acrylic UPy-functionalized monomer with a long polyethylene glycol (PEG) spacer. Such a PEG spacer allows for greater UPy chain mobility and is inspired by previous work into hard-soft block copolymer designs. The incorporation of a PEG spacer also allows the highly insoluble UPy monomer to transport through the water phase of an emulsion, and polymerize to form part of the waterborne latex without the need for large amounts of organic solvent.[29] Specifically, a library of four different UPy monomers with various PEG spacer lengths was synthesized, termed UPy-1, UPy-2, UPy-3 and UPy-4. UPy-1 represented the most hydrophobic design, with no PEG spacer, while the other three UPy monomers had PEG chains with MWs of 500, 360 and 2000 Da respectively. These four UPy monomers were compared to investigate how solubility and spacer length ultimately impacted self-healing capability. It was found that both UPy-2 and UPy-3 exhibited self-healing capability whose efficiency increased as the temperature increased from 25˚C to

60˚C. Of these two designs, UPy-2, with a longer PEG spacer, was noticeably superior. Furthermore, the UPy-2 coating was able to self-heal a crack over three damage/healing cycles, which is a key advantage of intrinsic, as opposed to extrinsic, self-healing designs. This work demonstrates a novel example of ambient self-healing both for acrylic coatings, an under-researched area in self-healing literature, and for stiffer, more rigid coatings, which remains a challenge for intrinsic self-healing strategies. This research also provides an important understanding of the mechanisms necessary for efficient intrinsic self-healing. Ultimately, such research represents an important step toward the design of self-healing commercial paints.

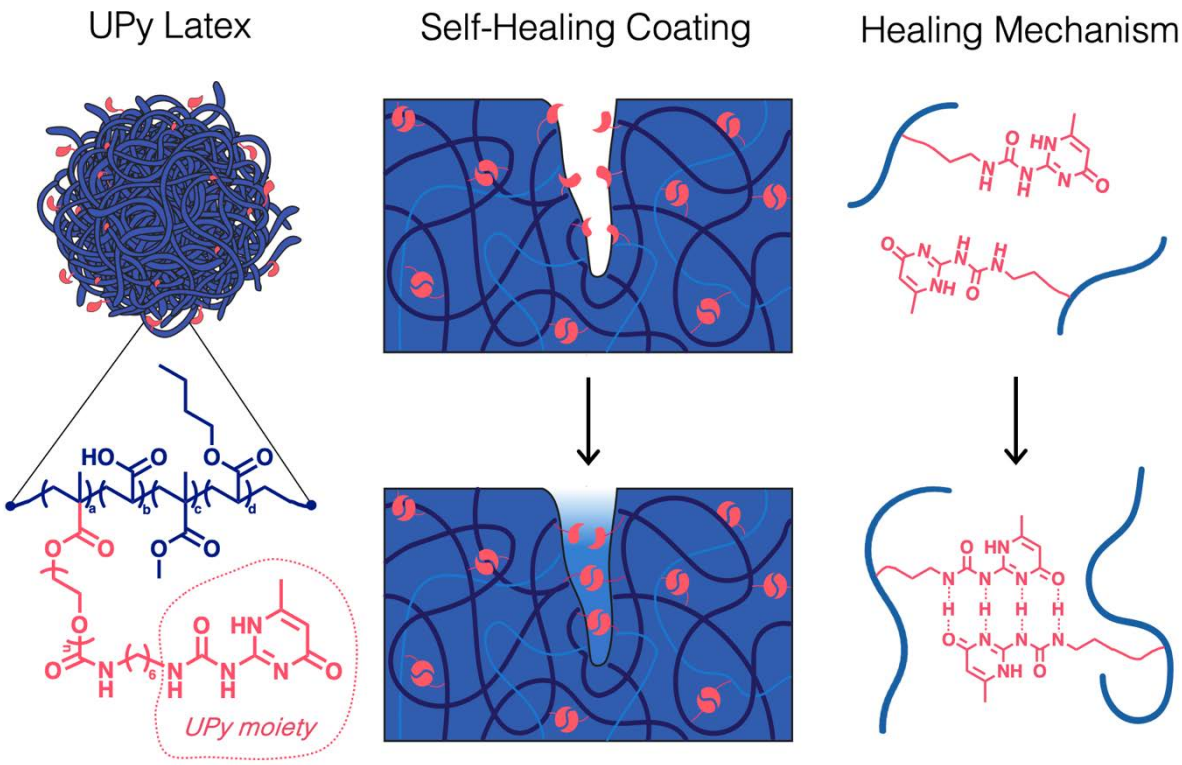

Figure 2.1 The concept of a self-healing acrylic coating. First, the hydrogen bonding unit UPy is incorporated into acrylic latex particles via the polymerization of a UPy-functionalized acrylic monomer. Then, as water evaporates, these latex particles coalesce to form an acrylic coating with a UPy-based hydrogen bonding network. Finally, following damage to the coating, intrinsic self-healing is generated through the attractive self-complementary hydrogen bonding of the UPy moieties.

2.2 EXPERIMENTAL

2.2.1 Materials

2-Amino-4-hydroxy-6-methylpyrimidine, ethanolamine, methacroyloyl chloride, hydroquinone, triethylamine (TEA), 1,1'-carbonyldiimidazole (CDI), poly(ethylene glycol) methacrylate (PEGMA) (molecular weight (MW) = 500 and 360), polyethylene glycol (PEG) (MW = 2000), hexamethylene diisocyanate, dibutyl tin dilaurate catalyst, as well as methyl methacrylate (MMA), butyl acrylate (BA), acrylic acid (AA), and sodium dodecyl sulfate (SDS) were all purchased from Sigma Aldrich and used as received. Ammonium persulfate, as well as the solvents dimethyl sulfoxide (DMSO), chloroform ($CHCl_3$), ethyl acetate, diethyl ether, acetone, pentane, hexane, methanol, dichloromethane (DCM) and dimethylformamide (DMF) were purchased from ChemSupply Australia. The deuterated solvents $CDCl_3$ and DMSO were purchased form Sigma Aldrich. The 3.5 kDa MWCO dialysis 'snakeskin' bag (Thermo-Fischer Scientific) was used according to instructions.

2.2.2 Characterization

^{1}H-NMR spectroscopy was performed on a 400 MHz Varian 400 MR spectrometer using deuterated chloroform ($CDCl_3$) as the solvent. ^{1}H NMR analysis was performed on MestreNova software. GPC analysis was performed on a Shimadzu system equipped with a Waters Styragel column (10μm pore size). THF was used as the eluent with a flow rate of 1 mL/min. The molecular weight and polydispersity of the samples were calculated relative to poly(methyl methacrylate) (PMMA) standards. Samples were prepared at 2 mg/mL and filtered (0.45μm) prior to measurement. IR spectroscopy was performed on a Perkin Elmer Spectrum 2 ATR-FTIR spectrometer, and UV Vis spectroscopy was performed on Cary 60 UV-Vis (Agilent technologies). Dynamic light scattering analysis of particle size was performed on a Horiba Nanopartica SZ-100 (Horiba Scientific, Japan), operating at 37℃ and a fixed scattering angle of 90˚. Optical microscopy images were taken on an optical microscope and TEM images were recorded on a FEI Talos L120C cryoTEM. Surface measurements were performed on a Bruker ContourGT Optical Profilometer. Tensile tests were carried out on an Instron 5944, 2kN microtester. Differential scanning calorimetry was performed on a Perkin Elmer 8500 Double Furnace HyperDSC from -50 to 70˚C at 10˚C per min.

2.2.3 Synthesis of the UPy functionalized monomers

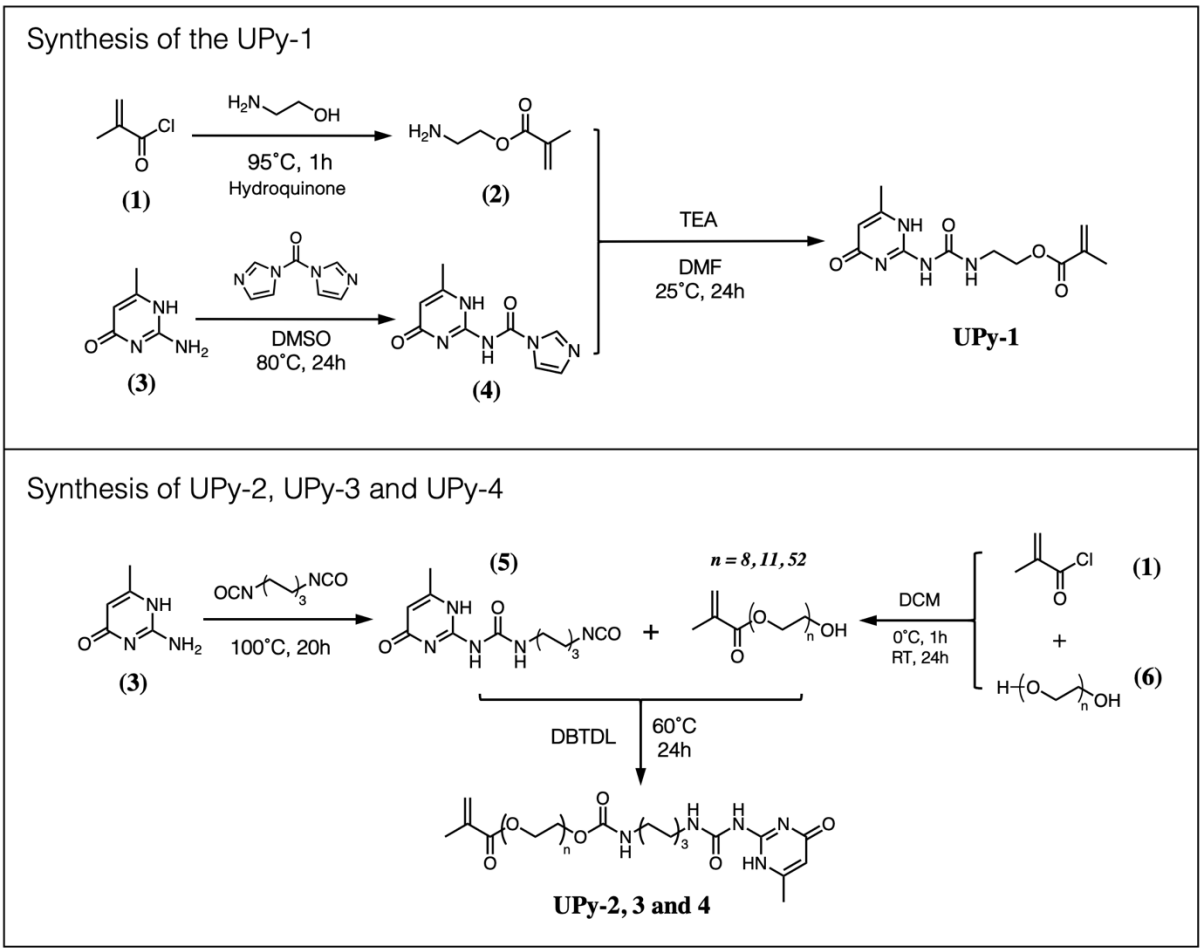

Scheme 1. The synthesis of UPy-1, as well as UPy-2, UPy-3 and UPy-4.

2.2.3.1 Synthesis of 2-aminoethyl methacrylate (2)

Ethanolamine (1.21 g, 12.5 mmol) and hydroquinone (0.01 g, 0.1 mmol) were mixed in a round bottom flask equipped with a condenser. The mixture was heated to 95˚C under nitrogen. Methacryloyl chloride (1) (2 mL, 18.4 mmol) was slowly added to the mixture over the course of an hour with vigorous stirring. The mixture was further stirred for half an hour and then cooled to 60˚C. The product in the form of a white powder (yield: 94%) was precipitated in ethyl acetate. ^{1}H NMR (400 MHz, $CDCl_3$): δ (ppm) 6.1 and 5.6 (C–CH_2), 4.3 (CH_2–CH_2–O), 3.3 (CH_2– CH_2–O), 1.8 (OC–CCH_2–CH_3) (Figure S1).

2.2.3.2 Synthesis of N-(6-methyl-oxo-1,4-dihydropyrimidin-2-yl)-1H-imidazole-1-carboxamide (4)

2-Amino-4-hydroxy-6-methylpyrimidine (3) (1.5 g, 12 mmol) was dissolved in 15 mL DMSO. 1,1'-Carbonyldiimidazole (2.52 g, 15 mmol) was added and the mixture was stirred for 24 hours at 80 °C under nitrogen. The mixture was then cooled to room temperature and acetone was added to precipitate the product. The precipitant was collected by filtration and washed with acetone. The white powder product, henceforth known as UPy-imidazole, was dried under vacuum (Yield: 90%). ^{1}H NMR (400 MHz, DMSO): δ (ppm) 7.6 (N–C*H*–N Imidazole), 7.1 (N–C*H*–CH–N Imidazole), 6.9 (N–CH–C*H*–N Imidazole), 5.4 (OC–C*H*–CCH_3), 1.9 (OC–CH–CC*H*$_3$) (Figure S2).

2.2.3.3 Synthesis of 2(6-isocyanatohexylaminocarbonylamino)-6-methyl-4[1H] pyrimidinone (5)

2-Amino-4-hydroxy-6-methylpyrimidine (3) (1.0 g, 8.0 mmol) was added in hexamethylene diisocyanate (8.0g, 48 mmol). The mixture was then heated to 100℃ and stirred for 20 hours under nitrogen. After this time, 20 mL of pentane was added to precipitate the product. The product was dried under vacuum to yield a white powder (yield: 95%). ^{1}H NMR (400 MHz, DMSO): δ (ppm) 5.8 (OC–C*H*–CCH_3), 3.2 (Hexyl chain), 2.2 (*CH*$_3$–C–NH), 1.4–1.6 (Hexyl chain), 10.6 12.0 and 13.1 (hydrogen bonding) (Figure S4). FTIR: v 2900 (CONH), 2270 (NCO), 1700 (aryl C=O) 1650 (NCON) 1100 (C–O) (Figure S5).

2.2.3.4 Synthesis of the UPy monomer, UPy-1

UPy-imidazole (4) (0.5 mmol, 110 mg) and 2-aminoethyl methacrylate (2) (0.75 mmol, 120 mg) were dissolved in 10 mL of dry DMF. 120 μL of TEA base was added and the reaction was stirred under nitrogen at room temperature overnight. The product was precipitated with water, and washed with water and acetone, before being vacuum dried to yield a white powder (yield: 90%). ^{1}H NMR (400 MHz, $CDCl_3$): δ (ppm) 6.2 and 5.8 (OC–CC*H*$_2$–CH_3), 5.6 (OC–C*H*–CCH_3), 4.3 (CH_2–C*H*$_2$–O), 3.6 (C*H*$_2$–CH_2–O), 2.2 (OC–CH–CC*H*$_3$), 1.8 (OC–CCH_2–C*H*$_3$), 10.5, 12.0 and 13.0 (hydrogen bonding) (Figure S3)

2.2.3.5 Synthesis of the UPy monomer, UPy-2

2(6-isocyanatohexylaminocarbonylamino)-6-methyl-4[1H] pyrimidinone (5) was added to a solution of poly(ethylene glycol) methyl methacrylate (PEGMA) (MW = 500 Da) in dry

chloroform at an even mol ratio. The mixture was heated to 60˚C under a nitrogen atmosphere, and a few drops of the catalyst, dibutyl tin dilaurate, were added. The reaction was then left to stir until all of the isocyanate precursor had converted. This was monitored via the IR peak at 2200 cm^{-1}. The product was then dried under vacuum (yield: ~98%). ^{1}H NMR (400 MHz, $CDCl_3$): ∂ (ppm) 6.1 and 5.6 (CH_3–C*CH_2*–CO), 5.8 (OC–*CH*–CCH_3), 4.0-4.4 and 3.6-3.8 (PEG chain), 3.1-3.4 (Hexyl chain), 2.2 (*CH_3*–C–NH), 1.8 (*CH_3*–CCH_2), 1.4-1.6 (Hexyl chain), 10.5, 12.0 and 13 (UPy hydrogen bonds) (Figure S6). FTIR: v 2900 (CONH), 1700 (aryl C=O), 1650 (NCON) 1100 (C–O) (Figure S7). The UPy monomers, UPy-3 (Figures S8–9) and UPy-4 (Figures S11–12), were synthesized as per the synthesis of UPy-2, however using PEGMA with MW = 360 and ~ 2000 Da respectively.

2.2.3.6 Synthesis of PEGMA (MW ~ 2000 Da)

Poly(ethylene glycol) (MW ~ 2000 Da) (6) (3.5 g, 1.75 mmol) was dissolved in 60 mL of dry dichloromethane and stirred under nitrogen. As the mixture was cooled to 0˚C in an ice bath, 245 mg of triethylamine (1.4 eq.) was added dropwise into the solution. Once the mixture had reached 0˚C, 218 mg of methacryloyl chloride (1) (1.2 eq.) was slowly added dropwise over a period of 1 hour. Following this, the reaction was left to stir at room temperature overnight. The resulting mixture was washed with 0.1 M HCl, followed by saturated $NaHCO_3$ solution and finally by brine. The crude product was then recrystallized in cold diethyl ether (yield: 84%). ^{1}H NMR (400 MHz, $CDCl_3$): ∂ (ppm) 6.1 and 5.6 (CH_3–C*CH_2*–CO), 4.0-4.4 and 3.6-3.8 (PEG chain), 1.8 (*CH_3*–CCH_2) (Figure S10).

2.2.4 Emulsion polymerization

REACTANTS	SOLIDS (wt%)
Butyl acrylate	47
Methyl methacrylate	47
Acrylic acid	2
UPy monomer	2.5
Sodium dodecyl sulfate (Surfactant)	1.2
Ammonium persulfate (Initiator)	0.3

The emulsion was performed in deionized water with a solid content of 20 wt%. Initially, a solution of de-ionized water and dissolved surfactant (sodium dodecyl sulfate) was deoxygenated under a nitrogen atmosphere and heated until the internal temperature rose to 80˚C. Following this, two separate feeds were prepared. The first was the monomer feed containing butyl acrylate, methyl methacrylate and acrylic acid (feed 1, S29). The UPy monomer (2.5 wt%) was added to this feed, and the solution was sonicated for 30 seconds. The second feed was the initiator (ammonium persulfate) dissolved in deionized water which was made up to the same volume as the monomer feed. Following the sonication of feed 1, both feeds were simultaneously fed into the reactor over a 3 hour period. After feeding, the reaction was left to run for a further hour for a total reaction time of 4 hours. The resulting latex was purified via dialysis for a week (MWCO 3.5kDa), displacing water twice a day. The latexes were characterized by ^{1}H NMR and UV-Vis spectroscopy to verify the presence of UPy monomer. DLS and TEM were employed to understand the shape and size of the latex particles.

2.2.5 Pencil hardness test

The surface hardness of the coatings (described in section 2.2.7) was determined via the pencil hardness test. The coatings were cleaned to remove dust or other impurities on the surface. A series of pencils ranging in hardness from 6B to 2H were conditioned by grinding on a piece of abrasive paper. The pencils were checked to make sure the edges of the graphite were smooth and level, not nipped or chipped. The pencils were then placed at a 45˚ angle to the coating and pushed forward with firm pressure. The hardness was defined as the hardest pencil which fails to cut the film, and the experiment was performed three times with a fresh pencil edge.

2.2.6 Water resistance test

The water resistance of the coatings was determined gravimetrically. The coatings were immersed for 24 hours under four different conditions: Deionized (neutral) water, saturated salt water, acidic (pH 5) water and 60˚C water. The weight gain after immersion was measured and reported as a fraction of the total weight.

2.2.7 Film formation and self-healing tests

To form the coatings, the latex was added to a silicone mold (30 mm x 30 mm x 1 mm) and left to dry at room temperature for 1 week and then at 50˚C for 2 days. As the water evaporated, the latex particles coalesced, forming the acrylic coating. Following this, the coating was cut

into a rectangular shape (30 mm x 12 mm x 600 μm). A 5 mm long horizontal cut was introduced to the coating via a razor blade, and penetrated the coating completely, with a depth of 600 μm. This cut was allowed to heal at room temperature over 24 hours with no intervention. Optical self-healing tests were performed via an optical microscope and a surface profilometer. The self-healing behaviour of the coating was photographed, and a 3D rendering of the surface topology was generated, yielding the depth and width of the crack at its widest point.

Tensile tests were carried out under the following conditions: a strain rate of 3 mm/min, a gauge length (fixture separation) of 17 mm and a temperature of 25˚C. An average result was calculated from three independent experiments. To evaluate the strain recovery of the coatings (a measure of self-healing efficiency), a 5 mm long horizon cut was introduced to the coating via a razor blade. The coatings were then gently pressed together for 5 seconds and left to heal for 24 hours over a given healing temperature (25, 40, 50 or 60˚C). The healed samples were then subject to tensile tests. The Young's modulus (E) and the strain at which the healed crack reopened (ε, strain-at-break, failure strain) was noted and compared to the strain at which an undamaged coating began to break apart. Given the malleability of the coatings, there was no sudden fracturing of the undamaged coating, rather, the failure strain was noted when the crack opened and the coating began to 'unzip'. This is contrasted with what is often defined as the strain-at-break for brittle materials, where the material breaks suddenly into two parts.

2.3 RESULTS

A library of four UPy-functionalized acrylic monomers were synthesized with varying PEG spacer lengths (Scheme 1, Figure 2.2). The monomer UPy-1 (Figure S3) was synthesized through the precursor UPy-imidazole (Figure S2), which then underwent a highly efficient nucleophilic addition reaction with aminoethyl methacrylate (Figure S1). UPy-1 represents the most hydrophobic possible UPy functionalized monomer, and lacks any PEG spacer separating its strong hydrogen bonding unit from the polymer backbone. The other three UPy monomers were synthesized via a two-step isocyanate-hydroxyl reaction, and contained both a long hydrophilic PEG spacer, and a hydrophobic hexyl chain end capped with the UPy unit, yielding amphiphilic character (Figure S4-12). Hydrophobicity is necessary for the monomer to polymerize and form part of the latex, while the partial hydrophilicity of the PEG chain allows for monomer transport through the aqueous phase of the emulsion.[29] Furthermore, the long

PEG spacer distances the UPy self-healing unit from the backbone of the hydrophobic polymer, potentially enhancing self-healing capability by maximizing the degrees of freedom of the UPy units. The synthesis of these monomers was highly efficient, generating high yields (> 90%) and was able to be performed under moderate conditions, chiefly due to the strength of the imidazole leaving group, in the case of UPy-1, and the reactivity of the isocyanate moiety, in the case of UPy-2 to 4.

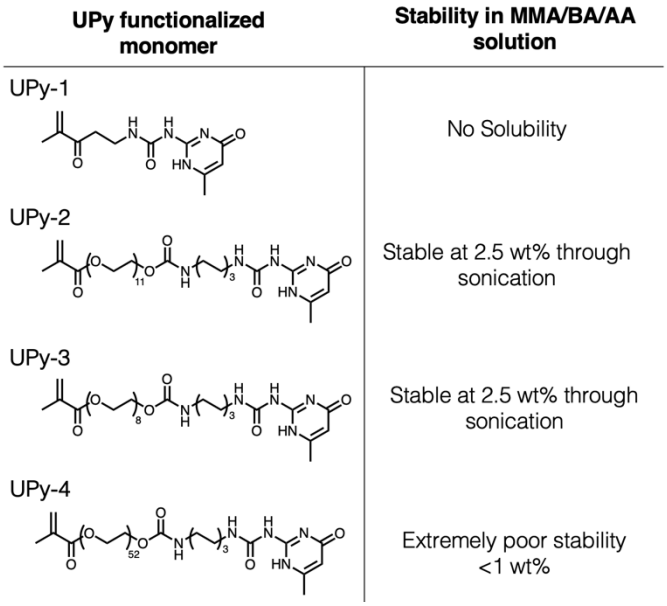

Figure 2.2 The chemical structure of the four UPy functionalized monomers (UPy-1 to UPy-4), as well as their respective stabilities in the acrylic monomer feed (MMA/BA/AA).

All four of the UPy monomers were tacky solids, and highly insoluble in both water and organic solvents, with the exception of chloroform and DMF. This fact makes their incorporation into a solvent-free waterborne emulsion polymerization problematic. To test their stability, the four monomers were added to a BA/MMA/AA feed at a concentration of up to 5 wt%, and the solution was then sheared for 30 seconds of sonication to accelerate the dissolution of the UPy-monomers. Figure 2.2 shows that only UPy-2 and UPy-3 could be stably incorporated into a BA/MMA/AA feed, each at a maximum concentration of 2.5 wt%. The fact that both UPy-1, the most hydrophobic design, and UPy-4, the most hydrophilic design, each had extremely poor solubility, implies the existence of an amphiphilic 'goldilocks zone', where both the hydrophobicity and hydrophilicity of UPy-2 and UPy-3 are sufficiently balanced to yield

stability up to 2.5 wt%. Therefore, due to the insolubility of UPy-1 and UPy-4, only UPy-2 and UPy-3 were incorporated into a waterborne MMA/BA/AA latex.

UPy-functionalized, waterborne MMA/BA/AA latexes were prepared through solvent-free emulsion polymerization. A monomer feed containing 2.5 wt% of either UPy-2 or UPy-3, and an initiator feed were added to an 80˚C reactor over 3 hours. The polymerization continued for another hour, yielding a gravimetric monomer conversion of ~ 91–92%, with no observed coagulum. The resultant latexes were then dialysed to remove unreacted monomer. DLS and TEM showed spherical latex particles with average sizes of around 100 nm, with DLS yielding average latex particle diameters of 80 nm, 91 nm and 110 nm for the control, UPy-2 and UPy-3 latexes respectively (Figure 2.3a–d). It is interesting to note that the dispersity of the latex particles increases slightly with the incorporation of the UPy functionalized monomers. This may be due to the strong self-complementary nature of the UPy units, causing a fraction of the nanoparticles to aggregate with each other, yielding larger particles and thus a higher dispersity. Nevertheless, all three latex particle samples are highly monodisperse. Furthermore, these latexes were also found to be highly stable over the course of a year, with the dispersity remaining essentially unchanged in the case of the control and UPy-3 latexes, while increasing from 0.1 to 0.3 between 6 and 12 months, in the case of the UPy-2 latex (Figure S25).

To determine where the UPy moieties were located on the latex particles, a UPy-2 latex was prepared in deuterium oxide, rather than water, and an ^{1}H NMR spectrum of this latex was obtained (Figure S67). ^{1}H NMR can be used to characterize the surface of nanoparticles as this surface is exposed to the solvent, whereas the core of the particle is shielded.[29] Figure S67 shows the presence of the UPy unit on the surface of the latex particles, which is indicated through its characteristic pyridinone proton, as well as MMA, whose methyl group is clearly visible on the surface.

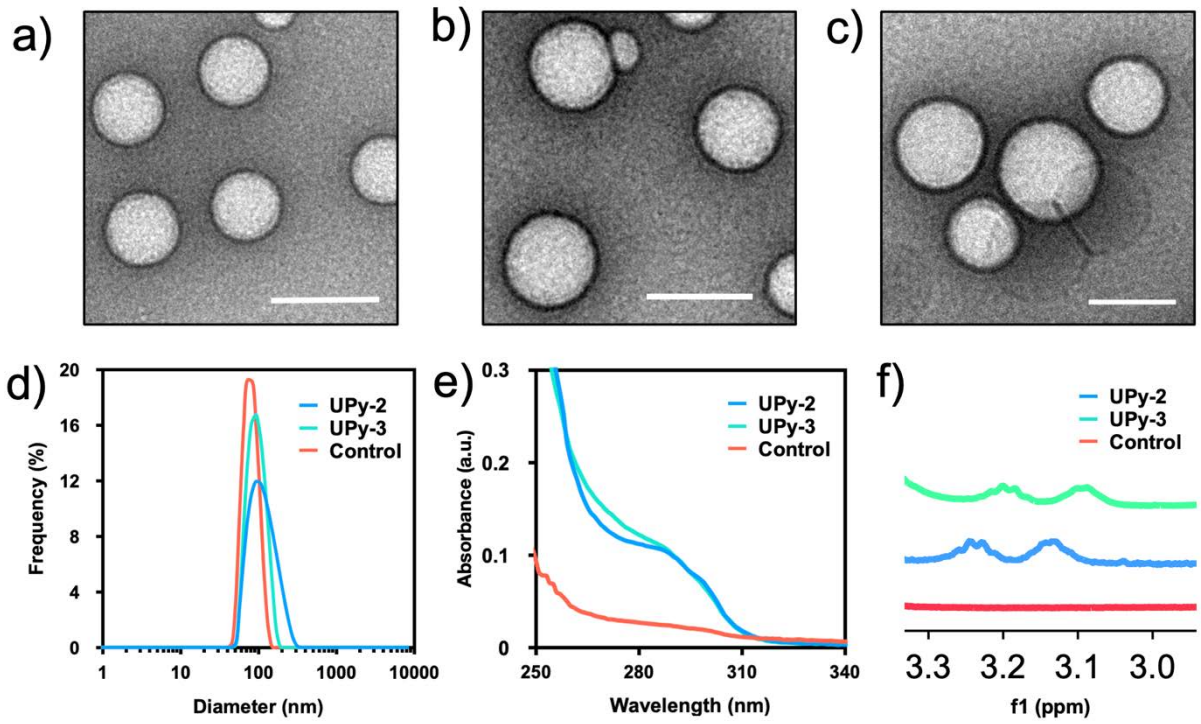

Figure 2.3 Characterization of the UPy functionalized BA/MMA/AA latex. TEM images of the latex particles for the control latex (a), the UPy-2 latex (b), and the UPy-3 latex (c) showing sizes of approximately 80-100 nm. The scale bar in white represents 100 nm. d) DLS intensity size distribution of the control, UPy-2 and UPy-3 latex particles. e) UV Vis spectrum of the control, UPy-2 and UPy-3 latexes. The shoulder between 250 and 300 nm corresponds to the absorbance of the UPy unit. f) A zoomed in ^{1}H NMR spectrum of the control, UPy-2 and UPy-3 latexes, where the peaks between 3.1 and 3.2 ppm correspond to the hexyl chain of the UPy monomers.

The successful incorporation of UPy into the latexes was verified by ^{1}H NMR of the latex, via monitoring the peaks from 3.3-3.1 ppm, which corresponds to the hexyl chain spacer on the UPy monomer (Figure 2.3f, S13-15). These peaks do not appear in the control latex. The UPy unit absorbs light between 250 and 300 nm. Therefore, the amount of UPy in the latex can be further quantified through UV/Vis spectroscopy using a standard curve of known concentrations of each monomer (Figure S16-17). 260 nm was selected to construct the absorbance calibration of UPy as it is distinct from the solvent cut off value (250 nm for $CHCl_3$). 250–300 nm is a relatively broad range of light absorption, and is due to the fact that UPy can form a variety of rotamers, as well as a tautomeric pyrimidin-4-ol conformation which absorbs ~ 290 nm.[30] At 260 nm, the absorbance is essentially independent of this UPy

tautomeric conformation behaviour.[31] At concentrations of 1 mg/mL, a shoulder is clearly visible between 250 and 300 nm for UPy-2 and UPy-3 latexes, and absent from the control latex, verifying the incorporation of the UPy functionalized monomers (Figure 2.3e). Comparing these absorbance values with standard curves yields a UPy monomer conversion of 84% for the UPy-2 latex, and 90% for the UPy-3 latex. 90% for UPy-3 is similar to the conversion of MMA and BA, which was calculated gravimetrically to be between 91% and 92%. However 84% obtained for UPy-2 is a slight decrease in conversion relative to the other monomers. One explanation for this may be the slightly reduced monomer feed solubility of UPy-2 relative to UPy-3, given the longer hydrophilic PEG spacer, which could cause the loss of some UPy-2 during the emulsion. Nevertheless, both UPy-2 and UPy-3 are capable of incorporation into an acrylic latex via emulsion polymerization without the need for large amounts of organic solvent, a significant marker of a more robust self-healing design. UV/Vis was also used to analyze the transparency (opacity) of the three resultant coatings (Figure S28). The coatings were transparent, with each having a transmittance of over 80%. Importantly, the addition of UPy-2 and UPy-3 did not affect the transparency of the acrylic films.

Mechanical tests were carried out on the control coating without UPy monomer and the two coatings containing 2.5 wt% UPy-2 and UPy-3. The glass transition temperature (*T*g) is the temperature at which an amorphous polymer matrix transitions from a glassy, brittle material to a softer, plasticized substance. It is theorized that *T*g plays an important role in intrinsic self-healing efficiency, given that polymer mobility and rearrangement is a far more pronounced above *T*g.[32] *T*g can be estimated according to Flory-Fox theory, and for a 1:1 BA/MMA latex with 2% AA, the theoretical *T*g is approximately 6˚C. The *T*g of each coating was measured by DSC and, the results are shown in Figure 2.4a and S18-20. All three coatings have a *T*g higher than their theoretical *T*g according to the Fox equation, while the range between the three coatings is very small (15-18˚C). The UPy monomer contains a long PEG spacer, whose low *T*g (approximately -50˚C) would seemingly lower the *T*g of the overall coating. However, other studies using UPy based monomers without flexible spacers, have reported slight increases in *T*g, due to the hydrogen bonding interactions between the UPy units.[33] DSC measurements show that the UPy-2 and UPy-3 monomers have very limited effect on the *T*g of the resultant coatings. Specifically, the control coating's *T*g was measured at 18˚C, with the UPy-2 and UPy-3 coatings measured at 16 and 15˚C respectively.

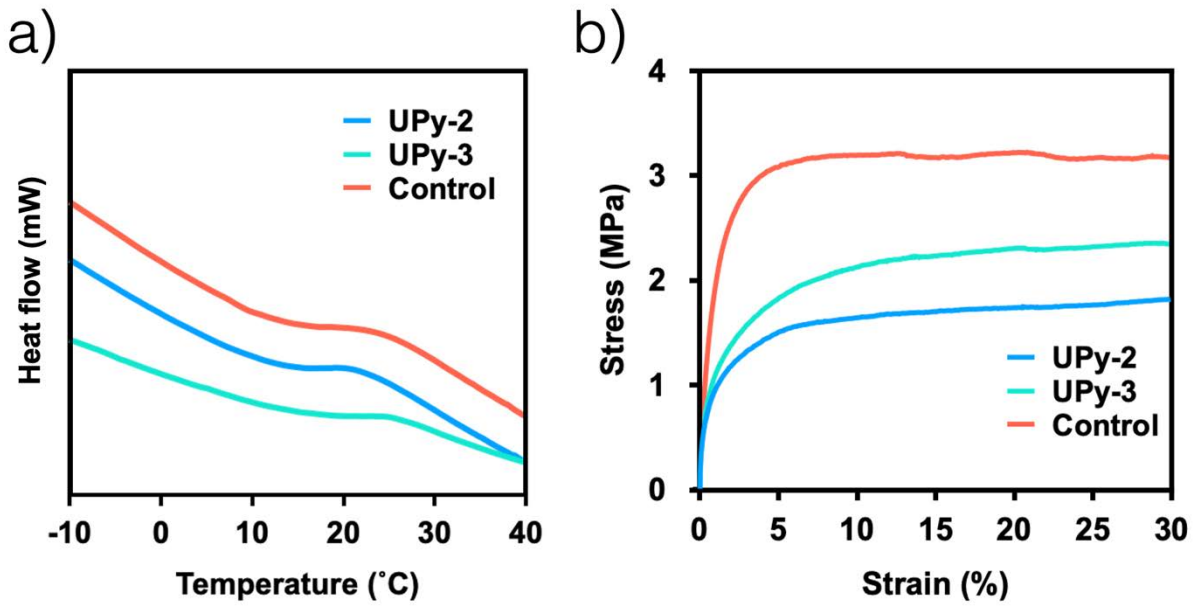

Figure 2.4 Mechanical properties of the UPy functionalized MMA/BA/AA acrylic coatings. a) DSC heat flow curves of the control, UPy-2 and UPy-3 coatings yielded the *Tg* of the coatings. b) Stress-strain curves of the control, UPy-2 and UPy-3 coatings yielded the Young's modulus (stiffness) and the ultimate strength of the coatings.

The coatings were subjected to tensile testing to yield stress strain curves (Figure 2.4b). Young's modulus, also known as the elastic modulus, is the ratio of stress to strain in the elastic deformation (linear region) of the curve, and measures how resistant a material is to deformation. It is the most common metric when defining and comparing the mechanical strength of different materials. Most intrinsic self-healing strategies rely on materials with a modulus from 0.1 MPa in the case of hydrogels to ~10 MPa in the case of stronger elastomers. Acrylic coatings, on the other hand, are generally stiffer materials with a Young's modulus > 100 MPa. The control, UPy-2 and UPy-3 coatings each have a Young's modulus of 0.20 and 0.22 GPa respectively, which is well within the operational range of such coatings. The control coating, at 0.3 GPa is slightly stiffer than the UPy based coatings, while also having a higher ultimate stress (~3 MPa), further reinforcing the idea that the PEG chains on the UPy monomers slightly soften the resulting coatings. Nevertheless, the UPy functionalized acrylic coatings maintained favorable mechanical strength, with Young's moduli two orders of magnitude above hydrogels and elastomers, and a *T*g similar to that of unaltered latex acrylic coatings.

As well as *T*g and Young's modulus, the surface hardness of the coatings was examined via a pencil hardness test (Figure S26). All three coatings displayed strong surface hardness, with the control and UPy-3 coatings displaying a hardness of H, and the UPy-2 coating displaying an average hardness of HB. Importantly, the addition of the UPy functionalized monomers did not significantly reduce the surface hardness of the resulting acrylic coating. The water resistance of each coating was measured gravimetrically under four separate conditions: de-ionized (neutral) water, saturated salt water, acidic (pH 5) water and hot water (60˚C) (Figure S27). Poor water resistance in the form of water uptake is a drawback of waterborne emulsion systems. In neutral water, all three coatings gained ~10% of their weight after 24 hours, and this weight gain increased upon increasing temperature. Crucially, however, the addition of the UPy-2 and UPy-3 monomer did not alter the water resistance properties of the MMA/BA/AA control coating.

To determine whether the UPy functionalized acrylic coatings gained any self-healing performance, optical self-healing tests were conducted by introducing a crack through the coatings via a razor blade, and then allowing the coatings to spontaneously heal at room temperature. Figure 2.5 displays images from the optical microscope immediately following the cutting of the films, and then after 24 hours of healing time. The control coating clearly displays no self-healing after 24 hours at room temperature, which is unsurprising, given the lack of UPy functionalization. However, as Figure 2.5b–c show, both the UPy-2 and UPy-3 coatings displayed noticeable optical self-healing capability, with the UPy-2 coating showing significant self-healing particularly near the top of the crack, which is shown within the dotted line in Figure 2.5b.

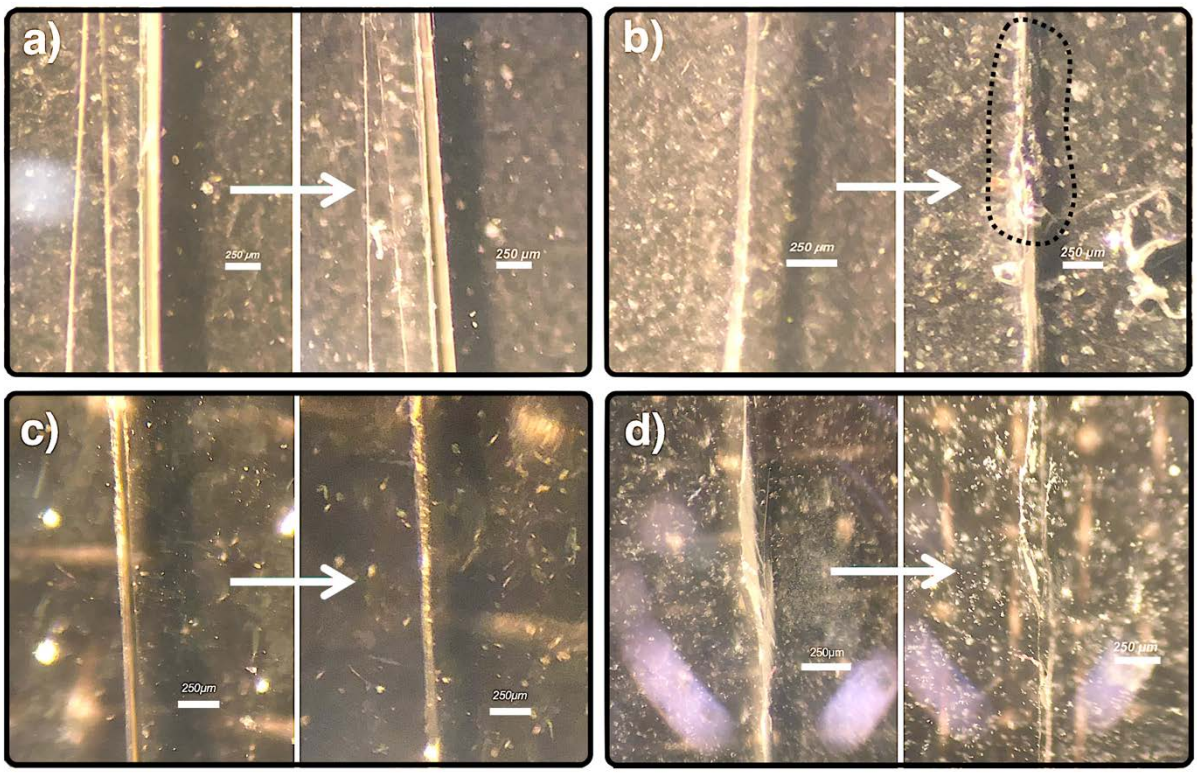

Figure 2.5 Optical self-healing tests. The coatings were cut through with a razor blade, and images were taken with an optical microscope immediately (left image) and after 24h at a given temperature (right image). a) Control coating at RT. b) UPy-2 coating at RT. c) UPy-3 coating at RT. d) UPy-2 coating at 60˚C. Scale bar represents 250 nm.

Figure 2.5d shows the self-healing of UPy-2 coating after 24 hours at 60˚C. Clearly the optical self-healing is significantly stronger than at room temperature, as the crack has fully closed, and the presence of damage is far more difficult to see. Interestingly, full optical healing of the crack, whereby there is almost no evidence of damage having ever occurred, remained absent, even when increasing the healing time over a week at 60˚C. Despite maintaining visual evidence of damage, Figure 2.5 shows that the UPy-2 and UPy-3 functionalized acrylic coatings were able to spontaneously heal damage and display clear optical self-healing capability, which increased with elevated temperature. Optical profilometry was used to gain a more quantitative understanding of crack self-healing, showing that almost all crack depth was recovered in the case of the UPy-2 coating, and that the UPy-3 coating's crack had an average depth of ~100 µm (Fig. S30). Furthermore, the widths of the cracks drastically reduced following 24 hours at room temperature, with UPy-3's width reducing by ~66% and UPy-2's width decreasing by ~80%, compared to the unhealed control.

To understand more about the self-healing potential of these systems, the strain recovery of each coating was measured to determine their self-healing efficiency. This method for calculating healing efficiency has been applied to various polymeric matrixes employing hydrogen bonding self-healing, including urea and barbiturate elastomers.[34, 35] Self-healing efficiency was calculated via the ratio between the strain-at-break of the undamaged coating and the damaged coating after a given set of self-healing conditions. Some materials are brittle and fracture sharply and completely, however polymeric coatings including acrylic coatings deform and elongate before eventually fracturing in the form of a crack which gradually 'unzips'. The strain-at-break for the virgin coating was defined as the point at which fracture in the form of an open crack first appears, before the crack unzips and the coating rips in half. The strain-at-break for the healed coating was defined as the strain at which the healed crack initially opens. For healed samples, the crack does not open up all at once, rather it opens from the center first, and unzips outwards.

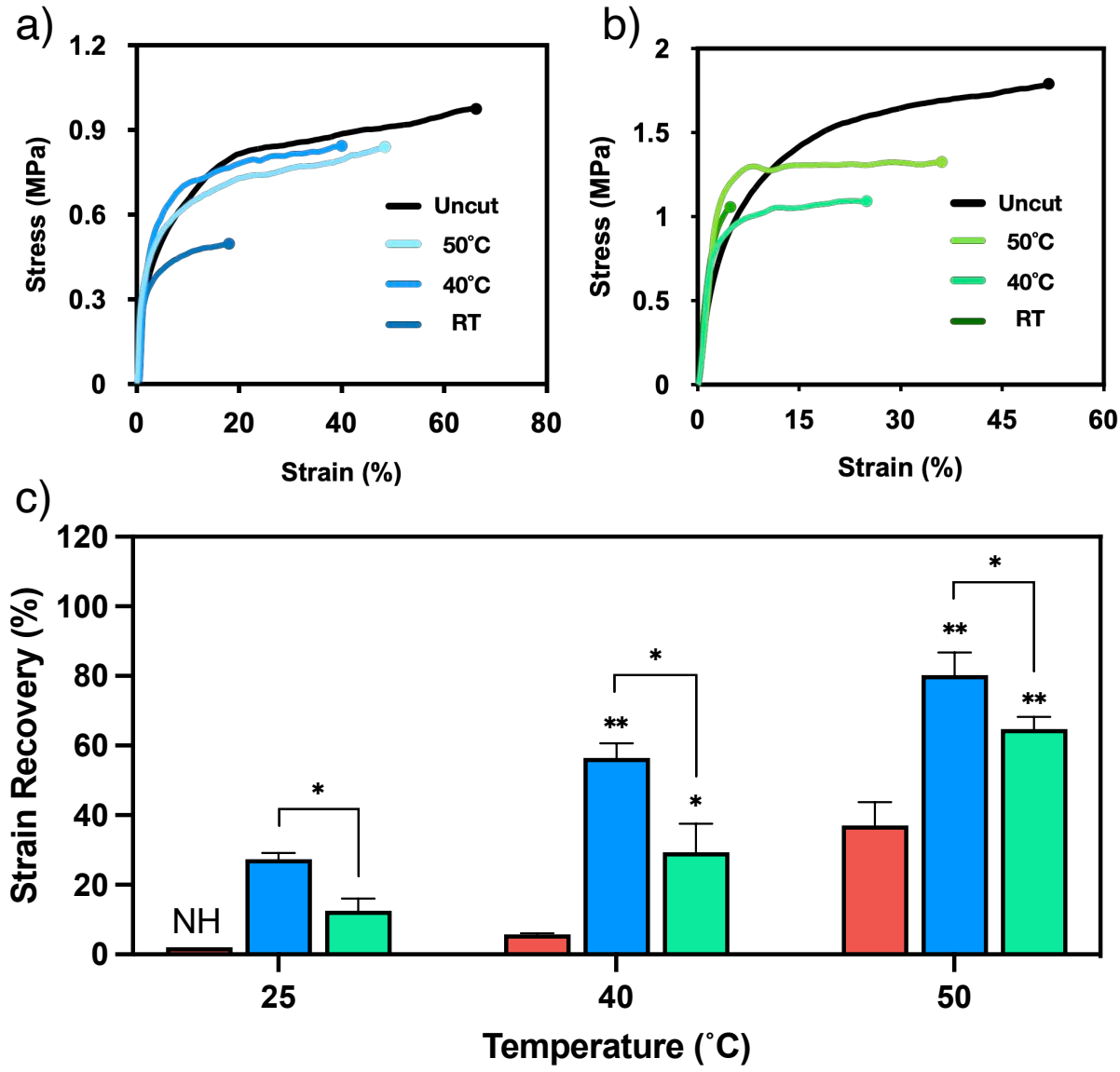

Figure 2.6 Self-healing efficiency was evaluated via strain recovery tests of the uncut coatings compared with the cut coatings allowed to heal for 24 hours over temperatures ranging from room temperature to 60˚C. a) An example stress strain curve for the UPy-2 coating. b) An example stress strain curve for the UPy-3 coating. c) The self-healing efficiency of the control (red), UPy-2 (blue) and UPy-3 (green) coatings for 25, 40 and 50˚C self-healing temperatures. NH indicates that no healing was observed. The data represents mean ± SD for n = 3 independent experiments. An unpaired t-test was used to analyze the statistical differences between the self-healing efficiency of each coating. *indicates $p \leq 0.05$, **indicates $p \leq 0.01$.

A cut was introduced to the control coating, along with UPy-2 and UPy-3 coatings via a razor blade and the samples were allowed to heal over 24 hours for a variety of different temperatures (Figure 2.6c, S21–22). At room temperature, both UPy coatings displayed self-healing activity in the form of strain recovery, with the UPy-2 coating having a higher strain recovery (~28%) compared to the UPy-3 coatings (~12%) (Figure 2.6a–c). The control coating, containing no UPy functionality, had no self-healing capability at room temperature, as upon tensile stress, the crack opened immediately. Figure 2.6c shows that self-healing efficiency increases with temperature, from ~60% at 40˚C to ~80% at 50˚C in the case of UPy-2, and from ~30% at 40˚C to ~60% at 50˚C in the case of the UPy-3 coating. At all three temperatures, there is a statistically significant difference between the self-healing efficiency of the UPy functionalized coatings and the control coating, indicating that the UPy moiety yields noticeable self-healing performance, due to the strong self-complementary hydrogen bonding.

The difference in healing performance between the UPy-2 and UPy-3 coatings suggests that the length of the spacer between the UPy unit and the polymer backbone impacts self-healing capacity. The superior self-healing efficiency of the UPy-2 coating is likely due to its longer poly(ethylene glycol) spacer, which increases polymer chain translational and rotational mobility, allowing the UPy units to rearrange and self-healing more efficiently. Furthermore, the elevated distance between the UPy unit and the polymer backbone likely reduces steric hindrance, which further enhances the ability of the UPy units to self-complement. Such enhanced polymer chain mobility is also the reason why self-healing performance increases with elevated temperature, as for polymeric materials, high temperatures maximize polymer chain mobility. Previous work on polymers with UPy functionalized backbones has also shown an increase in the association/dissociation dynamics of UPy at temperatures above 40˚C.[36] Interestingly, above 60˚C, the strain recovery for all three samples is very strong, which implies that at very high temperatures, the heightened polymer dynamics of an MMA/BA/AA acrylic coating can spontaneously self-heal by means analogous to melting (the most basic self-healing mechanism). It is important to note that because all three coatings have a similar Young's modulus and *T*g, self-healing is not occurring in the UPy functionalized coatings because they are inherently soft materials relative to the control. Rather, the self-complementary hydrogen bonding of the UPy unit itself is responsible for a significant fraction of self-healing performance. Interestingly, the MMA/BA/AA control coating begins to display self-healing activity >50˚C, likely due to the enhanced rheological properties of the polymers. However, the large difference between the self-healing efficiencies of the control and UPy-2 coatings

even at this elevated temperature (from ~30% and ~80% respectively) emphasizes the self-healing power of the UPy hydrogen bonding design.

One of the principal benefits of intrinsic self-healing is the potential to repeatedly heal damage in the same area of a coating. This is an advantage that microcapsule-based extrinsic designs lack, given their single-use encapsulated healing agent. To test whether the UPy-2 and UPy-3 self-healing designs provided any repeatable self-healing, the coatings were subjected to self-healing cycles. A crack was introduced, and the coating was left to heal over 24 hours at room temperature, after which the same crack was re-cut and reopened and allowed to heal again over the given conditions. This was repeated four times and the healing efficiency was recorded for each cycle (Figure S23). The results are shown in Figure 2.7a.

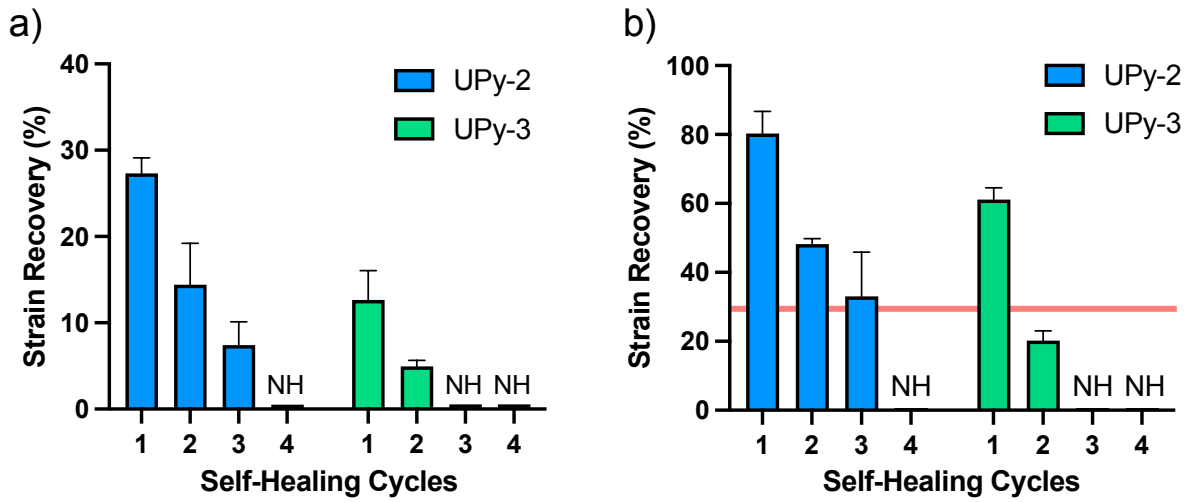

Figure 2.7 Self-healing cycles for damage in the same area, which was healed and recut and healed again over four cycles. The cycles were conducted at RT and 50˚C with a healing time of 24 hours. a) healing cycles for the UPy-2 and UPy-3 coatings at RT. b) healing cycles for the UPy-2 and UPy-3 coatings at 50˚C. NH refers to no observed self-healing relative to the control, and the red line in b) denotes the strain recovery of the control coating at 50˚C.

Figure 2.7a displays the measured strain recovery (healing efficiency) of the UPy-2 and UPy-3 coatings over four healing cycles at room temperature. Both coatings have repeatable self-healing capability which seems to degrade with each cycle. The UPy-2 coating's self-healing efficiency is notable for cycles 1-3, decreasing from ~28% to ~15% and finally to ~8%,

however by cycle 4 the efficiency has dropped to insignificant levels. The UPy-3 coating, whose healing efficiency is already lower than the UPy-2 coating, displays repeatable self-healing only after 2 cycles, where the healing drops from ~12% in cycle 1 to ~5% in cycle 2. No self-healing efficiency was observed after cycle 3. Both coatings seem to lose their self-healing performance completely after 4 cycles. This is an interesting observation, given that intrinsic self-healing materials, unlike extrinsic materials, should theoretically be able to self-heal a given area of damage repeatedly, due to their inherent healing functionality.

To fully understand the ability of the UPy functionalized coatings to self-heal damage repeatedly, the experiment was repeated at 50˚C, the temperature at which self-healing efficiency for both coatings is at its highest (Figure 2.7b, S24). Similar to the coatings at room temperature, self-healing efficiency decreases with each healing cycle. In the case of the UPy-2 coating, self-healing is observable for 2 cycles, before reducing to levels comparable to the control (shown by the red line in Figure 2.7b). UPy-3, on the other hand, displays no repeatable self-healing whatsoever. Such a loss of repeatable healing efficiency as the number of healing cycles increases is frequently seen in other intrinsic self-healing designs, when repeatable self-healing is tested, and has been posited to be the result of damage to the coating during cycling.[37, 38] One plausible reason for the observed reduction of repeatable self-healing efficiency in both the UPy-2 and UPy-3 coatings is that in the first healing cycle, both coatings are able to recover strain well into the plastic region of the material before the crack fails. This means that at the point of crack failure, the coatings have been permanently deformed into a 'crack open' position, so that when the experiment is repeated, self-healing efficiency is significantly reduced. A second explanation involves the fact that for each new healing/damage cycle, a greater number of unhealable bonds are broken. Given that the number of healable bonds in the same damage area does not change, the healing efficiency is thus minimized as more and more cycles are repeated. This mechanism of healing degradation, even in intrinsic self-healing systems, has been reported elsewhere.[39, 40] Nevertheless, it is important to note that though self-healing efficiency decreases with each cycle, the UPy-2 coating does display repeatable self-healing both at room temperature and at 50˚C, which is a key advantage of an intrinsic self-healing material, and an important benefit for any self-healing organic coating.

2.4 CONCLUSION

Self-healing technology has been applied to various kinds of organic coatings including epoxy resins and polyurethane anti-corrosive coatings via the microencapsulation of healing agents, reversible covalent bond functionalization and supramolecular networks. However, self-healing studies based on waterborne acrylic latex coatings, which comprise the majority of trade paints, are noticeably lacking. A self-healing acrylic coating was designed which showed self-healing capability at room temperature and moderate conditions while maintaining its mechanical properties. A library of four acrylic monomers based on the strong hydrogen bonding unit UPy was synthesized with varying amphiphilicity — termed UPy-1, UPy-2, UPy-3, and UPy-4. Of these four, UPy-2 and UPy-3, were able to undergo emulsion polymerization and form part of an MMA/BA acrylic latex. The resulting UPy-functionalized coatings displayed self-healing capability at room temperature, visually healing a crack and spontaneously recovering up to 28% of their strain-at-break after 24 hours. Self-healing efficiency was enhanced with elevated temperatures, and damage in the same spot was able to be healed repeatedly, albeit with a noticeable decline in healing efficiency as the number of healing cycles increased. Comparing the self-healing efficiency of the UPy-2 and UPy-3 coatings also yielded important information regarding the mechanism of self-healing, and what factors influence self-healing efficiency in organic coatings. Furthermore, the UPy functionalized acrylic coatings maintained good mechanical strength, with Young's moduli ~ 200 MPa, one to two orders of magnitude above the hydrogels and elastomers commonly associated with intrinsic self-healing. Finally, the design did not alter the optical properties of the acrylic coatings, which remained transparent, nor was undesirable organic solvent introduced into the emulsion procedure. This design is one of the first examples of latex acrylic self-healing at room temperature, without the often-accompanied loss of mechanical strength, and thus represents a significant step forward toward self-healing paint.

2.5 REFERENCES

1. Wicks, Z. W.; Jones, F. N.; Pappas, S. P.; Wicks, D. A., *Organic Coatings: Science and Technology*. Wiley: 2007.

2. García, S.; Fischer, H.; Van Der Zwaag, S., A critical appraisal of the potential of self healing polymeric coatings. *Progress in Organic Coatings* **2011,** *72* (3), 211-221.

3. White, S. R.; Sottos, N. R.; Geubelle, P. H.; Moore, J. S.; Kessler, M. R.; Sriram, S. R.; Brown, E. N.; Viswanathan, S., Autonomic healing of polymer composites. *Nature* **2001,** *409* (6822), 794-7.

4. Zhu, D. Y.; Rong, M. Z.; Zhang, M. Q., Self-healing polymeric materials based on microencapsulated healing agents: From design to preparation. *Progress in Polymer Science* **2015,** *49*, 175-220.

5. Wen, N.; Song, T.; Ji, Z.; Jiang, D.; Wu, Z.; Wang, Y.; Guo, Z., Recent advancements in self-healing materials: Mechanicals, performances and features. *Reactive and Functional Polymers* **2021,** *168*, 105041.

6. Bekas, D. G.; Tsirka, K.; Baltzis, D.; Paipetis, A. S., Self-healing materials: A review of advances in materials, evaluation, characterization and monitoring techniques. *Compos Part B-Eng* **2016,** *87*, 92-119.

7. Lee, J. K.; Hong, S. J.; Liu, X.; Yoon, S. H., Characterization of dicyclopentadiene and 5-ethylidene-2-norbornene as self-healing agents for polymer composite and its microcapsules. *Macromolecular Research* **2004,** *12* (5), 478-483.

8. Yin, T.; Rong, M. Z.; Zhang, M. Q.; Yang, G. C., Self-healing epoxy composites–preparation and effect of the healant consisting of microencapsulated epoxy and latent curing agent. *Compos Sci Technol* **2007,** *67* (2), 201-212.

9. Jin, H.; Mangun, C. L.; Stradley, D. S.; Moore, J. S.; Sottos, N. R.; White, S. R., Self-healing thermoset using encapsulated epoxy-amine healing chemistry. *Polymer* **2012,** *53* (2), 581-587.

10. Ahangaran, F.; Hayaty, M.; Navarchian, A. H.; Pei, Y.; Picchioni, F., Development of self-healing epoxy composites via incorporation of microencapsulated epoxy and mercaptan in poly (methyl methacrylate) shell. *Polymer Testing* **2019,** *73*, 395-403.

11. Song, Y.-K.; Chung, C.-M., Repeatable self-healing of a microcapsule-type protective coating. *Polymer Chemistry* **2013,** *4* (18), 4940-4947.

12. Hia, I. L.; Vahedi, V.; Pasbakhsh, P., Self-healing polymer composites: Prospects, challenges, and applications. *Polymer Reviews* **2016,** *56* (2), 225-261.

13. Zhong, N.; Post, W., Self-repair of structural and functional composites with intrinsically self-healing polymer matrices: A review. *Composites Part A: Applied Science and Manufacturing* **2015,** *69*, 226-239.

14. Sung, S.; Kim, S. Y.; Lee, T. H.; Favaro, G.; Park, Y. I.; Lee, S.-H.; Ahn, J. B.; Noh, S. M.; Kim, J. C., Thermally reversible polymer networks for scratch resistance and scratch healing in automotive clear coats. *Progress in Organic Coatings* **2019,** *127*, 37-44.

15. Liu, M.; Zhong, J.; Li, Z.; Rong, J.; Yang, K.; Zhou, J.; Shen, L.; Gao, F.; Huang, X.; He, H., A high stiffness and self-healable polyurethane based on disulfide bonds and hydrogen bonding. *European Polymer Journal* **2020**, 109475.

16. Zhang, F.; Ju, P.; Pan, M.; Zhang, D.; Huang, Y.; Li, G.; Li, X., Self-healing mechanisms in smart protective coatings: A review. *Corrosion Science* **2018,** *144*, 74-88.

17. Cheng, M.; Fu, Q.; Tan, B.; Ma, Y.; Fang, L.; Lu, C.; Xu, Z., Build a bridge from polymeric structure design to engineering application of self-healing coatings: A review. *Progress in Organic Coatings* **2022,** *167*, 106790.

18. Yang, Y.; Urban, M. W., Self-Healing of Polymers via Supramolecular Chemistry. *Advanced Materials Interfaces* **2018,** *5* (17), 1800384.

19. Thangavel, G.; Tan, M. W. M.; Lee, P. S., Advances in self-healing supramolecular soft materials and nanocomposites. *Nano convergence* **2019,** *6* (1), 29.

20. Hoogenboom, R., Hard Autonomous Self-Healing Supramolecular Materials—A Contradiction in Terms? *Angewandte Chemie International Edition* **2012,** *51* (48), 11942-11944.

21. Chen, Y.; Kushner, A. M.; Williams, G. A.; Guan, Z., Multiphase design of autonomic self-healing thermoplastic elastomers. *Nature chemistry* **2012,** *4* (6), 467.

22. Chen, Y.; Guan, Z., Multivalent hydrogen bonding block copolymers self-assemble into strong and tough self-healing materials. *Chem Commun* **2014,** *50* (74), 10868-10870.

23. Hentschel, J.; Kushner, A. M.; Ziller, J.; Guan, Z., Self-healing supramolecular block copolymers. *Angew Chem Int Ed Engl* **2012,** *51* (42), 10561-5.

24. Beijer, F. H.; Sijbesma, R. P.; Kooijman, H.; Spek, A. L.; Meijer, E. W., Strong Dimerization of Ureidopyrimidones via Quadruple Hydrogen Bonding. *J Am Chem Soc* **1998,** *120* (27), 6761-6769.

25. Liu, T.; Zhao, H.; Zhang, D.; Lou, Y.; Huang, L.; Ma, L.; Hao, X.; Dong, L.; Rosei, F.; Lau, W. M., Ultrafast and high-efficient self-healing epoxy coatings with active multiple hydrogen bonds for corrosion protection. *Corrosion Science* **2021,** *187*, 109485.
26. Hu, J.; Mo, R. B.; Jiang, X.; Sheng, X. X.; Zhang, X. Y., Towards mechanical robust yet self-healing polyurethane elastomers via combination of dynamic main chain and dangling quadruple. *Polymer* **2019,** *183*.
27. Cui, X. Y.; Zhang, C.; Camilo, R. P.; Zhang, H.; Cobaj, A.; Soucek, M. D.; Zacharia, N. S., Self-Healing Latex Containing Polyelectrolyte Multilayers. *Macromolecular Materials and Engineering* **2018,** *303* (8).
28. Qiu, T.; Wang, X. J.; Lin, X. Y.; Zhu, Z. Q.; Li, X. Y.; Guo, L. H., Emulsion polymerization to synthesize self-healing films toward healing on fractures: A feasible strategy. *Journal of Polymer Science Part a-Polymer Chemistry* **2016,** *54* (19), 3071-3078.
29. Chen, Y.; Jones, S. T.; Hancox, I.; Beanland, R.; Tunnah, E. J.; Bon, S. A. F., Multiple Hydrogen-Bond Array Reinforced Cellular Polymer Films from Colloidal Crystalline Assemblies of Soft Latex Particles. *Acs Macro Letters* **2012,** *1* (5), 603-608.
30. Zhang, J.; Qi, S.; Zhang, C.; Fan, Z.; Ding, Q.; Mao, S.; Dong, Z., Controlling Keto–Enol Tautomerism of Ureidopyrimidinone to Generate a Single-Quadruple AADD-DDAA Dimeric Array. *Organic Letters* **2020,** *22* (18), 7305-7309.
31. Appel, W. P. J.; Portale, G.; Wisse, E.; Dankers, P. Y. W.; Meijer, E. W., Aggregation of Ureido-Pyrimidinone Supramolecular Thermoplastic Elastomers into Nanofibers: A Kinetic Analysis. *Macromolecules* **2011,** *44* (17), 6776-6784.
32. Liu, X.; Gallavardin, T.; Burel, F.; Vuluga, D., Influence of quadruple hydrogen bonding on polyvinyl butyral resin properties. *Polymer Degradation and Stability* **2023,** *208*, 110243.
33. Faghihnejad, A.; Feldman, K. E.; Yu, J.; Tirrell, M. V.; Israelachvili, J. N.; Hawker, C. J.; Kramer, E. J.; Zeng, H., Adhesion and surface interactions of a self-healing polymer with multiple hydrogen-bonding groups. *Advanced Functional Materials* **2014,** *24* (16), 2322-2333.
34. Chen, S.; Mahmood, N.; Beiner, M.; Binder, W. H., Self-Healing Materials from V- and H-Shaped Supramolecular Architectures. *Angew Chem Int Ed Engl* **2015,** *54* (35), 10188-92.

35. Zhang, L.; Wang, D.; Xu, L.; Zhang, X.; Zhang, A.; Xu, Y., A highly stretchable, transparent, notch-insensitive self-healing elastomer for coating. *J Mater Chem C* **2020,** *8* (6), 2043-2053.

36. Kushner, A. M.; Vossler, J. D.; Williams, G. A.; Guan, Z., A Biomimetic Modular Polymer with Tough and Adaptive Properties. *J Am Chem Soc* **2009,** *131* (25), 8766-8768.

37. Zhang, M. Q.; Rong, M. Z., Application of alkoxyamine in self-healing of epoxy. *Journal of Materials Chemistry A* **2014,** *2* (18), 6558-6566.

38. Ling, J.; Rong, M. Z.; Zhang, M. Q., Coumarin imparts repeated photochemical remendability to polyurethane. *Journal of Materials Chemistry* **2011,** *21* (45), 18373-18380.

39. Heo, Y.; Malakooti, M. H.; Sodano, H. A., Self-healing polymers and composites for extreme environments. *Journal of Materials Chemistry A* **2016,** *4* (44), 17403-17411.

40. Guo, B.; Ji, X.; Chen, X.; Li, G.; Lu, Y.; Bai, J., A highly stretchable and intrinsically self-healing strain sensor produced by 3D printing. *Virtual and Physical Prototyping* **2020,** *15* (sup1), 520-531

Chapter 3. A Self-Healing Crosslinker

ABSTRACT

Self-healing technology offers the ability to repair and pre-emptively prevent crack formation in waterborne acrylic latex coatings. This can be achieved by functionalizing the acrylic polymers with the strong self-complementary hydrogen bonding unit, UPy, which provides a driving force for polymer rearrangement and self-healing. However, the self-healing efficiency of such a system remains modest, especially under ambient conditions. In order to enhance self-healing efficiency, a UPy functionalized crosslinker system was designed which could be added to a self-healing acrylic latex prior to coating formation. Such a crosslinker system offers the ability to increase the amount of UPy units in the coating, and potentially offset undesirable UPy self-complementation in the latex particles before coating formation. Given the poor solubility of UPy-based systems, two specific crosslinker architectures of varying molecular weights were designed based on hydrophilic polyethylene glycol: 1) linear poly(ethylene glycol) (PEG) crosslinkers end-capped by UPy moieties (UPy-Linear), termed UPy-XL-1 to 4; and 2) poly(poly(ethylene glycol methacrylate)) (poly(PEGMA)) brushes with 2 UPy units per polymer chain (UPy-Brush), termed UPy-Brush-5, 10 and 20. The crosslinkers with brush architecture represented the most promising design due to their enhanced solubility compared to the linear crosslinkers, and thus were incorporated into both a control and UPy-2 functionalized latex. Of the three UPy-Brush crosslinkers, UPy-Brush-10 displayed the strongest optical self-healing performance, and yielded enhanced self-healing at room temperature compared to the UPy-2 functionalized latex — ~38% as opposed to ~27%.

3.1 INTRODUCTION

As self-healing technology has rapidly accelerated over the past 20 years, a wide range of self-healing coatings have been successfully designed and highly optimized. However, designing a mechanically strong acrylic coating which can efficiently self-heal under ambient conditions remains exceedingly challenging. In fact, a coating which maintains robust mechanical strength while achieving highly efficient intrinsic self-healing has been described as a ‘contradiction in

terms'.[1] This is because intrinsic self-healing is inextricably linked to polymer mobility, as for self-healing to occur, polymeric segments must be mobile enough to reform due to the attractive forces of either reversible covalent bonds or supramolecular bonds.[1-4] Supramolecular bonds offer the best chance to design an acrylic coating which can self-heal at room temperature, but require the rearrangement of polymer chains to reform bonds broken by damage. Almost by definition, a mechanically strong acrylic coating is comprised of polymers which are hard, highly entangled and have significantly reduced mobility. The lack of progress regarding a self-healing acrylic coating design is highly undesirable, given that the majority of paints are based on a waterborne acrylic latex. Therefore, solving this dilemma and designing a strong self-healing coating is the subject of a significant research effort.

One plausible method to combine suitable mechanical strength with efficient self-healing is to introduce soft self-healing sections to a hard material, creating what is sometimes referred to as a multiphasic material.[5] This can involve the long flexible polymers grafted with healing functionality, where the polymers' increased mobility and degrees of freedom enhance self-healing efficiency. Multiphasic materials can also involve the introduction of smaller, highly mobile oligomers grafted with healing functionality. This second method is the basis by which ceramic automotive coatings self-healing at temperatures typically ranging from 50 to 60˚C.[2] The introduction of a hydrogen bonding network based on an acrylic monomer functionalized with 2-ureido-4[1H]-pyrimidinone (UPy) is a promising strategy to design a self-healing acrylic coating. Such a design relies both on UPy's self-complementary quadruple hydrogen bonding, which provides a strong self-healing driving force, as well as the presence of a long flexible spacer, which enhances polymer mobility and self-healing efficiency. A self-healing acrylic coating based on this UPy functionalized monomer design was shown in Chapter 2. It demonstrated the ability to self-heal at room temperature with an efficiency of ~25%, while maintaining sufficient mechanical strength.

In order to increase the self-healing efficiency of this self-healing acrylic coating, a UPy-functionalized crosslinker system was designed and investigated. The UPy-crosslinker was intended to be added to the aqueous phase of a UPy functionalized waterborne acrylic latex, and form a hydrogen bonding network with the UPy units in the latex polymers upon coalescence (Figure 3.1). Such a crosslinker system yields a number of potential benefits. First, it allows for a significantly greater number of UPy units to be incorporated into the coating. This results in a stronger and more highly concentrated hydrogen bonding network. Second, it

allows for the formation of hydrogen bonds between the UPy moieties grafted to the crosslinker and the UPy moieties attached to the latex polymers. This serves to reduce potentially undesirable UPy-UPy interactions within the latex particles, leading to a more evenly distributed hydrogen bonding network. Finally, the presence of a UPy functionalized crosslinker which is small and untethered to the high-MW acrylic polymers may yield significantly enhanced mobility and UPy rearrangement potential. Mobility-based crosslinker self-healing is somewhat analogous to the way in which automotive ceramic coatings self-heal at elevated temperatures. This final potential benefit is a double-edged sword, however, as the impact such a soft material has on other coating mechanical properties, such as Young's modulus, must be carefully monitored.

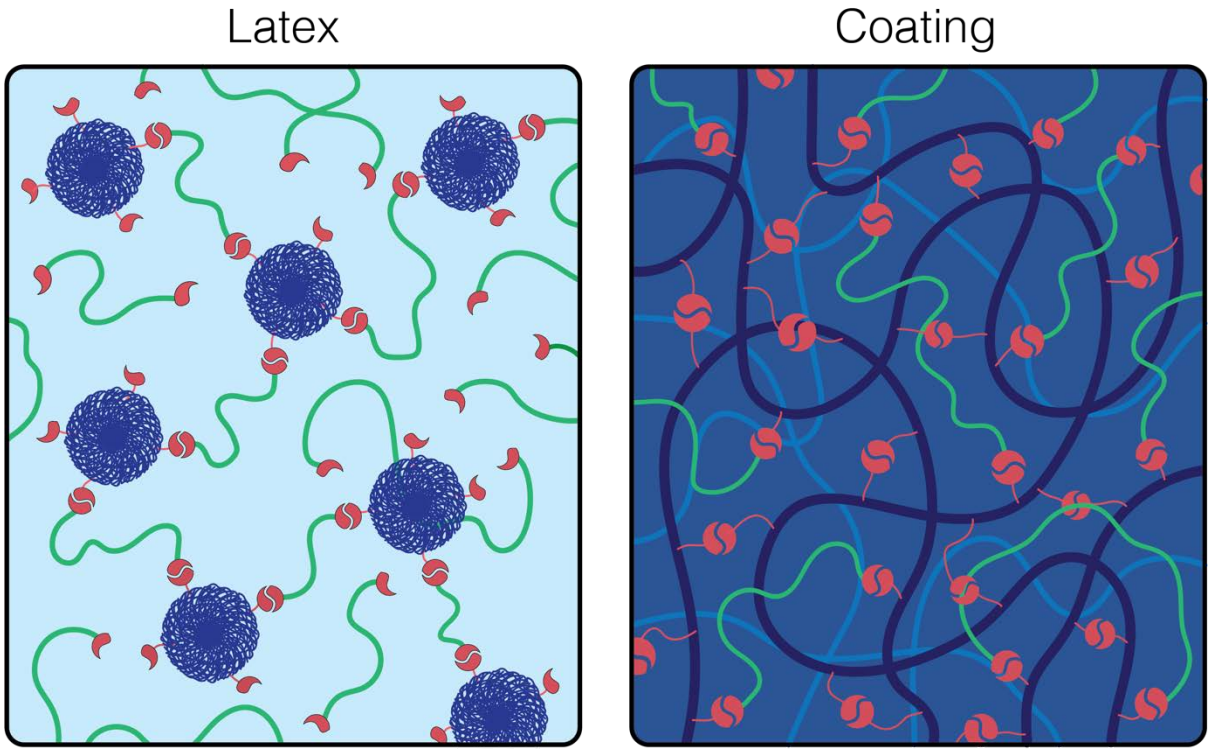

Figure 3.1 A system comprising a UPy-based crosslinker added to a UPy-functionalized MMA/BA/AA acrylic latex. The UPy crosslinker (green) is stable in a mixture of water and latex particles (blue). As the latex dries, the UPy units (red) form a hydrogen bonded network in the coating, resulting in self-healing capability.

Designing a UPy-functionalized crosslinker which can be added to an acrylic latex is no trivial task. Such a crosslinker must be hydrophilic, or at least hydrophilic enough to remain stable in a waterborne latex, which is a significant challenge, due to the strong self-complementation of

the UPy unit. In fact, hydrophilic UPy-based compounds that can dissolve in an aqueous environment are exceedingly rare. The vast majority of hydrophilic materials with a significant portion of UPy functionality are hydrogels. These hydrogels are typically longer hydrophilic polymers, where the UPy unit represents a crosslinking point either within the polymer backbone, or as a side chain grafted to the backbone.[6] Recent research has also incorporated UPy functionality into the hydrophilic shell component of core-shell nanoparticles for drug delivery, normally by associating the UPy unit with a hydrophilic polymer.[7]

Two different UPy functionalized crosslinkers were designed based on poly(ethylene glycol) (PEG), which is a stable, relatively cheap, and non-toxic hydrophilic polymer that is widely used in industry.[8] The two crosslinker designs were based on different architectures of PEG, so as to address solubility concerns based on UPy-UPy self-complementation. The first design, termed UPy-Linear, involved grafting UPy moieties onto both ends of a linear PEG chain (Figure 3.2).

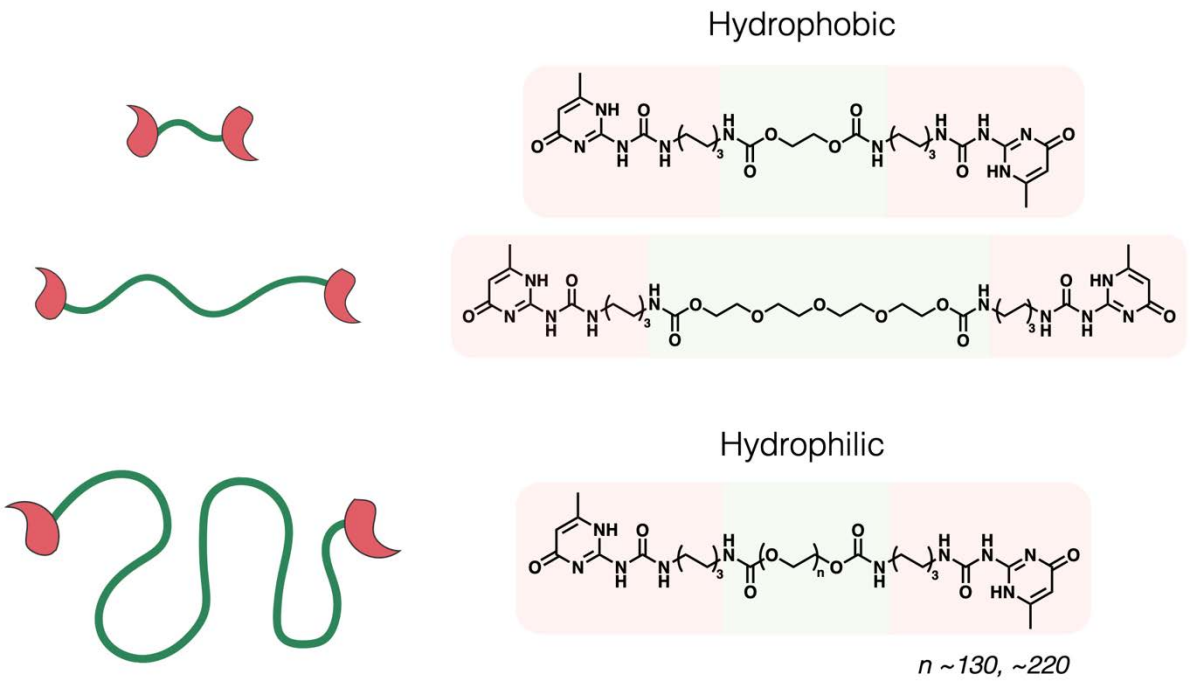

Figure 3.2 A UPy crosslinker design based on linear PEG. UPy units were grafted onto a hydrophilic PEG chain to create the crosslinkers. A library of four crosslinkers were synthesized with variable PEG lengths (*n* = 0, 4, ~ 130, ~ 220). Respectively, the first two crosslinkers with a smaller PEG length represent a hydrophobic design, and the two crosslinkers with a longer PEG chain represent a hydrophilic design.

The grafting of UPy functionality to both ends of a linear PEG chain through a hydroxyl–isocyanate reaction is one-pot and facile. It was hoped that the hydrophilicity of PEG would allow either complete solubility of the crosslinker, or that the UPy units would stably associate with the hydrophobic regions of the latex particles, while the PEG chain remained in the aqueous phase. By varying the length of the PEG chain, a library of four UPy-Linear crosslinkers was synthesized, spanning a range of hydrophilicity. The four crosslinkers each had PEG units of *n* = 1, 4, ~130 and ~220, and were termed UPy-XL-1, UPy-XL-2, UPy-XL-3 and UPy-XL-4 respectively. These UPy-Linear crosslinkers are somewhat similar to paint thickeners, which typically contain a very long PEG chain (*n* = 200 – 800), end-capped with two hydrophobic groups.[9] Therefore, a crosslinker length of ~220 was selected as the maximum length, given the possibility that higher PEG lengths might noticeably affect the viscosity and rheological properties of the latex.

As previously alluded to, solubility is likely a determining factor in the success of this UPy-Linear crosslinker system, and hence is a parameter that must be sufficiently optimized. In the case of extremely poor crosslinker solubility, precipitation occurs, meaning that the crosslinkers never form part of the self-healing coating. In the case of poor solubility, the crosslinker cannot exist stably in the latex, leading to self-crosslinking, aggregation, and the formation of nanostructures, likely drastically minimizing their self-healing potential. Therefore, a second UPy crosslinker design was investigated. This new crosslinker system was intended to have even greater aqueous solubility than the UPy-Linear crosslinkers.

Designing a polymeric system which is more hydrophilic than PEG is somewhat of a conceptual challenge, as PEG is considered the benchmark in hydrophilic polymer design.[10] Utilizing charged polymers such as polyelectrolytes is a plausible method to enhance hydrophilicity, however these polymers can be prone to form nanostructures and gels.[11] Moreover, such charged species are pH responsive, which presents two additional complexities. First, latex production in a wider industrial setting generally spans a range of moderately acidic to highly basic conditions, which may lead to pH-induced solubility issues in the case of charge crosslinker systems. Second, pH is a parameter that is carefully monitored in latex production, and would no doubt be affected by the addition of species with acidic or basic moieties.

Varying the architecture of linear PEG is another promising strategy to enhance water-solubility. Studies which have examined the relationship between PEG architecture and hydrophilicity report that nonlinear architectures such as brush, branched and dendritic polymers are generally more water-soluble than linear PEG.[12-15] The exact mechanism underlying this solubility effect is not well understood, although it is probably related to the maximized surface area/density of hydrophilic ethylene glycol units in non-linear polymers as compared to linear polymers.[16] Thus, to enhance aqueous solubility, a second UPy functionalized crosslinker was designed based on non-linear PEG with a brush architecture (Figure 3.3).

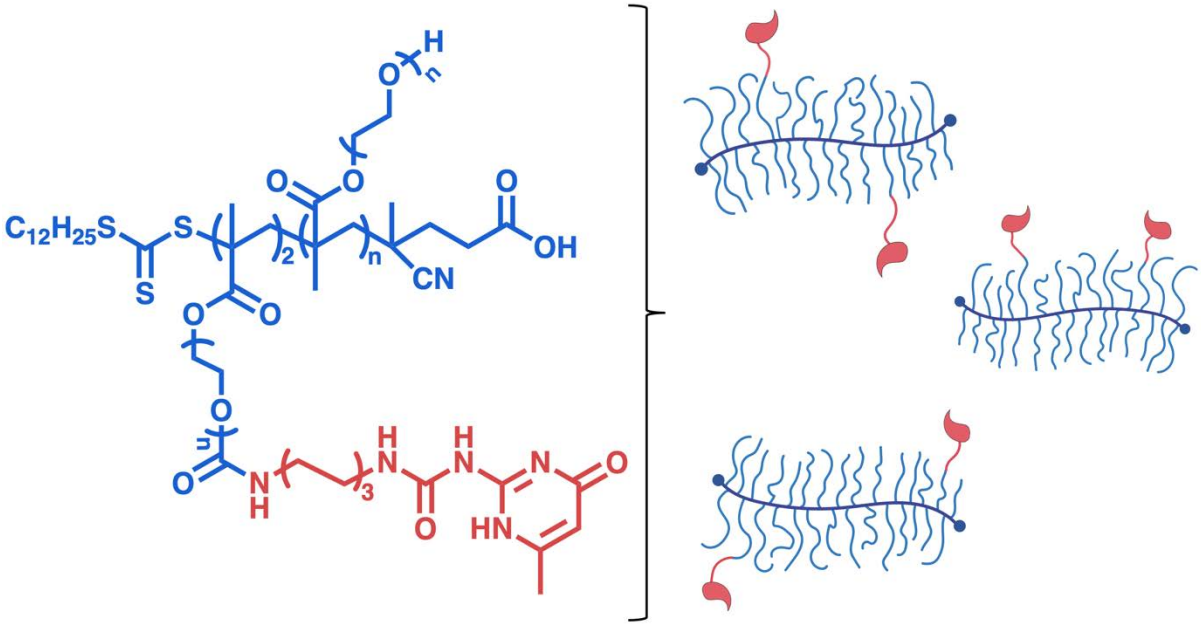

Figure 3.3 The UPy-Brush crosslinker design. UPy units were grafted onto a PEGMA brush polymer to create the crosslinkers. Three UPy-Brush crosslinkers were synthesized, with molecular weights of approximately 5, 10 and 20 kDa. Each crosslinker had on average two UPy moieties per polymer chain.

Specifically, this involved synthesizing a brush polymer, whereby PEG units in the form of poly(ethylene glycol methacrylate) (PEGMA) comprised individual brushes along a central polymer backbone. Following the formation of this brush, two UPy units were grafted to the crosslinker via a hydroxyl–isocyanate reaction. A total of three separate UPy-functionalized brush crosslinkers (UPy-Brush) were synthesized, each with varying molecular weights. These three UPy-Brushes were termed UPy-Brush-5, UPy-Brush-10 and UPy-Brush-20, as they had MWs of ~5, 10 and 20 kDa respectively.

Grafting UPy functionality onto this PEGMA brush polymer with any specificity or consistency requires accurate knowledge of the polymer's MW and thus its number of PEG side chains per polymer chain, as well as a somewhat monodisperse population of polymer chains. Synthesizing a brush polymer which meets these criteria is not possible via conventional radical polymerization methods, which would yield a heterogeneous mixture of very high MW polymers.[17] Reversible addition–fragmentation chain-transfer (RAFT) polymerization, on the other hand, is far more promising for this purpose. RAFT polymerization makes use of a chain transfer agent which controls an active/dormant

equilibrium between polymer chains, yielding slower and more even polymer growth.[18, 19] The resulting polymers are highly monodisperse, and both MW and architecture can be easily controlled.[20, 21]

The four UPy-Linear crosslinkers (UPy-XL-1 to 4), and the three UPy-Brush crosslinkers (UPy-Brush-5, 10 and 20), were successfully synthesized, and the aqueous solubility of each crosslinker was tested. All four of the UPy-Linear crosslinkers displayed poor solubility, either immediately precipitating, in the case of UPy-XL-1 and 2, or forming an unstable opaque solution, in the case of UPy-XL-3 and 4. The UPy-Brush crosslinkers, on the other hand, were soluble in water. When added to a latex, all three UPy-Brushes were found to affect the mechanical properties of the resulting coating, noticeably reducing Young's modulus by a factor of between 3 and 6, while reducing the glass transition temperature (*T*g) by 3 to 7˚C. The UPy-Brush coatings displayed strong optical self-healing capability at both room temperature and 50˚C, particularly in the case of UPy-Brush-10. The self-healing efficiency of the UPy-Brush crosslinkers was compared with the monomeric self-healing acrylic coating described in Chapter 2. Interestingly, though neither UPy-Brush-5 or UPy-Brush-20 enhanced self-healing efficiency, UPy-Brush-10 yielded a ~10% increase in self-healing efficiency. This finding shows that a specifically tailored UPy functionalized crosslinker can increase the self-healing efficiency of an acrylic coating, providing a useful strategy for the enhancement of future self-healing coating designs. Furthermore, the performance of these UPy functionalized crosslinkers yield valuable information regarding the mechanisms that underpin intrinsic self-healing in higher strength coatings, which is a complex, multifaceted process.

3.2 EXPERIMENTAL

3.2.1 Materials

2-Amino-4-hydroxy-6-methylpyrimidine, poly(ethylene glycol) methacrylate (PEGMA) (MW= 500 Da), hexamethylene diisocyanate, dibutyl tin dilaurate catalyst (DBTDL), methyl methacrylate (MMA), butyl acrylate (BA), acrylic acid (AA), sodium dodecyl sulfate (SDS), ammonium persulfate, tetraethylene glycol, linear polyethylene glycol (MW = 6 and 10 kDa appx.), azobisisobutyronitrile (AIBN), 4-cyano-4-[(dodecylsulfanylthiocarbonyl) sulfanyl]pentanoic acid (97%) (RAFT agent), chloroform ($CHCl_3$), dimethyl sulfoxide (DMSO), dimethylformamide (DMF) and dioxane were all purchased from Sigma Aldrich and used as received. The 3.5 kDa MWCO dialysis 'snakeskin' bag (Thermo-Fischer Scientific) was used according to the instructions.

3.2.2 Characterization

^{1}H-NMR spectroscopy was performed on a 400 MHz Varian 400 MR spectrometer using deuterated chloroform (CDCl3) as the solvent. ^{1}H NMR analysis was performed on MestreNova software. GPC analysis was performed on a Shimadzu system equipped with a Waters Styragel column (10μm pore size). THF was used as the eluent with a flow rate of 1 mL/min. The molecular weight and polydispersity of the samples were calculated relative to *poly*(methyl methacrylate) (PMMA) standards. Samples were prepared at 2 mg/mL and filtered with a syringe filter (0.45μm) prior to measurement. IR spectroscopy was performed on a Perkin Elmer Spectrum 2 ATR-FTIR spectrometer. Tensile tests were carried out on an Instron 5944, 2kN microtester. Differential scanning calorimetry was performed on a Perkin Elmer 8500 Double Furnace HyperDSC from –50 to 70˚C at 10˚C per min.

3.2.3 Synthesis of the crosslinkers

Two separate UPy functionalized crosslinkers were synthesized: a linear crosslinker, formed from the grafting of two UPy units to a linear PEG chain of variable MW; and a brush crosslinker, formed from the grafting of UPy units to a PEG brush polymer, synthesized through RAFT polymerization. Their synthetic pathways are shown in Scheme 1 below.

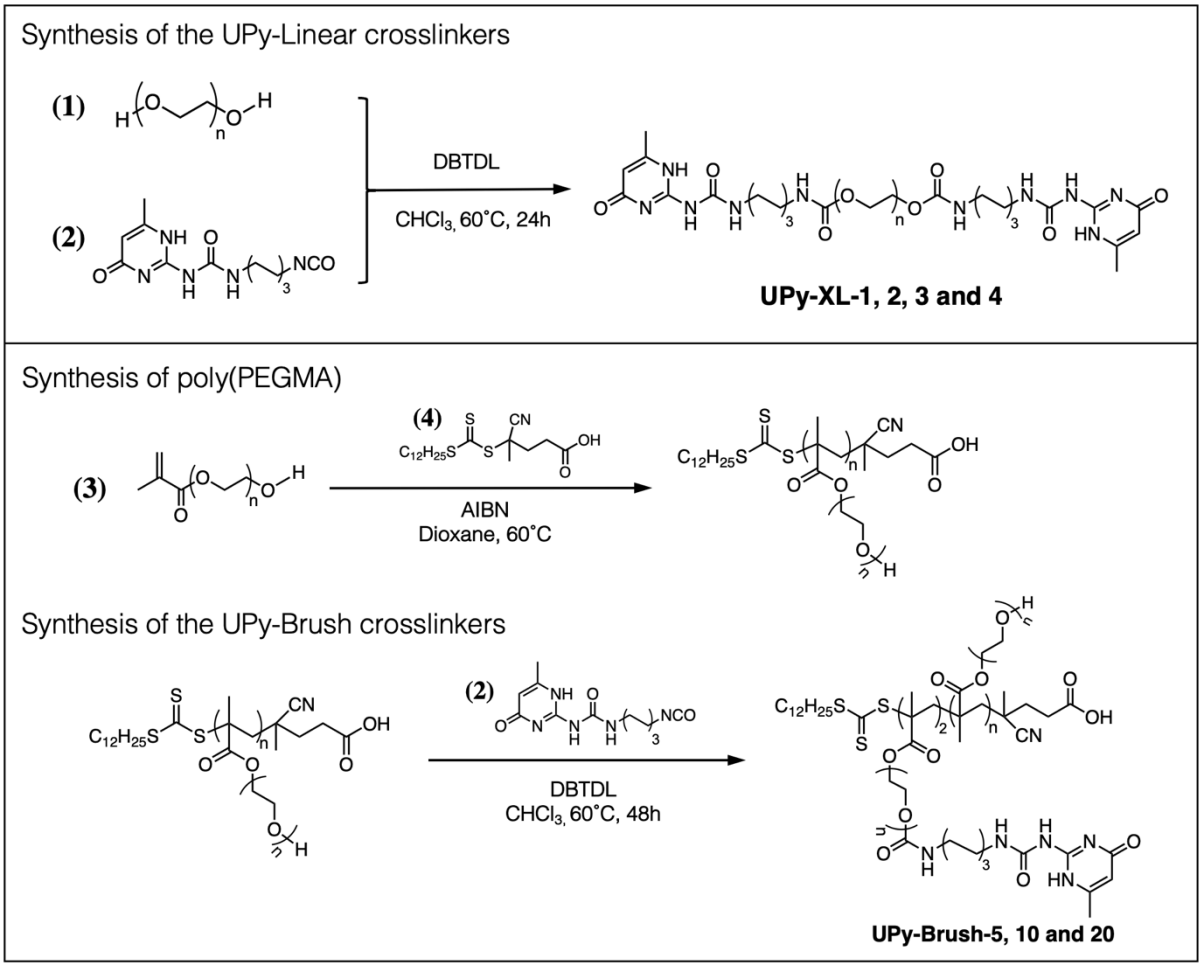

Scheme 1. The synthesis of the linear UPy crosslinkers, the PEGMA brush polymers, and the UPy-functionalized brush crosslinkers.

3.2.3.1 Synthesis of 2(6-isocyanatohexylaminocarbonylamino)-6-methyl-4[1H] pyrimidinone (2)

2-Amino-4-hydroxy-6-methylpyrimidine (1.0 g, 8.0 mmol) was added in hexamethylene diisocyanate (8.0g, 48 mmol). The mixture was then heated to 100℃ and stirred for 20 hours under nitrogen. After this time, 20mL of pentane was added to precipitate the product. The product was dried under vacuum to yield a white powder. ^{1}H NMR (400 MHz, DMSO): δ (ppm) 5.8 (OC-C*H*-CCH3), 3.2 (Hexyl chain), 2.2 (*CH3*-C-NH), 1.4–1.6 (Hexyl chain), 10.6 12.0 and 13.1 (UPy–UPy hydrogen bonding). FTIR: v 2900 (CONH), 2270 (NCO), 1700 (aryl C=O) 1650 (NCON) 1100 (C-O).

3.2.3.2 Synthesis of the UPy-2 monomer

2(6-isocyanatohexylaminocarbonylamino)-6-methyl-4[1H] pyrimidinone was added to a solution of polyethylene glycol methyl methacrylate (PEGMA, MW = 500 Da) in dry chloroform at 1:1 mol ratio. The mixture was heated to 60˚C under a nitrogen atmosphere, and a few drops of the catalyst, DBTDL, were added. The reaction was then left to stir until all of the isocyanate precursor had converted. This was monitored via the IR peak at 2200 cm^{-1}. The product was then dried under vacuum. ^{1}H NMR (400 MHz, $CDCl_3$): ∂ (ppm) 6.1 and 5.6 (CH_3–CCH_2–CO), 5.8 (OC–*CH*–CCH_3), 4.0–4.4 and 3.6–3.8 (PEG chain), 3.1–3.4 (Hexyl chain), 2.2 (*CH*$_3$–C–NH), 1.8 (*CH*$_3$–CCH_2), 1.4–1.6 (Hexyl chain), 10.5, 12.0 and 13 (UPy–UPy hydrogen bonds). FTIR: v 2900 (CONH), 1700 (aryl C=O), 1650 (NCON) 1100 (C–O).

3.2.3.3 Synthesis of the UPy-Linear crosslinkers:

Ethylene glycol, tetraethylene glycol or linear polyethylene glycol (MW = 6000 or 10,000 Da) (1) was dissolved in dry chloroform, into which UPy-NCO (2) was added. In order to react fully with both hydroxyl ends of the linear PEG chain, the UPy isocyanate precursor was added in excess at a 3:1 mol ratio. The reaction was heated to 60˚C under an inert nitrogen atmosphere, and a few drops of the catalyst, DBTDL, were added. The reaction was left to stir for 24 hours. Subsequently, ~ 500 mg of silica and three more drops of the catalysts was added to the reaction, which was left to stir for a further 2 hours. Finally, the reaction was filtered to remove the silica, and the product was dried under vacuum. The ethylene glycol and tetraethylene glycol based crosslinkers were dull-pink and white powders respectively, while the longer PEG chain crosslinkers were rocky white solids. ^{1}H NMR (400 MHz, $CDCl_3$): ∂ (ppm) 5.8 (OC–*CH*–CCH_3), 4.0–4.4 and 3.6–3.8 (PEG chain), 3.1–3.4 (Hexyl chain), 2.2 (*CH*$_3$–C–NH), 1.4–1.6 (Hexyl chain), 10.5, 12.0 and 13 (UPy–UPy) hydrogen bonds). FTIR: v 2900 (CONH), 1700 (aryl C=O), 1650 (NCON) 1100 (C–O).

3.2.3.4 Synthesis of the PEGMA brush polymers

RAFT polymerization was used to synthesize a library of polyethylene glycol brush polymers with varying molecular weights: (5, 10 and 20 kDa). The relative amount of each reactant is shown in the table below.

Polymer MW (kDa)	**PEGMA (mmol)**	**PEGMA (g)**	**RAFT agent (mmol)**	**AIBN (mmol)**	**Time (h)**
5	6	3	0.12	0.012	4
10	6	3	0.12	0.012	7
20	6	3	0.03	0.003	4

PEGMA (3), the RAFT agent 4-cyano-4-[(dodecylsulfanylthiocarbonyl)sulfanyl] pentanoic acid, and the initiator AIBN were dissolved in dioxane. The solution was then thoroughly degassed via four freeze-pump-thaw cycles to completely remove residual oxygen. The solution was then backfilled with nitrogen, and the reaction proceeded under gentle stirring at 60˚C. Termination of the reaction was achieved by exposing the reaction to air. The resultant polymers were purified via precipitation in diethyl ether five times to remove unreacted monomer. The brush polymers were yellowish and had a viscous, honey-like consistency. ^{1}H NMR (400 MHz, $CDCl_3$): ∂ (ppm) 4.0–4.4 and 3.6–3.8 (PEG chain), 2.1–1.6 (backbone C–*CH_2*–C), 1.3–1.2 (CH_2–*C_8H_{16}*–CH_3), 1.1–0.8 (backbone CH_2–C–*CH_3*).

3.2.3.5 Synthesis of the UPy-Brush crosslinkers

The PEGMA brush polymers (~5, ~10 and ~20 kDa) were dissolved in dry DMF. UPy-NCO (2) was added into this solution at a mol ratio of 2:1, so as to functionalize two brushes per polymer chain with the UPy moiety. The reaction was heated to 80˚C and, once the material was dissolved, a few drops of DBTDL catalyst was added. IR spectroscopy showed the disappearance of the isocyanate peak after 48 hours, signalling that all the starting material had been grafted. The product was dried under vacuum, yielding a tacky solid ranging from yellow to dull orange depending on the MW of the brush. ^{1}H NMR (400 MHz, $CDCl_3$): ∂ (ppm) 5.8 (OC–*CH*–CCH_3), 4.0–4.4 and 3.6–3.8 (PEG chain), 3.1–3.4 (Hexyl chain), 2.2 (*CH_3*–C–NH), 2.1–0.8 (brush backbone) 10.5, 12.0 and 13 (UPy–UPy hydrogen bonds).

3.2.4 Emulsion polymerization

REACTANTS	SOLIDS (wt%)
Butyl acrylate	47
Methyl methacrylate	47
Acrylic acid	2
UPy-2	2.5
Sodium dodecyl sulfate	1.2
Ammonium persulfate	0.3

The emulsion polymerization was performed in de-ionized water with a solid content of 20 wt%. Initially, the surfactant (sodium dodecyl sulfate) was dissolved in de-ionized water (11 mM). This solution was deoxygenated under a nitrogen atmosphere and heated in an oil bath until an internal temperature probe displayed 80˚C. Following this, two separate feeds were prepared, the first was the monomer feed containing butyl acrylate, methyl methacrylate, acrylic acid and dissolved UPy-2 if required. The second feed was the initiator (ammonium persulfate) dissolved in de-ionized water which was made up to the same volume as the monomer feed. Both these feeds were simultaneously fed into the reactor over a 3 hour period. Following this, the reaction was left to run for a further hour for a total reaction time of 4 hours. The resulting latex was purified via dialysis for a week (MWCO 3.5 kDa), displacing water twice a day.

3.2.5 Pencil hardness test

The surface hardness of the coatings (described in section 3.2.6) was determined via the pencil hardness test. The coatings were cleaned to remove dust or other impurities on the surface. A series of pencils ranging in hardness from 6B to 2H were conditioned by grinding on a piece of abrasive paper. The pencils were checked to make sure the edges of the graphite were smooth and level, not nipped or chipped. The pencils were then placed at a 45˚ angle to the coating and pushed forward with firm pressure. The hardness was defined as the hardest pencil which fails to cut the film, and the experiment was performed three times with a fresh pencil edge.

3.2.6 Film formation and self-healing tests

To form the coatings, the latex was added to a silicone mold (30 mm x 30 mm x 1 mm) and left to dry at room temperature for 1 week and then at 50˚C for 2 days. As the water evaporated, the latex particles coalesced, forming the acrylic coating. Following this, the coating was cut into a rectangular shape (30 mm x 12 mm x 600 μm). The tensile tests were carried out under the following conditions: a strain rate of 3 mm/min, a gauge length (fixture separation) of 17 mm. An average result was calculated from three independent experiments.

To evaluate the strain recovery of the coatings (a measure of self-healing efficiency), a 5 mm long horizon cut was introduced to the coating via a razor blade. The coatings were then gently pressed together for 5 seconds and left to heal for 24 hours at RT and 50˚C. The healed samples were then subject to tensile tests. The Young's modulus (E) and the strain at which the healed crack reopened (ε, strain-at-break, failure strain) was noted and compared to the strain at which an undamaged coating began to break apart. Given the malleability of the coatings, there was no sudden fracturing of the undamaged coating, rather, the failure strain was noted when the crack opened and the coating began to 'unzip'. This is contrasted with what is often defined as the strain-at-break for brittle materials, where the material breaks suddenly into two parts.

3.3 RESULTS

3.3.1 UPy-Linear crosslinkers

A library of four UPy-crosslinkers were synthesized, whereby a linear PEG chain with varying molecular weight was end capped with UPy functionality (Figure 3) (Figures S31–40). This was achieved through a high yield hydroxyl–isocyanate reaction between both ends of the PEG chain and a UPy-isocyanate precursor. The reaction was allowed to run to completion, which was verified through the disappearance of the isocyanate peak at 2200 cm^{-1} in the IR spectrum. ^{1}H NMR verified that all four crosslinkers had been successfully grafted with UPy functionality, forming two hydrophobic crosslinkers, with PEG chain lengths of 0 and 4 units, and two hydrophilic designs, with PEG chain lengths of ~130 and ~220 units.

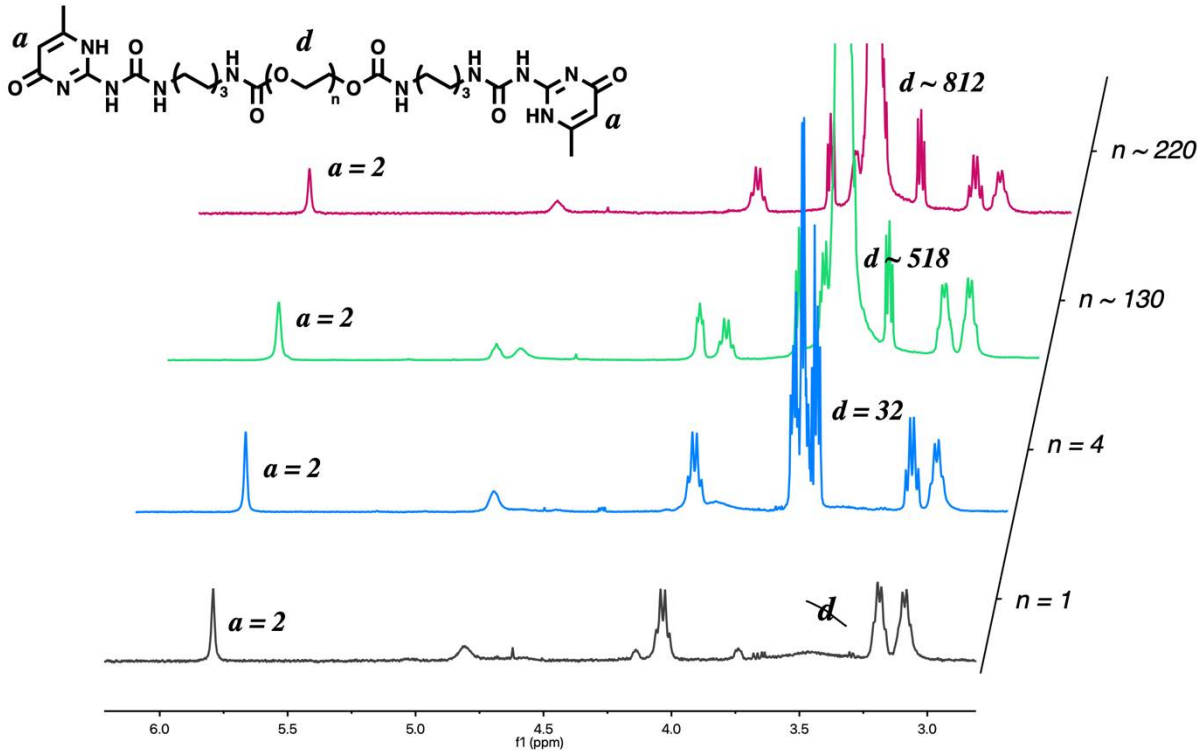

Figure 3.4 ^{1}H NMR spectra of the four UPy crosslinkers with varying PEG lengths. Two peaks, *a* and *d*, corresponding to UPy's pyridinone proton and the PEG chain respectively, are shown. The ratio between peak *a*, set to 2H, and peak *d* can be used to verify the successful synthesis of the UPy crosslinkers.

Figure 3.4 compares the integrated intensity of the peak *a* (~ 5.8 ppm), which corresponds to a single hydrogen on UPy's pyridinone moiety, to peak *d* (~ 3.5 ppm), which corresponds to four hydrogens for each unit of the PEG spacer. Given both PEG end groups are grafted with UPy functionality, integrating peak *a* to 2 gives the total numbers of hydrogens associated with the PEG chain (peak *d*). Dividing peak *d* by four gives the total number of PEG units for each crosslinker, which verifies that all four crosslinkers were completely grafted with UPy functionality. The exact integration values, as well as the fully assigned spectra, are shown in Figures S33–39. IR spectra of the four crosslinkers also showed that the grafting of UPy to each end of the linear PEG chain was completed, given the clear lack of a peak ~2200 cm^{-1}, which is indicative of the precursor's isocyanate moiety (Figures S32–40).

All four crosslinkers were solids, with UPy-XL-1 and UPy-XL-2 dull-pink and white powders respectively, and UPy-XL-3 and UPy-XL-4 harder, rocky white solids. The rationale behind these crosslinkers was to imitate associative thickeners, where the crosslinkers would dissolve into the aqueous phase of the latex, and the UPy units would associate with the monomeric UPy units in the latex, forming a stronger hydrogen bonding network in the resulting coating. In order to achieve this function, each crosslinker required enough aqueous solubility to remain stable in the latex. The solubility of all four crosslinkers was tested in both de-ionized water and in a UPy-2 functionalized latex. The crosslinkers were added to this latex at a mol ratio of 1:2, so that the number of UPy units in the latex particles was equal to the number of UPy units on the crosslinkers. This corresponded to 1.8, 2.1, 16.5 and 27.5 g/L for UPy-XL-1, 2, 3 and 4 respectively. The results are shown in Figure 3.5 below.

a)

Crosslinker	PEG length	Water	Latex
UPy–XL–1	n = 0	Insoluble	Insoluble
UPy–XL–2	n = 4	Insoluble	Insoluble
UPy–XL–3	n ~ 130	Opaque (stable < 1 day)	Precipitates
UPy–XL–4	n ~ 220	Opaque (stable ~ 3 days)	Precipitates (~ 3 days)

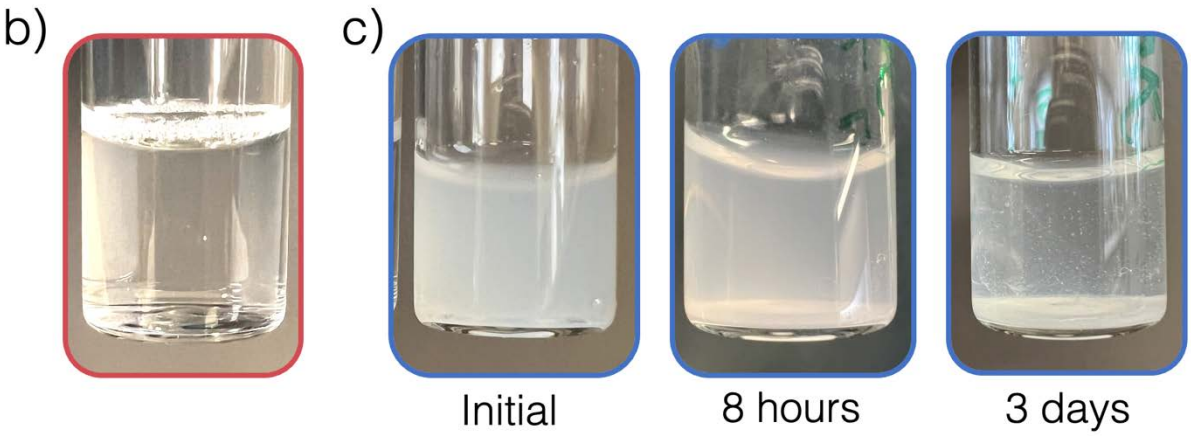

Figure 3.5 a) A table describing the stability of each crosslinker, UPy-XL-1 to 4, formed from a linear PEG chain functionalized with UPy end groups. Photographs were taken of the most soluble crosslinker, UPy-XL-4, in water after 8 hours and after 3 days (c), compared to linear PEG with a MW of 10 kDa (b).

Figure 3.5a underscores the poor solubility of all four crosslinkers. Specifically, the hydrophobic crosslinker designs, UPy-XL-1 and UPy-XL-2, displayed no solubility in water or stability in the latex, retaining their powdered form even under vigorous stirring. This result is unsurprising, given that the crosslinkers contain both a hexyl chain spacer and two UPy moieties, which are extremely hydrophobic, due to their tendency to form strong self-complementary bonds. The insolubility of these two UPy crosslinkers is emphasized by the fact that UPy-1, the short-chain UPy monomer discussed in Chapter 2, is also completely insoluble in water, the vast majority of organic solvents, and a mixture of acrylic monomers. Intriguingly, even the two nominally hydrophilic crosslinkers, UPy-XL-3 and UPy-XL-4, were not completely soluble in either water or a latex environment (5 mg/mL). It was hoped that the very long hydrophilic PEG chain — ~130 and ~220 units respectively — would yield sufficient crosslinker solubility. However, as Figure 3.5b demonstrates, this is clearly not the case. The

hydrophilic crosslinkers initially form opaque solutions in water, before slowly precipitating out, presumably due to aggregation. In the case of UPy-XL-4, which has a PEG chain over 200 units long (roughly equivalent to smaller associative thickeners), this opaque solution is maintained over a period of hours. Such an opaque solution may indicate the presence of nanostructures. In the case of UPy-XL-4, a long hydrophilic linear chain with highly hydrophobic end units, two plausible structures are shown below in Figure 3.6a.

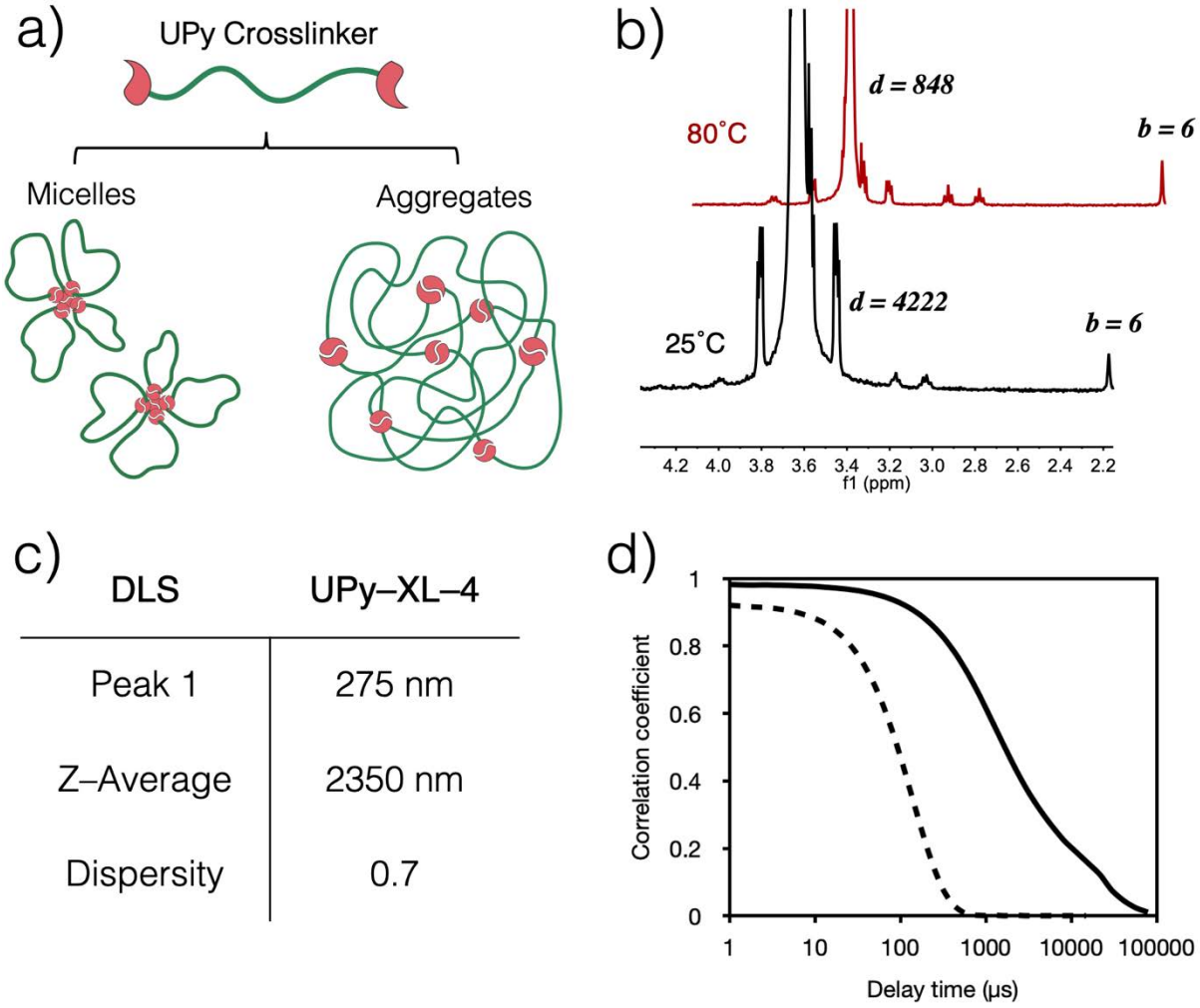

Figure 3.6 Examining the morphology of UPy-XL-4 in an aqueous solution. a) UPy-XL-4 may form temporarily stable micelle-like nanostructures with a UPy based core and a PEG shell, or irregular aggregates which grow and eventually precipitate over time. b) ^{1}H NMR spectra of UPy-XL-4 in D_2O at two different temperatures: RT (black) and 80˚C (red). c) DLS analysis of UPy-XL-4 in water, including two nanoparticle size measurements and dispersity. d) the DLS correlation function of UPy-XL-4 (bold line), and a typical suspension of monodisperse nanoparticles (dotted line).

UPy-XL-4 contains a very long PEG chain (MW ~ 10,000) separating the two strong self-complementing hydrophobic UPy moieties. This PEG chain may be hydrophilic enough to form a shell/corona around the extremely hydrophobic UPy moieties, thus stabilizing a suspension of micelle-like structures, albeit temporarily. Indeed, other studies into self-healing hydrogels show that UPy–Urea systems with similarly long PEG spacers form micelles between 5 and 10 nm at both room temperature and at temperatures up to 50˚C.[22] Furthermore, micelles with hydrophilic PEG shells and hydrophobic cores based on UPy-UPy hydrogen bonding have been employed in drug delivery applications.[7]

The structure of these possible UPy-PEG nanoparticles can be analyzed through ^{1}H NMR. This is possible due to the fact that particle shell components are free to interact with the deuterated solvent environment and hence appear clearly on the spectrum, while core components are typically not observed, as their isolation from the bulk solvent minimizes spin–spin relaxation time (T_2).[23] The black spectrum in Figure 3.6b shows that at room temperature, the signal of UPy moieties is drastically reduced by a factor of 5 compared to the PEG spacer. This can be seen through the ratio between peak *d*, which corresponds to the PEG chain, and peak *b*, which corresponds to the pyrimidinone's methyl group (~700:1) (Figure S41). This ratio is significantly higher than a PEG:UPy ratio of 133:1 for fully dissolved UPy-XL-4 (the red spectrum in Figure 3.6b, S12), indicating that, at room temperature, the hydrophobic UPy sections of the crosslinker are forming a packed structure isolated from the bulk aqueous environment, while the PEG chains are more easily able to access the solvent, indicating they may exist as a shell/corona.

Dynamic light scattering (DLS) was used to substantiate the presence of micelle-like UPy-PEG structures, and the results are shown in Figures 3.6c–d. DLS measures the scattered light of a solution of nanoparticles, and generates a correlation function based on the Brownian motion of the particles, which are assumed to be spherical. This correlation function roughly describes how long a particle is located in the same spot.[24] Because smaller particles undergo more rapid Brownian motion than larger nanoparticles, the time at which the correlation function decays is an indirect measurement of particle size, and the gradient of this decay is a measure of particle dispersity. Figure 3.6d displays a correlation function which begins to decay after a very prolonged period of time. This is in contrast to the correlation function of a typical solution of monodisperse nanoparticles, which shown by the dotted line in Figure 3.6d.[25] Furthermore, the rate of decay is very shallow rather than steep, indicating a highly dispersed sample of

particles. The DLS parameters for UPy-XL-4 displayed in Figure 3.6c confirm this, with a dispersity of ~ 0.7, where ~ 0.1 represents typical value for monodisperse particles. The dispersity of UPy-XL-4 was measured over a period of 48 hours (Figure S64a), and the dispersity increased from ~0.7 to 3.4 after 24 hours, indicating aggregation over time. This aggregation over time was further reinforced via the increase in delay time and the broadening of the correlation function (Figure S64b). The dispersity of a highly dilute (1:100) sample of UPy-XL-4 was also found to increase more slowly over time (Figure S64a–c), indicating that aggregation was concentration dependent, and that there was likely no concentration at which a suspension of UPy-XL-4 nanostructures was stable. These parameters reveal that UPy-XL-4 does not form stable micelles in an aqueous environment, but rather forms large aggregates similar to those depicted in Figure 3.6a, which gradually precipitate in both water and a latex environment.

This instability and precipitation can be most obviously seen through the difference between a UPy-2 functionalized coating with and without added UPy-XL-4 crosslinker (Figure 3.7). The crosslinker was added to the latex with the hope that the aggregates would sufficiently coalesce with the latex particles as the coating formed. As Figure 3.7a clearly shows however, the resultant coating is highly opaque, due to the fact that as the water evaporated, UPy-XL-4 precipitated out of the latex before coalescence occurred.

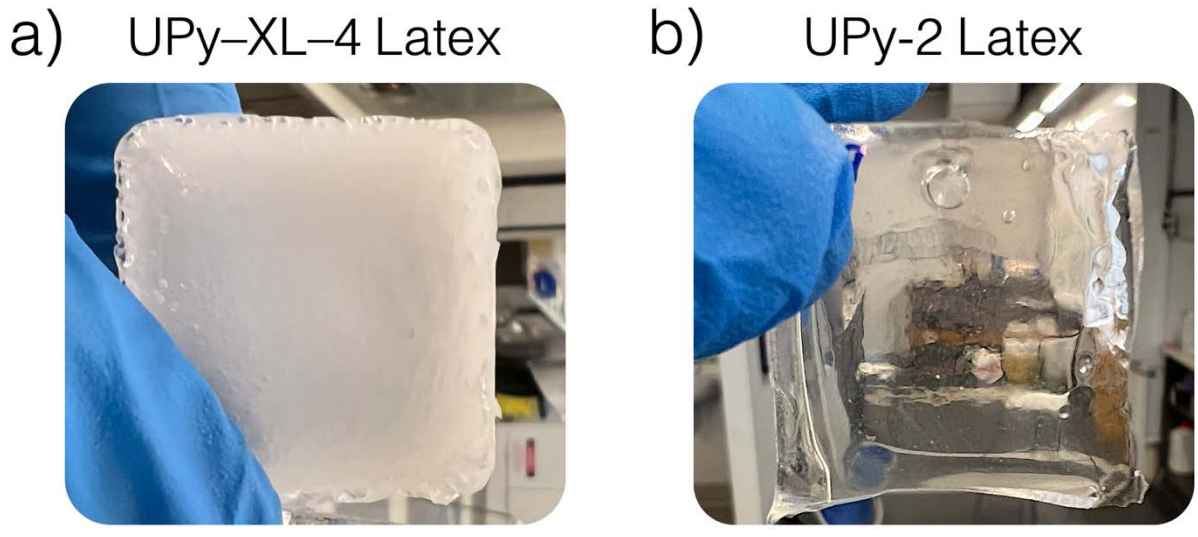

Figure 3.7 Images of a UPy-2 functionalized acrylic coating with the UPy-XL-4 crosslinker (a) and without the addition of crosslinker (b). The clear difference in opacity clearly emphasizes the instability and precipitation of UPy-XL-4.

Such instability ultimately prevents UPy-XL-4, along with the other three linear crosslinkers, from being stably incorporated into a latex and forming an enhanced hydrogen bonding network in the UPy-functionalized coating. Therefore, a new crosslinker design was necessary.

3.3.2 UPy-Brush crosslinkers

In order to synthesize a UPy-functionalized crosslinker with brush architecture, as opposed to linear architecture, a poly(PEGMA) brush was first synthesized via RAFT polymerization. Specifically, a library of three PEGMA brushes were synthesized, with molecular weights of roughly 5, 10 and 20 kDa. This was achieved by keeping a constant [monomer: RAFT agent: initiator] ratio, while varying the reaction time to increase monomer conversion. In the case of the 20 kDa brush polymer, however, the concentration of the RAFT agent was reduced to increase the length of the resultant polymer chains, according to the equation 1:

$$MW = X \frac{[\mathrm{PEGMA}]}{[\mathrm{RAFT}]} M_{\mathrm{PEGMA}} + M_{\mathrm{RAFT}} \quad (1)$$

Where, M_{PEGMA} and [PEGMA] are the molecular weight and concentration of PEGMA, M_{RAFT} and [RAFT] are the molecular weight and concentration of the RAFT agent, X is the monomer conversion (%), and MW is the molecular weight of the resultant polymer. The three crosslinkers were synthesized, and their molecular weights were verified through ^{1}H NMR (Figures S43–45). This was achieved through examining the ratio between the RAFT agent peak at 1.26 ppm and the PEG peak at 4.2. Given there is only one RAFT agent per polymer chain, this ratio yields the number of PEG units per polymer chain and hence the molecular weight of the polymer.

Purification of these PEGMA brushes was difficult, as even after four precipitations in diethyl ether followed by dialysis in water over 1 week, ~5–8% of unreacted PEG monomer remained. This unreacted monomer is shown by red asterisks in Figures S43–45. Entanglement due to the steric hinderance of the brush polymers may be responsible for this small amount of residual monomer. Another plausible explanation is based on the fact that PEG forms physicochemical bonds with itself, either in the form of Van Der Waal's forces or intermolecular (self-complementary) hydrogen bonds.[26] This effect is likely maximized in the case of PEGMA brush polymers, given the higher density of PEG moieties for a given volume, compared to

typical linear PEG polymers. This physicochemical bonding is also responsible for another phenomenon that must be carefully considered when synthesizing PEGMA brushes, gelation. Gelation typically occurs when PEG systems form covalently crosslinked structures due to the addition of hydrophobic moieties or a reactive crosslinker. For brushes, star polymers and polymers with other exotic architectures, however, this crosslinking process can occur due to the inherent intermolecular physicochemical bonding between PEG chains.[27, 28] In this system specifically, gelation begins to occur at a monomer conversion of roughly 60%. Therefore, to avoid gelation, conversion was intentionally kept low at around 10 to 20%. In fact, using equation 1 to tailor the concentration of the RAFT agent such that a monomer conversion of 100% would yield suitable brush polymers, is a strategy to eliminate unreacted monomer that is made unfeasible due to gelation. All of that is to say that the RAFT protocol to design these brushes was specifically designed to avoid the complexities associated with synthesizing PEG-based homopolymers with a non-linear architecture.

Following the synthesis of these PEGMA brush polymers, UPy units were grafted to the brushes at a ratio of two UPy moieties per polymer chain through a hydroxyl–isocyanate reaction. The UPy-functionalized monomers described in Chapter 2 were synthesized through this reaction at 60˚C in anhydrous chloroform over 24 hours. However, these conditions proved highly inefficient for the formation of UPy-Brush crosslinkers, likely due to the enhanced steric hinderance of the poly(PEGMA) brush polymers. Therefore, the reaction was performed in DMF at 80˚C for two days, which allowed the reaction to go to completion (Figures S46–54). This was verified by the lack of any IR isocyanate peak corresponding to the UPy-NCO precursor (Figure 3.8b)

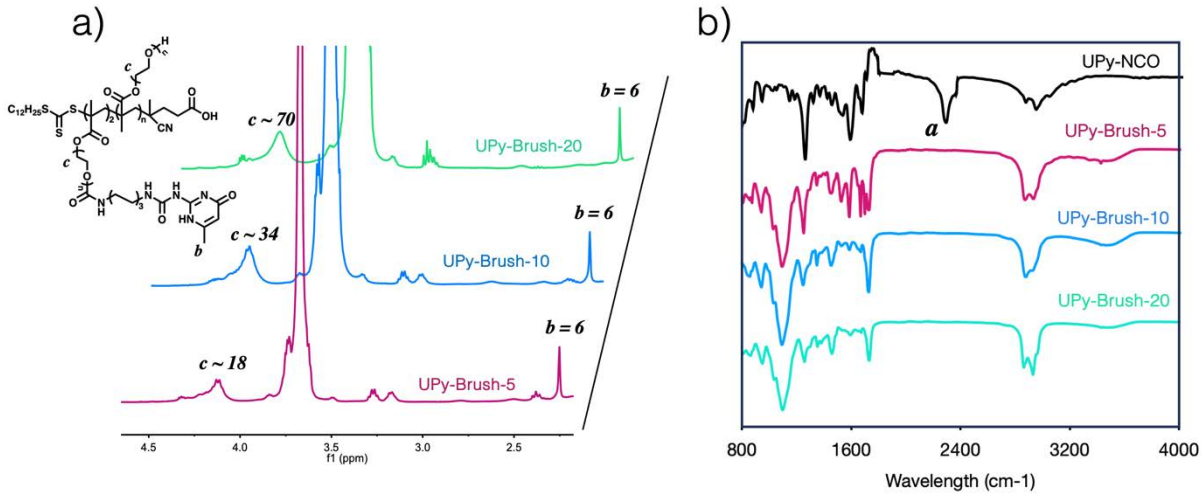

Figure 3.8 Three UPy brush crosslinkers were synthesized with MWs of 5, 10 and 20 kDa, termed UPy-Brush-5, UPy-Brush-10, and UPy-Brush-20 respectively. a) A section of the ^{1}H NMR spectra for the three crosslinkers. Two peaks, *b* and *c*, are shown, allowing a calculation of the number of UPy units per polymer chain. b) IR spectra of the UPy brush crosslinkers compared to the UPy-NCO precursor, whose isocyanate peak is shown as peak *a*. The fully assigned ^{1}H NMR and IR spectra are shown in Figures S46–54

The successful synthesis of the three crosslinkers, termed UPy-Brush-5, UPy-Brush-10 and UPy-Brush-20, was further verified by ^{1}H NMR (Figure 3.8a). The ratio between peak *b*, corresponding to the pyrimidinone's methyl group (6H), and peak *c*, corresponding to a section of the PEG chain (2H) was compared. For all three crosslinkers, the average number of UPy moieties per polymer chain was ~2, as intended. All three UPy-Brush crosslinkers, which took the form of tacky solids, were soluble in water (Figure S55), although in the case of UPy-Brush-5, the solution was cloudy, and full dissolution took over an hour. For coating tests, the UPy-brush crosslinkers were added to either the UPy-2 functionalized latex or the unfunctionalized (control) MMA/BA/AA latex at a 2:1 mol ratio compared to the UPy-2 latex, which represents an effectively equal number of UPy moieties between monomer and crosslinker.

The glass transition temperature (*T*g) is an important parameter when analyzing the mechanical and self-healing properties of organic coatings. *T*g is the temperature at which a polymeric coating transitions from a brittle glassy substance (< *T*g) to a rubbery, plasticized coating (> *T*g). This transition is due to the rheological properties of the polymers which comprise the

coating. As the temperature rises, the polymers, which initially had no mobility below *T*g, gain enough energy to slide past each other when force is applied, resulting in a more malleable substance. To investigate how the UPy-Brush crosslinkers affected *T*g, the three crosslinkers were added to a control MMA/BA/AA latex, from which coatings were formed. Differential scanning calorimetry (DSC) was used to measure the *T*g, and the results are shown in Figure 3.9 below.

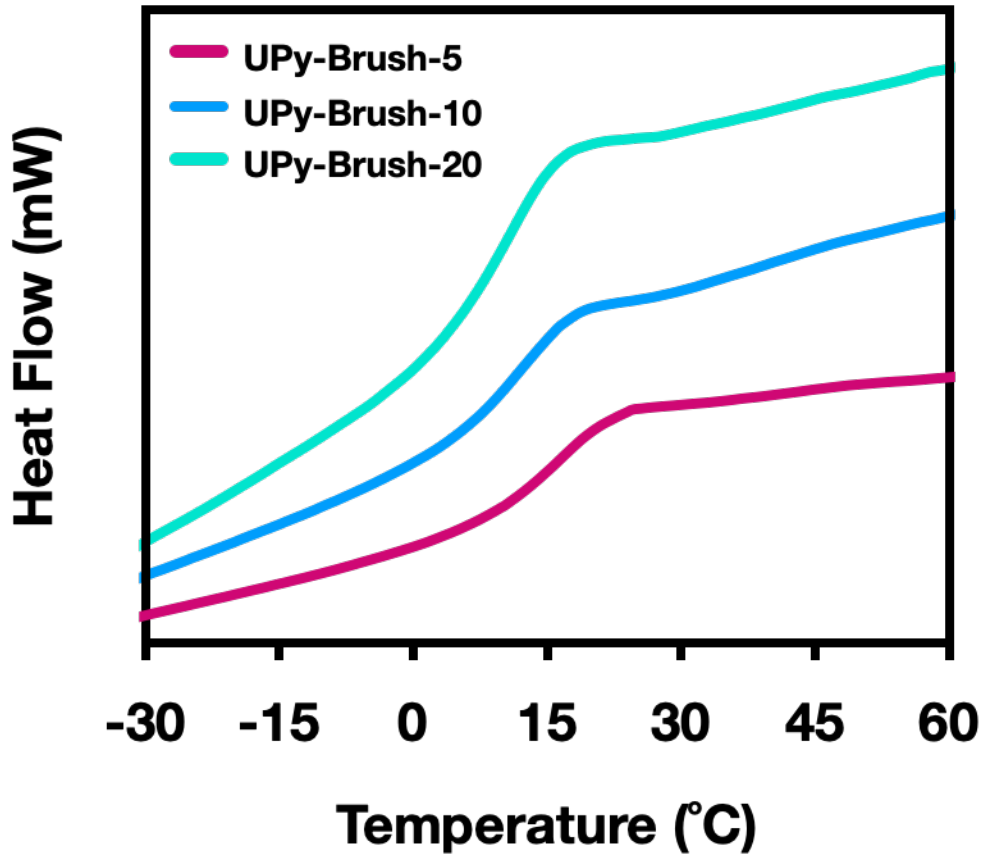

Figure 3.9 DSC was used to investigate how the UPy-Brush crosslinkers impacted *T*g, an important coating mechanical property. Heat flow curves were obtained for a MMA/BA/AA acrylic coating with the three crosslinkers added following latex synthesis.

The *T*g of the UPy-Brush-5, 10 and 20 coatings was measured at 15˚C ± 0.24, 13˚C ± 0.53 and 11˚C ± 0.33 respectively (Figures 3.9 and S56–58). Given that the measured *T*g of the MMA/BA/AA latex in Chapter 2 was 18˚C, clearly each brush crosslinker noticeably reduces *T*g, and hence provides a slight softening effect to the coating. Flory–Fox theory can be used

to roughly estimate the *T*g of each UPy-Brush crosslinker according to the following simplified equation (2):

$$\frac{1}{T_{g(coating)}} = \frac{\omega_{(control)}}{T_{g(control)}} + \frac{\omega_{(XL)}}{T_{g(XL)}} \quad (2)$$

Where *T*g and ω are the glass transition temperatures (K) and weight fractions of the crosslinker-functionalized coatings, the unfunctionalized MMA/BA/AA control coating (measured with a *T*g of 18˚C in Chapter 2), and the unknown UPy-Brush crosslinkers (abbreviated to *XL* in this equation). According to Flory–Fox theory, the estimated *T*g of UPy-Brush-5, UPy-Brush-10, and UPy-Brush-20 crosslinkers are approximately –130˚C, –120˚C, and –85˚C respectively. These values are markedly lower than soft acrylic monomers typically used in the paint industry, such as BA, which has a *T*g of –54˚C. Such low *T*g is due to the length and flexibility of PEG, which is a very soft material. Hydrogels comprised of poly(PEGMA) brushes have a *T*g ranging from –90˚C to –35˚C, with hydrogels based on PEGMA (MW = 500 Da) — the closest analogue to these UPy-Brush crosslinkers — having a *T*g between –75˚C and –65 ˚C.[29] Given the UPy-Brushes do not take the form of a highly crosslinked hydrogel, one would expect the true *T*g of PEGMA 500 to be well below –75˚C. In fact, the *T*g of PEG systems increases with the length and MW of PEG, as well as the crosslinking density for PEG-based hydrogel systems. This is the likely reason for the observed increase in *T*g from –130˚C in the case of UPy-Brush-5, to –80˚C in the case of UPy-Brush-20. As well as the physicochemical properties of PEG, the additional free volume that exists due to the addition of the crosslinkers, which are around two orders of magnitudes smaller than the latex polymers, allows the polymers more 'room to maneuver', thus decreasing *T*g.[30] This method of reducing the *T*g by increasing the free volume within a coating underpins the performance of plasticizers and coalescents, two crucial additives in the production of paint and other organic coatings.

In addition to *T*g, a coating's Young's modulus is a vital parameter that yields important insight into a coating's mechanical strength and self-healing efficiency. In fact, Young's modulus and *T*g are highly correlated, and low modulus materials typically self-heal at higher efficiencies, especially when the healing mechanism is intrinsic rather than extrinsic. As previously mentioned in Chapter 2, Young's modulus is a measure of how well a material is able to resist deformation, and is the gradient of the linear section of a stress-strain curve (corresponding to

elastic deformation). Three coatings, obtained from a UPy-2 functionalized latex with added UPy-Brush crosslinker, were subjected to tensile testing via a universal testing machine (UTM). The stress-strain curves of each coating are shown in Figure 3.10 below.

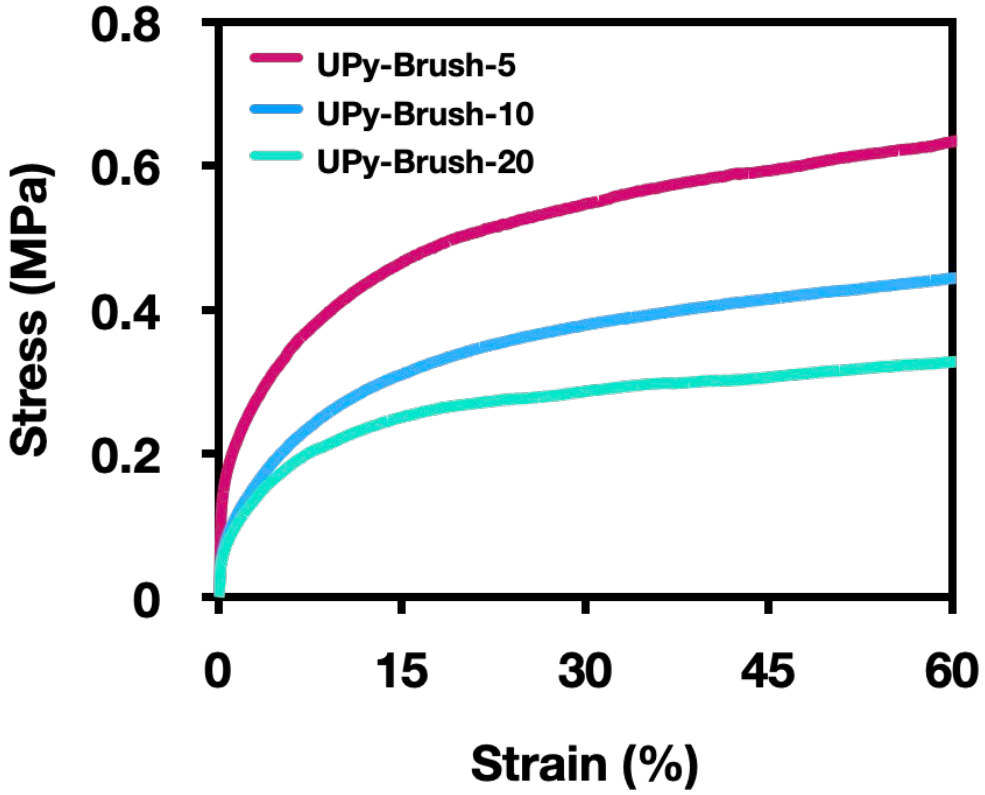

Figure 3.10 Stress-strain curves of a UPy-2 functionalized coating with the three UPy-Brush crosslinkers were obtained. The gradient of the linear section of the curves represents the Young's modulus — a measure of resistance to deformation — which is an important coating mechanical parameter.

As previously mentioned, Young's modulus is the most common metric when analyzing and comparing the mechanical strength of different materials, as well as investigating the self-healing efficiency. The vast majority of intrinsic self-healing strategies rely on materials with a very low modulus. Hydrogels, for example, have a Young's modulus typically below 0.1 MPa, whereas stronger thermoplastic elastomers have a Young's modulus of ~10 MPa. For acrylic coatings, Young's modulus ranges anywhere from 100 to 2000 MPa. The stress-strain curves in Figure 3.10 yield Young's moduli of ~60, ~40 and ~30 MPa for the UPy-Brush-5, 10 and 20 coatings respectively. Given that Chapter 2's UPy-2 functionalized coating without any added crosslinker had a Young's modulus of ~200 MPa, it is clear that the addition of the UPy-brush crosslinkers significantly reduces the strength of the coating. A Young's modulus

of ~30 MPa in the case of the UPy-Brush-20 coating is roughly equivalent to a strong thermoplastic elastomeric coating. This decrease in mechanical strength is unsurprising, given that the length and flexibility of PEG-based materials yield low modulus materials such as hydrogels. Figure 3.10 also shows that the mechanical strength of the coating decreases with increasing MW of the UPy-Brush crosslinkers. As a 1:1 mol ratio between the crosslinker and latex UPy units is kept constant, the amount of PEG units is maximized as a fraction of the total material in the case of the UPy-Brush-20 crosslinker system. A minor decrease in *T*g and a noticeable decrease in Young's modulus demonstrates that the UPy-Brush functionalized coatings represent an overall weaker material than either an MMA/BA/AA acrylic coating, or a coating functionalized with the monomer UPy-2. This decrease in strength might be problematic for certain paint-based applications, but may also allow for greater intrinsic self-healing efficiency, due to the enhanced polymer mobility associated with softer materials.

As well as *T*g and Young's modulus, the surface hardness of the UPy-Brush coatings was evaluated via the pencil hardness test (Figure S65). All three coatings had an average score of B, with the UPy-Brush-20 scoring 2B for one out of three repeats. B represents a pencil hardness one step below HB, which was the average hardness of the UPy-2 coating, and two steps below H, the hardness of the control acrylic coating. These results show that the UPy-Brush crosslinkers have a slightly detrimental effect on coating hardness, and reinforce the conclusions drawn from Young's modulus and *T*g — that the crosslinker coatings represent an overall softer material.

To analyze the self-healing potential of the three UPy-Brush crosslinkers, a crack was introduced with a razor blade to six separate coatings, and the damaged coatings were allowed to self-heal for 24 hours at room temperature. The six coatings included three coatings formed from an MMA/BA/AA control latex and each UPy-Brush crosslinker, and another three coatings formed from the self-healing UPy-2 functionalized latex and each UPy-Brush crosslinker. Optical microscopy was used to take images at the initial time of damage and after 24 hours (Figures 3.11 and S59–60).

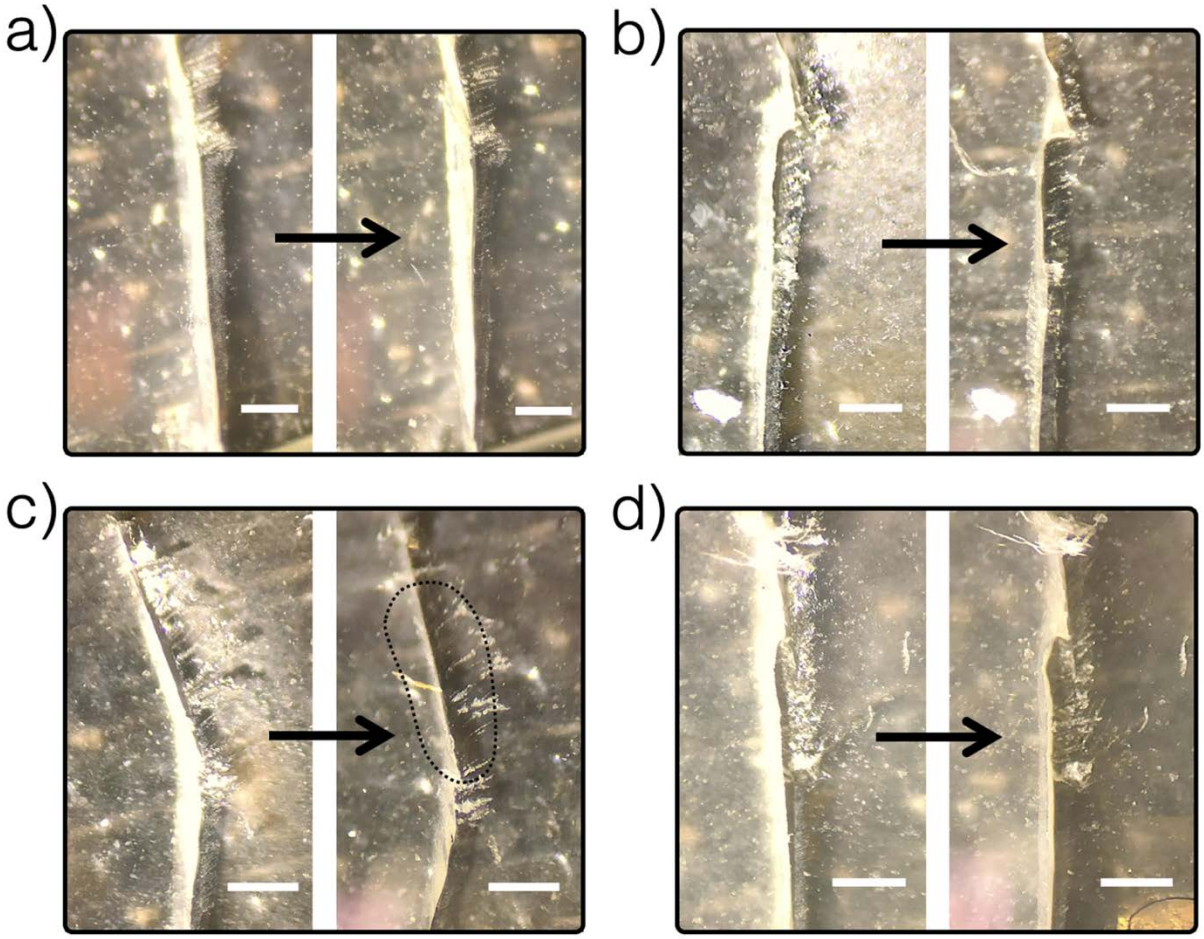

Figure 3.11 The self-healing potential of four coatings was analyzed through the healing of a crack after 24 hours at room temperature. a) The control latex with added UPy-Brush-10. b) The UPy-2 functionalized latex with added UPy-Brush-5. c) The UPy-2 functionalized latex with added UPy-Brush-10. d) The UPy-2 functionalized latex with added UPy-Brush-20. Control images are shown in Figures S59–60. The images were taken on an optical microscope, and the scale bar represents 250 µm.

Given that the control latex shows no self-healing capability at room temperature, it was expected that the control latex with added UPy-Brush crosslinker would also display minimized self-healing. This is due to the fact that the latex polymers, which make up the bulk of the acrylic coating, contain no UPy functionality, minimizing their hydrogen bonding-induced rearrangement. Figure 3.11a, which shows just the UPy-Brush-10 control coating, and Figure S54 supports this hypothesis, as neither the UPy-Brush-5, UPy-Brush-10 or UPy-Brush-20 control latex coatings display any visible healing of a crack over 24 hours at room temperature. All three UPy-2 functionalized coatings with added crosslinker, however, do

display self-healing potential compared to the control coatings, as can be seen through Figures 3.11b–d. The self-healing appears strongest for the UPy-XL-10 coating, specifically at the part of the crack shown within the dotted line (Figure 3.11c).

Given that elevated temperatures enhance the self-healing efficiency of intrinsic materials, the UPy-Brush coatings were also subjected to a self-healing temperature of 50˚C for a further 24 hours. The results are shown in Figure 3.12 and S55. Even at 50˚C, Figures 3.12a and S59–60 show that the control latex coatings with added crosslinker display slight self-healing capability. This is evident in both the UPy-Brush-10 control coating, and the UPy-Brush-5 control coating, where some self-healing is evident near the bottom of the crack (Figure S59). The UPy-2 functionalized coatings with added crosslinker, on the other hand, display very strong self-healing (Figures 3.12b–d). Specifically, the UPy-Brush-10 coating displays exceptional self-healing compared to the control coating, and the UPy-Brush-20 also displays very strong self-healing. This pattern mirrors the self-healing of the coatings at room temperature; however, the UPy-Brush-5 coating's self-healing is seemingly reduced compared to the other coatings. In fact, there does not appear to be a large difference between the control latex and UPy-2 functionalized latex coatings with added UPy-Brush-5. This suggests UPy-Brush-5 is likely the weakest crosslinker in terms of self-healing efficiency. Though the UPy-2 functionalized coating with added UPy-Brush crosslinker displays noticeable self-healing at room temperature and very strong self-healing at 50˚C (at least in the case of UPy-Brush-10), this pattern in also evident in the UPy-2 functionalized coating without any crosslinker, as shown in Chapter 2.

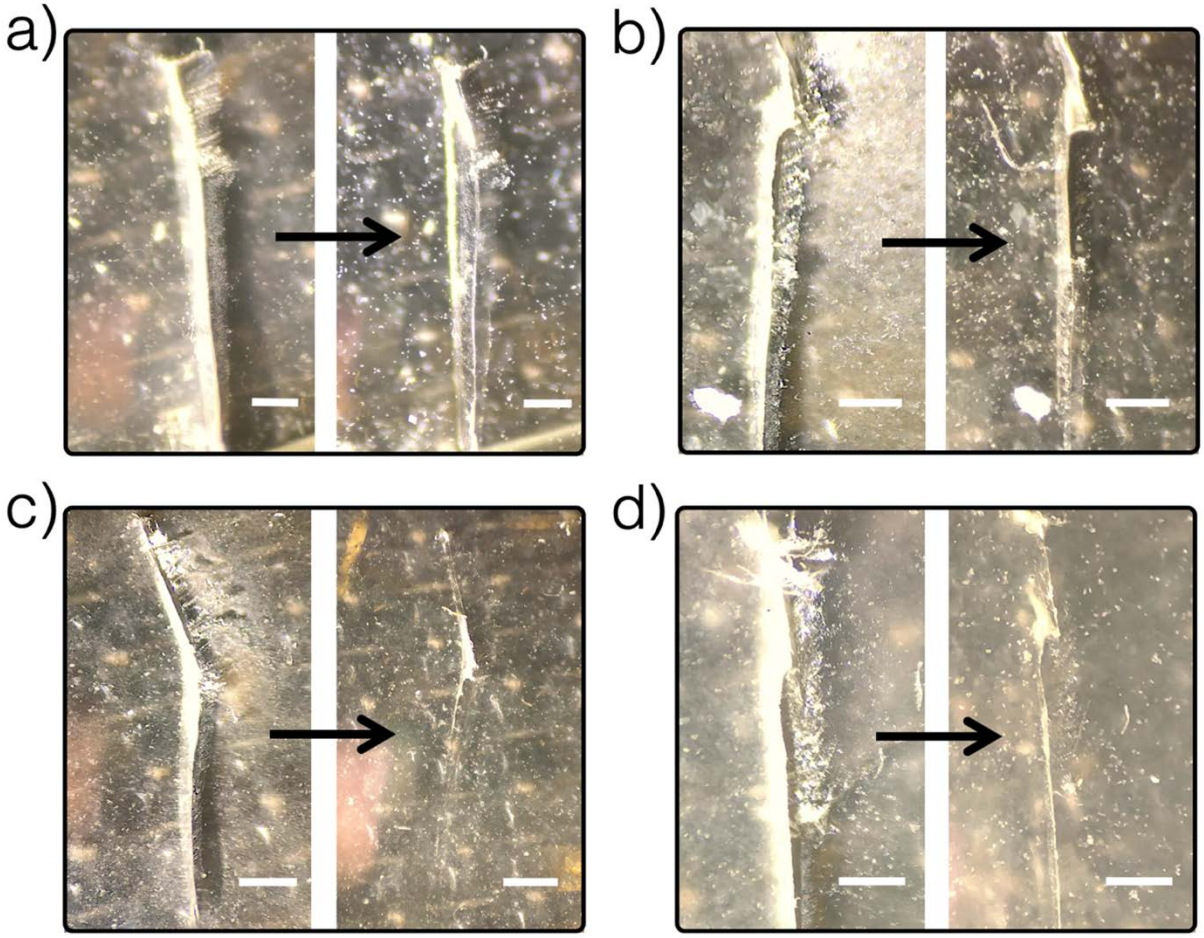

Figure 3.12 The self-healing of four coatings was analyzed through the healing of a crack after 24 hours at 50˚C. a) The control latex with added UPy-Brush-10. b) The UPy-2 functionalized latex with added UPy-Brush-5. c) The UPy-2 functionalized latex with added UPy-Brush-10. d) The UPy-2 functionalized latex with added UPy-brush-20. Control images are shown in Figure S59–60. The images were taken on an optical microscope, and the scale bar represents 250 µm.

Optical images are able to provide clear qualitative evidence of self-healing, however they cannot accurately quantify self-healing efficiency. In order to understand self-healing efficiency, the strain recovery of each coating was measured and compared. Strain recovery involves measuring the strain-at-break for both an undamaged coating, and a damaged coating allowed to heal under certain conditions, and comparing the two values as a ratio. This method is a common measure of self-healing efficiency for intrinsic polymeric materials, and is described in detail in Chapter 2.

Four specific coatings were designed which represent three control coatings and one self-healing system (Figure 3.13). The first two controls, termed C1 and C2, comprised an MMA/BA/AA control coating with either the UPy-Brush crosslinker or the un-grafted PEGMA brush (no UPy moieties) added respectively. The UPy-2 functionalized coating without any added crosslinker, which was described in Chapter 2, constitutes a third control (C3). The coating with the hypothesized maximum amount of self-healing is the combination of the UPy-2 functionalized coating with the UPy-Brush crosslinker, termed UPy-Brush.

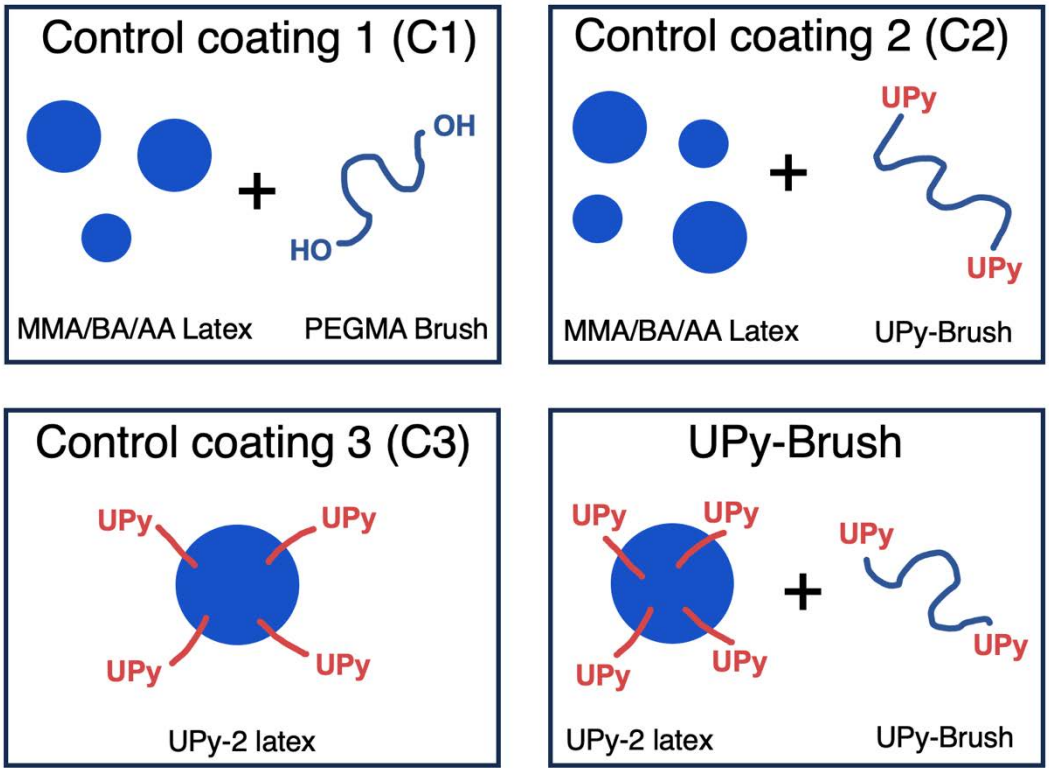

Figure 3.13 Strain recovery tests were conducted on four separate coatings. These coatings are comprised of an MMA/BA/AA latex and the PEGMA brush crosslinkers with no UPy units (C1); an MMA/BA/AA latex with the UPy-Brush crosslinkers (C2); a UPy-2 functionalized latex (C3); and a UPy-2 functionalized latex with the UPy-Brush crosslinkers. This last coating is termed UPy-Brush, and is expected to have the highest self-healing efficiency.

Any difference between C1 and C2 would indicate that the UPy-Brush crosslinkers had self-healing potential without the need for UPy moieties covalently conjugated to the latex polymers themselves. Such a result would be surprising, given that the optical images in Figures 3.11, 3.12 and S59–60 do not indicate any self-healing capacity for the control latex/UPy-Brush crosslinker system. Any difference between C3 and the UPy-Brush coatings would prove that the addition of UPy-Brush crosslinkers to a UPy-functionalized latex increases the self-healing efficiency of the coating. These four coatings combined with three crosslinkers represent 12 total experiments. A crack was introduced to the coatings via a razor blade, and the coatings were allowed to heal over 24 hours at both room temperature and 50˚C (Figure 3.14, S61–63).

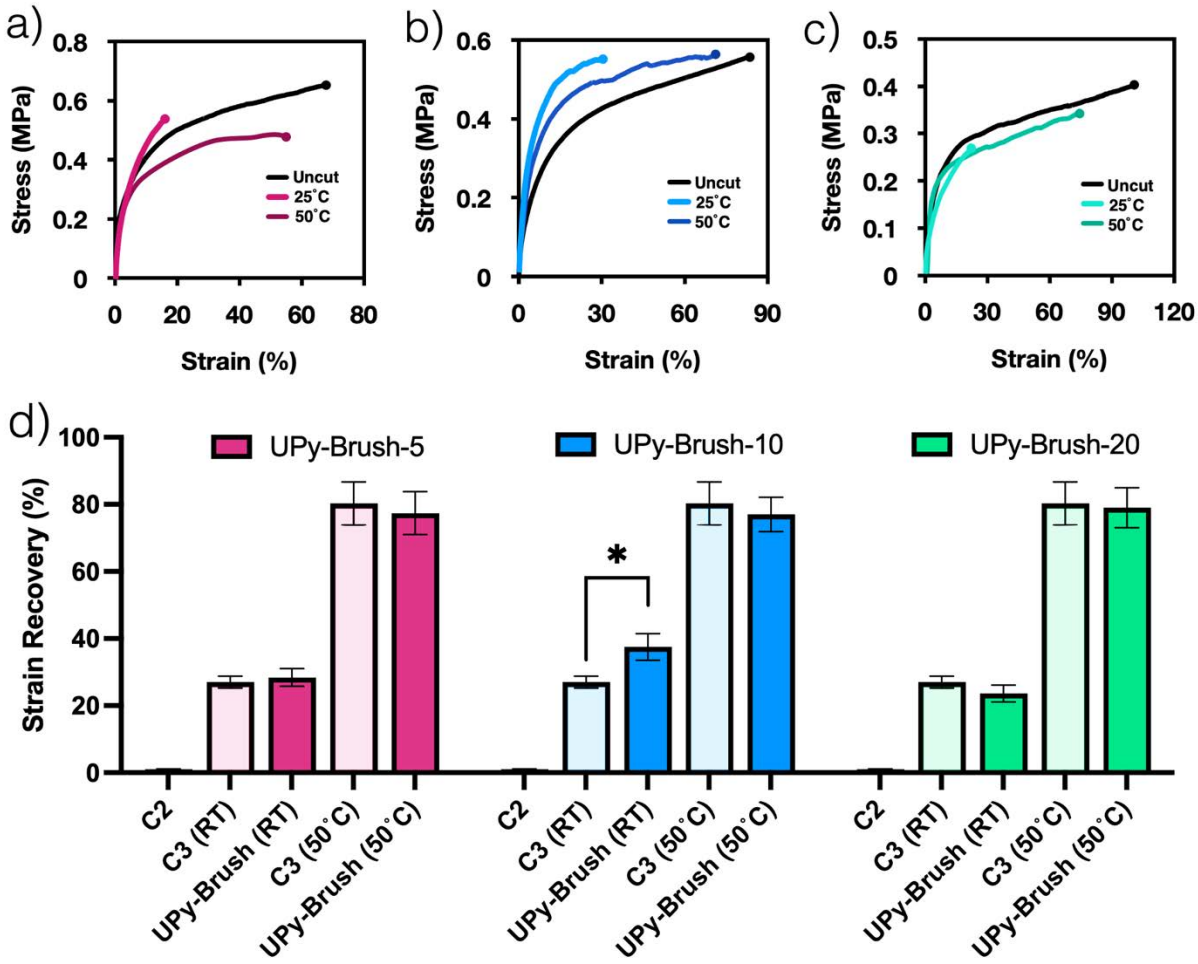

Figure 3.14 Self-healing efficiency was evaluated via strain recovery tests of the uncut coatings compared with the cut coatings allowed to heal for 24 hours at RT and 50˚C. a) An example stress strain curve for the UPy-functionalized coating with UPy-Brush-5. b) An example stress strain curve for the UPy-functionalized coating with UPy-Brush-10. c) An example stress strain curve for the UPy-functionalized coating with UPy-Brush-20. d) The strain recovery (self-healing efficiency) of the MMA/BA/AA coating + the UPy-Brush crosslinkers (C2) at RT, the UPy-2 functionalized coating alone (C3) at RT and 50˚C, and the UPy-2 functionalized coating + the UPy-Brush crosslinkers (UPy-Brush) at RT and 50˚C. The data represents mean ± SD for n = 3 independent experiments. An unpaired t-test was used to analyze the statistical differences between the self-healing efficiency of each coating. *indicates $p \leq 0.05$.

Figures 3.14a–c show strain recovery curves for the three UPy-Brush coatings at both RT and 50˚C. The UPy-Brush-5, 10 and 20 coatings all displayed noticeable self-healing efficiency at room temperature — 28%, 38% and 24% respectively — and very strong healing at 50˚C (~80%). Such self-healing is radically stronger than both C1 and C2, which together displayed no observable self-healing (Figures 3.14d and S61–63). This implies that the addition of the brush crosslinkers, whether with or without UPy moieties, does not alone imbue acrylic coatings with any self-healing capability. The most plausible reason for this is that latex polymer rearrangement requires that the self-healing functionality be covalently attached to the latex polymers themselves. Thus, the UPy-Brush coatings were also compared with the UPy-2 functionalized latex design described in the Chapter 2 (C3) (Figure 3.14d).

At 50˚C, there is no observable difference between the UPy-functionalized coating with or without the addition of any of the three UPy-Brush crosslinkers. This lack of additional self-healing efficiency is also evident for the UPy-Brush-5 and UPy-Brush-20 crosslinkers at room temperature. Interestingly, the UPy-Brush-10 coating had a higher healing efficiency at room temperature compared to the UPy-2 functionalized coating. Furthermore, this difference in self-healing efficiency — 38% as compared with 27% — is statistically significant. The enhanced self-healing efficiency of UPy-Brush-10 is interesting, given that it sits between the other two crosslinkers in terms of its PEG length, MW and its impact on mechanical properties of the coating. The self-healing efficiency of UPy-Brush-20, which is significantly larger than the other UPy-Brush-10, may be diminished due to its increased steric hinderance. This steric hinderance may minimize the extent to which the UPy units of UPy-Brush-20 can form a hydrogen bonding network with the UPy units covalently connected to the latex polymers, resulting in a weaker hydrogen bonding network. Furthermore, the increased length of UPy-Brush-20 may allow for three-dimensional rearrangement and intramolecular hydrogen bonding — an effect observed in longer linear UPy systems [31] — thus minimizing the evenness of the resulting hydrogen bonding network and minimizing self-healing efficiency. It is more difficult to explain why UPy-Brush-10 has superior healing efficiency compared to UPy-Brush-5, but solubility may play a role. As the crosslinker with the highest relative fraction of hydrophobic UPy functionality, UPy-Brush-5 likely has the weakest aqueous solubility. This fact is suggested by UPy-Brush-5's increased dissolution time in water compared with the other two crosslinkers. In a latex, which represents an opaque suspension of hydrophobic particles in water, it is possible that UPy-Brush-5, due its reduced solubility, preferentially adheres to

the latex particles rather than existing in the bulk solution, which results in the crosslinker effectively behaving like the UPy-functionalized monomer, UPy-2.

The strain recovery values for the three UPy-Brush crosslinkers paint a clear overall picture regarding self-healing efficiency. Neither the UPy-Brush-5 nor the UPy-Brush-20 crosslinkers provide any superior self-healing efficiency compared to a UPy-functionalized latex system. UPy-Brush-10, on the other hand, provides a noticeable improvement in self-healing efficiency at room temperature, as it likely exists in a 'goldilocks zone' in regard to size, solubility and the fraction of UPy functionality relative to PEG. However, it is not a substantial step-change improvement. This reveals important information regarding the nature and potential mechanisms of intrinsic self-healing in an acrylic coating:

i) Simply increasing the amount of self-healing functionality — UPy in this case — does not necessarily enhance self-healing efficiency.
ii) Even a significant reduction in mechanical strength and *T*g — which occurred due to the addition of the UPy-Brush crosslinkers — does not necessarily enhance self-healing efficiency.
iii) How the self-healing functionality is incorporated into the acrylic coating is vital to self-healing efficiency. In this particular system, the bulk latex polymers themselves need to rearrange for self-healing to occur. Consequently, the UPy moieties covalently attached to the latex polymers in the form of a UPy-monomer, as opposed to a UPy-crosslinker, provided the strongest benefit to self-healing efficiency.

Both the UPy monomeric designs in Chapter 2 and the crosslinker designs in Chapter 3 clearly show that self-healing efficiency increases with increasing temperature above Tg. The self-healing efficiency data provided by strain recovery measurements allows a semi-quantitative trend to be established. In the case of the UPy-Brush-10 crosslinker, self-healing efficiency increases by 1.8% per degree, as compared to 2.1% per degree in the case of the monomer UPy-2. Such a trend provides a useful model for predicting the self-healing behaviour of other coatings with different Tgs, however, more temperature data points between 20 and 60 ˚C are necessary to fully refine this trend.

3.4 CONCLUSION

In order to enhance the self-healing efficiency of an acrylic coating, a self-healing crosslinker system was designed based on varied architectures of PEG, grafted with the strong hydrogen bonding unit UPy. Firstly, a library of four UPy-functionalized linear PEG chains of varying length and hydrophilicity was synthesized, representing the simplest possible UPy crosslinker design. The negligible solubility of all four crosslinkers prevented their incorporation into an MMA/BA/AA latex, necessitating a more complex crosslinker design with enhanced aqueous solubility. Therefore, RAFT polymerization was employed to design PEG-based polymers with a brush, as opposed to a linear architecture. These polymers were then grafted with UPy functionality to form three UPy-Brush crosslinkers termed UPy-Brush-5, UPy-Brush-10, and UPy-Brush-20, due to their respective MWs of 5, 10 and 20 kDa. All three UPy-Brushes were incorporated into an MMA/BA/AA latex, yielding coatings with a reduced *T*g and Young's modulus.

The self-healing efficiency of these crosslinkers was tested by imaging the recovery of a crack over 24 hours. When added to UPy functionalized acrylic coating, all three crosslinkers showed self-healing capability, with the UPy-Brush-10 and 20 both displaying very strong optical self-healing at room temperature and 50°C. The self-healing efficiency of each crosslinker was tested by measuring strain recovery. It was found that the crosslinkers did not have any noticeable self-healing efficiency when added to an unfunctionalized MMA/BA/AA latex. When combined with the UPy functionalized latex, UPy-Brush-5 and UPy-Brush-20 did not impart any additional self-healing. However, the addition of UPy-Brush-10 yielded a ~10% increase in self-healing efficiency at room temperature. These results show that under specific conditions, a UPy-functionalized crosslinker system can increase self-healing efficiency. Despite this, the general performance of these crosslinker systems suggests that, at best, they can only modestly enhance self-healing efficiency. Nevertheless, such a UPy-Brush crosslinker system provides a valuable insight into the nature and mechanism of intrinsic self-healing in an acrylic coating, and thus represents an important step toward developing self-healing paint.

3.5 REFERENCES

1. Hoogenboom, R., Hard Autonomous Self-Healing Supramolecular Materials—A Contradiction in Terms? *Angewandte Chemie International Edition* **2012,** *51* (48), 11942-11944.

2. Beach, M.; Davey, T.; Subramanian, P.; Such, G., Self-healing organic coatings – Fundamental chemistry to commercial application. *Progress in Organic Coatings* **2023,** *183*, 107759.

3. Fujisawa, Y.; Asano, A.; Itoh, Y.; Aida, T., Mechanically Robust, Self-Healable Polymers Usable under High Humidity: Humidity-Tolerant Noncovalent Cross-Linking Strategy. *J Am Chem Soc* **2021,** *143* (37), 15279-15285.

4. Peng, Y.; Gu, S.; Wu, Q.; Xie, Z.; Wu, J., High-Performance Self-Healing Polymers. *Accounts of Materials Research* **2023,** *4* (4), 323-333.

5. Hentschel, J.; Kushner, A. M.; Ziller, J.; Guan, Z., Self-healing supramolecular block copolymers. *Angew Chem Int Ed Engl* **2012,** *51* (42), 10561-5.

6. Guo, M.; Pitet, L. M.; Wyss, H. M.; Vos, M.; Dankers, P. Y.; Meijer, E., Tough stimuli-responsive supramolecular hydrogels with hydrogen-bonding network junctions. *J Am Chem Soc* **2014,** *136* (19), 6969-6977.

7. Chen, J.; Yan, B.; Wang, X.; Huang, Q.; Thundat, T.; Zeng, H., Core cross-linked double hydrophilic block copolymer micelles based on multiple hydrogen-bonding interactions. *Polymer Chemistry* **2017,** *8* (20), 3066-3073.

8. Fruijtier-Pölloth, C., Safety assessment on polyethylene glycols (PEGs) and their derivatives as used in cosmetic products. *Toxicology* **2005,** *214* (1-2), 1-38.

9. Jones, F. N.; Nichols, M. E.; Pappas, S. P., *Organic coatings: science and technology*. John Wiley & Sons: 2017.

10. Knop, K.; Hoogenboom, R.; Fischer, D.; Schubert, U. S., Poly (ethylene glycol) in drug delivery: pros and cons as well as potential alternatives. *Angewandte chemie international edition* **2010,** *49* (36), 6288-6308.

11. Meka, V. S.; Sing, M. K. G.; Pichika, M. R.; Nali, S. R.; Kolapalli, V. R. M.; Kesharwani, P., A comprehensive review on polyelectrolyte complexes. *Drug Discov Today* **2017,** *22* (11), 1697-1706.

12. Ooya, T.; Lee, J.; Park, K., Effects of ethylene glycol-based graft, star-shaped, and dendritic polymers on solubilization and controlled release of paclitaxel. *J Control Release* **2003,** *93* (2), 121-127.

13. Wang, J.; Del Rosario, L. S.; Demirdirek, B.; Bae, A.; Uhrich, K. E., Comparison of PEG chain length and density on amphiphilic macromolecular nanocarriers: self-assembled and unimolecular micelles. *Acta Biomaterialia* **2009,** *5* (3), 883-892.

14. Jee, J. P.; Kim, H. J., Development of Hydrogel Lenses with Surface-immobilized PEG Layers to Reduce Protein Adsorption. *Bulletin of the Korean Chemical Society* **2015,** *36* (11), 2682-2687.

15. Sim, S. L.; He, T.; Tscheliessnig, A.; Mueller, M.; Tan, R. B.; Jungbauer, A., Branched polyethylene glycol for protein precipitation. *Biotechnology and bioengineering* **2012,** *109* (3), 736-746.

16. Gillich, T.; Acikgöz, C.; Isa, L.; Schlüter, A. D.; Spencer, N. D.; Textor, M., PEG-stabilized core–shell nanoparticles: Impact of linear versus dendritic polymer shell architecture on colloidal properties and the reversibility of temperature-induced aggregation. *Acs Nano* **2013,** *7* (1), 316-329.

17. Lovell, P. A.; Schork, F. J., Fundamentals of Emulsion Polymerization. *Biomacromolecules* **2020,** *21* (11), 4396-4441.

18. Chiefari, J.; Chong, Y. K.; Ercole, F.; Krstina, J.; Jeffery, J.; Le, T. P. T.; Mayadunne, R. T. A.; Meijs, G. F.; Moad, C. L.; Moad, G.; Rizzardo, E.; Thang, S. H., Living free-radical polymerization by reversible addition-fragmentation chain transfer: The RAFT process. *Macromolecules* **1998,** *31* (16), 5559-5562.

19. Moad, G.; Rizzardo, E.; Thang, S. H., Living radical polymerization by the RAFT process–a second update. *Aust J Chem* **2009,** *62* (11), 1402-1472.

20. Corrigan, N.; Jung, K.; Moad, G.; Hawker, C. J.; Matyjaszewski, K.; Boyer, C., Reversible-deactivation radical polymerization (Controlled/living radical polymerization): From discovery to materials design and applications. *Progress in Polymer Science* **2020,** *111*, 101311.

21. Destarac, M., Industrial development of reversible-deactivation radical polymerization: is the induction period over? *Polymer Chemistry* **2018,** *9* (40), 4947-4967.

22. Dankers, P. Y. W.; Hermans, T. M.; Baughman, T. W.; Kamikawa, Y.; Kieltyka, R. E.; Bastings, M. M. C.; Janssen, H. M.; Sommerdijk, N. A. J. M.; Larsen, A.; van Luyn, M. J. A.; Bosman, A. W.; Popa, E. R.; Fytas, G.; Meijer, E. W., Hierarchical Formation of Supramolecular Transient Networks in Water: A Modular Injectable Delivery System. *Advanced Materials* **2012,** *24* (20), 2703-2709.

23. Gao, Y.; Xu, J.; Zhang, C.; Venugopal, H.; Kermaniyan, S. S.; Such, G.; Ritchie, C., Rationale Design of pH-Responsive Core–Shell Nanoparticles: Polyoxometalate-Mediated Structural Reorganization. *Acs Appl Nano Mater* **2020,** *3* (11), 11247-11253.

24. Hassan, P. A.; Rana, S.; Verma, G., Making Sense of Brownian Motion: Colloid Characterization by Dynamic Light Scattering. *Langmuir* **2015,** *31* (1), 3-12.

25. Beach, M. A.; Teo, S. L. Y.; Chen, M. Z.; Smith, S. A.; Pouton, C. W.; Johnston, A. P. R.; Such, G. K., Quantifying the Endosomal Escape of pH-Responsive Nanoparticles Using the Split Luciferase Endosomal Escape Quantification Assay. *ACS Appl Mater Interfaces* **2022,** *14* (3), 3653-3661.

26. McNamee, C. E.; Yamamoto, S.; Higashitani, K., Effect of the Physicochemical Properties of Poly(Ethylene Glycol) Brushes on their Binding to Cells. *Biophys J* **2007,** *93* (1), 324-334.

27. Gao, H.; Matyjaszewski, K., Synthesis of functional polymers with controlled architecture by CRP of monomers in the presence of cross-linkers: From stars to gels. *Progress in Polymer Science* **2009,** *34* (4), 317-350.

28. Zhao, T.; Zhang, H.; Zhou, D.; Gao, Y.; Dong, Y.; Greiser, U.; Tai, H.; Wang, W., Water soluble hyperbranched polymers from controlled radical homopolymerization of PEG diacrylate. *RSC Advances* **2015,** *5* (43), 33823-33830.

29. Czaderna-Lekka, A.; Kozanecki, M.; Matusiak, M.; Kadlubowski, S., Phase transitions of poly(oligo(ethylene glycol) methyl ether methacrylate)-water systems. *Polymer* **2021,** *212*, 123247.

30. Ramesh, N.; Davis, P.; Zielinski, J.; Danner, R.; Duda, J., Application of free-volume theory to self diffusion of solvents in polymers below the glass transition temperature: A review. *Journal of Polymer Science Part B: Polymer Physics* **2011,** *49* (23), 1629-1644.

31. de Greef, T. F.; Nieuwenhuizen, M. M.; Sijbesma, R. P.; Meijer, E., Competitive intramolecular hydrogen bonding in oligo (ethylene oxide) substituted quadruple hydrogen bonded systems. *The Journal of Organic Chemistry* **2010,** *75* (3), 598-610.

Chapter 4. Self-Healing Paint

ABSTRACT

Paints are an acrylic polymer matrix containing inorganic pigment particles and a variety of other function-specific additives, which impart both protective and decorative functionality on the surfaces they coat. Paints encompass a majority of the coatings market, yet a self-healing paint has never been successfully designed, let alone implemented in a manner that is commercially feasible. In this study, Weathershield™, a decorative paint marketed by the international paint company DuluxGroup, was functionalized with a self-healing monomer in order to investigate a potential self-healing paint. This monomer comprised the strong hydrogen bonding unit UPy, which was separated from a methacrylate backbone by a long amphiphilic spacer (UPy-2). UP-2 was able to successfully undergo an industrial-scale emulsion polymerization as well as paint formulation, and the resultant UPy functionalized paint (UPy-Paint) was subjected to a variety of industry standard tests as well as self-healing evaluation. The UPy-Paint largely maintained the mechanical properties necessary for effective paint performance, but had slightly reduced adhesion and scrub resistance properties. The UPy-Paint also displayed optical self-healing of a crack at room temperature relative to unfunctionalized Weathershield. However, this self-healing performance was suppressed when the paint was applied to a substrate, and it displayed minimal strain recovery following self-healing either at room temperature or elevated temperature (50˚C). Nevertheless, this UPy-Paint design further enhances our understanding of the factors that influence self-healing, and represents a foundation for future studies on designing a commercially viable paint with self-healing performance.

4.1 INTRODUCTION

All organic coatings are susceptible to mechanical damage in the form of cracking, which over time can severely reduce their ability to protect an underlying substrate.[1] Self-healing technology offers the opportunity to radically enhance the performance and service lifetime of coatings, through the ability to spontaneously heal damage without external intervention. The commercial benefits of such technology include enormous reductions in maintenance costs, which according to some estimates range into the trillions of dollars per year,[2] as well as

enhanced protective and aesthetic functionality. Thus, there is a clear incentive in materials science to develop effective and commercially viable self-healing coatings.

The mechanism by which self-healing occurs can generally be divided into two categories. The first category, known as extrinsic self-healing, generally involves the microencapsulation of a healing agent distinctly separate from the coating matrix.[3] Upon mechanical damage, the capsules break, allowing the healing agent to flow into cracks and initiate healing, normally through auto-polymerization in the presence of a catalyst. The second category, intrinsic self-healing, involves functionalizing the coating with either reversible covalent or supramolecular bonds.[4] Upon damage these bonds are ripped apart, and self-healing occurs due to the attractive forces between these bonds.

Epoxy resins and polyurethane anticorrosive coatings are the principal subjects of fundamental self-healing studies, and have therefore garnered the most attention as commercially viable self-healing coatings — a fact clearly evident in the patent literature. For example, the microencapsulation of self-healing agents has been applied to develop self-healing polyurethane coatings,[5] via the release and auto-polymerization of liquid diisocyanate monomer, and self-healing epoxy resins,[6] via the release of solvent-borne alkoxysilane sealant, which hardens as the solvent evaporates. These patented designs both utilize non-toxic microcapsules, comprised of a wax shell and a polymeric shell respectively, which is a necessity for wide industrial application. Autonomic Materials Inc have utilized microcapsule-based self-healing to design AMP-UP™, a product range of self-healing epoxy resins based on the release of healing agent from damaged microcapsules. These self-healing coatings are designed to protect metal substrates from corrosion or concrete from damage and represent the first commercially available self-healing organic coating.

Organic coatings which are comprised of acrylic polymers form the basis of paints, which are arguably the most important type of coating, representing over half of the total coatings market in value, and around 60% of all coatings produced globally by volume.[7] It would be expected that such an important kind of coating should spark significant research and investment into self-healing designs. However, over the last 20 years, progress into commercially viable self-healing acrylic coatings, let alone paints, has been limited.[8] Companies have recently employed intrinsic strategies to design self-healing acrylic coatings. Covestro, for example, obtained a patent describing the creation of a hydrogen bonding-based self-healing acrylic coating for

protecting optical fibers.[9] This self-healing acrylic resin relied both on UV curing, and the presence of a very high amount of self-healing oligomers (up to 80 wt% of the coating), minimizing its wider applicability. Another patent, obtained by Behr in 2020, claims to have developed a self-healing acrylic coating based on the widely studied reversible covalent bond reaction, the Diels–Alder reaction.[10] The primary drawback of employing reversible covalent bonds for the design of a commercially viable intrinsic self-healing coating is the high temperatures needed to induce self-healing, which are often greater than 100 ˚C. However, Hentschel and the other inventors of the patent were able to reduce this healing temperature to a relatively mild 60˚C. Furthermore, their self-healing polymer was incorporated into paint at a maximum of only ~10 mol%. However, the self-healing efficiency of this design was poor. Given the lack of significant patent literature describing self-healing acrylic coatings, as well as the obvious drawbacks with the minimal amount of designs that do exist, there exists an incentive to design an efficient and commercially viable self-healing paint.

Paints are based on acrylic polymeric matrix, known as a binder, but are in fact a complex mixture of many parts. In a wet state, these acrylic polymers exist as a suspension of nanoparticles, known as a latex. A paint's colour and opacity (transparency) is derived from pigments, which are insoluble inorganic particulates that absorb and scatter certain wavelengths of light. Titanium dioxide nanoparticles (200–300 nm), which provide the paint's opacity and a bright white colour, are the most common, and most expensive additive. Larger inorganic fragments (~5 μm), known as extenders, scatter light by roughening the surface of the paint, thus providing a glossy or matte appearance depending on concentration. Dispersants are charged species which adsorb onto the surface of pigments, stabilizing them in wet paint. Thickeners, as the name suggests, increase the viscosity of the paint, and are bulky, often cellulosic, compounds. Thickeners which contain hydrophobic end-groups that adsorb to the surface of pigment particles are known as associative thickeners. Coating formation relies on the coalescence of the acrylic latex particles which make up the binder. This is only possible if the particles are soft enough to entangle, and coalescence will not occur if the polymer particles are glassy and rigid. Volatile organic compounds (VOCs) such as texanol are added to the paint to temporarily soften the polymer particles. Once coalescence has occurred, these VOCs evaporate, hardening the film and giving the dried paint its distinctive smell. Figure 4.1 shows a typical latex acrylic paint made up with its principal components in both the wet and dry stage.

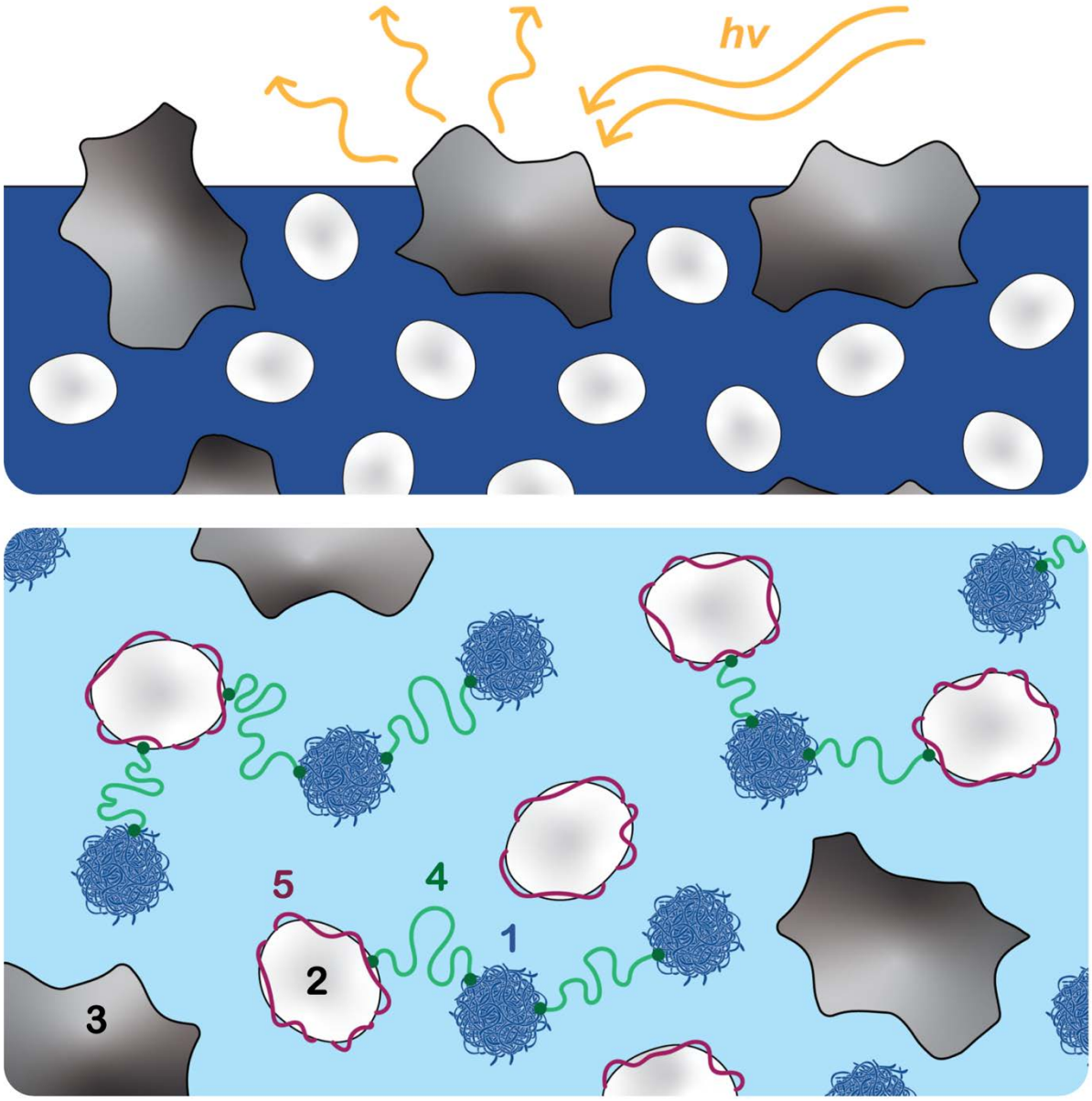

Figure 4.1 A typical acrylic paint in its dry (top) and wet (bottom) film forms. Polymeric latex particles (1) are suspended in water, and coalesce to form the body of the paint, 'binding' the other materials in place. Titanium dioxide nanoparticles (2) provide the paint's colour and opacity, while the extenders (3) scatter light, controlling its gloss. In the wet stage, associative thickener (4) increases the viscosity of the paint, and dispersant (5) stabilizes the insoluble pigment particles.

It is possible to design an acrylic monomer containing a flexible amphiphilic spacer end-capped with the strong hydrogen bonding unit 2-ureido-4[1H]-pyrimidinone (UPy). This monomer can be incorporated into an acrylic latex and instill the subsequent coating with self-healing performance via a self-complementary hydrogen bonding network. This self-healing is viable under ambient conditions and grows more efficient with increasing temperatures. In Chapter 2, four such monomers were synthesized, and the monomer UPy-2 displayed the most promising self-healing efficiency. Such healing in the context of a transparent acrylic film represents a significant step forward in the study of self-healing organic coatings, which has traditionally focused on epoxy and polyurethane coatings. It also allows for an investigation into the next logical step for this UPy-based healing technology, incorporation into paint. This chapter investigates a design which has shown promise as a self-healing technology at smaller scale under laboratory conditions, and scaling it up to assess whether the design is applicable in a wider industrial setting. UPy-2 was selected as the basis for a paint binder as its self-healing properties proved the most efficient at room temperature and at elevated temperature. Furthermore, the addition of a single monomer to the paint formulation represents a facile design, and the synthetic accessibility of UPy-2 allows it to be synthesized at a scale applicable to paint production (> 10g).

Pigments, extenders, dispersants, thickeners and other additives drastically increase the complexity and scale of paint relative to a simpler acrylic coating. This increased complexity raises important questions regarding the self-healing capability of the UPy-monomer design: 1) will self-healing be maintained as the latex represents a smaller fraction of the material? 2) will the introduction of inorganic fragments and particles impact the ability of the UPy functionalized polymers to spontaneously rearrange? And 3) how will the different mechanical and rheological properties of the paint affect self-healing?

The comparison between UPy-2 and UPy-3 in Chapter 2 demonstrates that UPy based self-healing is inextricably linked to the mobility of polymer chains, and the capacity of the UPy units to rearrange and self-complement, reforming the hydrogen bonding network. The longer spacer of UPy-2 maximizes this effect relative to other self-healing monomer designs. The fact that general healing efficiency increases markedly with increasing temperature further reinforces this conclusion. In addition, the introduction of a bis-UPy crosslinker (MW = 10 kDa) slightly enhanced the healing efficiency of the polymer film, suggesting that a higher amount of UPy units increases the overall self-healing effect (Chapter 3). These two principles

yield clear hypotheses regarding the questions posed. The reduction of UPy units as a fraction of the overall material will reduce self-healing efficiency, and the material properties of the paint will significantly impact self-healing. The introduction of pigments and other elements will also impact the stiffness and rheological properties of the paint, likely affecting self-healing efficiency.

Titanium dioxide nanoparticles as pigments and opacifiers are the most prolific compound in a paint mixture other than the polymeric binder, and therefore will have the greatest impact on the mechanical properties of the paint. The effects of pigments on a coating's mechanical properties are well studied, and in general, given an even dispersion of pigment nanoparticles, serves to increase both the Young's modulus (resistance to deformation), tensile strength, toughness and stiffness of the coating, while decreasing its ductility.[11, 12] This is due to the fact that pigments such as titanium dioxide have a Young's modulus two orders of magnitude higher than most acrylic binders (~ 200 GPa as opposed to ~ 0.1–2 GPa respectively).[13] The introduction of pigments into a coating is often framed as an enhancement of its mechanical properties. While this is certainly true, pigments are also likely to have a detrimental effect on the self-healing capacity of the paint, relative to its functionalized binder, as they stiffen the material and reduce the degrees of freedom associated with the UPy functionalized polymers.

To determine how these various additives might impact self-healing performance, and to investigate the feasibility of a commercially viable self-healing trade paint, the monomer UPy-2 was incorporated into a scaled-up synthesis of an acrylic latex, which then formed a commercially available paint binder. The synthesis and formulation of this UPy functionalized acrylic latex followed the procedures practiced at DuluxGroup, a leading marketer and manufacturer of architectural paints. The UPy-functionalized latex was then added to a paint formulation based on Weathershield, one of Dulux's exterior paint product ranges. First, this UPy-Paint was subjected to a variety of industry standard paint tests, including scrub resistance and adhesion tests. The UPy-Paint was found to maintain ~75% of Weathershield's scrub resistance, and showed strong adhesion to wood and metal — albeit slightly less than Weathershield. The self-healing performance of the UPy-Paint was analyzed through both optical and strain recovery tests. Free UPy-Paint showed optical self-healing compared to Weathershield, however this healing was diminished when the paint was applied to a substrate. Furthermore, the UPy-Paint did not exhibit any notable strain recovery. Despite this loss of self-healing efficiency in the paint, relative to a transparent acrylic coating, this work provides

a valuable insight into both the mechanisms that govern intrinsic self-healing and the challenges associated with commercializability, and serves as a promising foundation to design effective self-healing paint in the future.

4.2 EXPERIMENTAL

4.2.1 Materials

Paint synthesis and experiments were conducted at the DuluxGroup Innovation Centre in Clayton, Victoria. Poly(ethylene glycol) methacrylate (PEGMA) (molecular weight (MW) = 500), hexamethylene diisocyanate and the catalysts dibutyl tin dilaurate were sourced from Sigma Aldrich. All other materials were provided by DuluxGroup.

4.2.2 Characterization

^{1}H-NMR spectroscopy was performed on a 400 MHz Varian 400 MR spectrometer using deuterated chloroform (CDCl3) as the solvent. ^{1}H NMR analysis was performed on MestreNova software. IR spectroscopy was performed on a Perkin Elmer Spectrum 2 ATR-FTIR spectrometer, and UV Vis spectroscopy was performed on Cary 60 UV-Vis (Agilent technologies). Dynamic light scattering analysis of particle size was performed on a Horiba Nanopartica SZ-100 (Horiba Scientific, Japan), operating at 37℃ and a fixed scattering angle of 90˚. Optical microscopy images were taken on an optical microscope and TEM images were recorded on a FEI Talos L120C cryoTEM. Sample areas were exposed to a constant stream of electrons to remove ice crystals from the images. Tensile tests were carried out on an Instron 5944, 2kN microtester. Differential scanning calorimetry was performed on a Perkin Elmer 8500 Double Furnace HyperDSC from –50 to 70˚C at 10˚C per min. An Elcometer 1720 Abrasion and Washability Tester measured scrub resistance, and Elcometer adhesive tape was used during adhesion testing.

4.2.3 Latex formulation

This latex formulation is based on Optima™, a widely used latex at Dulux.

REAGENTS	Wt %	
Dosed Water	57.53	
Surfactant (sodium dodecyl sulfate)	2.06	
Ammonium Persulfate	0.204	
Sodium Carbonate	0.052	
Ammonia	0.67	
t-butyl Perbenzoate	0.12	
Sodium Erythorbate	0.07	
Biocides	0.275	
Anti-Foam	0.01	
Monomers	**Wt %**	**Monomer %**
MMA	18.62	47.75
BA	18.62	47.75
AA	0.78	2.00
UPy-2	0.975	2.50
Total	*99.98 wt%*	

Sodium dodecyl sulfate was mixed with deionized water to form the pre-emulsion, which was added into a reactor containing an internal temperature probe, two feed lines, a metal u-shaped agitator, and a condenser (Figure 4.2). The reactor was heated to 80˚C under nitrogen and stirred at 100 rpm. Four feeds were set up: an initiator spike, a monomer seed, an initiator feed, and a monomer feed. The monomer feed was sheared with a sawtooth agitator to form a white, creamy emulsion. The initiator spike and the monomer seed were initially added to the reactor, and the exotherm increased the reactor temperature to 83˚C. When the temperature returned to 80˚C and solution became blue, indicative of pre-nanoparticles (<50 nm), the monomer and initiator feeds were fed into the reactor over 3 hours. Following this, the reaction was neutralized with ammonia, and the remaining unreacted monomer (<5%) was polymerized via the addition of sodium erythorbate, a reducing agent, and tert-butyl-perbenzoate, an oxidizing agent. The reactor was then left to cool, and at 40˚C, 1 drop of antifoam was added to reduce foaming, and biocides were added to prevent the buildup of mold.

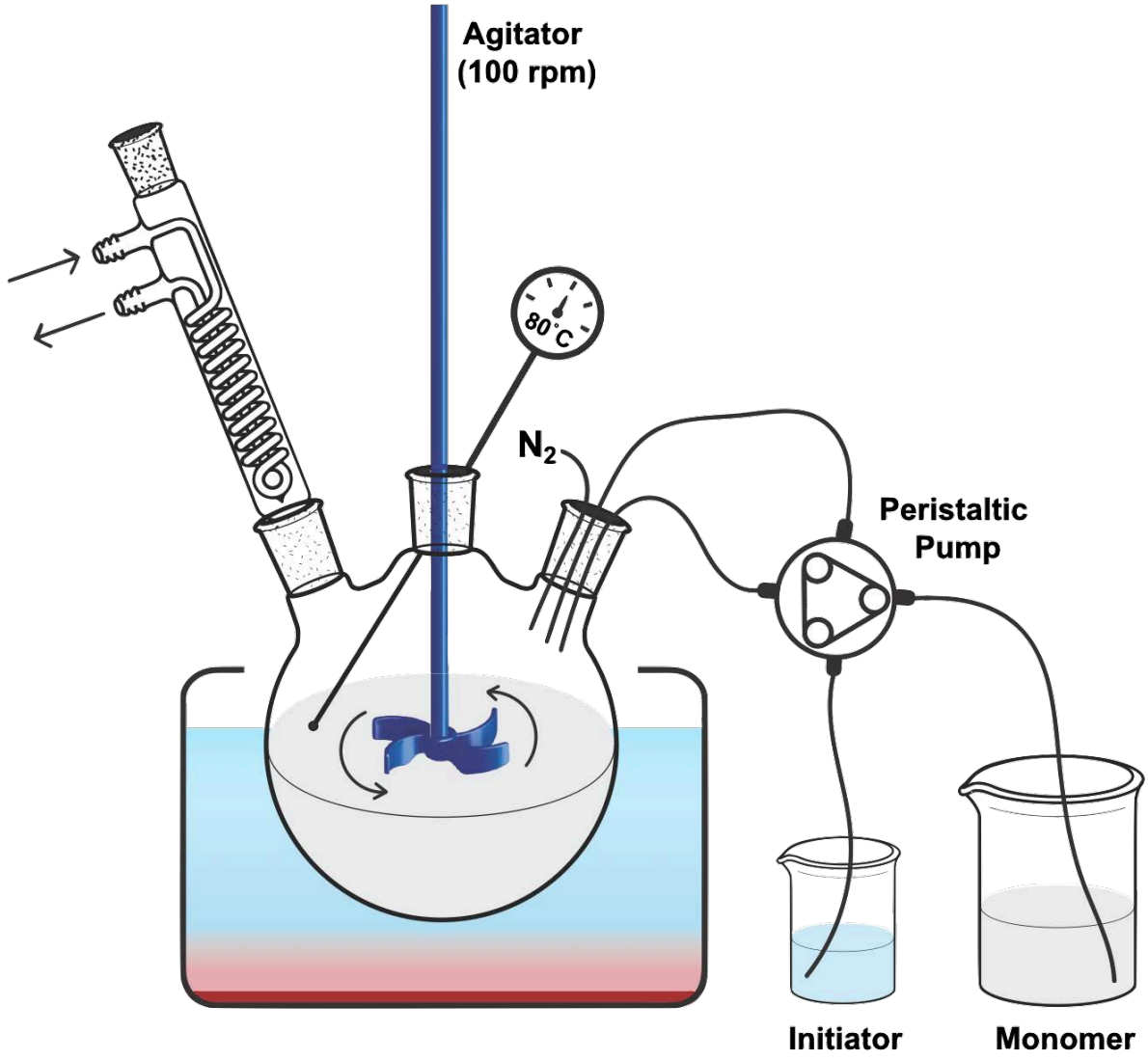

Figure 4.2 A simplified diagram of a typical large scale (1 kg) emulsion polymerization setup, whereby the monomers are evenly fed into the 80˚C reactor via a peristaltic pump. The monomer feed, in combination with water and surfactant, is first sheared to form a white creamy emulsion.

4.2.4 Paint formulation

REAGENTS	Wt %
Water	10.55
Latex	46.87
Pigment/Opacifier	21.26
Extender	13.22
Thickener	2.38
Surfactant	0.39
Dispersant	1.46
Coalescent	0.76
Biocide	0.6
Defoamer	0.37
Zinc oxide	0.32
Propylene glycol	1.73
Amino methyl propanol	0.1
Total	*100.01 wt%*

Deionized water was mixed with associative thickener in a 1L plastic container, and subjected to 30 seconds of strong shear force via a speedmixer. Then water, non-ionic surfactant, and a urethane-based thickener were added, and the mixture was further sheared for 30 seconds. To this mixture, water, titanium dioxide nanoparticles and ~5 μm calcium carbonate fragments were added, as well as a small amount of dispersant and thickener. Zinc oxide and amino methyl propanol were added, and the entire mixture was sheared for 120 seconds. This mixture, primarily comprised of titanium dioxide opacifiers and calcium carbonate extenders in water, is known as the millbase. The latex was added to this millbase, as well as trace amounts of coalescent and biocides. Hollow polystyrene microcapsules were added to further opacify the paint. The paint was sheared for 120 seconds. Once completed, the paint was a highly viscous, bright white liquid.

4.2.5 Scrub resistance

Scrub resistance was measured using an Elcometer 1720 Abrasion and Washability Tester. 5mL of paint was drawn down on a black plastic scrub resistance panel using a 200μm doctor blade. Care was taken to make sure the paint was drawn down evenly, and that there were no

impurities or irregularities in the film. This paint was left to dry at 25˚C for 7 days. Jif cleansing cream was dispersed onto a nylon brush, and two shims (16.8 cm x 1.3 cm x 0.025 cm) were inserted under the panel to raise it to contact with the nylon brush. The raised section of film was then scrubbed by the nylon brush in cycles. Abrasion was defined by the number of scrub cycles necessary to completely remove paint across the 1.3 cm width of each shim. Complete abrasion appeared as a clear and continuous black line across the paint. 4 repeats were taken for the UPy-Paint, and Weathershield (no UPy-2).

4.2.6 Adhesion testing

A wood substate, a metal substrate and an alkyd substrate were chosen for testing the adhesion properties of the paint. Paint was drawn down onto each substrate using a 150 μm doctor blade. The paint was left to dry for a week, and four measurements were taken for each substrate: dry adhesion after 1 day, dry adhesion after 1 week, wet adhesion after 1 day, and wet adhesion after 1 week. Adhesion was tested by cutting a 7x7 square grid through the paint with a pen knife, and then Elcometer adhesive tape was applied to the grid. The tape was then ripped off, and coating adhesion was determined by the number of grid squares ripped off the substrate.

4.2.7 Film formation and self-healing tests

The films were cast in a silicone mold and left to dry at room temperature for 1 week and then at 50˚C for 2 days. Following this, rectangular films (30 mm x 12 mm x 800 μm) were cut. The tensile tests were carried out under the following conditions: a strain rate of 3 mm/min, a gauge length (fixture separation) of 17 mm and a temperature of 25˚C. An average result was calculated from three independent experiments.

To evaluate the strain recovery of the coatings (a measure of self-healing efficiency), a 5 mm long horizon cut was introduced to the coating via a razor blade. The coatings were then gently pressed together for 5 seconds and left to heal for 24 hours over a given healing temperature. The healed samples were subject to tensile tests. The Young's modulus (E), maximum stress (σ) and the strain at which the healed crack reopened (ε, failure strain, strain-at-break) was noted and compared to the strain at which an undamaged coating began to break apart.

4.3 RESULTS

4.3.1 UPy-2 latex

UPy-2 (2.5 wt%) was incorporated into a 1kg MMA/BA/AA latex emulsion (40% solids) following Dulux's Optima™ procedure. Initially a pre-emulsion seed stage was formed to control the polymerization rate and particle size, and then the monomer and initiator feeds were fed into the emulsion over 3 hours. Extremely high monomer conversion is required for any commercially viable system, and so following the emulsion feeds, a small amount of sodium erythorbate and tert-butyl perbenzoate–reducing and oxidizing agents respectively–was added to introduce enough radicals to drive monomer conversion from ~90% to >99.5%. Biocide was added to increase long-term storage capability by preventing the buildup of mold. Previously, a maximum of 2.5 wt% of UPy-2 was incorporated into the BA/MMA/AA monomer feed by sonication, as opposed to stirring. This process is impractical given scaled-up industrial conditions, and therefore UPy-2 was stirred overnight in the monomer feed. This resulted in an opaque solution whose stability over 3 hours was suspect. This solution however was emulsified with water and surfactant before being fed into the reactor, and the extreme shear of the blade, coupled with the quasi-stability of this emulsion, allowed UPy-2 to be stably fed into the reaction over 3 hours. This UPy-2 latex was employed as the binder of a UPy functionalized paint, which was formulated according to Dulux's Weathershield. This paint was compared to Weathershield itself, with the only difference between the two paints being the presence of UPy-2, added to the binder at 2.5 wt%.

In the context of paint, the Minimum Film Formation Temperature (MFFT) is defined as the lowest temperature at which a latex forms a film, upon solvent evaporation. Above this temperature, the hydrophobic polymers that comprise a latex particle are plastic enough to coalesce together, forming a transparent, isotropic coating. Below this temperature, glassy polymers prevent the deformation and coalescence of latex particles, locking them in place with void spaces in between. This results in a powdered, turbid film with extremely poor mechanical properties.[14] MFFT is a vital waterborne paint metric. To adequately decorate and protect surfaces, a paint cannot be applied below its MFFT. But MFFT is not as problematic for solvent-based paints, given that in solvent the polymers are already evenly dissolved, rather than present as a dispersion of nanoparticles in water.

For waterborne paints, MFFT is influenced by a complex set of factors including the monomer composition of the polymeric binder, the substrate, and various other additives, including surfactants, coalescents (plasticizers) and VOCs. Coalescents, for example, embed themselves between the polymer chains in latex particles, enhancing the free volume of the polymer chains and 'softening' them, allowing for film formation at lower temperatures.[15] These coalescents slowly evaporate, re-hardening the paint overtime. Predictably, MFFT is closely aligned with the *Tg* of the polymer binder (the temperature at which the polymers transition from glassy to rubbery). When temperatures are below *T*g, the glassy polymers will prevent the deformation and coalescence of latex particles, unless a coalescent is present. Above *T*g, the softer more malleable polymers allow for easy deformation and coalescence of these latex particles.

In order to verify that both the unfunctionalized MMA/BA/AA latex (control) and UPy-2 latexes formed transparent films, and to assess what impact the UPy monomer had on the coalescence properties of the latex, the MFFT was measured. This was done by forming long films of the UPy-2 latex and control latex (200 μm thickness), and subjecting the film to a temperature gradient, from –5˚C to 20˚C. MFFT was defined as the temperature at which the middle of the film was consistent and totally transparent, as opposed to opaque and powdery. The results are shown in Figure 4.3.

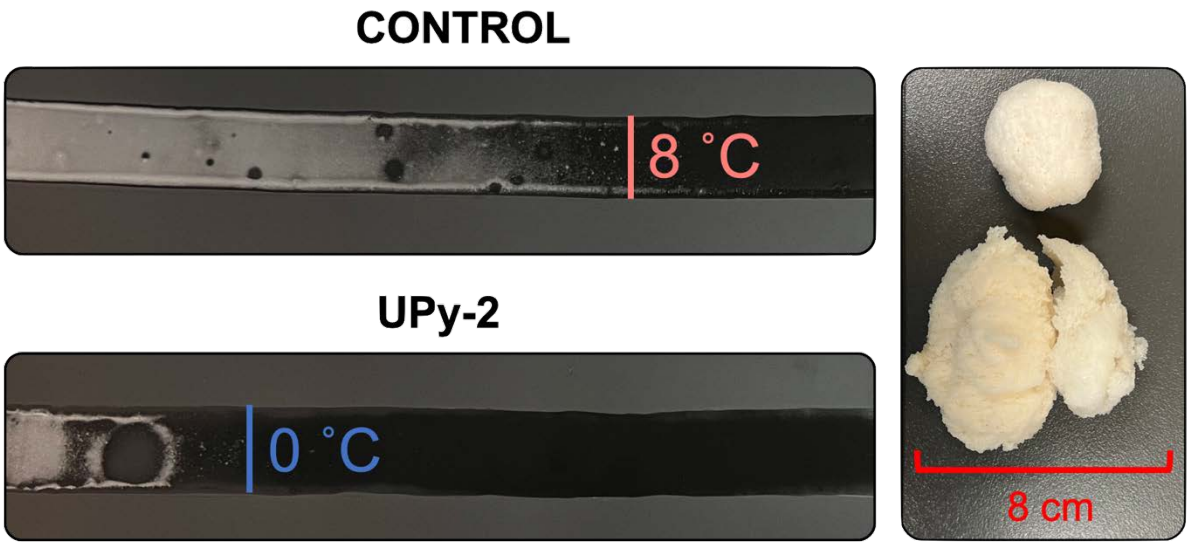

Figure 4.3 MFFT measurements for the control latex (top left) and the UPy-2 latex (bottom left). MFFT was the temperature at which the latex formed a clear coating, as opposed to an opaque, graining material. Significant coagulum is associated with the 1kg UPy-2 latex procedure, and an example of coagulum is shown on the right.

Figure 4.3 shows both the MFFT for the control, approximately 8˚C, and the UPy-2 latex, approximately 0˚C. The turbidity of the coatings is obvious below MFFT, and this section of the coating was powdery, immediately disintegrating upon external force. Above the MFFT, the coating is strong and optically transparent, due to the lack of distinct latex particles scattering light. This is indicative of polymer coalescence. The fact that the UPy-2 latex has a slightly lower *T*g than the control latex (Chapter 2), suggests that the MFFT of the UPy-2 latex will also be slightly below the control latex. Furthermore, the presence of UPy units on the surface of the latex particles, as shown in Figure S67, likely accelerates particle compaction, due to their strong self-complementary attraction, further lowering MFFT. Figure 4.3 verifies this hypothesis, with a difference of ~8˚C between the UPy-2 and control coatings. Undoubtedly the lower *T*g of the UPy-2 monomer reduces to some extent the MFFT of the resultant coating, however such a magnitude difference suggests that the self-complementary hydrogen bonding of the UPy units may provide a further driving force for latex particle coalescence.

The fact that the MFFT of the UPy-2 latex is significantly below the control may also yield insight into the conformation of the UPy functionalized polymers in latex particles. One might

expect the UPy units on the shell of the latex particles to hydrogen bond with each other, thus locking the particles in place and preventing coalescence. The lowered MFFT implies that either this mechanism does not occur, or is significantly minimized when compared to the other forces driving coalescence. The UPy-2 monomer is amphiphilic, where the hydrophobic section of the monomer, an aliphatic hexyl chain, is closest to the UPy unit itself. Thus, the UPy units may face inward to the hydrophobic latex particles, while only the hydrophilic PEG spacer is found on the particle surface. This conformation would minimize UPy complementation on the surface of particles, allowing for coalescence to occur. With all that said, Figure 4.3 shows that both the UPy-2 and control latexes easily form films both at room temperature, and at temperatures only slightly above freezing.

Figure 4.3 also illustrates the relatively high amount of coagulum (large lumps of polymer not present in latex form) which occurs during the emulsion polymerization of UPy-2. The amount of coagulum is significant, and varies between 3 and 4 wt% for repeated 1 kg emulsions. Notably, such coagulum is not present in the control latex, whose coagulum is <0.1 wt%. This implies that the presence of UPy-2, and the strong attractive forces between UPy units, are responsible for the increased coagulum. ^{1}H-NMR analysis of this coagulum showed that it was comprised of latex polymers and was not UPy-rich, therefore having no impact on the relative amount of UPy in the resultant latex (Figure S68)."

4.3.2 UPy-Paint

The UPy-2 latex was then incorporated into a paint formula based on Weathershield, a range of outdoor trade paints manufactured by Dulux. The latex comprised roughly 47 wt% of the final paint, with inorganic pigment (TiO_2) and calcium carbonate extender making up roughly 35 wt%, giving the paint a bright white, glossy appearance. Figure 4.4 displays a cryo-TEM image of the wet paint *in situ* (diluted in de-ionized water, 1:1000).

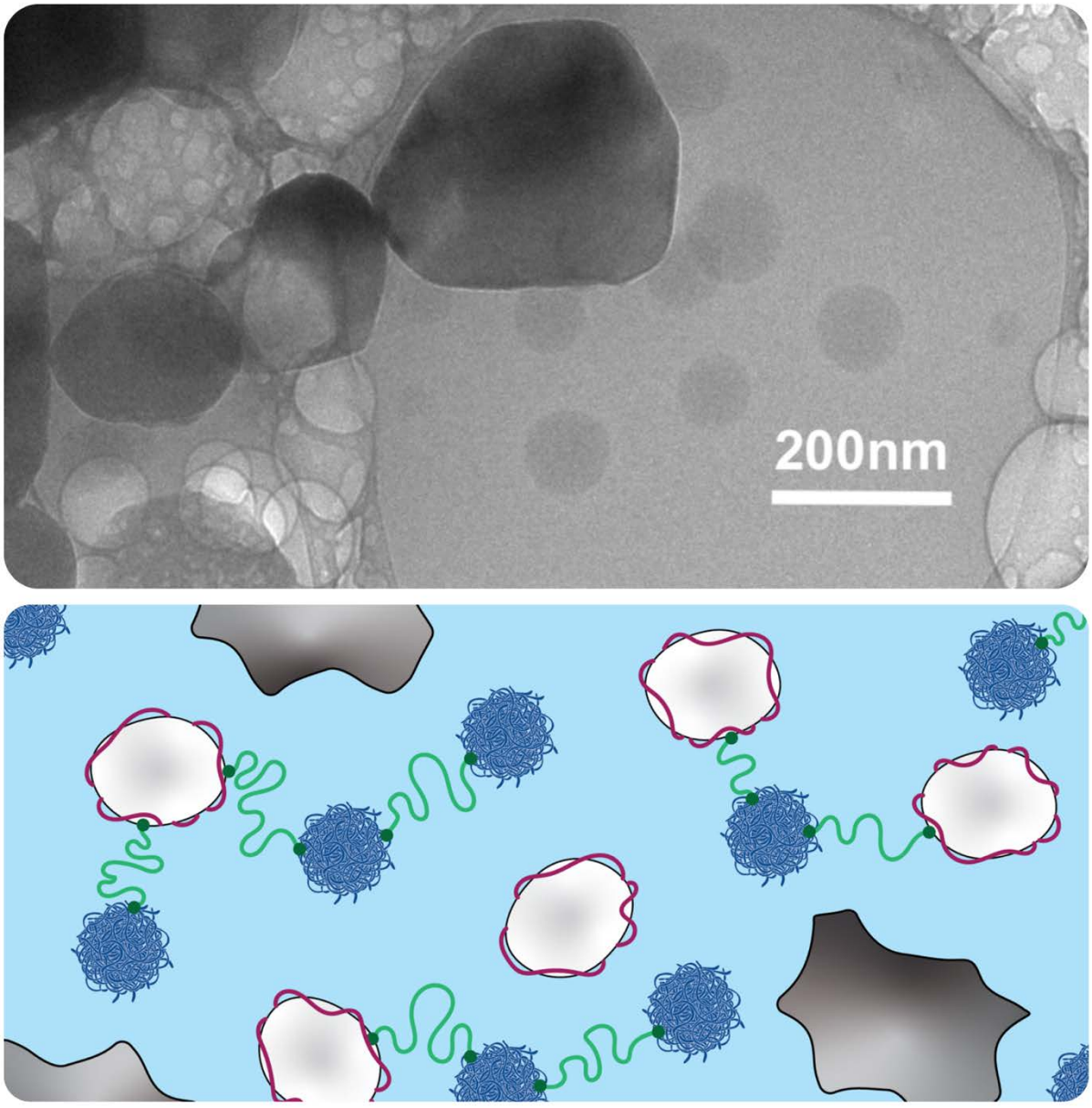

Figure 4.4 A Cryo-TEM image of the paint (top), in comparison to a theoretical image of the paint in its wet state (bottom). Cryo-TEM shows the presence of spherical latex nanoparticles, as well as the larger, darker TiO_2 pigment particles.

Of the myriad of paint components, one would expect to see both latex nanoparticles, which are spherical and have a diameter ~100nm, and TiO2 pigment particles, which appear as darker asymmetrically shaped rocks (200–300nm). The other paint components are either too small or, in the case of extenders, too large (>5μm) to be adequately viewed by TEM. Both latex nanoparticles and TiO2 pigment particles are clear in the image. Cryo-TEM shows that the latex particles are relatively monodispersed spheres approximately 100nm in diameter, and the TiO2 pigment particles are non-spherical and dark, with a greater variety in size (200–300nm). Interestingly, the TiO2 nanoparticles appear as agglomerates, rather than well dispersed particles. These agglomerations are generally apparent in TEM studies of TiO2 particles,[16] and may be an artifact of cryo-TEM sample preparation.

4.3.2.1 Adhesion

The function of a trade paint is to coat a substrate — normally the surface of a structure — in order to provide protection and decoration. Therefore, a paint's adhesive capability is vital to its overall performance. Dulux's Weathershield is designed to have strong adhesion to both wood and metal substrates, but displays weak adhesion to alkyd coated substrates. The adhesion of the UPy functionalized paint was compared with Weathershield using an industry standard test. A wood, metal and alkyd board were coated with the paints at a thickness of 200 μm, and a grid was cut into each. Tape was then applied to the grid and ripped off, and the adhesive properties were analyzed. This process was applied after 24 hours and then after a week, for both a dried and wet coating environment. The results are shown in Figure 4.5.

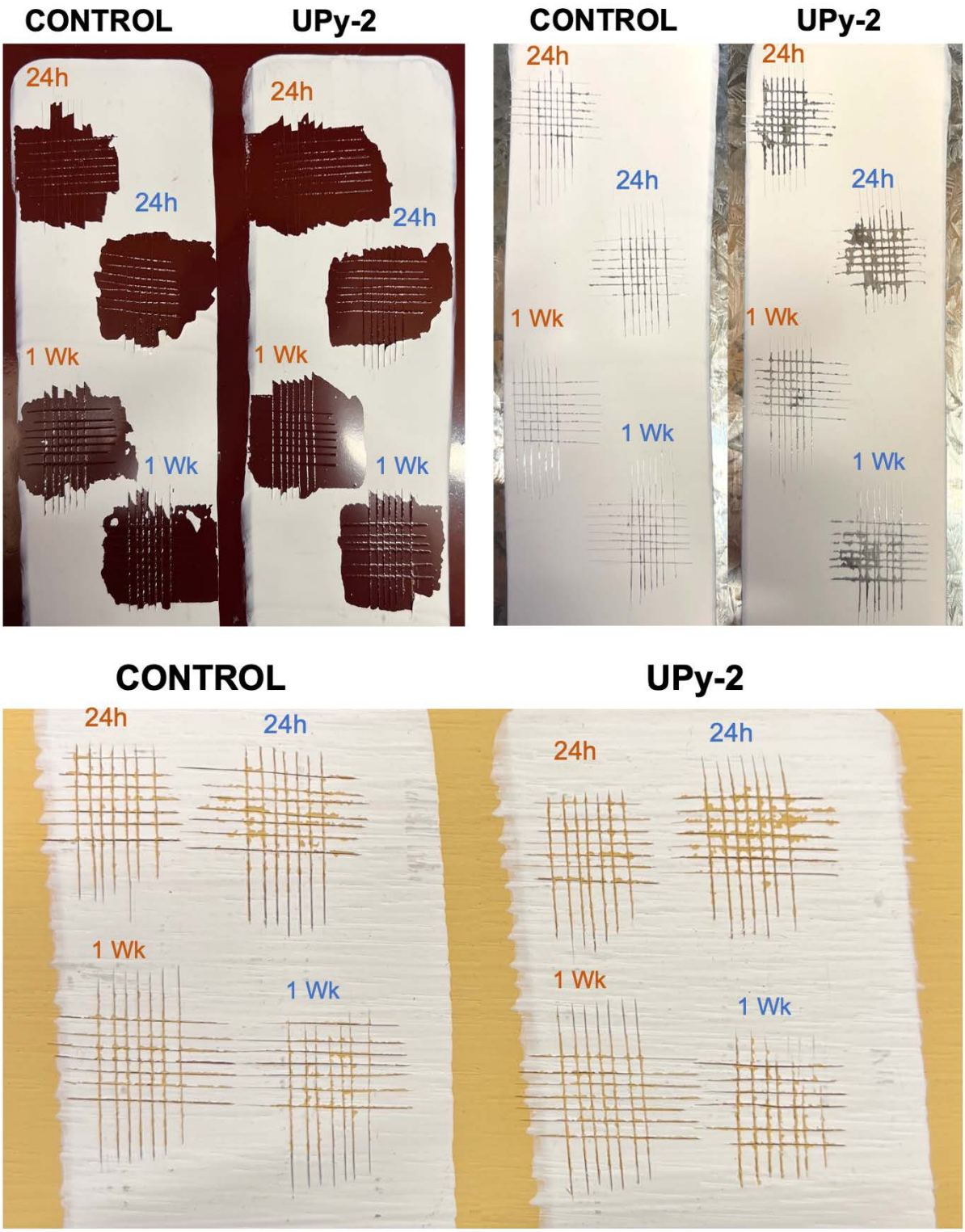

Figure 4.5 Adhesion testing for Weathershield (control) and the UPy-Paint. Three substrates were tested: Alkyd (top left), metal (top right) and wood (bottom). The tests were run in dry (orange) and wet (blue) conditions over 1 day and after 1 week (indicated in the figure).

The poor adhesion of both the UPy-Paint and Weathershield when applied to the alkyd substrate is readily apparent, with no paint remaining across the grid for any test. This is unsurprising, given that all waterborne acrylic paints have poor adhesion to alkyd surfaces, and solvent borne paints are generally required for alkyd coating. Both the UPy-Paint and Weathershield have very strong adhesion to the surface of wood after both 24 hours and a week. There is also little difference between dry adhesion, and adhesion when the paint is saturated with water. However, there is a slight loss of adhesion for the UPy-Paint when saturated with water after 24 hours, compared to the control. This pattern, while only very slight for adhesion to wood, is more pronounced for the paints when applied to a metal substrate. There is a very clear difference in adhesion between Weathershield and UPy-Paint after 24 hours under both dry and wet conditions. For 24 hours in wet conditions, a significant amount of the UPy-Paint is removed from the metal substrate. This pattern is apparent, though not as strong, for adhesion after 1 week.

The relatively poorer adhesion of the UPy-Paint when compared to Weathershield for both the wood and metal surfaces is surprising, given that hydrogen bonding moieties are readily used in paints to enhance adhesion. Ureido methacrylate, for example, is used in paint formulations for wood adhesion, as the ureido groups form hydrogen bonds with cellulose. Paradoxically, the incredible strength of UPy's quadruple self-complementary hydrogen bonding may be one of the sources of its poorer adhesion. Rather than form attractive bonds with the substrate, the self-complementation of UPy may dominate when the paint coalesces, providing no additional substrate adhesion. Another possible reason for the slight diminishment in adhesion is the presence of the long PEG spacer attached to the UPy-2 monomer. PEG is strongly hygroscopic, meaning that it absorbs and maintains moisture from its surroundings, and therefore may slightly increase the amount of water held within the coating, even after it dries, diminishing adhesion. This would also explain why the difference in adhesion between Weathershield and the UPy-Paint is more pronounced after 1 day, where a small amount of water is expected to be present in the coating, compared to one week, where only trace amounts of water should remain. Water reduces adhesion by preferentially forming hydrated layers on a substrate surface, inhibiting contact between the surface and coating.

4.3.2.2 Scrub resistance

Scrub resistance measures the durability of a dried coat of paint. Given the common occasions of wear due to abrasive materials, and repeated mechanical stress that paint is frequently subjected to, durability is a vital indicator of paint performance. Durability relies not only on substrate adhesion, but also on the chemistry and rheology of the coating itself. Failure to sufficiently maximize durability via scrub resistance undermines both the protective and aesthetic functionality of paint. Both the UPy-2 functionalized paint and Weathershield were subjected to controlled and repeated cycles of scrubbing with a nylon brush, and failure was defined by the presence of a continuous black line, indicative of complete paint removal. The results are displayed in Figure 4.6.

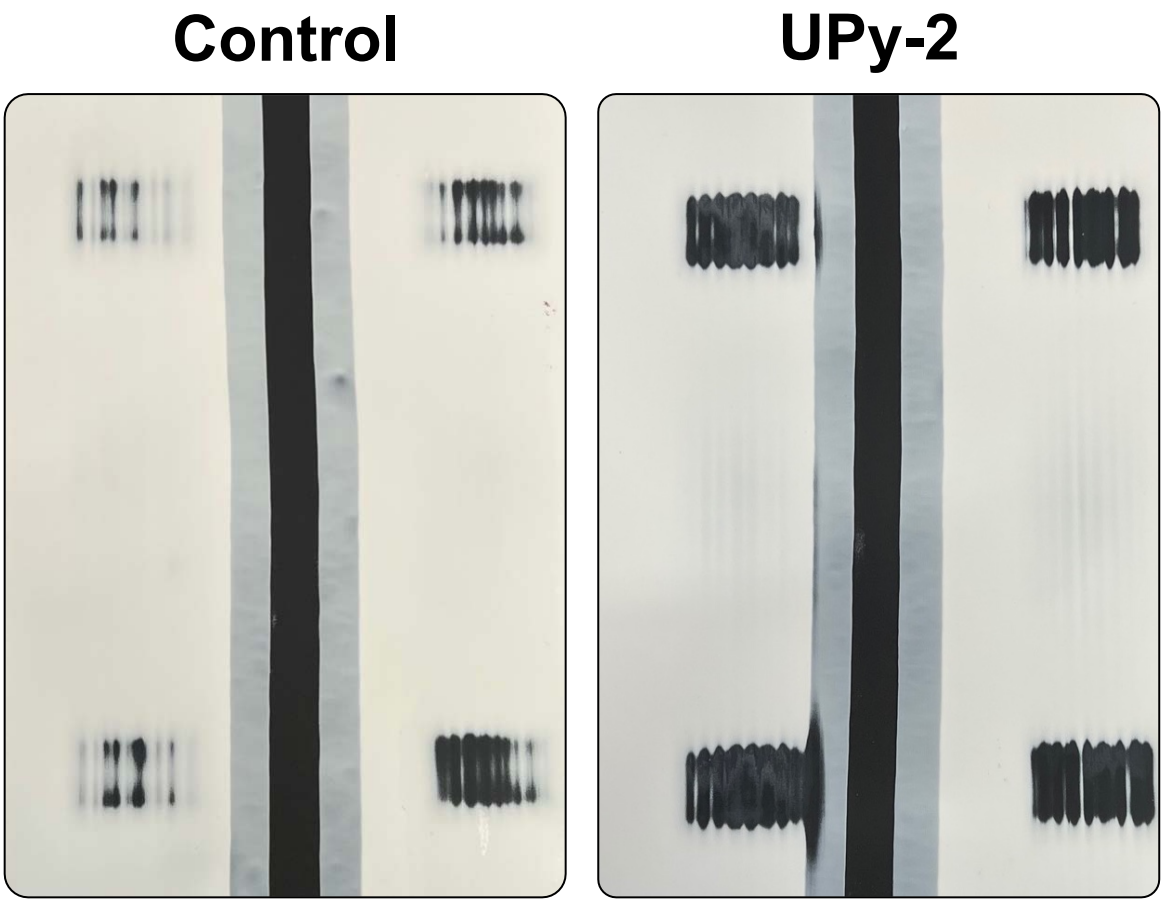

Figure 4.6 Scrub resistance tests for the UPy-2 functionalized paint and Weathershield. The paints were scrubbed with a nylon brush until the paint was fully removed, visualized by a continuous black line. The number of scrubs was noted for two different measurements of two independent experiments and averaged.

Figure 4.6 shows the results of four different scrubs for both Weathershield and the UPy-Paint. The number of scrubs required to induce failure was noted and averaged yielding 667 scrubs required to fail the control, and 490 scrubs required to fail the UPy-Paint. Both paints had strong scrub resistance, but Weathershield had a 26% superior scrub resistance to the UPy-Paint. Certainly, the UPy-Paint's diminished adhesive properties may also be affecting its scrub resistance, but given that scrub resistance is based on abrasion from the top of the coating, rather than the coating–substrate interface, rheology is likely to be a more influential factor. The UPy-Paint's only difference compared to Weathershield is the presence of UPy-2 in its binder. UPy-2, as shown in Chapter 2, slightly lowers both *T*g and Young's modulus, resulting in a coating that is slightly more susceptible to deformation. This change in the mechanical properties, though slight, is likely the primary reason for the difference in scrub resistance between Weathershield and the UPy-Paint.

Both adhesion and scrub resistance are two important metrics when considering the performance of a paint under real-world conditions, and must be taken into account for any newly designed product. Both tests conclude that the UPy-Paint has a diminished performance when compared to Weathershield. Given that the only difference between the two paints is the presence of UPy-2 in the polymeric binder, one must conclude that UPy-2 reduces both the durability and adhesion of paint. Nevertheless, both paints display strong scrub resistance, and the difference in adhesion on both wood and metal substrates, though visually apparent, is not prohibitively large. Therefore, any self-healing capability of the UPy functionalized paint would still represent a significant addition of highly sought-after functionality.

4.3.2.3 Paint self-healing experiments

The self-healing capability of the UPy-Paint was investigated and compared against Weathershield. Using a microscope, optical images of the paints before and after healing were obtained. The paints were dried in a silicon mold and cut with a razor, and then left to heal at room temperature over 24 hours. Previously, the UPy-2 functionalized latex, which is transparent, showed a clear visual difference in crack healing when compared to an unfunctionalized MMA/BA/AA coating (Chapter 2). Optical images of the UPy-Paint and Weathershield are shown below in Figure 4.7.

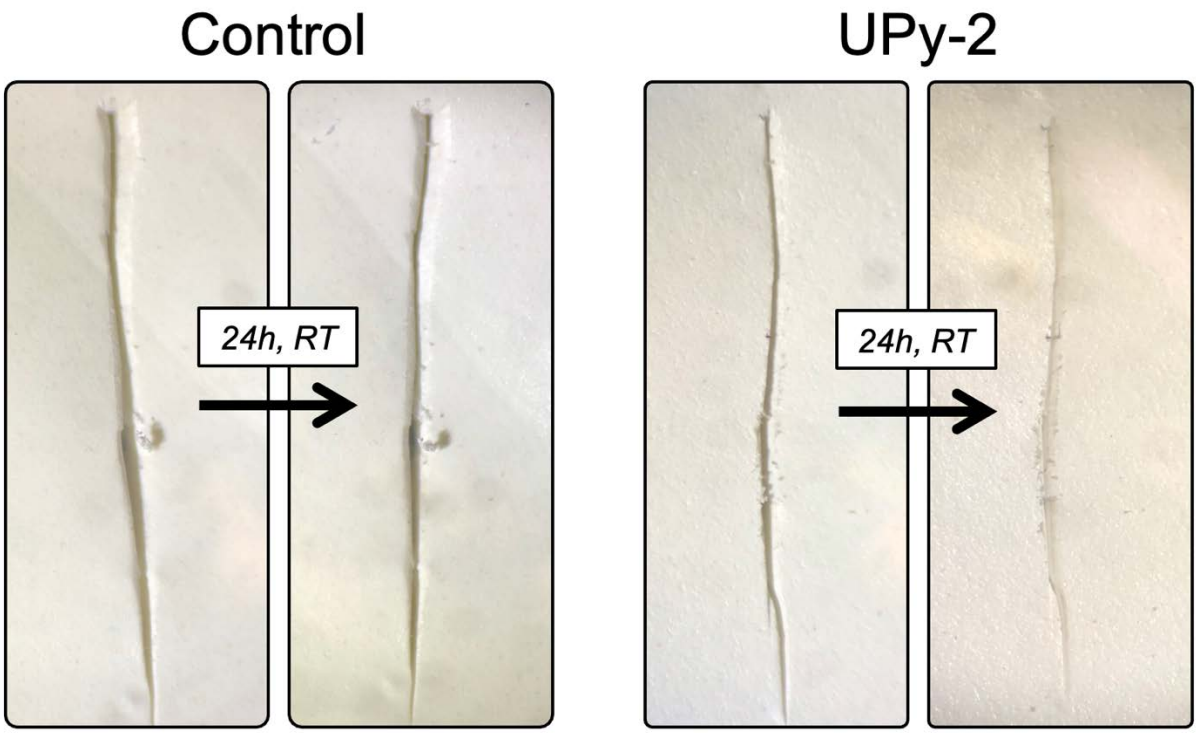

Figure 4.7 Optical microscopy images of Weathershield (control) and UPy functionalized paints, which were cut with a razor and allowed to heal spontaneously at room temperature over 24 hours.

Figure 4.7 displays what happens when the paints, in this case bright white due to the presence of titanium dioxide, are cracked and left to heal over 24 hours at room temperature. As expected, when Weathershield, which represents a typical range of trade paints already on the market, is subjected to cracking, there is essentially no evidence of self-healing. Interestingly, the UPy-Paint initially shows a distinct crack which appears to close, having spontaneously healed over 24 hours at room temperature. The gap between the sheared edges appears minimized, and the overall crack has faded and is less clearly apparent. Unsurprisingly, as with the UPy-2 polymer coating, the indentation of a crack still exists. Given the predicted stiffening of the paint film relative to the unpigmented transparent polymer coating, this is a noteworthy result.

As well as the predicted increase in toughness of the paint relative to the binder alone, another potential challenge to self-healing paint is the fact that paint adheres to a substrate. This adherence potentially limits the ability of the polymers within the coating to undergo sufficient rearrangement to reform broken hydrogen bonds, thus reducing self-healing efficiency.

Furthermore, most paint applications rely on a very thin coat of paint, below 200 µm thickness. Therefore, optical self-healing tests were repeated, with both Weathershield and the UPy-Paint drawn down on a metal substrate, rather than dried in silicone as a coating in free space. Then the coatings were cut with a razor, and their healing was monitored over 24 hours and 1 week at room temperature and at 50˚C. The results are displayed in Figures S66 and 4.8 below.

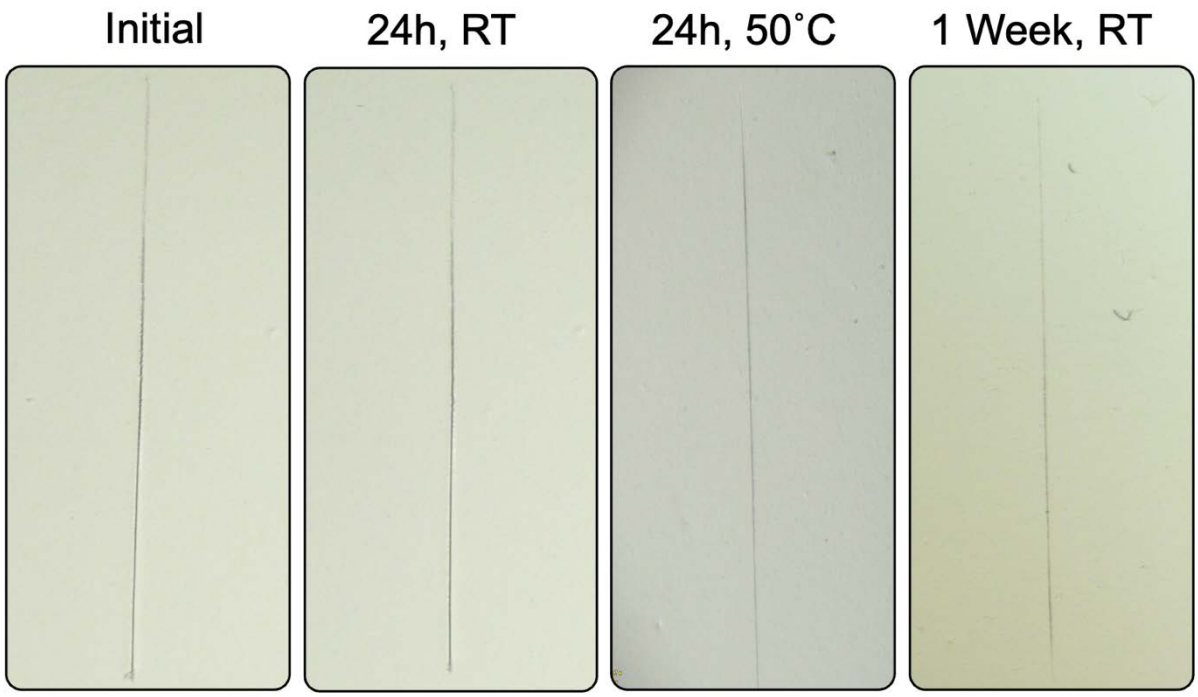

Figure 4.8 Optical microscope images of the UPy-Paint applied to a metal substrate and cut with a razor. The paint was left to heal at room temperature over 24 hours and 1 week, and at 50˚C over 24 hours.

Figure 4.8 displays the UPy-Paint cut with a razor and left to heal first over 24 hours at room temperature. Unfortunately, no self-healing was apparent over this time, as there is no discernible difference between the initial crack, and the crack after 24 hours. The paint was heated to 50˚C in an oven, and another image was taken after 24 hours. The temperature of 50˚C was chosen, as the greatest difference in self-healing efficiency between the UPy-2 latex coating and the control latex coating was observed at this temperature (Chapter 2). Again, there is no difference between the crack initially, and after 24 hours at this elevated temperature. Finally, the crack was left for 1 week, which also did not lead to any observable self-healing. The obvious lack of any noticeable self-healing performance is strong evidence supporting the

idea that anchoring the coating to a substrate drastically reduces its self-healing capability. The significant difference in visual self-healing performance between the UPy functionalized paint in free space, which shows some spontaneous crack healing, and the paint when adhered to a substrate, which displays negligible self-healing, is worthy of discussion.

One of the ways in which self-healing can be achieved in lower modulus materials with very little added functionality, is through the shape-memory effect. This effect involves a material which, when deformed, inherently wants to return to its original shape. In the case of polymeric coatings, the shape memory effect is instigated through high molecular weight, highly entangled and highly crosslinked polymers, which when deformed, are forced into an undesirable formation, like a 'coiled spring'.[17] The polymers, due to their conformational entropy, intrinsically 'uncoil', partially restoring the original shape.[18] In the present context, the polymeric binder of the paint is made up of coalesced, highly entangled, hydrophobic copolymers of MMA and BA primarily, and thus may have a small amount of shape-memory activity. However, the addition of UPy-2 into the polymeric matrix allows for crosslinking between the polymers due to the self-complementarity of the UPy moieties. Furthermore, the UPy-UPy self-complementary hydrogen bond is a quadruple hydrogen bond, with a strength more comparable to covalent bonds rather than conventional supramolecular bonds, resulting in a stronger crosslinked system. Therefore, there is likely to be a difference in the shape-memory activity between Weathershield and the UPy-Paint, so that upon deformation (in the form of a cut), UPy-Paint is observed to have superior self-healing (Figure 4.7). However, the adherence of the UPy functionalized paint to a metal substrate, drastically limits or may even negate the ability of the coating to reform via the shape memory effect. This is because the adhesion force of the paint to the substrate far outweighs the slight changes in polymer conformational entropy brought about by a cut. This effect is further enhanced by the fact that a drawn paint coating is very thin, maximizing the area of the substrate-coating interface relative to its bulk volume. Thus, when applied to a substrate, neither Weathershield nor the UPy-Paint shows any self-healing activity.

4.3.2.4 Dried paint films

Testing the self-healing efficiency of paint via the strain recovery method involves forming a rectangular paint specimen which is dry, thick, and of known cross sectional area. It is vital for this film to be completely dry, as residual water acts as a plasticizer, altering the film's mechanical properties and serving as an incorrect representation of a dried coating. Furthermore, the presence of water as a plasticizer effectively lowers *T*g and enhances the mobility of polymer chains, likely leading to overestimation of self-healing efficiency.

Further, simply heating the paint, or the polymer film, results in cavities throughout the coating caused by escaping steam. These cavities significantly alter a coating's mechanical properties and are as undesirable as residual water. A latex polymer film is dry when it is completely transparent, after which it can be heated in an 80˚C oven to remove trace amounts of water. But it is more difficult to determine when a paint film is sufficiently dry, due to the presence of titanium dioxide nanoparticles as opacifiers. Therefore, IR spectroscopy was used to chart the evaporation of water from the paint film through the disappearance of the broad OH peak (Figure 4.9).

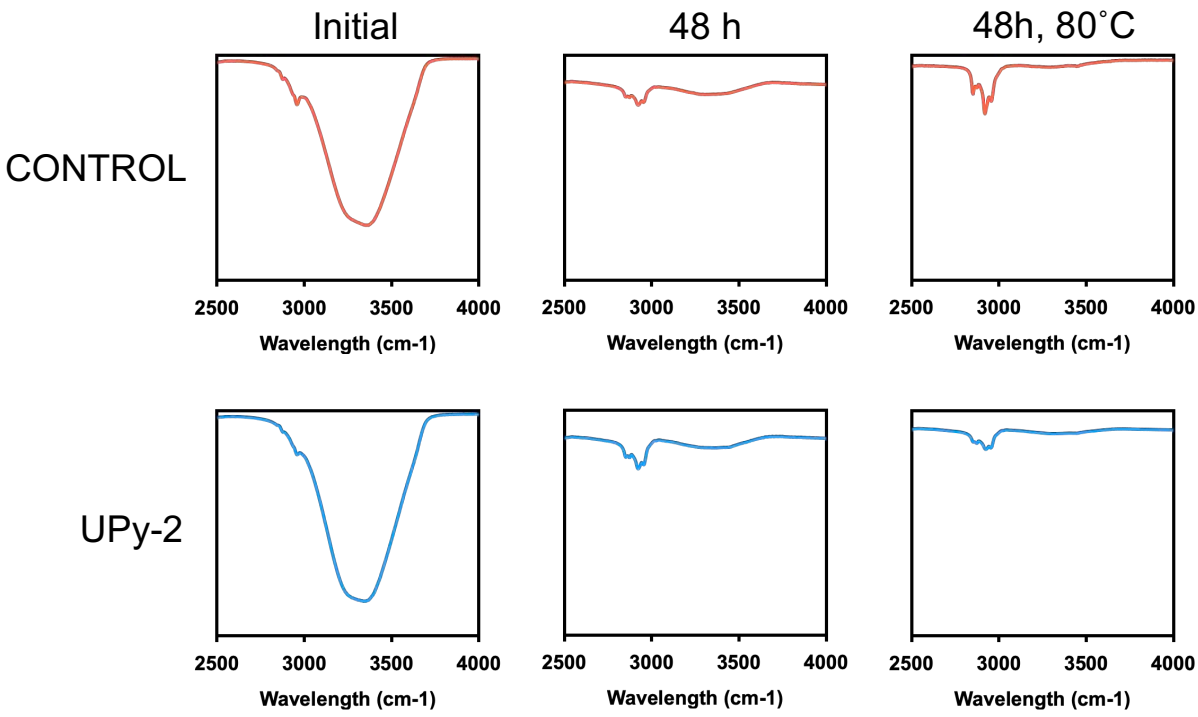

Figure 4.9 IR spectra of Weathershield (red) and UPy-Paint (blue) initially in the wet state (left), and after 48 hours at room temperature (middle), and then another 48 hours at 80˚C (right).

Figure 4.9 displays a clear broad peak between 3300 and 3600 cm^{-1} in the paint's wet state, indicative of the symmetric and asymmetric stretching of the O–H bond associated with bulk water. Upon 48 hours at room temperature, the evaporation of water is clear through the noticeable disappearance of the OH peak, and further drying at 80˚C for 48 hours resulted in an almost flat baseline where a water peak would occur. Therefore, the paint films were left to dry at room temperature for 1 week to remove the vast majority of water without forming cavities in the coating, then the films were heated to remove the remaining trace elements. Further heating did not diminish the peak between 3300 and 3600 cm^{-1}.

4.3.2.5 Paint mechanical properties

To understand the mechanical properties of both Weathershield and the UPy-Paint, stress-strain curves were obtained. Two important metrics can be calculated from stress-strain curves: the Young's modulus, which characterizes a material's ability to resist deformation; and the strain-at-break, which roughly corresponds with a material's brittleness. Analyzing these two values yields insight into the differences between the two paint formulations, and the differences between a paint, and a latex polymer coating. Stress-strain curves of Weathershield and the UPy-Paint are shown in Figure 4.10.

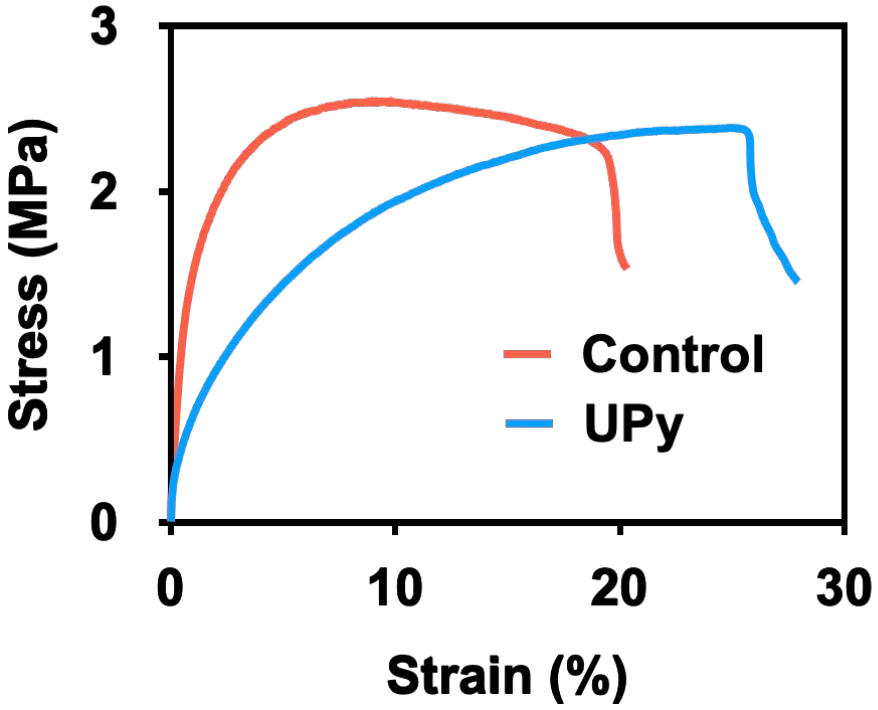

Figure 4.10 Stress-strain curves of Weathershield (red) and the UPy-Paint (blue). These curves show that the UPy-Paint has a lower Young's modulus, meaning it is less resistant to deformation or more malleable than the control. The UPy-Paint also has a higher strain-at-break, meaning it is less brittle than Weathershield.

Figure 4.10 illustrates a noticeable difference between the mechanical properties of Weathershield and the UPy-Paint. Most clearly, the UPy-Paint has a higher strain-at-break (~28%) in comparison to Weathershield (~20%). This indicates that the UPy-Paint is less brittle and more malleable/ductile than the control. The presence of the UPy monomer in the paint's polymer binder is the cause of this difference, given the lack of any other difference between the two paint samples. This effect is unsurprising, as it is also present between the UPy-2 and control transparent latex coatings (Chapter 2). As well as the presence of a long flexible amphiphilic spacer (roughly 800 Da), which serves to 'soften' the material, the strain-at-break may also be enhanced by the presence of a hydrogen bonding network within the coating. The reversibility of this network, and its ability to distribute the applied force (stress) that may otherwise impact the coalesced polymers, may also contribute to a higher strain-at-break.

It also follows that the Young's modulus of the UPy-Paint should also decrease, due to the flexibility and relative softness of UPy-2's spacer. This reduced Young's modulus is also

observed in the transparent polymeric films (Chapter 2). For the UPy-Paint, this reduction is apparent, as the stress-strain curves in Figure 10 yield a Young's modulus of 300 MPa for Weathershield and roughly 200 MPa for the UPy-Paint. The Young's modulus is defined as the slope of the linear region of a stress-strain curve, where deformation is elastic, rather than plastic. Elastic deformation is reversible, and allows the material to return to its original shape when stress is no longer applied. However, plastic deformation involves the loss of mechanical energy and results in the irreversible deformation of the material. Plastic deformation is represented by the non-linear region of a stress-strain curve. Interestingly Weathershield has a more clearly defined linear region, compared to the UPy functionalized paint, which does not have a clearly defined linear region. This implies that Weathershield undergoes significant elastic deformation before becoming permanently deformed, whereas the UPy-Paint becomes irreversibly deformed very rapidly. The presence of a UPy based hydrogen bonding network may account for this difference, as the applied strain may induce UPy-UPy rearrangement within the material that becomes permanent when stress is removed, resulting in plastic, rather than elastic deformation.

Further, given that titanium dioxide pigment particles comprise a significant fraction of the paint formulation, the UPy-Paint and Weathershield were predicted to be less ductile and more brittle than the transparent acrylic coatings that their binders are based upon. This hypothesis is drawn from three notions: 1) Pigment particles have a far higher *T*g than the acrylic polymers in question; 2) ductility is primary determined by the extent to which polymer chains can rearrange, which pigment particles minimize by taking up significant free volume in the coating; and 3) pigments and extenders increase the probability of voids forming in the coating, and voids provide a genesis for crack formation and propagation. The drastically reduced strain-at-break values for the two paints (20% - 30%) compared to those of their polymeric counterparts (~60% – 80%) clearly illustrates how much more brittle the paints are. Furthermore, Figure 4.10 also shows how suddenly the paints fail, which is shown by the steep drop in stress at the strain-at-break of the materials. This sudden failure is more analogous to harder glassy polymer coatings, rather than the low *T*g transparent acrylic coatings, which do not fail suddenly.

4.3.2.6 Strain recovery

Finally, optical microscopy analysis of Weathershield and the UPy-Paint showed that for an introduced crack, neither paint was able to self-heal when applied to a substrate. However, for the paint films in free space, Figure 4.7 showed that spontaneous crack closure appeared to some degree only in the UPy-Paint, as opposed to Weathershield. To determine whether this observed spontaneous healing was robust, both paints were cut through with a razor, and left to heal for 24 hours at room temperature and 50˚C. Their strain recovery was measured and compared to the strain-at-break of the uncut paints respectively, to yield self-healing efficiency. Regarding the healing conditions, 50˚C was selected along with room temperature, as Chapter 2 showed that the self-healing efficiency difference between the UPy-2 and control coatings was maximized at this elevated temperature. If the UPy-Paint had any ability to self-heal a fraction of its mechanical properties, testing at 50˚C provided the best chance to observe this phenomenon. As in Chapters 2 and 3, strain-at-break was defined as the point at which the crack first breaks, rather than when the material completely fractures.

Given the increased brittleness of the paints relative to the purely polymeric coatings in Chapters 2 and 3, as well as the reduction of UPy as a fraction of the total material, it was hypothesized that the self-healing capability of the paints would be reduced, minimized or even vanish entirely. Unfortunately, the latter appears to have been the correct prediction, as when both Weathershield and the UPy-Paint were subjected to strain recovery tests after healing at room temperature and 50˚C for 24 h, there was no observed healing whatsoever, and the crack opened instantly upon the application of stress.

4.4 CONCLUSION

The organic coatings industry has already begun to reap the benefits of self-healing technology, which has rapidly developed in scope and sophistication since the year 2000. Specialized epoxy resins and polyurethane anti-corrosive coatings, imbued with self-healing performance via both extrinsic and intrinsic designs, are approaching widespread commercialization. Paradoxically, the most prevalent and important type of organic coating–architectural paints–remains an under-researched frontier of self-healing coatings. These paints, which are based on a waterborne acrylic latex combined with pigments and other function-specific additives, stand to benefit from self-healing due to: 1) increased service lifetime; 2) significantly reduced costs associated with damage; and 3) a general enhancement of the paint's decorative and protective function. To investigate the feasibility of a self-healing paint, a paint recipe derived from Weathershield, a product marketed by the international paint company DuluxGroup, was imbued with UPy-2 — the self-healing monomer design outlined in Chapter 2.

This design was rigorous enough to undergo a scaled-up industrial emulsion synthesis and form part of a latex, which made up the binder of a paint. This UPy functionalized paint was subjected to various industry-standard tests which showed a slight reduction in its scrub resistance and adhesive qualities compared to Weathershield. Though the UPy-Paint showed some optical self-healing capability in free space, when applied to a substrate, which is more reflective of paint in its applied context, this self-healing ability was nullified. Furthermore, the paint was unable to recover any of its mechanical properties when left to heal either at room temperature or 50˚C. This lack of self-healing stands in contrast to the significant healing of the UPy-2 functionalized acrylic coating observed in Chapter 2. Such an absence of healing is likely due to the reduction of UPy as a fraction of the ultimate material, coupled with the added pigment, which serves to rigidify the paint and suppress spontaneous polymer rearrangement. Nevertheless, evaluating the limits of a UPy-based hydrogen bonding network's capacity to impart healing functionality is necessary to deeply understand self-healing in the context of paints. Furthermore, the lack of healing ability displayed by this UPy-Paint hints at possible future enhancements to self-healing efficiency. Two such enhancements are increasing the amount of healing agent (in this case a UPy based polymer) and designing a polymer system with rheological properties able to offset the addition of pigments and other additives, while maintaining sufficient mechanical strength. This final point likely represents the limiting factor in the design of efficient self-healing paint, and will no doubt require a highly creative solution.

4.5 REFERENCES

1. Wicks, Z. W.; Jones, F. N.; Pappas, S. P.; Wicks, D. A., *Organic Coatings: Science and Technology*. Wiley: 2007.

2. Zhang, F.; Ju, P.; Pan, M.; Zhang, D.; Huang, Y.; Li, G.; Li, X., Self-healing mechanisms in smart protective coatings: A review. *Corrosion Science* **2018,** *144*, 74-88.

3. Zhu, D. Y.; Rong, M. Z.; Zhang, M. Q., Self-healing polymeric materials based on microencapsulated healing agents: From design to preparation. *Progress in Polymer Science* **2015,** *49*, 175-220.

4. Zhong, N.; Post, W., Self-repair of structural and functional composites with intrinsically self-healing polymer matrices: A review. *Composites Part A: Applied Science and Manufacturing* **2015,** *69*, 226-239.

5. Henry, J. J. M., Nano-based self-healing anti-corrosion coating. US20140134426A1: 2014.

6. Dayton, C. R.; Wilson, G. O.; Kasisomayajula, S. V.; Shukla, S.; Navarro, A. G. R.; Rodriguez, D., One-component waterborne self-healing epoxy formulation. US11613668B2: 2023.

7. Jones, F. N.; Nichols, M. E.; Pappas, S. P., *Organic coatings: science and technology*. John Wiley & Sons: 2017.

8. Beach, M.; Davey, T.; Subramanian, P.; Such, G., Self-healing organic coatings – Fundamental chemistry to commercial application. *Progress in Organic Coatings* **2023,** *183*, 107759.

9. He, M.; Fauvell, T.; Urruti, E., Self-healing optical fibers and the compositions used to create the same. US11358899B2: 2022.

10. Williams, G. A.; Hentschel, J.; Satpute, A., Self-healing resin. US10800866: 2020.

11. Cazan, C.; Enesca, A.; Andronic, L., Synergic Effect of TiO2 Filler on the Mechanical Properties of Polymer Nanocomposites. *Polymers* **2021,** *13* (12), 2017.

12. Perera, D. Y., Effect of pigmentation on organic coating characteristics. *Progress in Organic Coatings* **2004,** *50* (4), 247-262.

13. Sun, J.; Forster, A. M.; Johnson, P. M.; Eidelman, N.; Quinn, G.; Schumacher, G.; Zhang, X.; Wu, W.-l., Improving performance of dental resins by adding titanium dioxide nanoparticles. *Dental Materials* **2011,** *27* (10), 972-982.

14. Winnik, M. A., Latex film formation. *Current Opinion in Colloid & Interface Science* **1997,** *2* (2), 192-199.

15. Maeda, Y.; Paul, D. R., Effect of antiplasticization on gas sorption and transport. I. Polysulfone. *Journal of Polymer Science Part B: Polymer Physics* **1987,** *25* (5), 957-980.

16. Yang, W.; Shen, H.; Min, H.; Ge, J., Enhanced visible light-driven photodegradation of rhodamine B by Ti3+ self-doped TiO2@Ag nanoparticles prepared using Ti vapor annealing. *Journal of Materials Science* **2020,** *55* (2), 701-712.

17. Hornat, C. C.; Urban, M. W., Shape memory effects in self-healing polymers. *Progress in Polymer Science* **2020,** *102*, 101208.

18. Ji, G.; Zhang, P.; Nji, J.; John, M.; Li, G., 11 - Shape memory polymer-based self-healing composites. In *Recent Advances in Smart Self-healing Polymers and Composites*, Li, G.; Meng, H., Eds. Woodhead Publishing: 2015; pp 293-363.

Chapter 5. Conclusions and Perspectives

All coatings are widely susceptible to mechanical damage. This damage initially occurs in the form of microcracks, which, if left unchecked, grow into large macrocracks visible to the naked eye, ultimately resulting in the complete failure of the coating. Paints — the most widely applicable and well-known class of coating — are significantly affected by cracking for two fundamental reasons. First, cracking undermines and ultimately eliminates a paint's protective function over a substrate. Second, cracking harms a paint's decorative function over time. Furthermore, healing a damaged coat of paint involves simply replacing it with a new coat. This "solution" is energy consuming, time consuming and above all, costly. In fact, some estimates suggest that the global yearly cost of replacing damaged coatings reaches into the trillions, rather than the billions of dollars.

Self-healing technology offers the ability to heal cracks spontaneously and without external diagnosis, and hence is the best possible strategy to radically enhance a coating's protective function and, in the case of paints, its decorative function. Over the past 20 years, various coatings have been imbued with self-healing capability, amongst which epoxy resins and polyurethane anticorrosive coatings are the most thoroughly investigated. In these designs, self-healing is normally attained either through the encapsulation of extrinsic healing agent in microcapsules, or the addition of intrinsic healing functionality to the coating's polymeric components. Crucially however, a successful self-healing acrylic coating, which comprises the body of a paint, remains elusive. Three challenges largely exclusive to self-healing paint explain this decades-long lack of progress.

1. *Stiffness*. Paints are generally strong materials composed of a highly entangled acrylic polymer matrix. They generally have a Young's modulus anywhere between 0.1–2 GPa, making them highly resistant to deformation in the form of polymer mobility – a necessity for self-healing performance.

2. *Opacity*. The acrylic coating that comprises a paint is transparent, so that colour, opacity, and gloss can be tailored through the introduction of pigments. Microcapsules, which represent the principal design strategy for self-healing stiff coatings, almost always have a refractive index mismatch with the surrounding coating, resulting in undesirable opacification.
3. *Healing conditions*. The vast majority of stiff-material self-healing occurs at very high temperatures (80 – 150˚C) for prolonged periods of time (> 1 month). These systems can work well for specialized anticorrosive coatings; however, such healing conditions are unfeasible for the vast majority of paints. An effective self-healing paint must be able to heal under ambient, or close to ambient conditions.

As well these three central problems, cost, toxicity, and synthetic complexity are additional factors that must be carefully monitored in the design of self-healing paint.

The research contained in this thesis represents the culmination of a three-and-a-half-year effort to create an acrylic coating which is able to maintain high mechanical strength while self-healing cracks at room temperature, and to apply this self-healing coating to a paint formulation, as would be sold to consumers. Briefly, room temperature self-healing was successfully introduced to an acrylic latex via the self-complementary quadruple hydrogen bonding unit, UPy. The strong attractive forces between the UPy units, as well as the nature of their distribution in the acrylic polymer coating, provided the driving force necessary for self-healing.

The first project, described in Chapter 2, involved the design of a series of UPy functionalized monomers. A typical paint-based acrylic coating was formed from the emulsion polymerization of typical paint-based acrylic monomers to form a suspension of waterborne hydrophobic polymer nanoparticles known as a latex. Upon the evaporation of water, these particles coalesced to form a tangled coating of acrylic polymers. The UPy-monomers were intended to form part of this polymer latex to imbue the ultimate acrylic coating with a self-healing hydrogen bonding network. The key to this monomeric design was the introduction of a large amphiphilic spacer to separate the UPy unit from the polymer backbone. This spacer comprised both a hexyl chain and a PEG chain whose length was varied. Such a long spacer serves two purposes. First, it allows for the UPy monomer to effectively transport through the aqueous

phase of the emulsion and undergo polymerization. Second, the long flexible spacer allows the UPy unit a significantly greater degree of freedom and distance away from the sterically hindered backbone. This enhances its ability to self-heal via the rearrangement of polymers and reformation of UPy–UPy bonds. Out of a library of four monomers with differing spacer lengths, UPy-2, with a PEG length of ~11 units, was able to imbue an acrylic coating with self-healing capability. Crucially, this self-healing occurred at room temperature, and the UPy-2 functionalized acrylic coating maintained almost all of its mechanical strength. Strain recovery, a measure of self-healing efficiency, showed that the introduction of UPy-2 yielded self-healing efficiency from 25% to 80% between room temperature and 50˚C. This represents an enormous improvement compared to an unfunctionalized control coating, which displayed no self-healing at room temperature, and drastically reduced healing at 50˚C.

In order to enhance the self-healing efficiency of this UPy-functionalized monomer design, particularly at room temperature, a self-healing UPy-functionalized crosslinker system was investigated. The hypothetical self-healing benefits of such a crosslinker design are twofold. First, increasing the total amount of UPy functionality strengthens the coating's hydrogen bonding network, enhancing self-healing. Second, such a crosslinker system provides a means to prevent undesirable UPy–UPy self-complementation in the latex particles before coalescence, yielding a more evenly distributed hydrogen bonding network. Chapter 3 describes the theory, synthesis, characterization, and self-healing performance of this crosslinker system. Specifically, the crosslinkers were based on hydrophilic poly(ethylene glycol) (PEG) grafted with two UPy moieties per polymer chain. Two different PEG architectures, linear (UPy-Linear) and brush (UPy-Brush), were investigated, and a library of crosslinkers with varying molecular weight was synthesized for each architecture. The UPy-Brush crosslinkers, as opposed to the UPy-Linear crosslinkers, were soluble enough to allow crosslinker incorporation into an acrylic latex. The UPy-Brush crosslinkers yielded strong optical self-healing at room temperature and at 50˚C, while resulting in a noticeable reduction in the *T*g and Young's modulus of the coatings. Of the three different UPy-Brushes, only UPy-Brush-10, with a molecular weight of ~10 kDa, displayed improved self-healing efficiency compared to both the other UPy-Brush coatings, and the UPy-2 functionalized coating described in Chapter 2.

Having both designed a self-healing acrylic coating based on a UPy-functionalized monomer and enhanced this self-healing through the incorporation of a carefully tailored UPy-functionalized crosslinker, Chapter 4 explores how to imbue a paint with self-healing capability. To achieve this, UPy-2 was incorporated into a paint formulation. UPy-2 was chosen because it provided the greatest impact on self-healing efficiency, and was able to self-heal most efficiently at room temperature and 50˚C. Though the crosslinker UPy-Brush-10 provided enhanced self-healing when coupled with UPy-2 at room temperature, it was decided that its impact on the coating mechanical properties, as well as the scaling costs associated with synthesizing > 100g, practically offset any modest benefits to self-healing efficiency. UPy-2 was successfully incorporated into a 1kg latex, and this UPy-functionalized latex was then combined with inorganic TiO_2 pigment nanoparticles and a myriad of other paint additives to form a UPy functionalized paint (UPy-Paint). The paint was formulated at DuluxGroup's Innovation Center, and was based on their outdoor protective paint range Weathershield™ . The UPy-Paint was compared to Weathershield™ through a number of industry-specific tests including scrub resistance and adhesion, and its mechanical properties were also analyzed compared to a transparent acrylic polymer coating. The ability of the paint to self-heal a crack when both attached and unattached to a substrate was evaluated, and any strain recovery properties were investigated. Interestingly, though the paint showed some optical self-healing when unattached to a substrate relative to Weathershield™ , the self-healing capacity of the paint was severely diminished when attached to a substrate, and no strain recovery potential was observed.

The summation of these three research projects represents the successful design of a paint-based acrylic coating which is able to self-heal damage at room temperature. As previously mentioned, though research has yielded a significant body of literature regarding self-healing epoxy resins, polyurethane coatings, and other specialized coatings — namely anticorrosive coatings — the lack of a necessarily strong acrylic latex coating which is able to self-heal at ambient conditions through intrinsic functionality remains a significant shortcoming. This work presents a viable solution to that problem in the form of a hydrogen bonding network, which arises through the addition of a monomer with both a flexible amphiphilic spacer and a strong hydrogen bonding unit UPy. Where this work sits in regard to other intrinsic self-healing designs is illustrated in Figure 5.1 below.

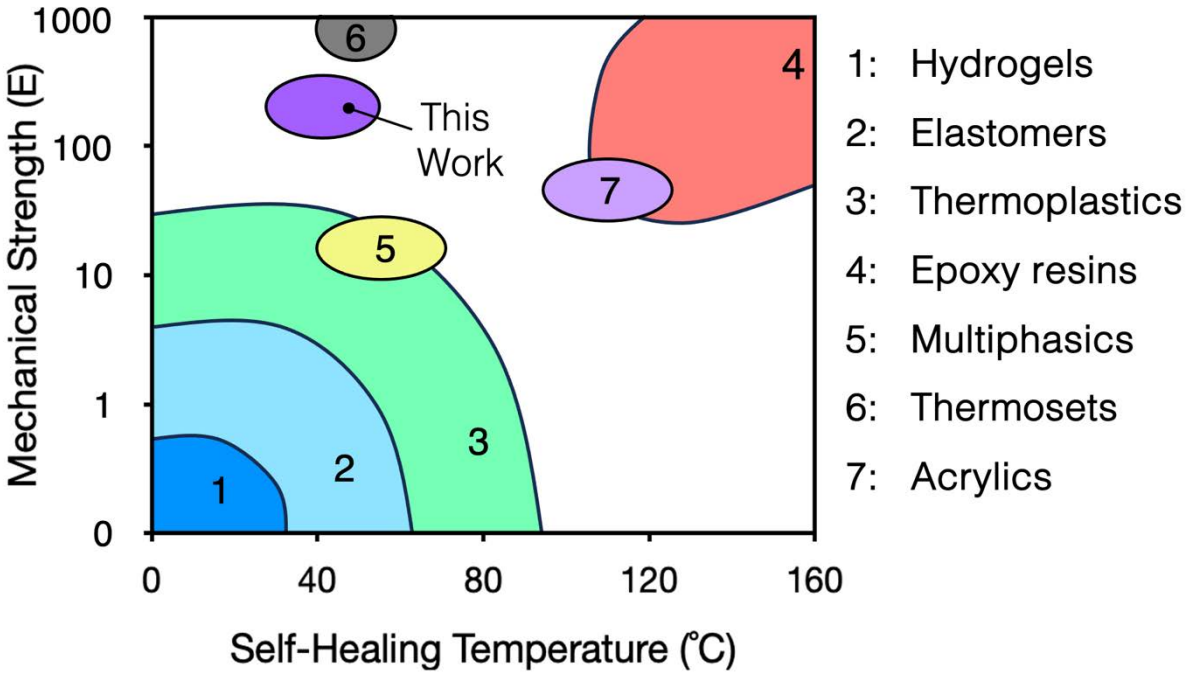

Figure 5.1 Coatings with different mechanical strengths self-heal across a wide range of temperatures. Generally, the temperature at which self-healing occurs is proportional to a coating's mechanical strength. This work represents a strong acrylic coating which is able to self-heal at ambient temperatures.

Low modulus materials such as hydrogels and elastomers are well known to self-heal efficiently at room temperature. Stronger coatings such as epoxy resins are able to self-heal intrinsically, however, require significantly elevated temperatures. Materials with distinct hard and soft polymeric domains — known as multiphasic materials — can also heal under moderate conditions, due to the rheology of their softer portions. This work is able to imbue a strong paint-based acrylic coating with self-healing capacity at room temperature, which is a benefit that is normally confined only to precisely designed thermoset polymers.

As well as successfully designing a self-healing acrylic coating, this work has also yielded invaluable insight into the mechanisms governing self-healing, the potential of self-healing acrylic coatings and future research directions toward creating commercially viable self-healing paint. For example, the superior self-healing efficiency of UPy-2 compared to UPy-3, as demonstrated in Chapter 2, shows that a longer flexible chain separating the self-healing unit from the polymer backbone enhances self-healing efficiency. This is due to the UPy unit's

maximized degree of freedom and thus its heightened ability to rearrange. The principle of polymer mobility-induced self-healing forms the basis of multiphasic materials, whose soft domains allow for self-healing under mild conditions while maintaining moderate mechanical strength (~1 order of magnitude below this work).

Interestingly, the fact that only one UPy-Brush crosslinker is able to enhance self-healing efficiency at room temperature, implies that increased polymer mobility alone does not result in self-healing. If the opposite were true, then the addition of each UPy-Brush crosslinker would enhance self-healing, given that in all three cases, the ultimate coating formed is more malleable, lower *T*g and lower modulus than the UPy-2 coating alone. Such healing does not occur for UPy-Brush-5 and UPy-Brush-20 however, which reinforces the idea that self-healing is generated via the attractive forces of the UPy units, rather than simply as a biproduct of a weaker material with enhanced viscoelastic flow. This finding is particularly valuable, as some multiphasic coatings, as well as other self-healing designs, rely on simply heating a coating well above *T*g to initiate 'flow' across a certain domain within the material. The self-healing efficiency of designs such as these would be significantly enhanced by the addition of some form of self-healing functionality, as efficient intrinsic self-healing requires a driving force, generated from a hydrogen bonding network or otherwise.

The research outcomes in Chapter 3 also yield a second important insight into the mechanism underpinning intrinsic self-healing in strong polymer coatings. Only one crosslinker design, UPy-Brush-10, imparts any additional room temperature strain recovery (~10%) compared to a UPy-2 functionalized latex alone. UPy-Brush-5 and 20 yielded no additional self-healing, and the efficiency of UPy-Brush-10 declines at 50˚C. This is despite the fact that for all three UPy-Brush crosslinker coatings, the number of UPy units is effectively doubled compared to the UPy-2 coating. Therefore, the lack of significantly enhanced self-healing on the part of the crosslinkers heavily implies that for efficient self-healing to occur, the driving force must come from the bulk material, in this case latex polymers, rather than an additional additive which represents only a small fraction of the total material. Such an effect is likely magnified given the size difference between the latex polymers (~200 kDa) and the crosslinkers (~ 10 kDa). Nevertheless, this insight is important given the number of coating designs which employ crosslinkers as a source of self-healing, as well as design strategies which purport to utilize the smaller additives in paint as a source of self-healing functionality.

Chapter 4 clearly identifies the significant challenges associated with designing a self-healing paint. In order to disperse the monomer UPy-2, sonication was used in Chapters 2 and 3, which represents a significant problem for large-scale industrial production. However, it was found that the shear forces imparted by a sawtooth metal blade sufficiently dispersed UPy-2, allowing for a successful emulsion polymerization. However, The self-healing efficiency of UPy-2 seemingly allows for some optical self-healing of a crack compared to Weathershield™ paint. This self-healing however, does not yield any strain recovery, and becomes non-existent when paint is applied to a substrate, even at 50°C. The most likely reason for this drastic reduction in self-healing performance is twofold. First, the self-healing functionality (UPy) represents a much smaller fraction of paint, compared to the transparent acrylic coating (~40%), thus limiting the effectiveness of the hydrogen bonding network. Second, the materials properties and polymer rheology of the paint is noticeably different to the acrylic coating. Specifically, the addition of pigment particles, which have a far higher Young's modulus than the surrounding polymer coating, make the paint stiffer and more brittle, minimizing the ability of the UPy units on the polymers to rearrange and self-heal. Indeed, the performance of the UPy-Paint ostensibly reinforces the widely held notion that room temperature self-healing of a high strength coating represents a 'contradiction in terms'. Nevertheless, where before there was no feasible self-healing acrylic coating design, this work shows that room temperature self-healing in an acrylic paint binder is possible (and effective) through the careful design and incorporation of UPy-functionalized monomers and crosslinkers. Furthermore, this self-healing of a clear acrylic film (clearcoat), as opposed to a paint, may prove useful for clear protective outdoor coatings as well as wood coatings. These coatings are subjected to thermally induced expansion and contraction cycles overtime, potentially leading to the formation and propagation of microcracks. The presence of a UPy hydrogen bonding network within these coatings, combined with sufficient polymer chain mobility, would allow for the self-healing of these microcracks, potentially enhancing the service lifetime and overall performance of these clearcoats.

How then, might one increase the self-healing capacity of a pigmented paint, using the insights gained in this work? Increasing the amount of UPy in the bulk polymeric material, thus yielding a stronger hydrogen bonding network, is a good starting point. If a strong acrylic coating was able to self-heal at room temperature with an efficiency of >25% and a UPy-2 monomer

concentration of just 2.5 wt%, then what self-healing efficiency is possible for UPy-2 concentrations above 5 wt%? Or 10 wt%? Given the poor solubility profile of UPy-1 to UPy-4, a significant increase in concentration well above 2.5 wt% would likely involve a noticeably different monomer design. One possible strategy would be to alter the hydrophobic section of the monomer's spacer — which is derived from hexamethylene diisocyanate — rather than its PEG-based hydrophilic section, as was done in Chapter 2. Employing n-dodecyl diisocyanate would effectively double the length of the monomer's hydrophobic chain from 6 to 12 carbons, and likely enhance its solubility in a mixture of acrylic monomers. Introducing aryl functionality, rather than relying on an aliphatic carbon chain, may also be worth investigating, and would likely enhance monomer solubility in styrene, a common acrylic paint monomer. Designing a UPy functionalized monomer in liquid form is perhaps the best way to allow high monomer concentrations, as this would completely negate the limitations associated with dissolving a solid monomer in a mixture of acrylic monomers, or worse, organic solvent. The strong self-complementation of UPy makes such a design challenging, however.

Utilizing a different hydrogen bonding system which, though weaker than UPy, can be incorporated at much higher concentrations into an acrylic latex, is another possible strategy to enhance self-healing. Many weaker hydrogen bonding units such as amide and urea moieties, which form the basis of self-healing gels and elastomers, are already widely incorporated into acrylic coatings and display no self-healing activity. Two stronger hydrogen bonding units, barbiturate groups and thiourea adducts, have, under certain circumstances, displayed self-healing potential in tougher materials, and therefore present a possible alternative to UPy. Furthermore, some research has also focused on designing systems with multiple different hydrogen bonding functionalities, such as UPy + urea bonds, and UPy + amide bonds, to enhance self-healing efficiency.

The photothermal effect, which involves the conversion of light into heat, presents a strategy to develop self-healing paint which is worthy of investigation. Simply through the addition of specific nanoparticles to a material, IR irradiation can yield local temperatures of over 150°C. Such high local temperatures generated through light irradiation, which is a comparatively non-invasive technique, would no doubt radically enhance intrinsic self-healing efficiency at a damage site. Furthermore, these high local temperatures open up the possibility of employing reversible covalent bonds, which are stronger even than UPy hydrogen bonds, as self-healing

functionality. Furthermore, given that photothermal activity normally comes from the introduction of specialized nanoparticles, utilizing these particles both as heat generators and pigments at the same time would yield a highly rational 'two-in-one' self-healing paint design. However, as with any other technique, the costs and additional synthetic complexities associated with photothermal self-healing must be carefully considered if such a design is to be commercially viable.

All of these sophisticated self-healing techniques and strategies seek to solve the most fundamental problem confounding the creation of self-healing paint: how to imbue ambient self-healing in mechanically strong coatings. This work demonstrates that designing a tough, high modulus acrylic coating which is able to self-heal at room temperature is indeed possible, and achieved through the introduction of a strong hydrogen bonding network with flexibility sufficient to allow self-healing through polymer rearrangement and hydrogen bond reformation. Thus, self-healing acrylic paint, which was left largely unexplored over the past 20 years, is one step closer to reality.

Chapter 6. Appendix

The supplementary information contained in this chapter is crucial to the arguments made in the main body of this thesis. In particular, characterization data for the various synthetic materials is displayed.

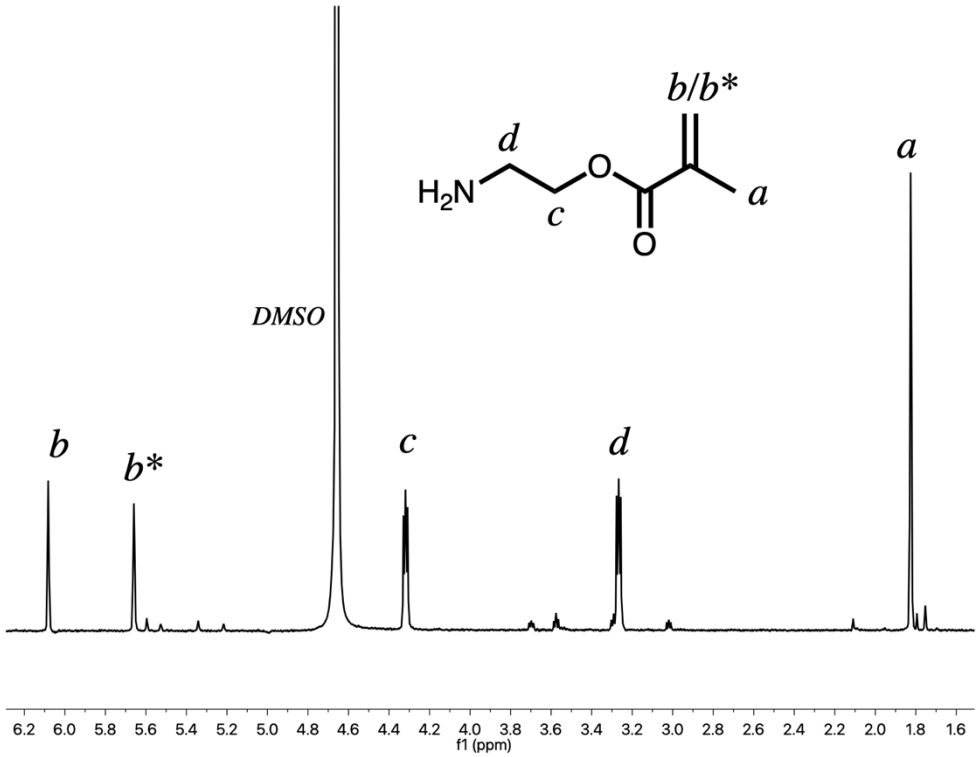

Figure S1. ^{1}H-NMR (400 MHz, DMSO) of 2-aminoethyl methacrylate

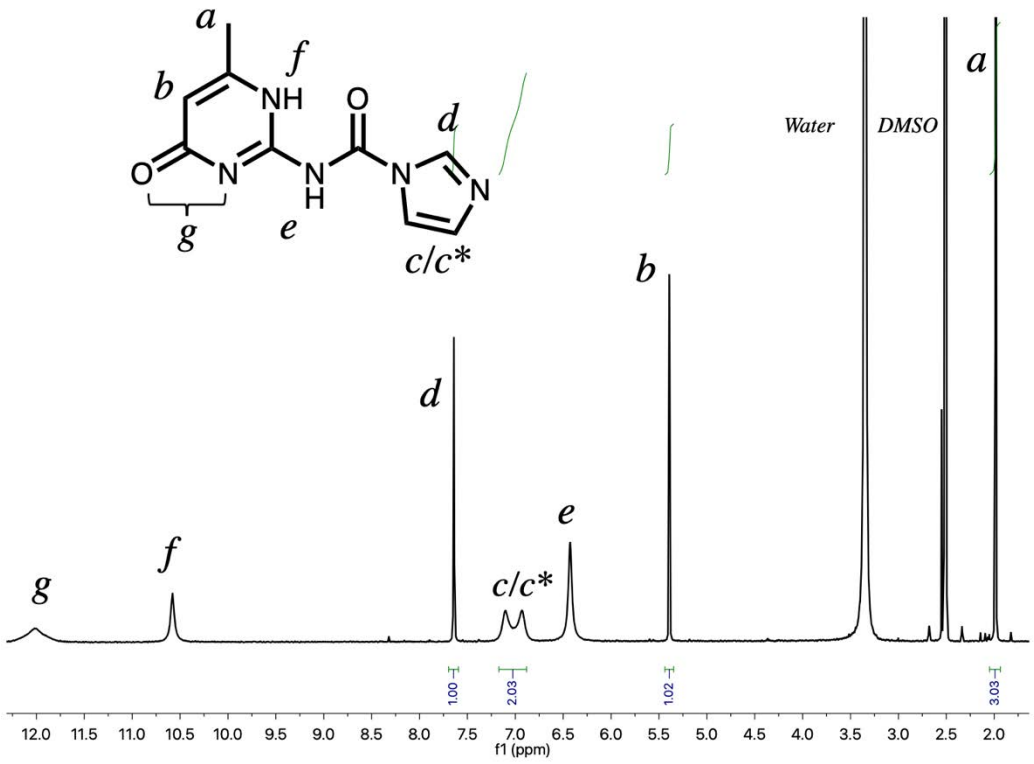

Figure S2. ^{1}H-NMR (400 MHz, DMSO) of N-(6-methyl-oxo-1,4-dihydropyrimidin-2-yl)-1H-imidazole-1-carboxamide (UPy-imidazole)

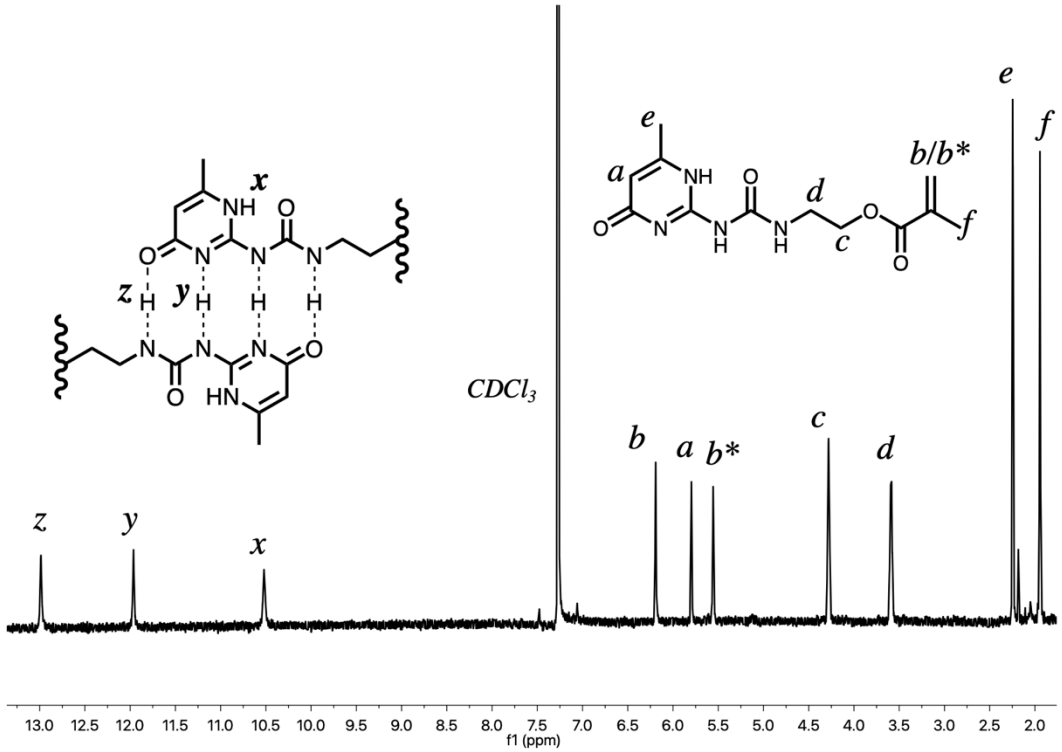

Figure S3. ^{1}H-NMR (400 MHz, $CDCl_3$) of UPy-1

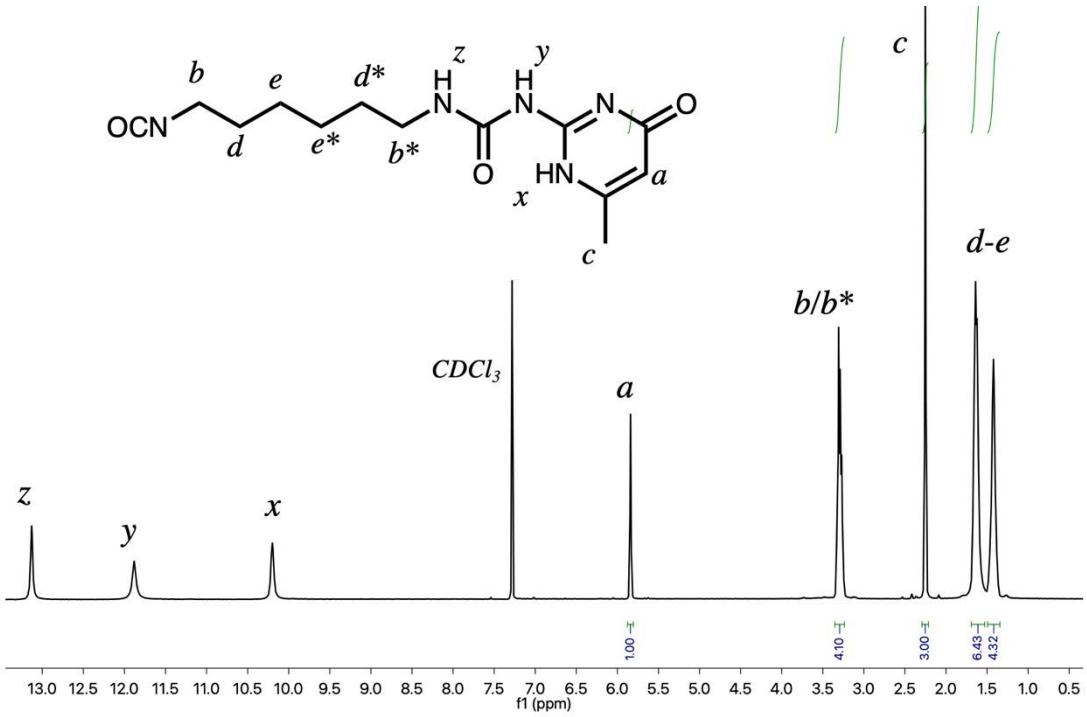

Figure S4. ^{1}H-NMR (400 MHz, $CDCl_3$) of 2(6-isocyanatohexylaminocarbonylamino)-6-methyl-4[1H] pyrimidinone

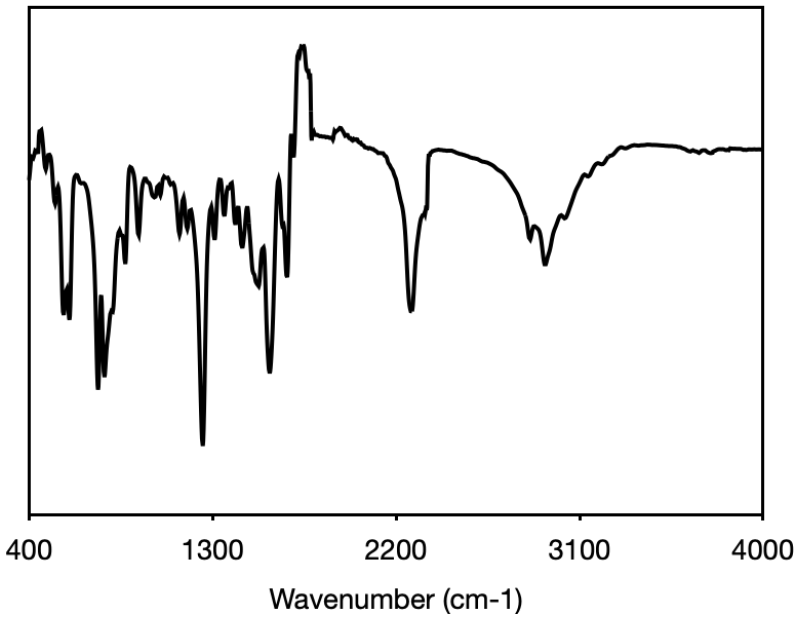

Figure S5. FTIR spectrum of 2(6-isocyanatohexylaminocarbonylamino)-6-methyl-4[1H] pyrimidinone

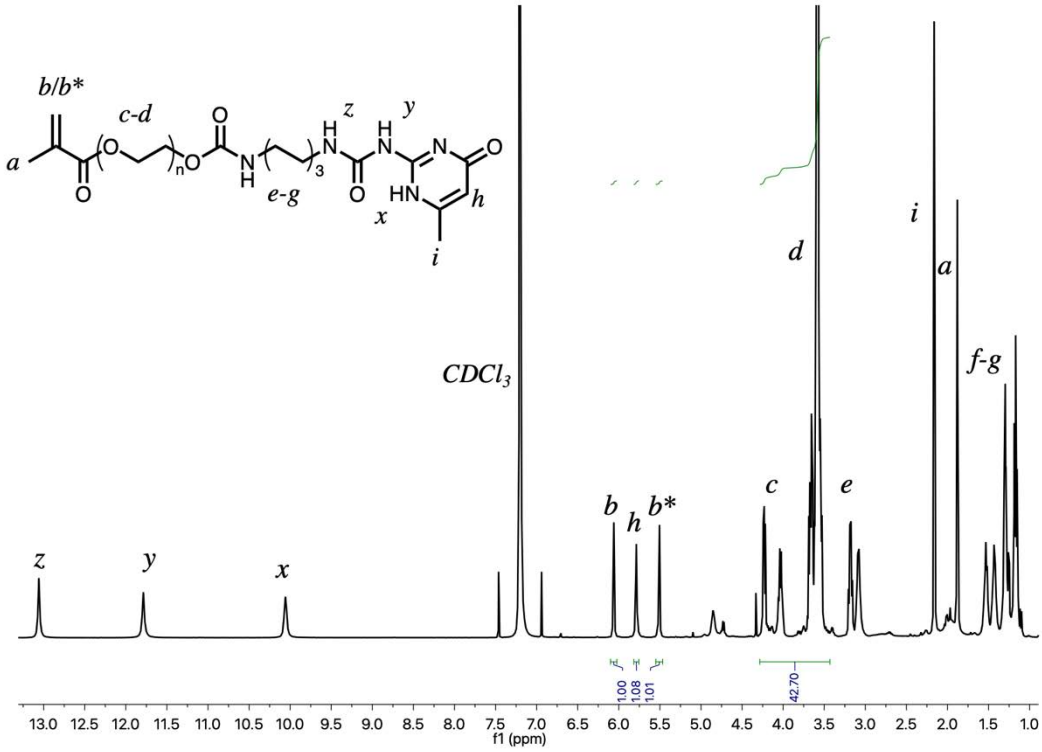

Figure S6. ^{1}H-NMR (400 MHz, $CDCl_3$) of the monomer UPy-2

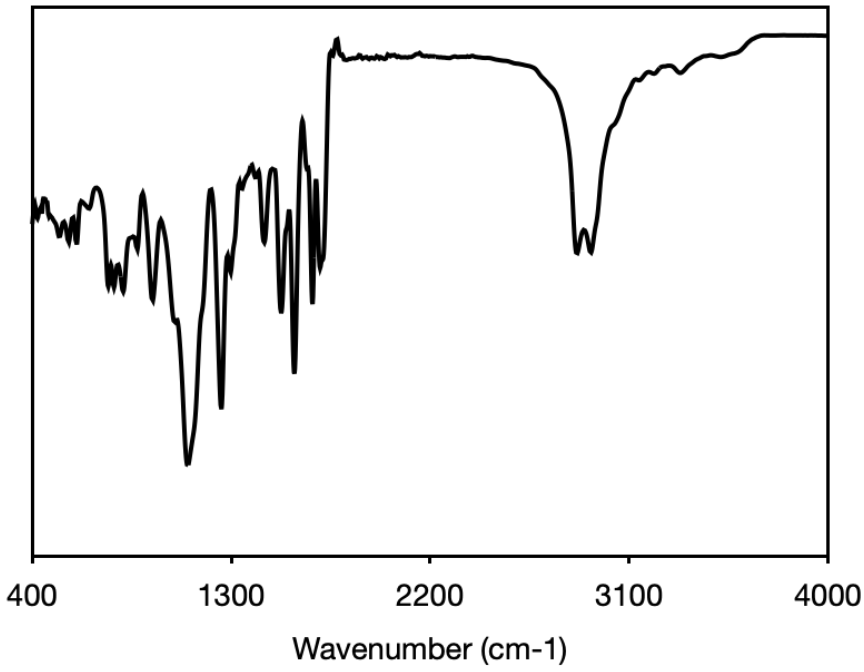

Figure S7. FTIR spectrum of UPy-2

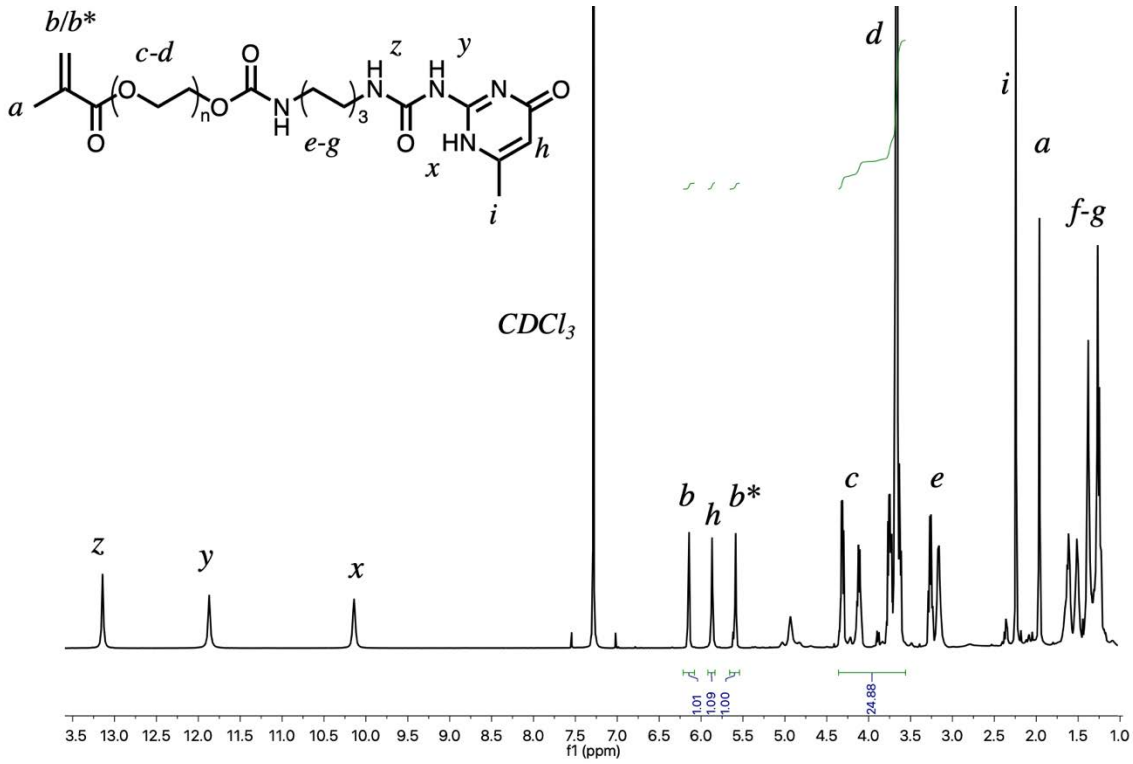

Figure S8. ^{1}H-NMR (400 MHz, $CDCl_3$) of the monomer UPy-3

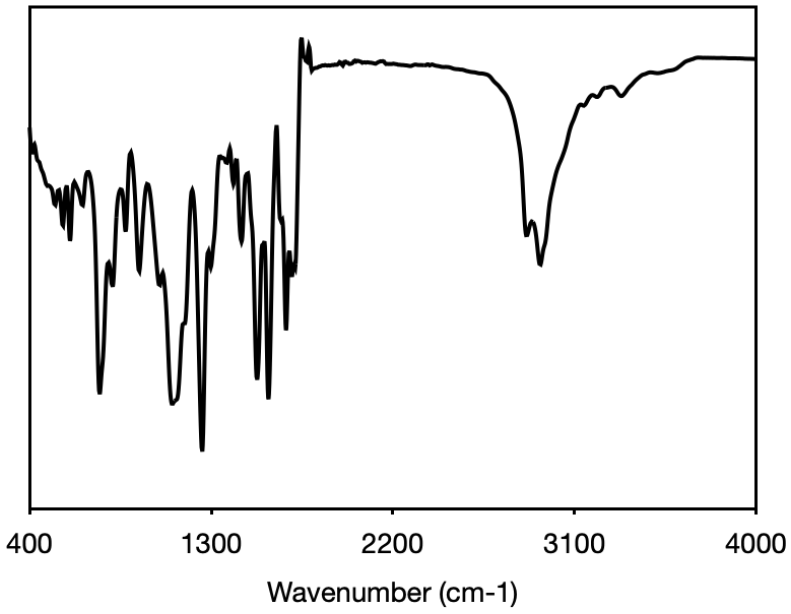

Figure S9. FTIR spectrum of UPy-3

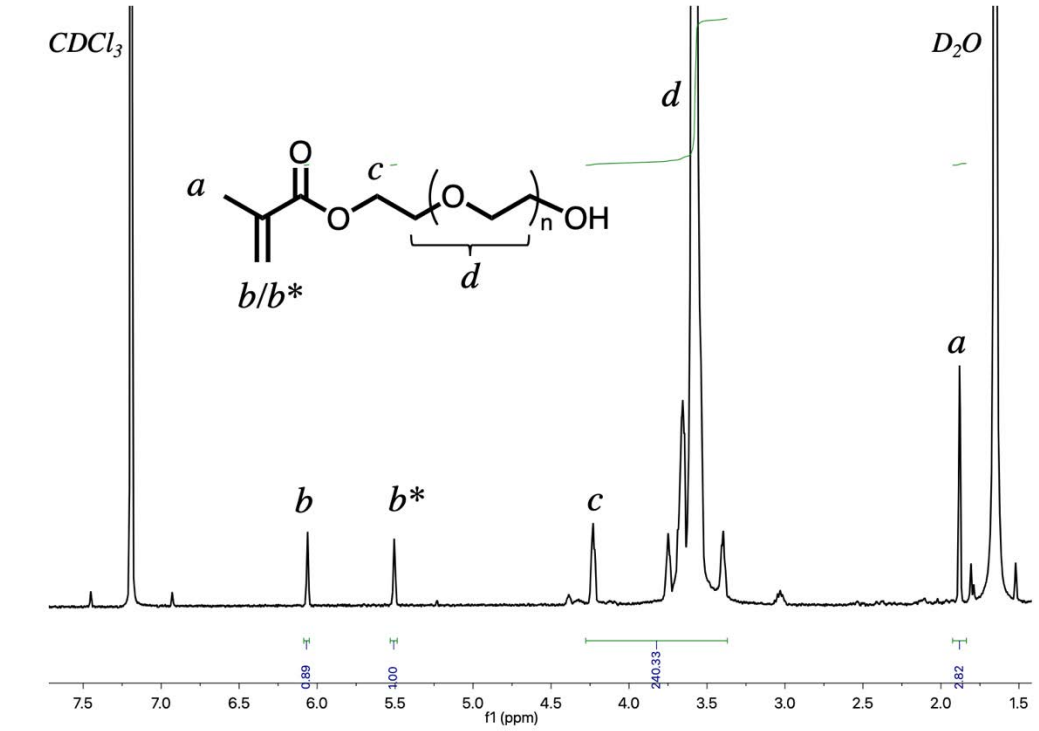

Figure S10. ^{1}H-NMR (400 MHz, $CDCl_3$) of PEGMA (MW = 2000)

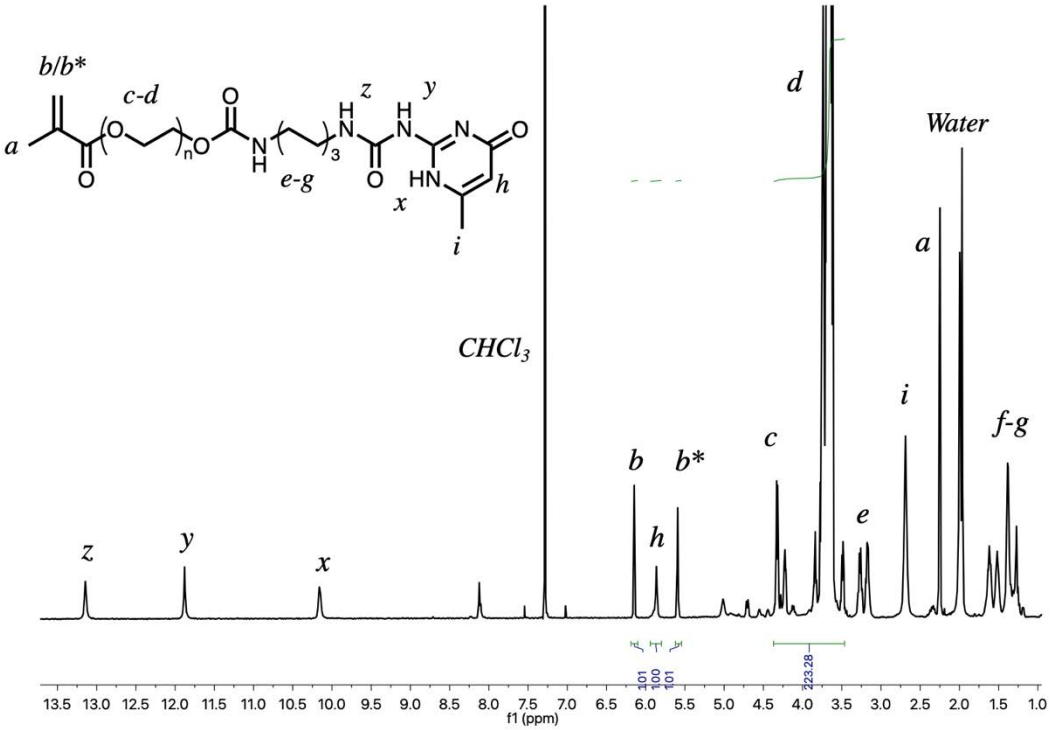

Figure S11. ^{1}H-NMR (400 MHz, $CDCl_3$) of the monomer UPy-4

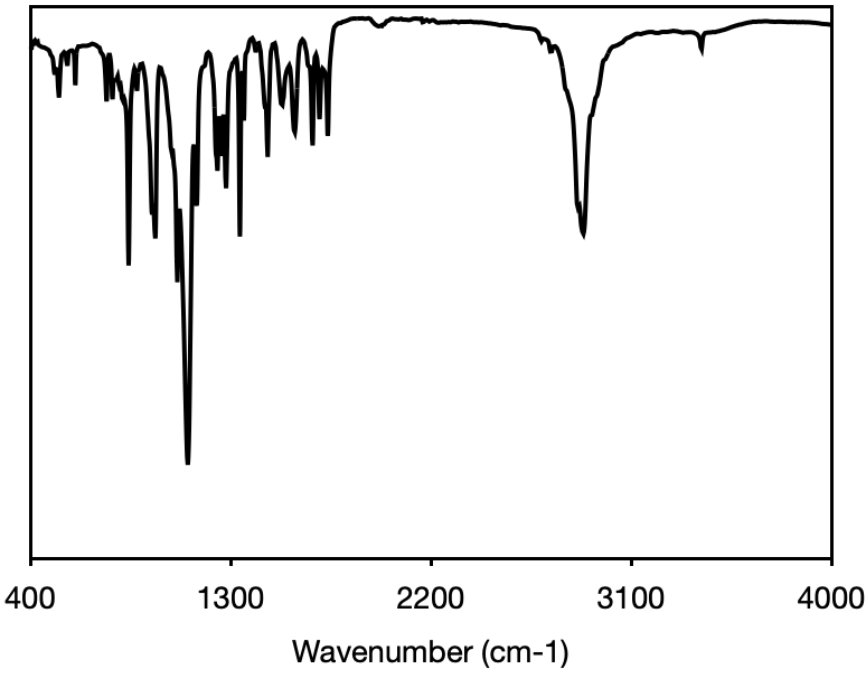

Figure S12. FTIR spectrum of UPy-4

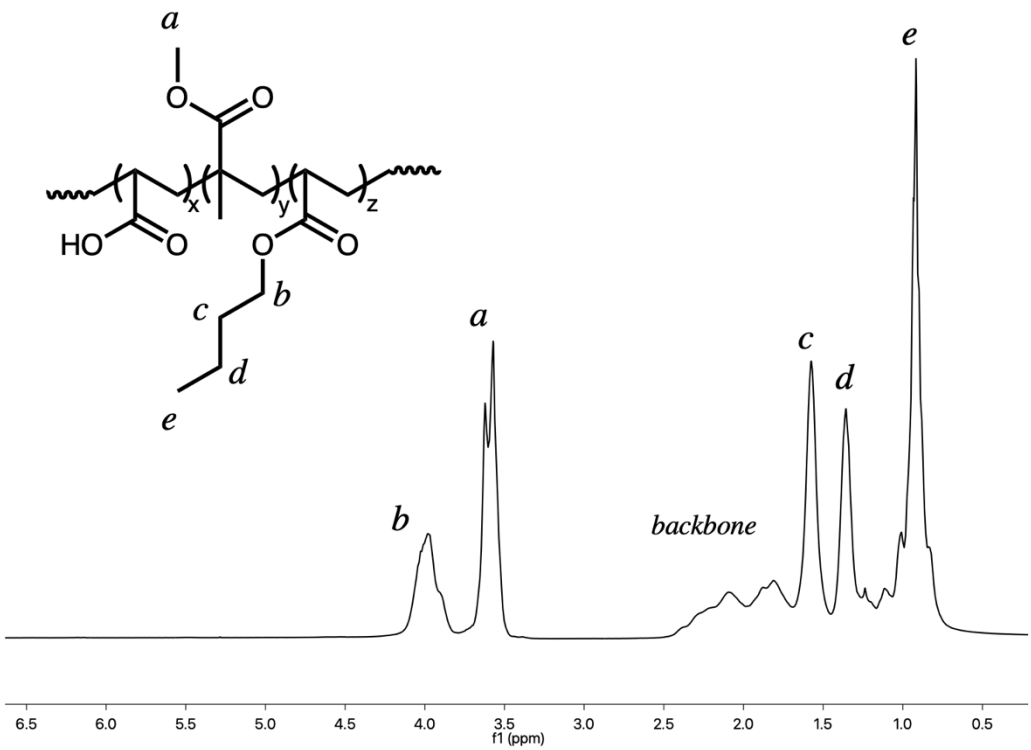

Figure S13. ^{1}H-NMR (400 MHz, $CDCl_3$) of the MMA/BA/AA control acrylic coating

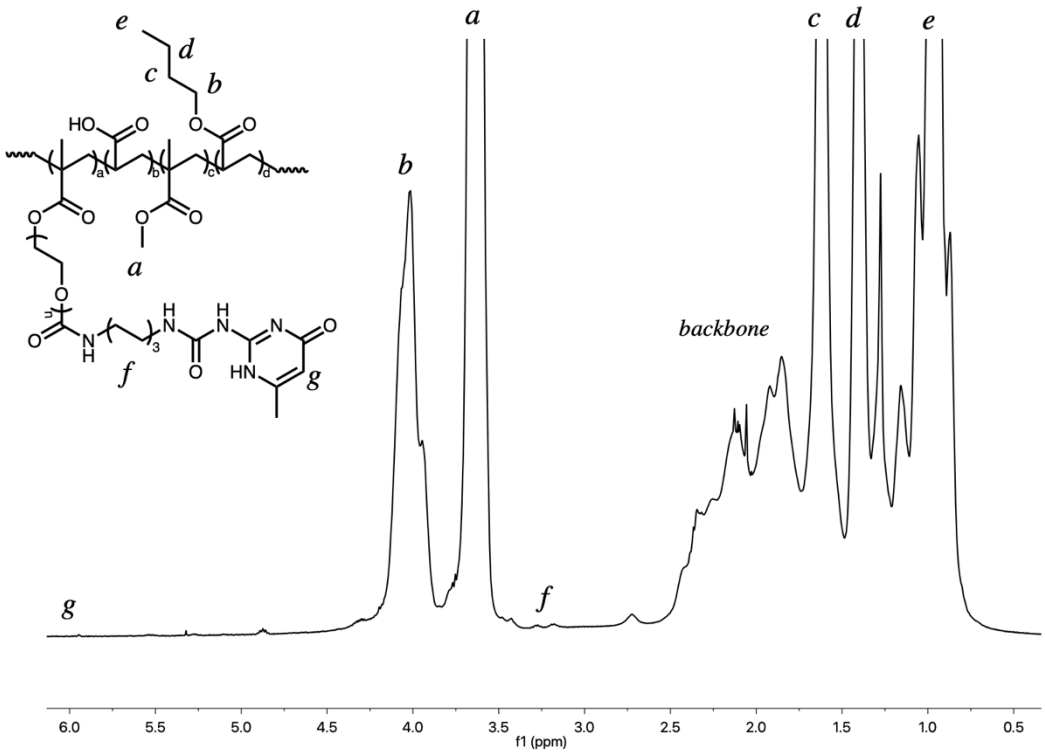

Figure S14. ^{1}H-NMR (400 MHz, $CDCl_3$) of the UPy-2 coating.

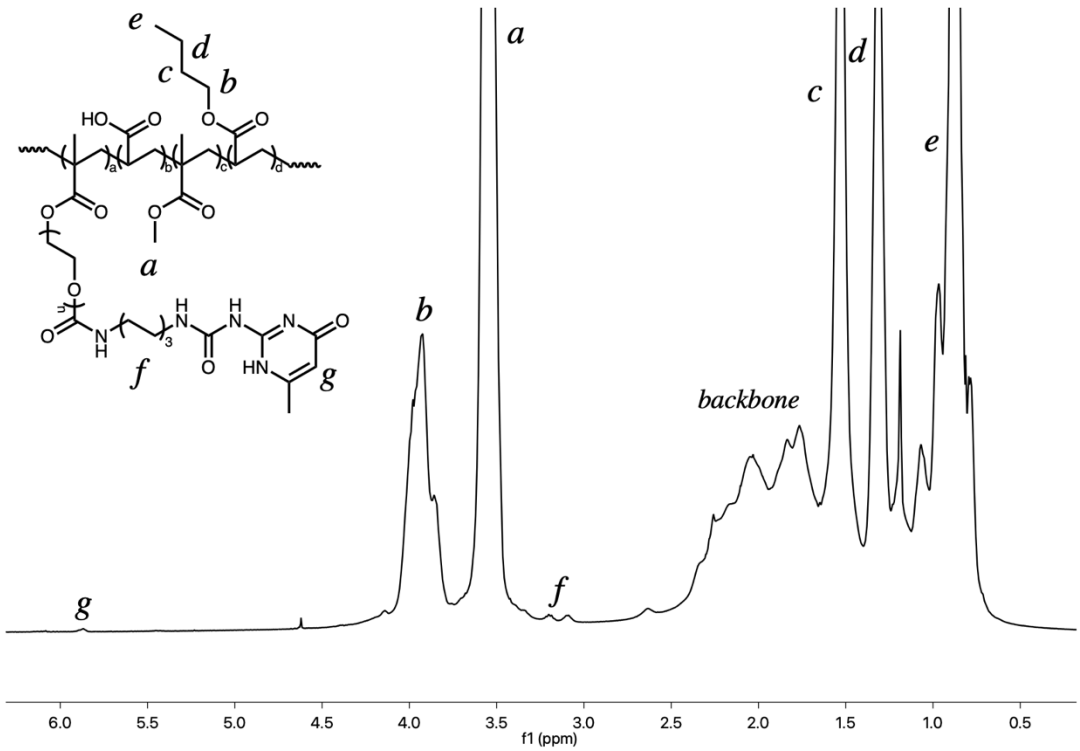

Figure S15. ^{1}H-NMR (400 MHz, $CDCl_3$) of the UPy-3 coating

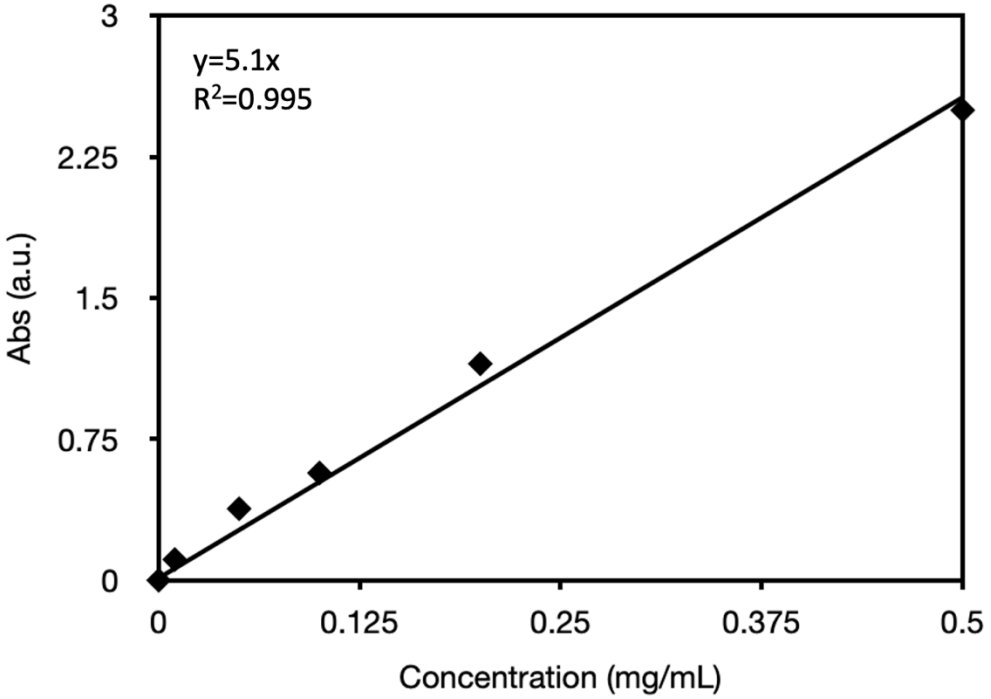

Figure S16. UPy-2 UV-Vis standard curve

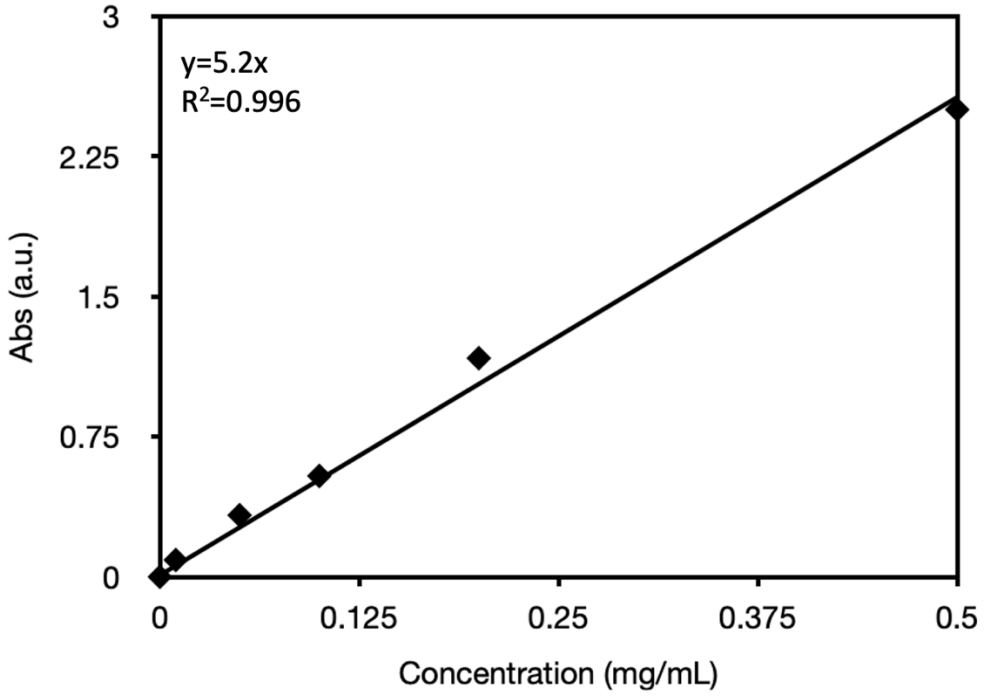

Figure S17. UPy-3 UV-Vis standard curve

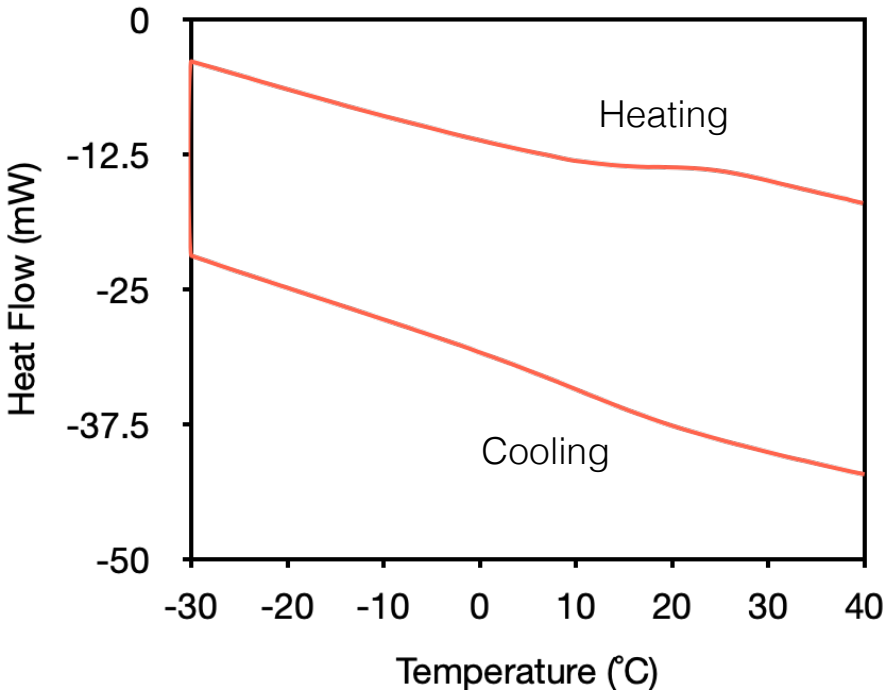

Figure S18. Heat flow curves of the control coating measured via DSC

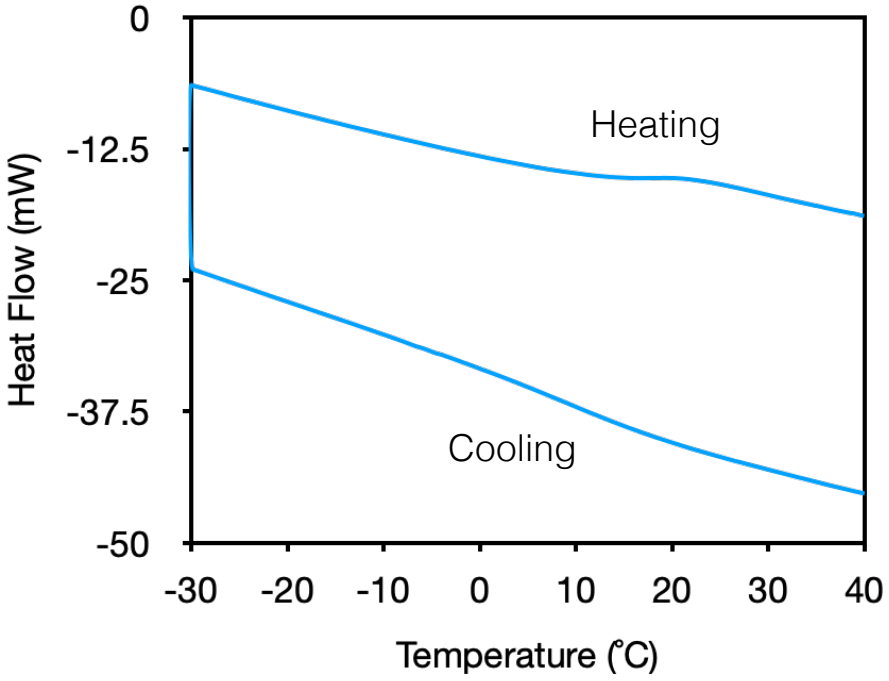

Figure S19. Heat flow curves of the UPy-2 coating measured via DSC

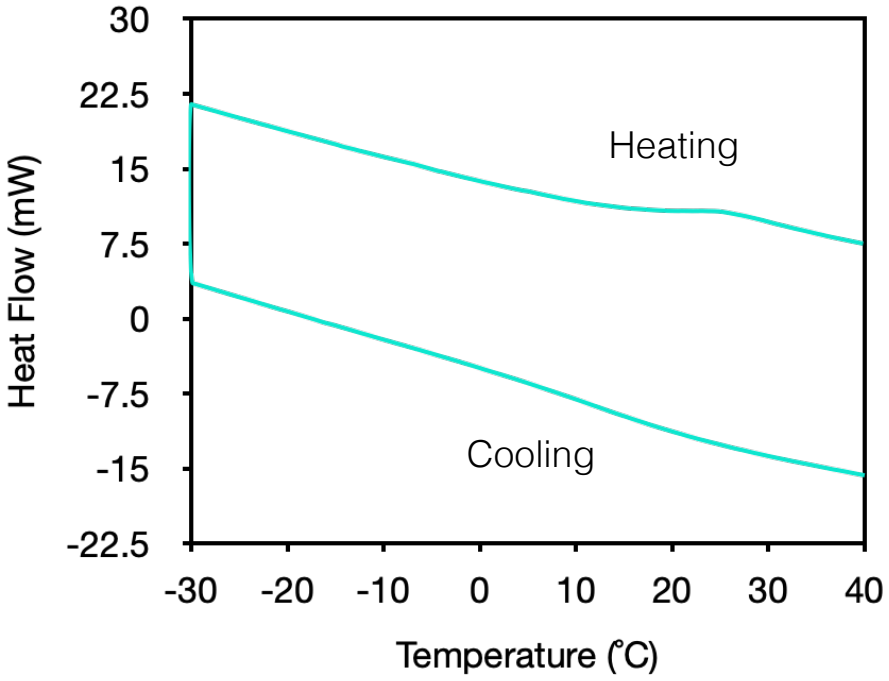

Figure S20. Heat flow curves of the UPy-3 coating measured via DSC

Strain recovery

Self-healing efficiency was calculated by comparing the strain-at-break (ε) between an undamaged coating and a damaged coating allowed to self-heal under certain conditions. Shown below are the raw values for the strain recovery of both the UPy-2 and UPy-3 functionalized coatings across a range of temperatures. No self-healing was observed for the control MMA/BA/AA latex without UPy. The UPy-2 and UPy-3 were also subjected to four healing cycles, also shown below.

	Uncut	**RT**		**40˚C**		**50˚C**	
	ε (%)	*ε (%)*	*Healing (%)*	*ε (%)*	*Healing (%)*	*ε (%)*	*Healing (%)*
	79.6	23.4	29.4	41.7	52.3	58.9	74.0
	67.0	17.6	26.3	40.7	60.7	58.2	86.8
	61.0	16.0	26.2	34.3	56.2	48.8	80.0
Mean	69.2	19.0	27.3	38.9	56.4	55.3	80.3
σ	9.5	3.8	1.8	4.0	4.2	5.6	6.4

Figure S21. A table of the strain-at-break (ε) and the strain recovery (self-healing) (%) of the UPy-2 coating is shown for three independent experiments. The mean and standard deviation (σ) values are also shown at the bottom of the table. The healing conditions were 24 hours at temperatures ranging from RT to 50˚C. Self-healing was calculated by comparing the strain-at-break of the healed coatings with the undamaged coating.

	Uncut	RT		40˚C		50˚C	
	ε (%)	*ε (%)*	*Healing (%)*	*ε (%)*	*Healing (%)*	*ε (%)*	*Healing (%)*
	61.5	8.4	13.6	22.0	35.8	37.6	61.1
	51.5	4.6	8.9	10.4	20.2	33.8	65.6
	53.1	8.2	15.4	17.1	32.2	36.0	67.8
Mean	55.4	7.1	12.6	16.5	29.4	35.8	64.8
σ	5.3	2.1	3.4	5.8	8.2	1.9	3.4

Figure S22. A table of the strain-at-break (ε) and the strain recovery (self-healing) (%) of the UPy-3 coating is shown for three independent experiments. The mean and standard deviation (σ) values are also shown at the bottom of the table. The healing conditions were 24 hours at temperatures ranging from RT to 50˚C. Self-healing was calculated by comparing the strain-at-break of the healed coatings with the undamaged coating.

	UPy-2			UPy-3		
	ε (%)	*Healing (%)*	*σ*	*ε (%)*	*Healing (%)*	*σ*
Cycle 1	19.0	27.3	1.8	7.1	12.6	3.4
Cycle 2	9.9	14.4	4.8	2.7	4.9	0.7
Cycle 3	5.1	7.4	2.7	NH	NH	NH
Cycle 4	NH	NH	NH	NH	NH	NH

Figure S23. A table of the strain-at-break (ε), the strain recovery (self-healing) (%) and the standard deviation (σ) values for the UPy-2 and UPy-3 coatings following self-healing after 24 hours at RT. The self-healing was measured over four healing cycles. NH refers to no observed self-healing, i.e. no difference between the strain-at-break of the UPy coatings as opposed to the control. The data represents the mean and standard deviation of three independent experiments.

	UPy-2			UPy-3		
	ε (%)	*Healing (%)*	*σ*	*ε (%)*	*Healing (%)*	*σ*
Cycle 1	55.3	80.3	6.4	37.6	61.1	3.4
Cycle 2	33.4	48.2	1.6	11.2	20.2	2.8
Cycle 3	22.8	33.0	12.9	NH	NH	NH
Cycle 4	NH	NH	NH	NH	NH	NH

Figure S24. A table of the strain-at-break (ε), the strain recovery (self-healing) (%) and the standard deviation (σ) values for the UPy-2 and UPy-3 coatings following self-healing after 24 hours at 50˚C. The self-healing was measured over four healing cycles. NH refers to no observed self-healing, i.e. no difference between the strain-at-break of the UPy coatings as

opposed to the control. The data represents the mean and standard deviation of three independent experiments.

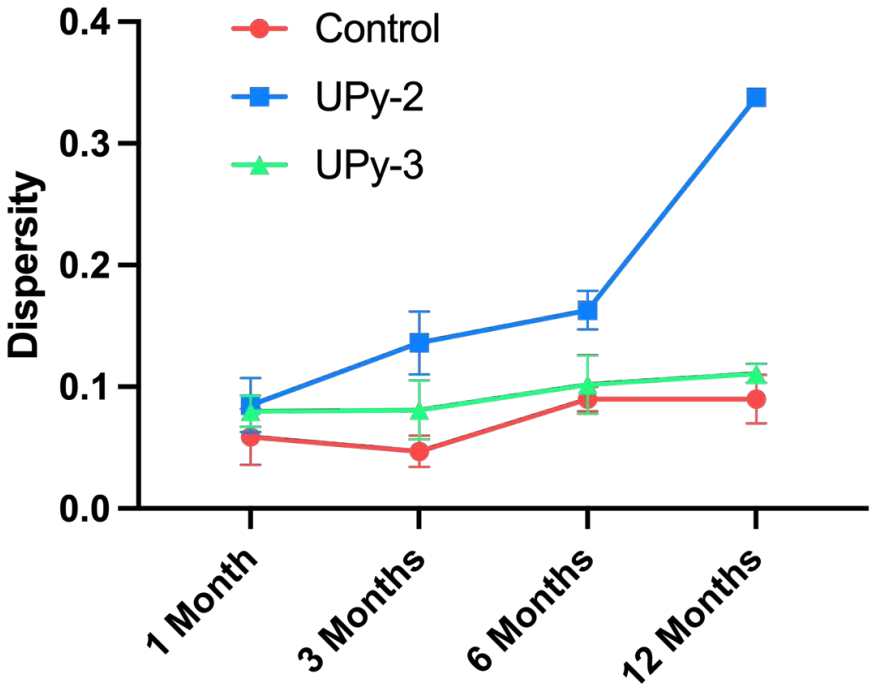

Figure S25. The long term stability of the control, UPy-2 and UPy-3 latexes was examined. The dispersity of each latex was measured via DLS at 1 month, 3 months, 6 months and 12 months. The data represents the mean ± SD for 3 independent experiments

Control	UPy-2	UPy-3
H	H	H
H	HB	H
H	HB	H

Figure S26. The surface hardness of each coating was measured via the pencil hardness test. The hardness results are shown above for 3 separate measurements.

	Water	Salt	pH 5	60˚C
Control	11%	<1%	7%	33%
UPy-2	8%	<1%	4%	33%
UPy-3	11%	1%	5%	29%

Figure S27. The water resistance of each coating was measured gravimetrically under four different conditions: deionized water, saturated salt water, acidic (pH 5) water, and water at elevated temperature (60˚C). The increase in weight (%) for each coating under each condition is shown.

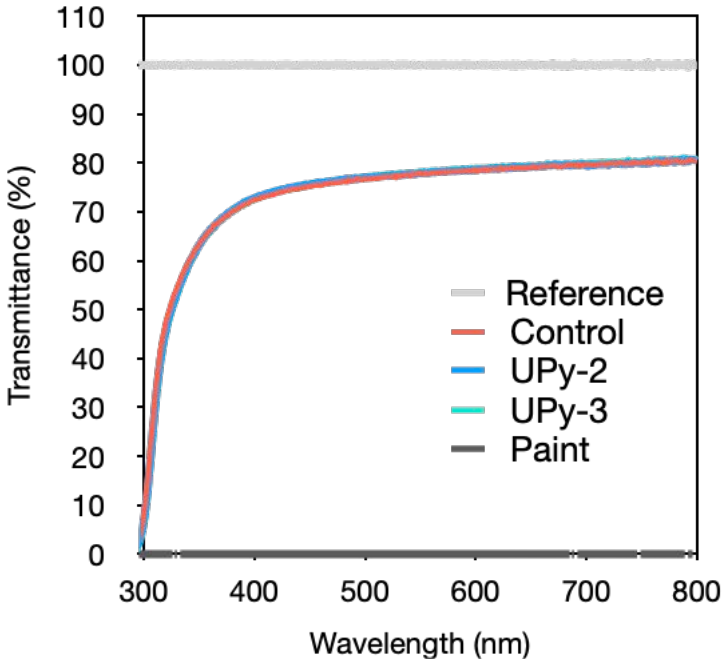

Sample	T (%)
Reference	99
Control	80
UPy-2	81
UPy-3	81
Paint	<1

Figure S28. The transparency of each coating (600µm thickness) was analyzed by measuring the transmittance (T) via UV/Vis spectroscopy. a) The UV/Vis spectra of the three coatings, as well as a reference and opaque paint sample. b) The transmittance values for each sample (λ = 650 nm).

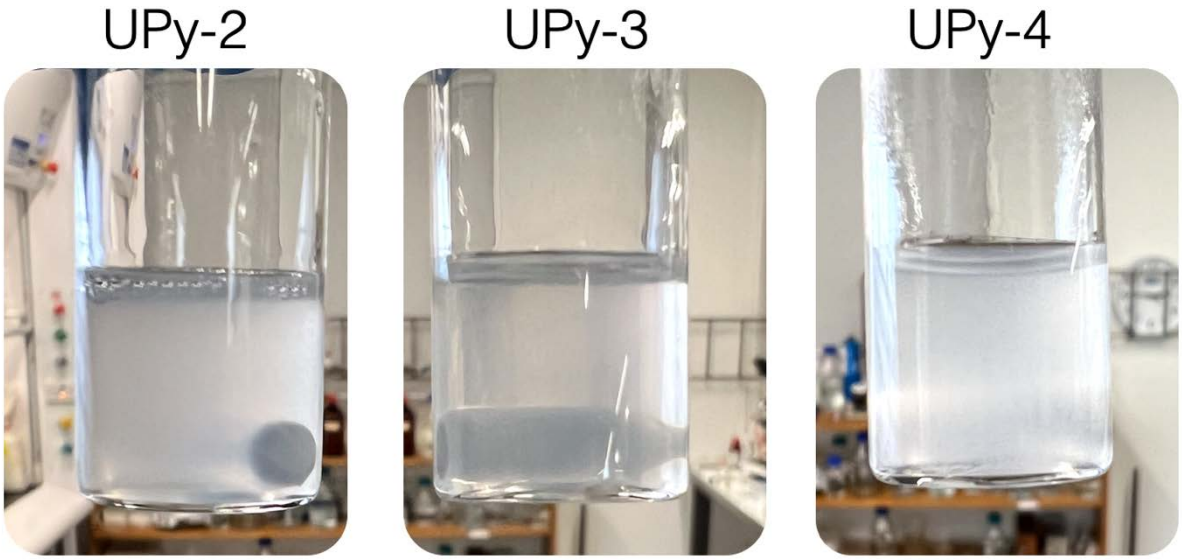

Figure S29. Images of the monomer feeds for the UPy-2, 3, and 4 monomers respectively at 2.5 wt%. At this concentration, only UPy-2 and 3 are stable in MMA/BA/AA. UPy-4 begins to aggregate.

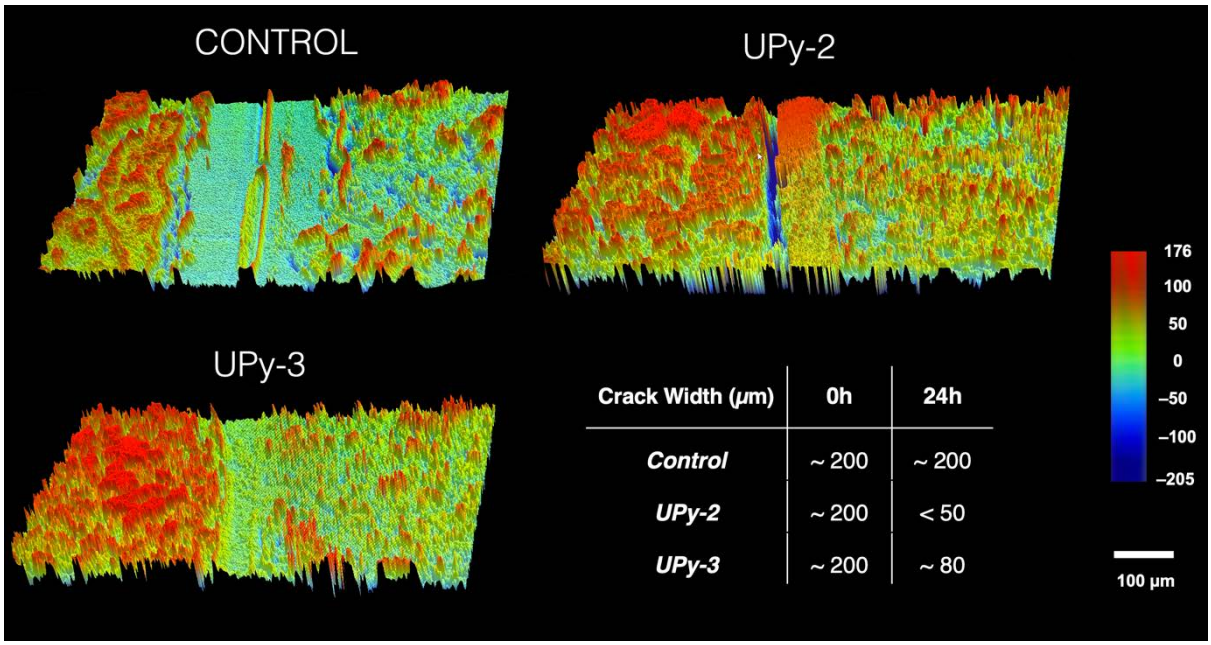

Figure S30. 3D rendered images of the control, UPy-2 and UPy-3 coatings with a 200μm cut allowed to self-heal over 24 hours at room temperature. The images were taken via optical surface profilometry, and the respective widths of the healed coatings are shown.

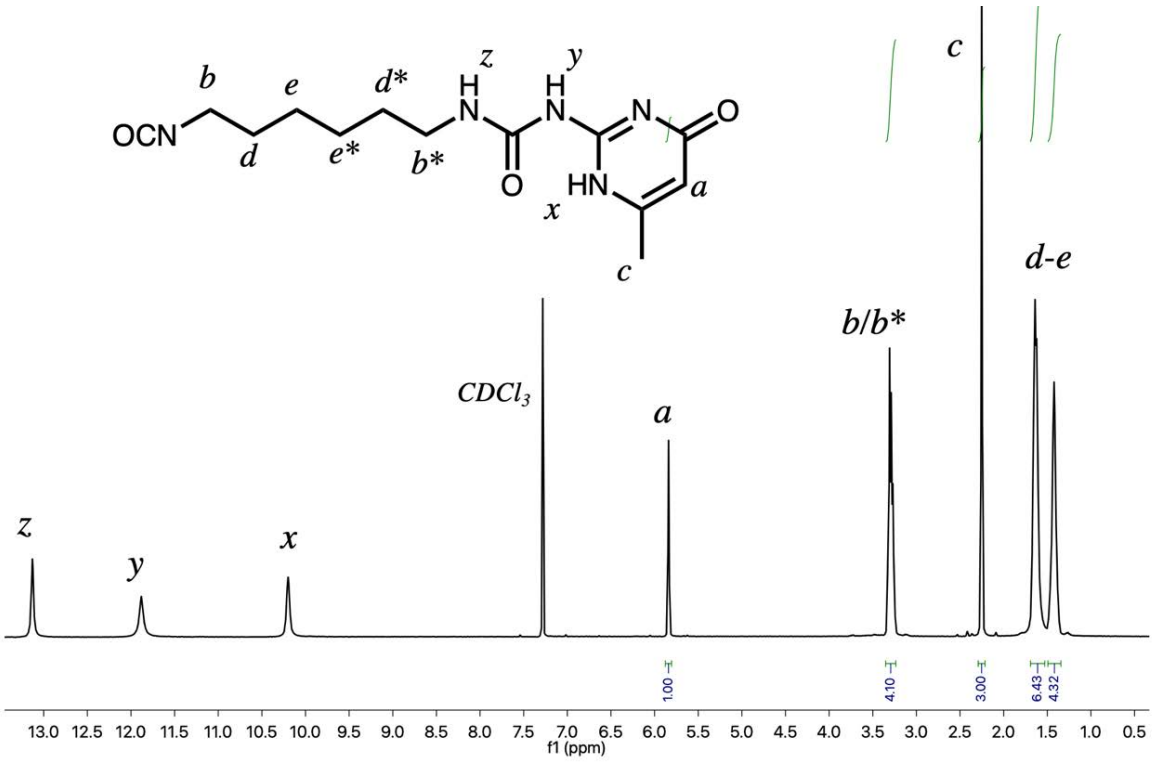

Figure S31. ^{1}H-NMR (400 MHz, $CHCl_3$) of 2(6-isocyanatohexylaminocarbonylamino)-6-methyl-4[1H] pyrimidinone

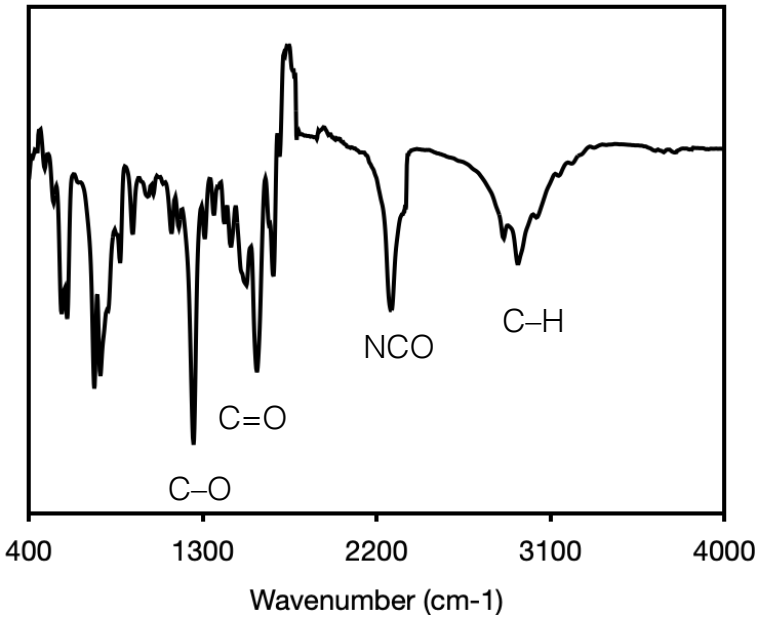

Figure S32. FTIR spectrum of 2(6-isocyanatohexylaminocarbonylamino)-6-methyl-4[1H] pyrimidinone

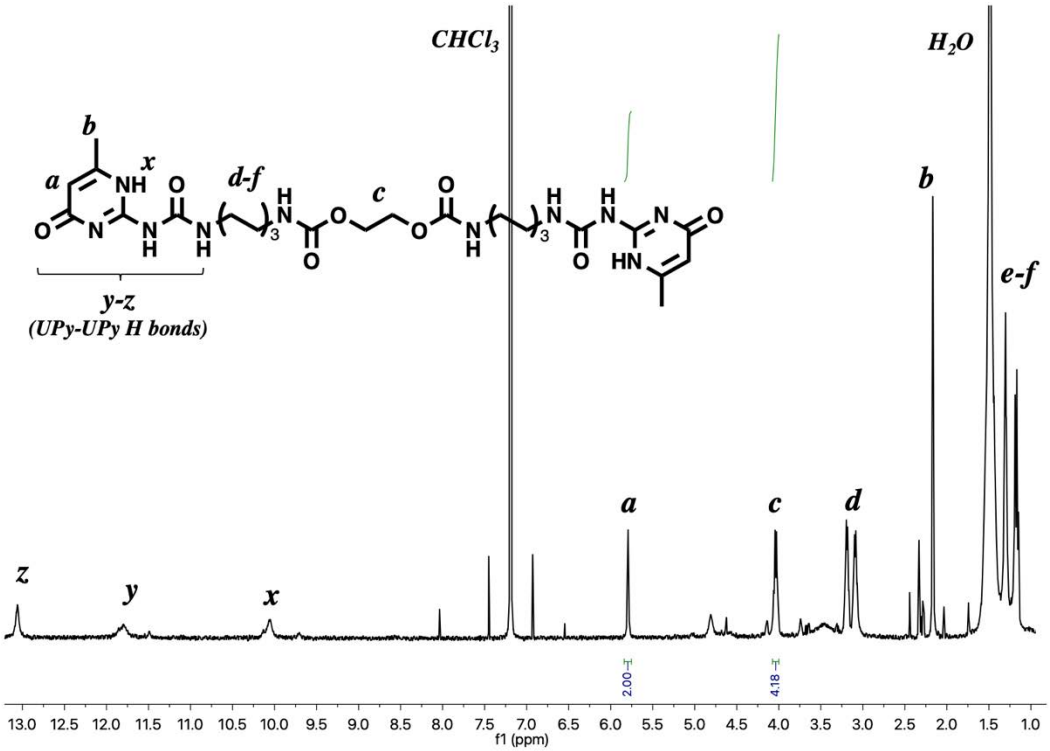

Figure S33. ^{1}H NMR (400 MHz, $CHCl_3$) of UPy-XL-1

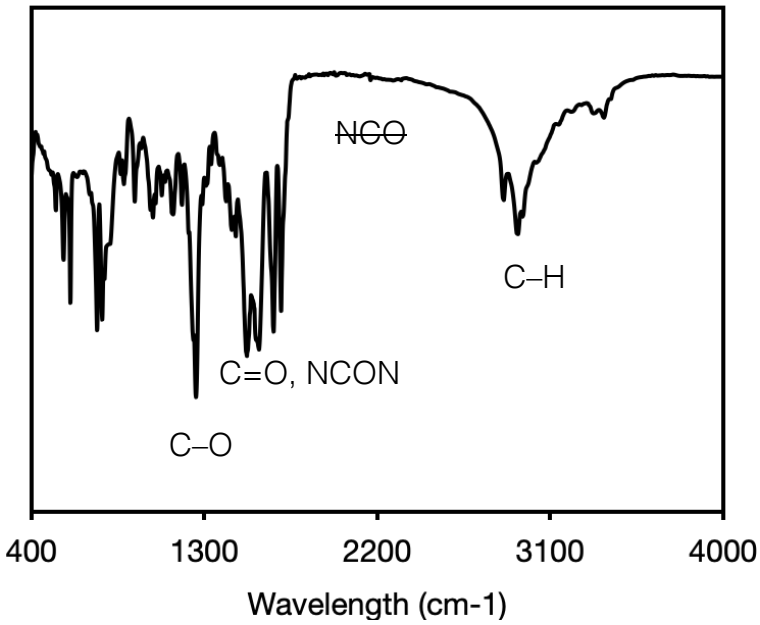

Figure S34. FTIR spectrum of UPy-XL-1

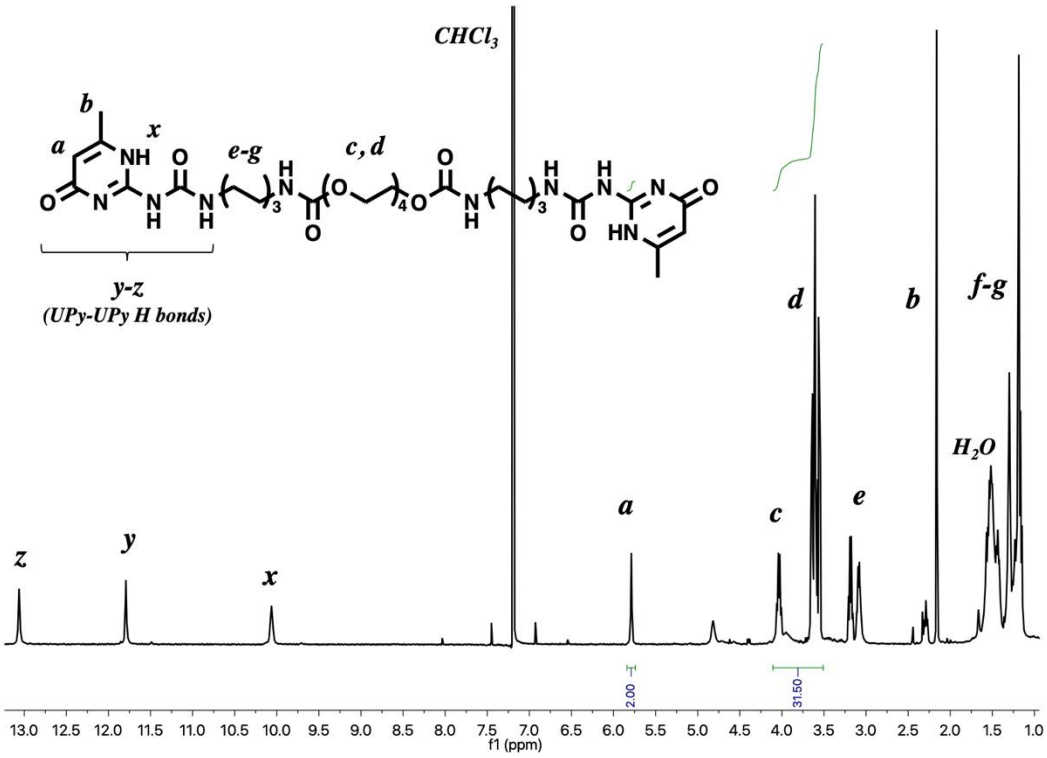

Figure S35. ^{1}H NMR (400 MHz, $CHCl_3$) of UPy-XL-2

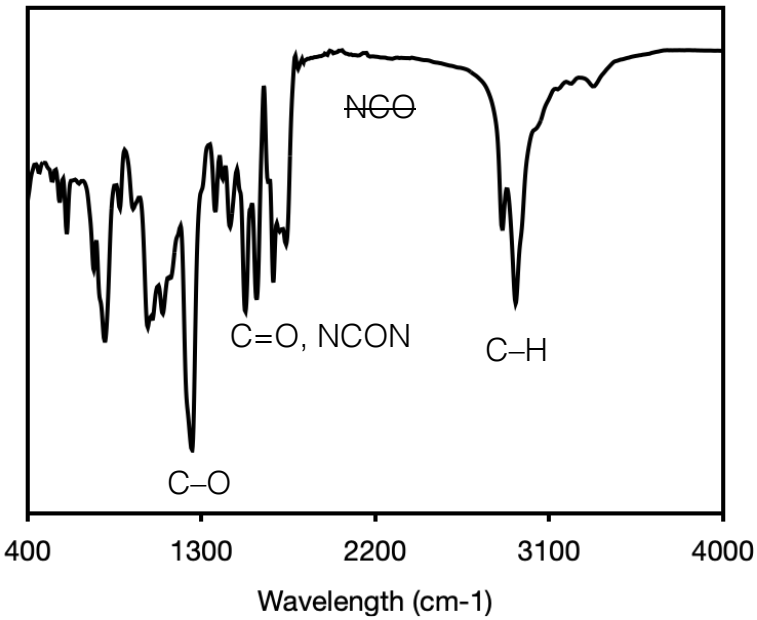

Figure S36. FTIR spectrum of UPy-XL-2

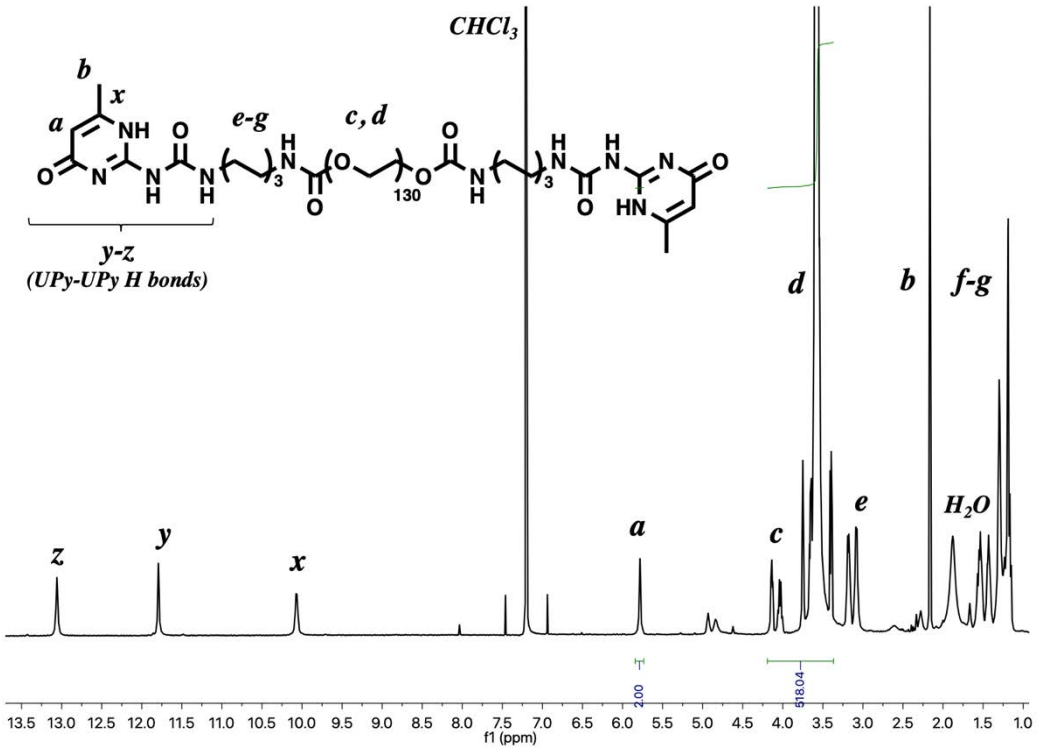

Figure S37. ^{1}H NMR (400 MHz, $CHCl_3$) of UPy-XL-3

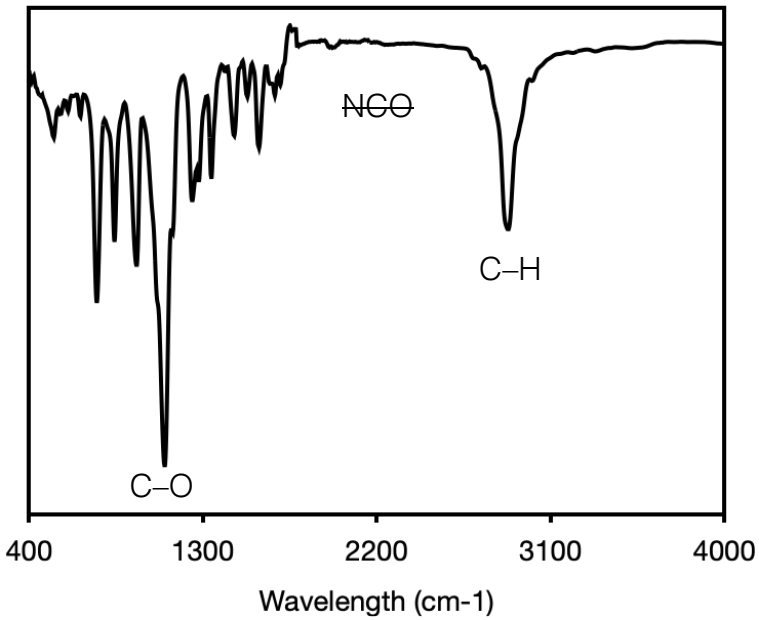

Figure S38. FTIR spectrum of UPy-XL-3

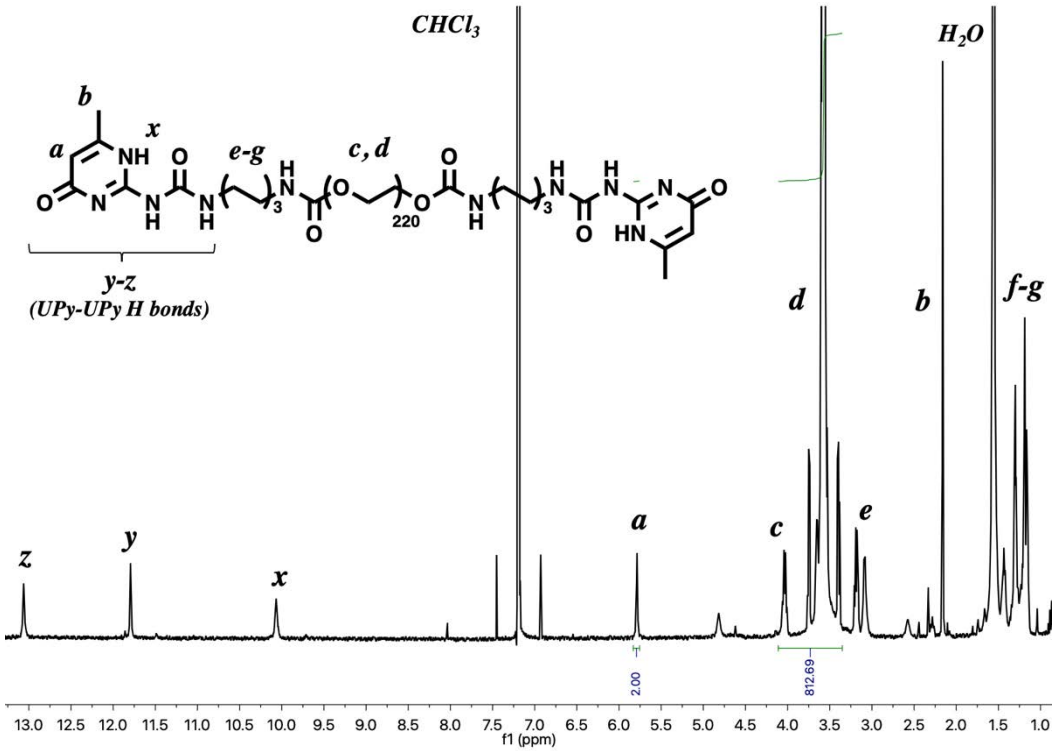

Figure S39. ^{1}H NMR (400 MHz, $CHCl_3$) of UPy-XL-4

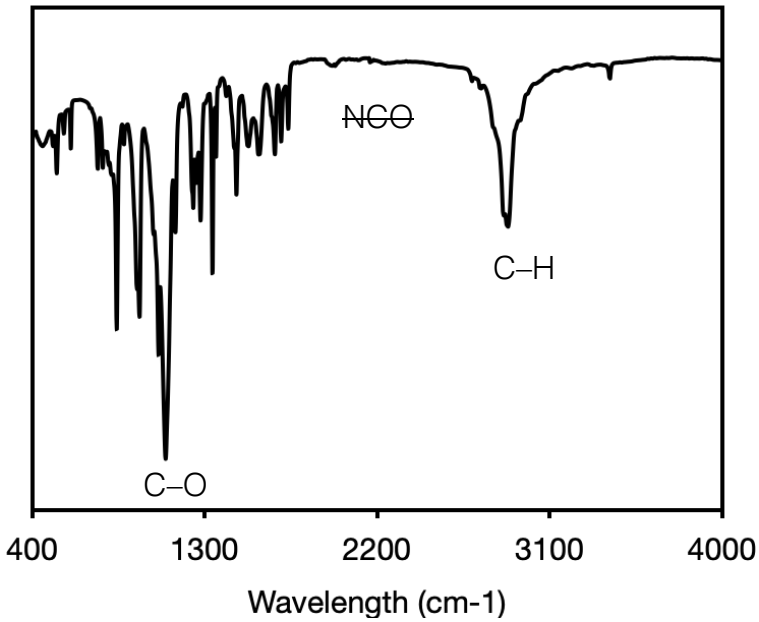

Figure S40. FTIR spectrum of UPy-XL-4

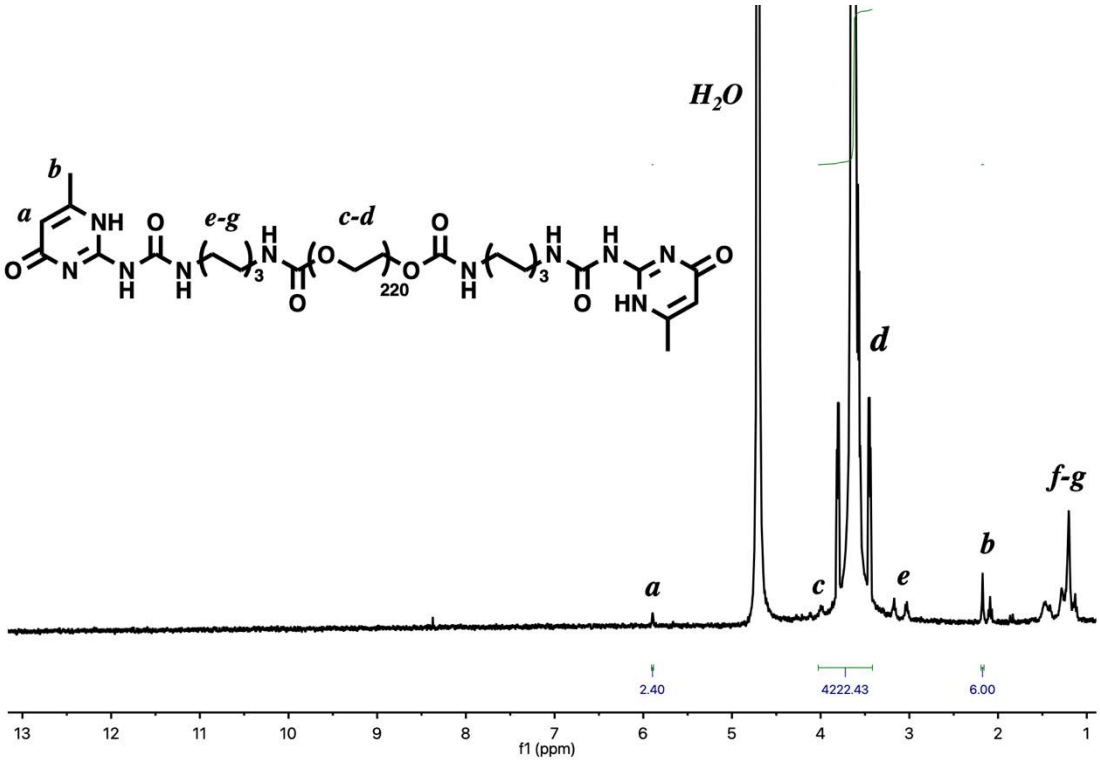

Figure S41. ^{1}H NMR (400 MHz, D_2O) of UPy-XL-4 at 25°C

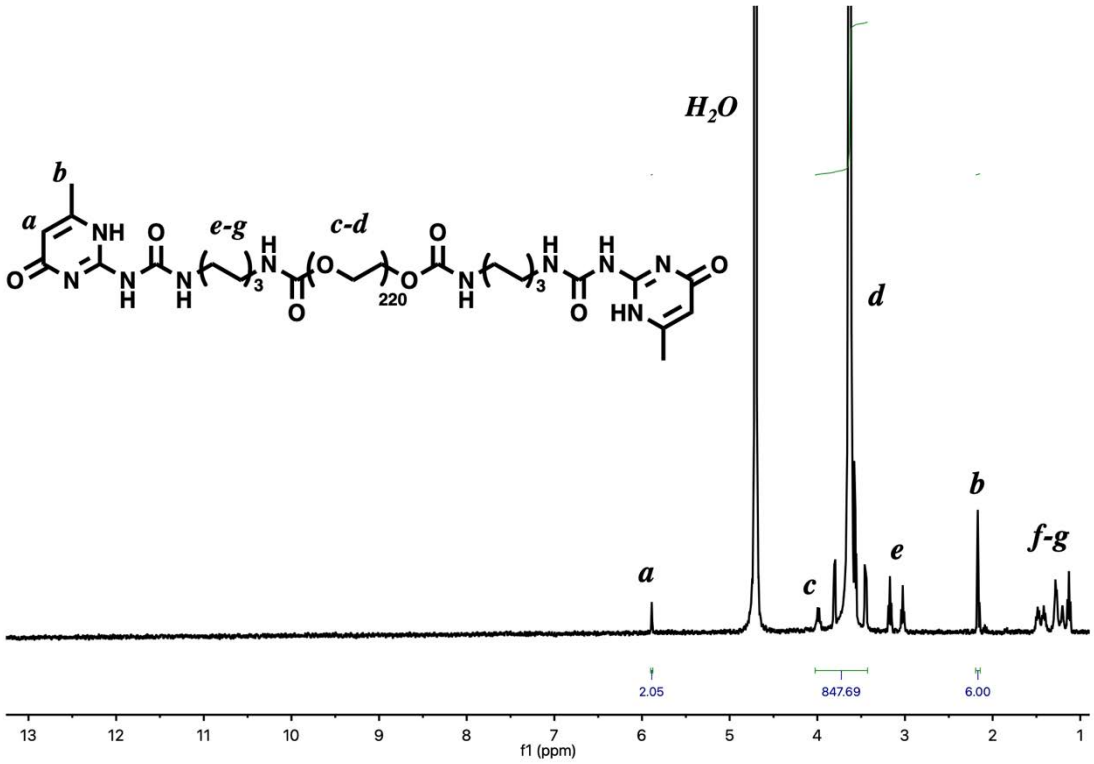

Figure S42. ^{1}H NMR (400 MHz, D_2O) of UPy-XL-4 at 80˚C

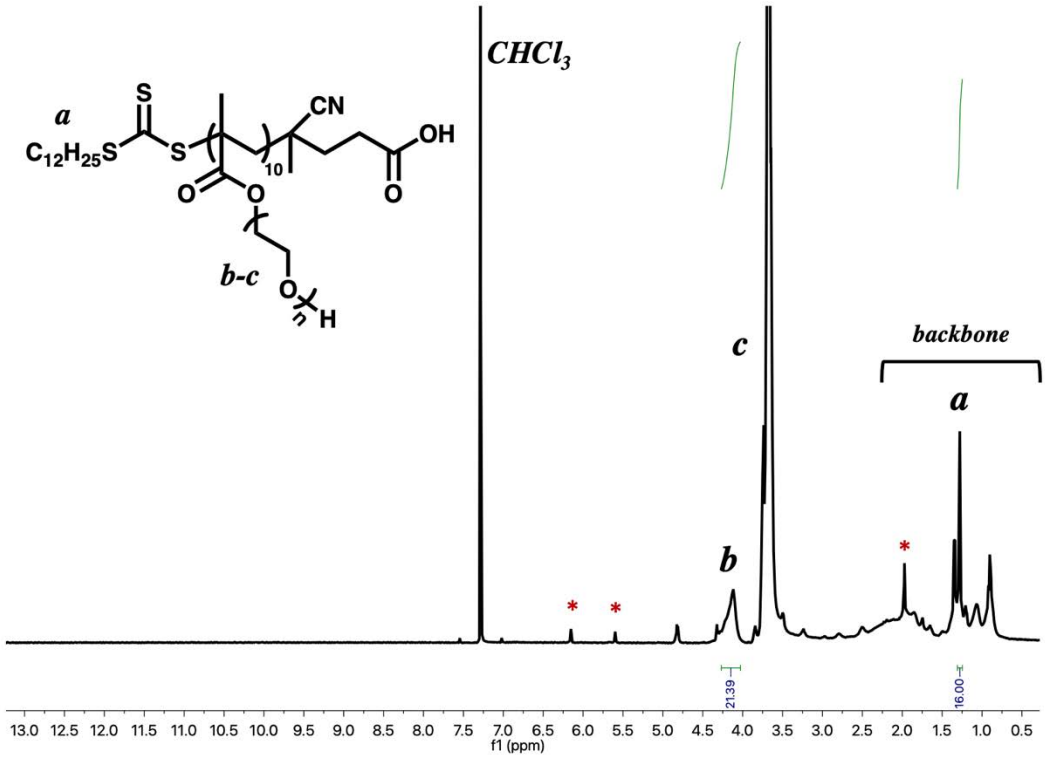

Figure S43. ^{1}H NMR (400 MHz, $CHCl_3$) of the poly(PEGMA) brush (MW ~ 5000 Da). Red asterisks indicate residual monomer peaks.

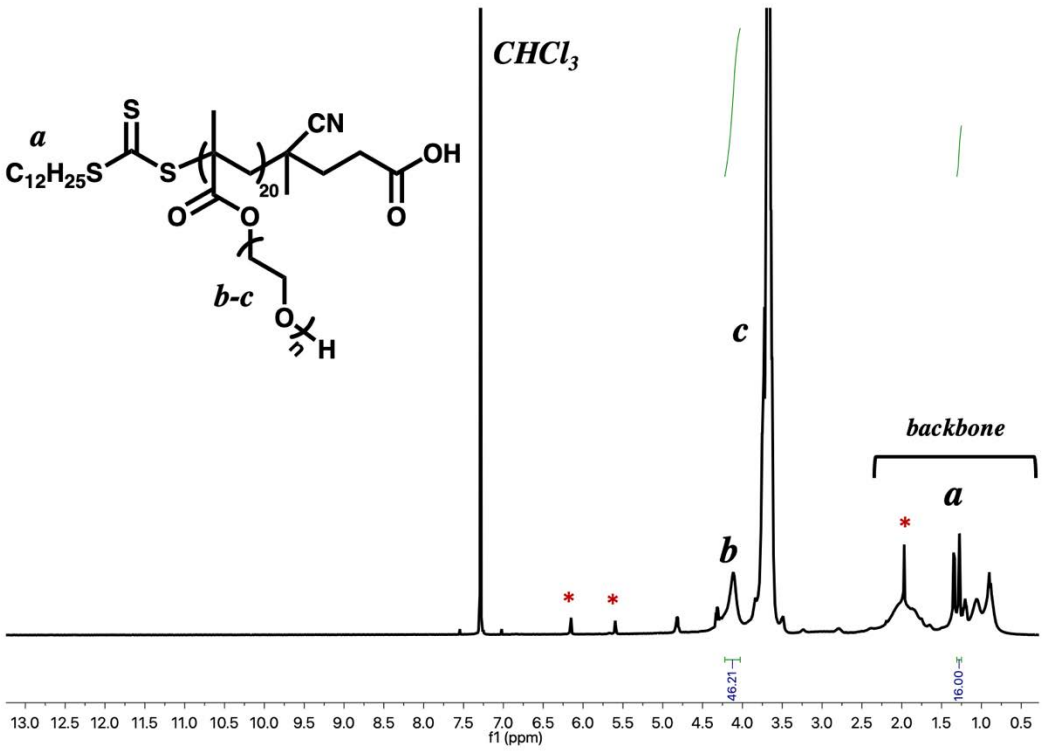

Figure S44. ^{1}H NMR (400 MHz, $CHCl_3$) of the poly(PEGMA) brush (MW ~ 10,000 Da). Red asterisks indicate residual monomer peaks.

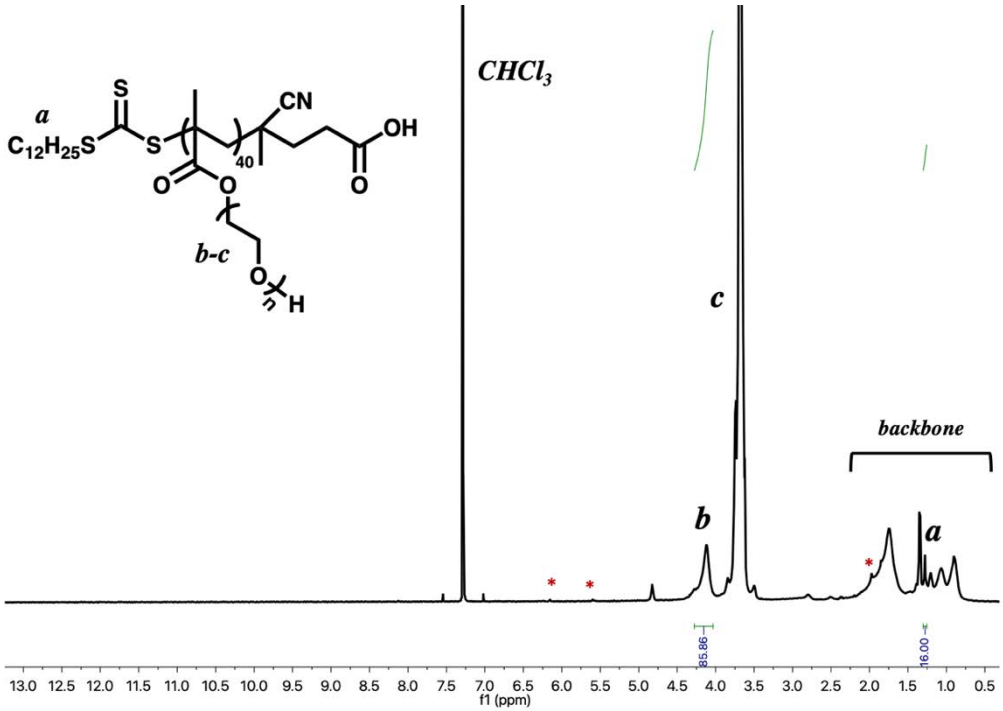

Figure S45. ^{1}H NMR (400 MHz, $CHCl_3$) of the poly(PEGMA) brush (MW ~ 20,000 Da). Red asterisks indicate residual monomer peaks.

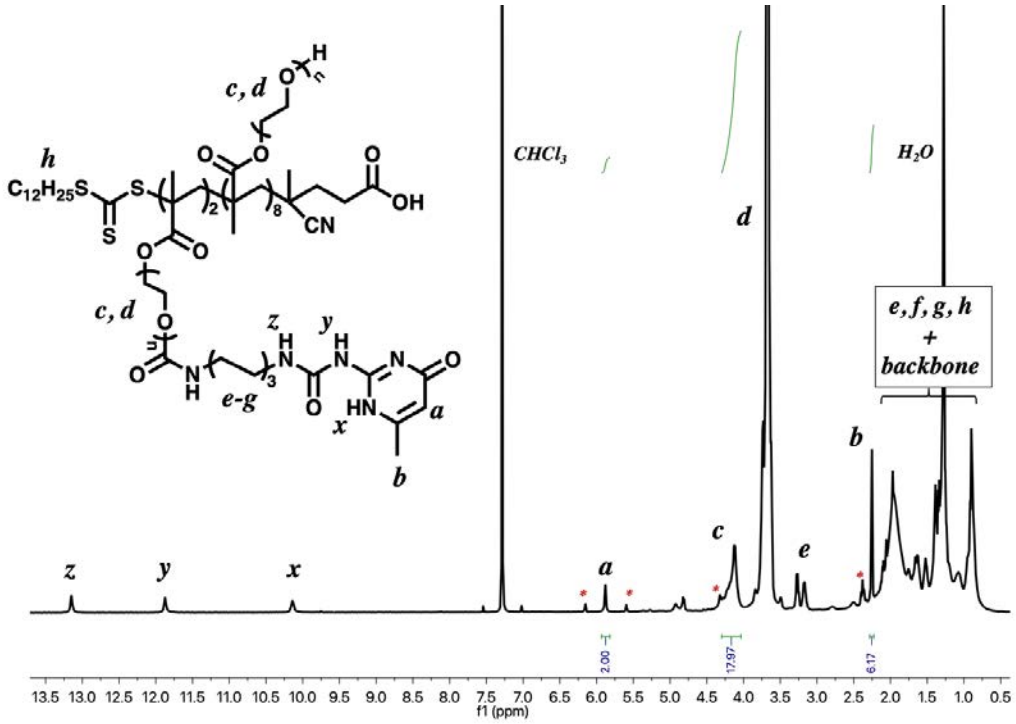

Figure S46. ^{1}H NMR (400 MHz, $CHCl_3$) of UPy-Brush-5. The red asterisk represents unreacted monomer peaks.

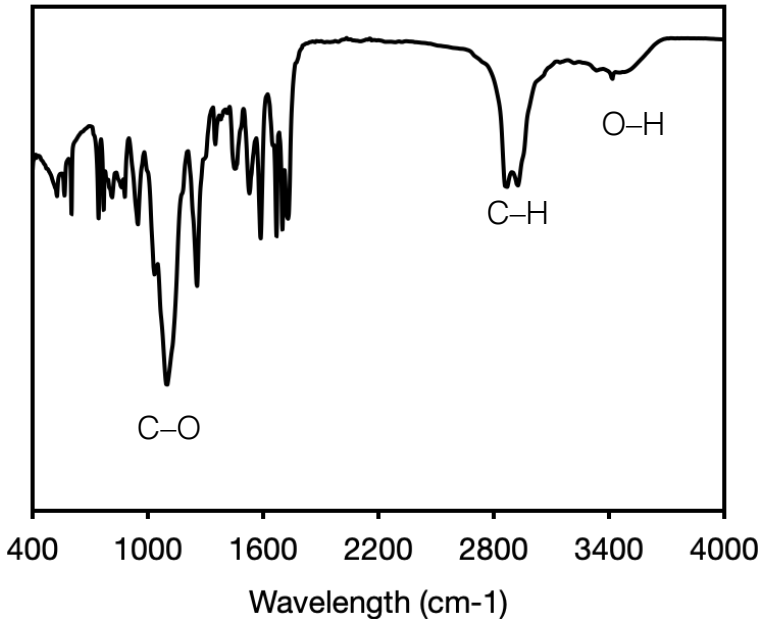

Figure S47. FTIR spectrum of UPy-Brush-5

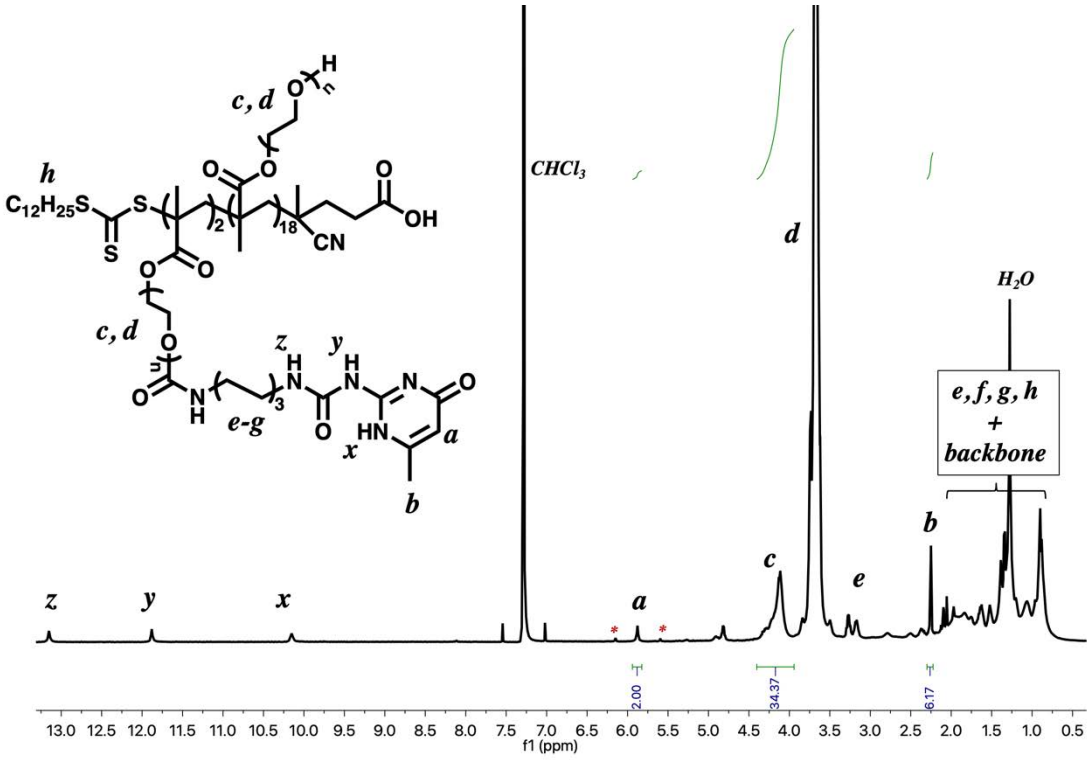

Figure S48. ^{1}H NMR (400 MHz, $CHCl_3$) of UPy-Brush-10. The red asterisk represents unreacted monomer peaks.

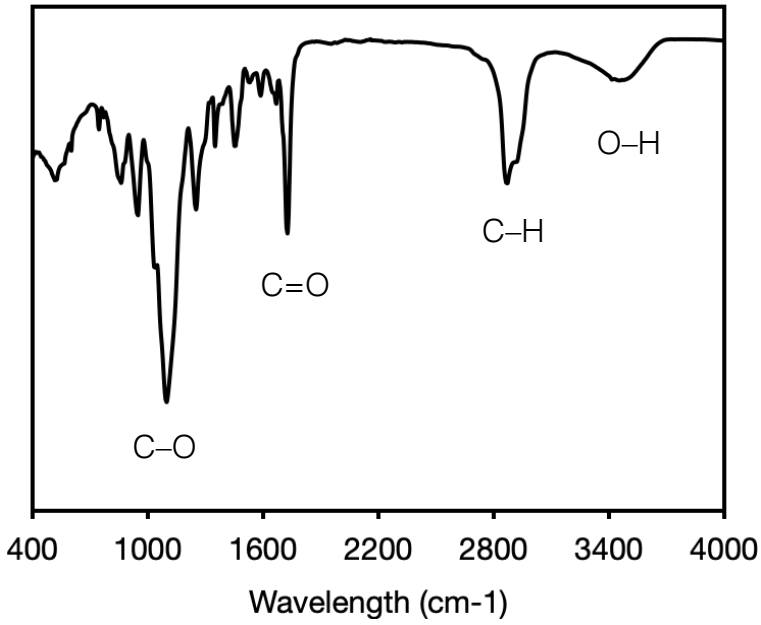

Figure S49. FTIR spectrum of UPy-Brush-10

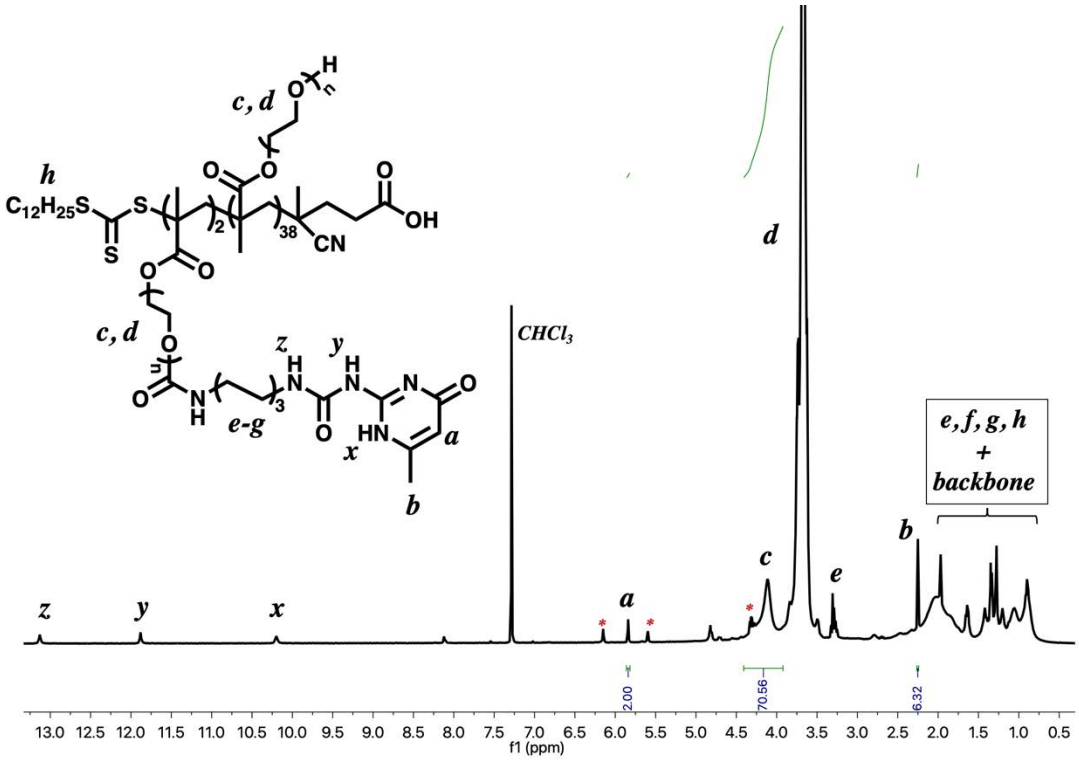

Figure S50. ^{1}H NMR (400 MHz, $CHCl_3$) of UPy-Brush-20 The red asterisk represents unreacted monomer peaks.

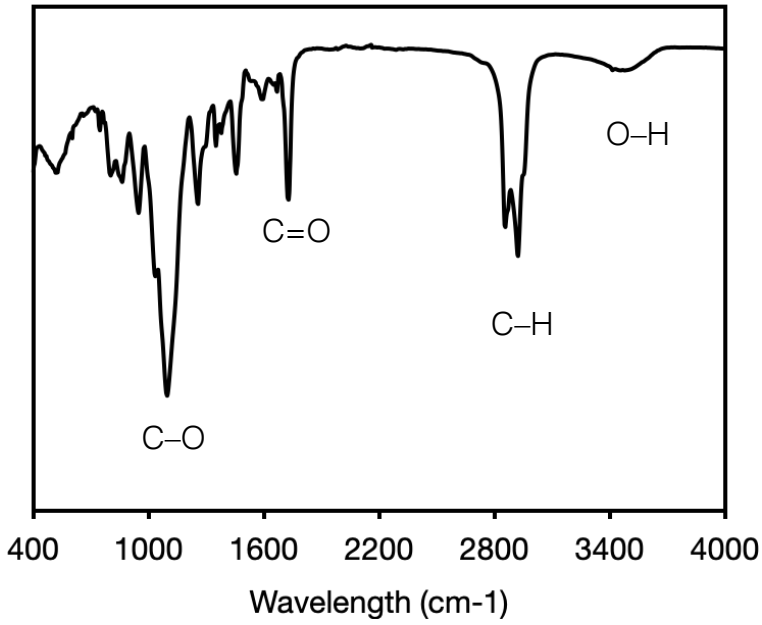

Figure S51. FTIR spectrum of UPy-Brush-20

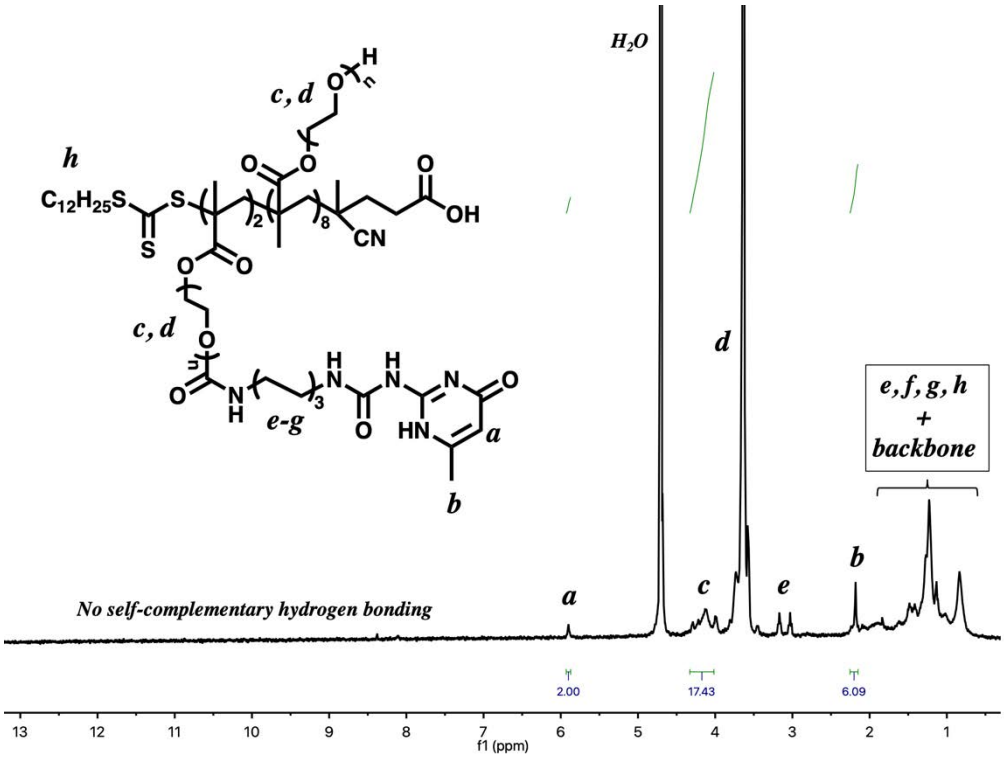

Figure S52. ^{1}H NMR (400 MHz, H_2O) of UPy-Brush-5

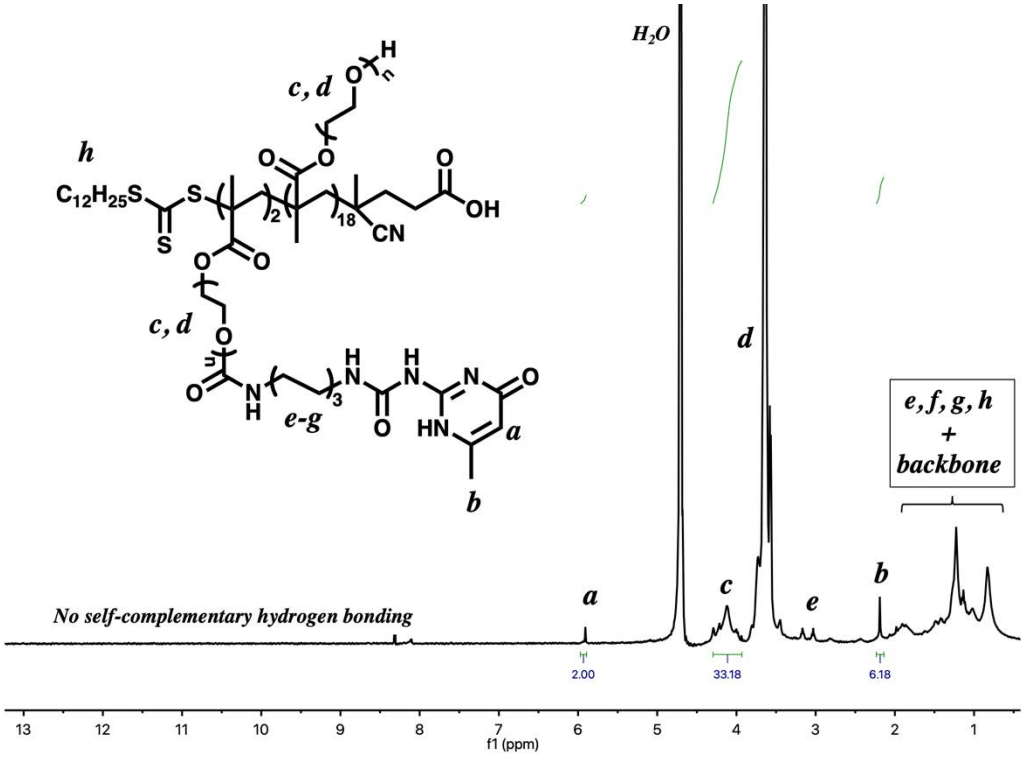

Figure S53. ^{1}H NMR (400 MHz, H_2O) of UPy-Brush-10

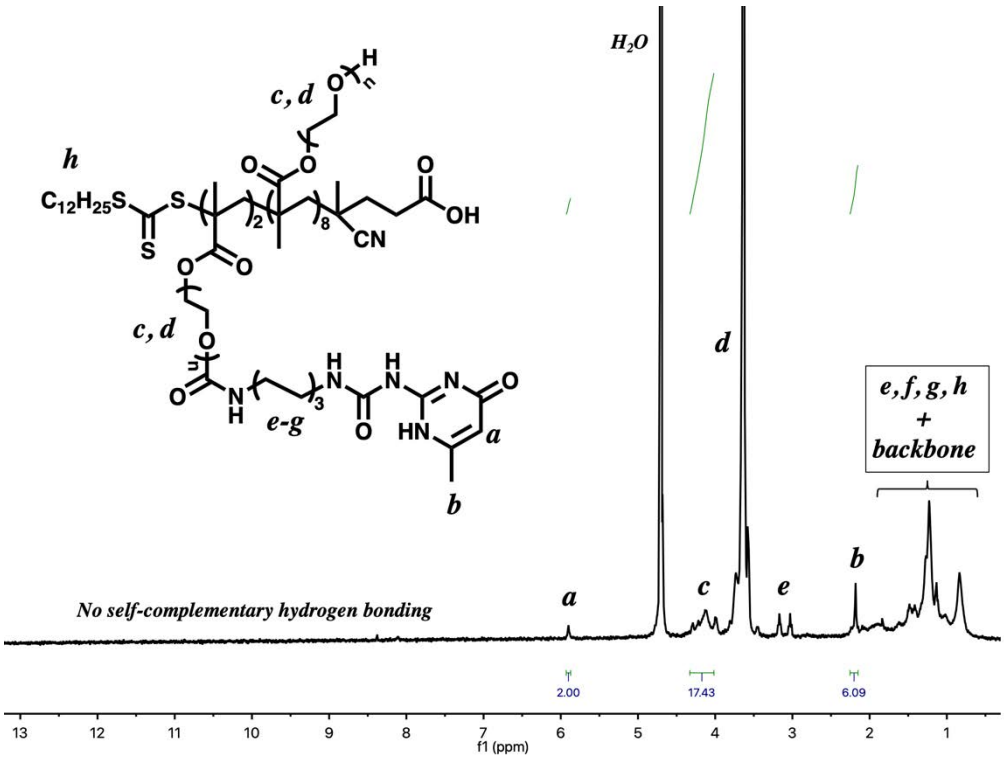

Figure S54. ^{1}H NMR (400 MHz, H_2O) of UPy-Brush-20

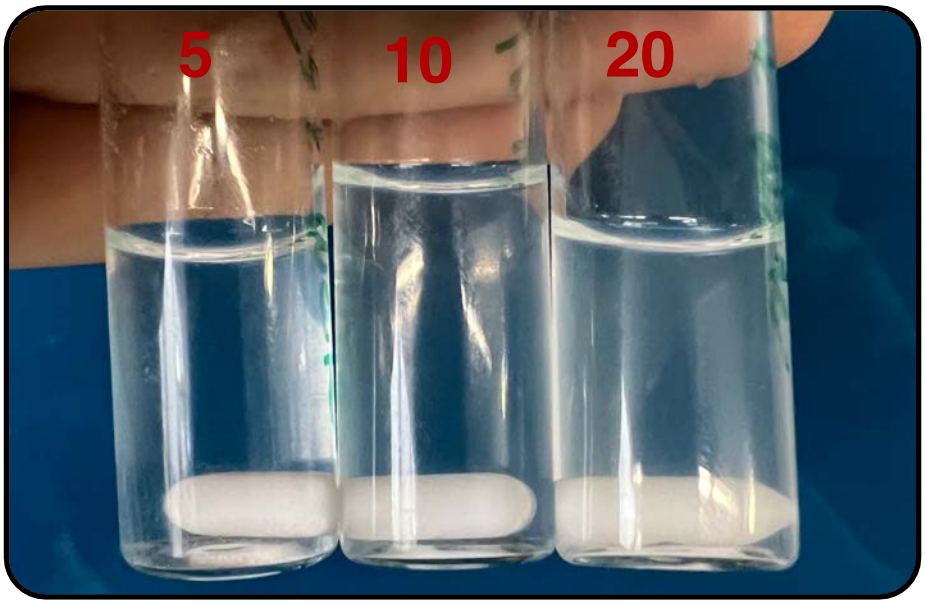

Figure S55. The three UPy-Brush crosslinkers dissolved in de-ionized water

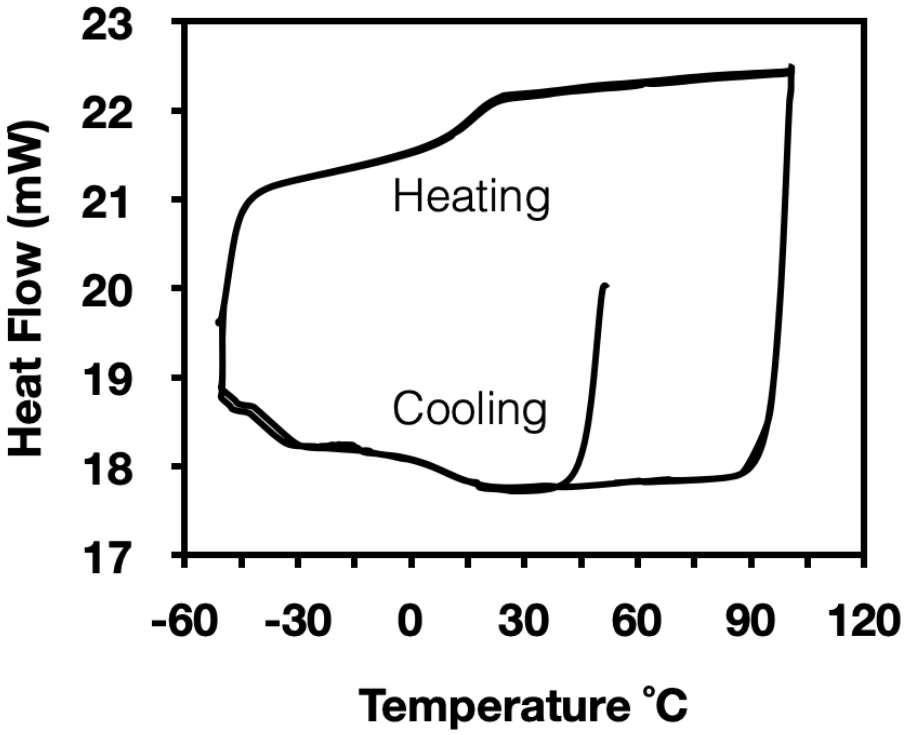

Figure S56. Heat flow curves of the UPy-Brush-5 coating measured by DSC, which shows two heating cycles and two cooling cycles between –50 and 100°C.

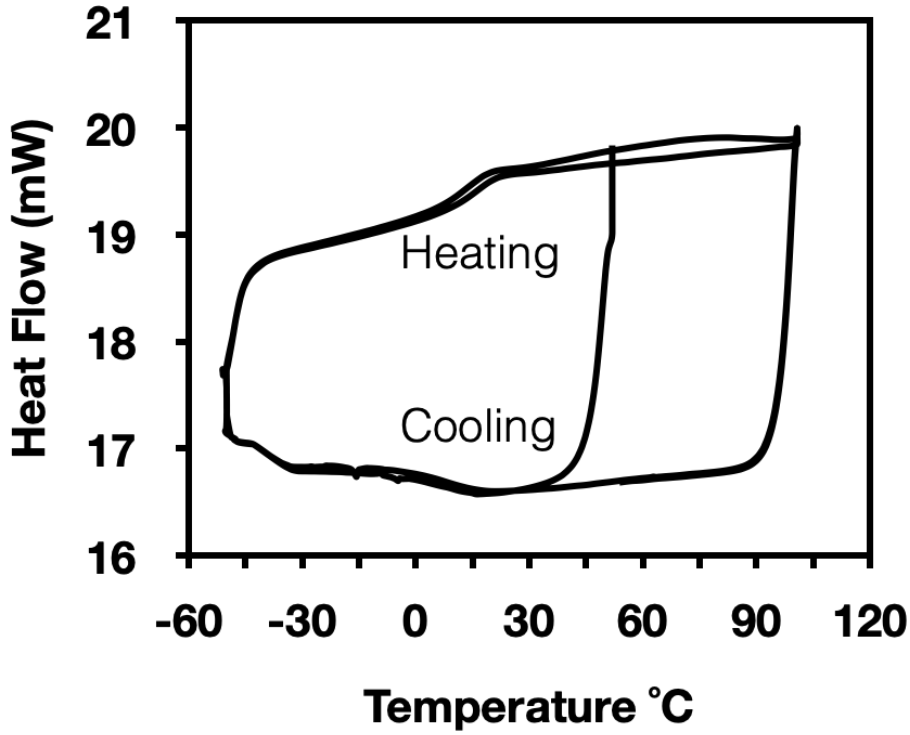

Figure S57. Heat flow curves of the UPy-Brush-10 coating measured by DSC, which shows two heating cycles and two cooling cycles between –50 and 100˚C.

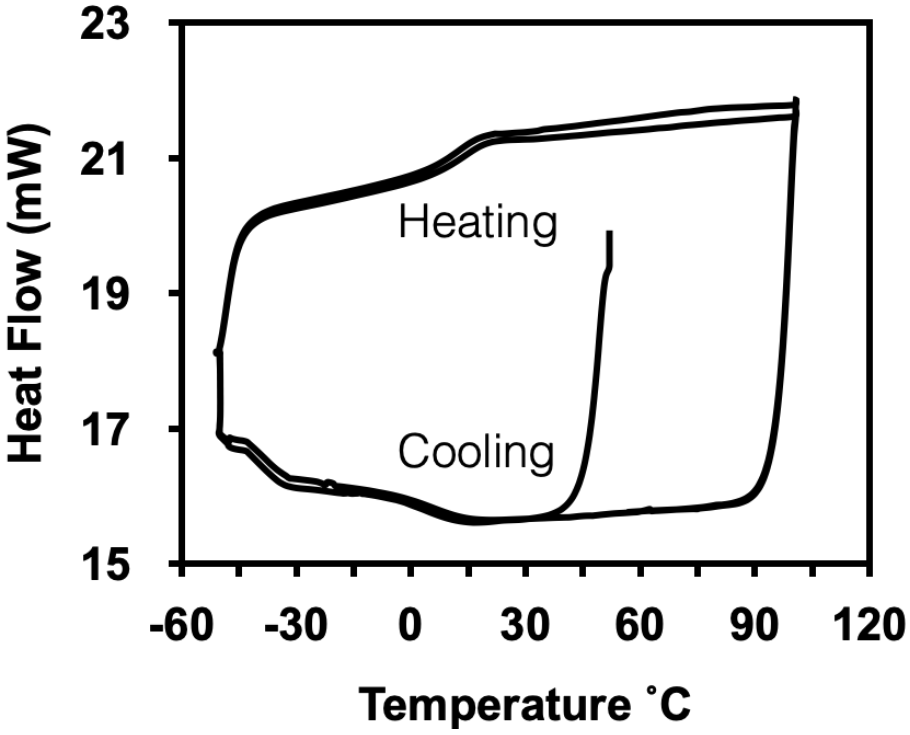

Figure S58. Heat flow curves of the UPy-Brush-20 coating measured by DSC, which shows two heating cycles and two cooling cycles between –50 and 100˚C.

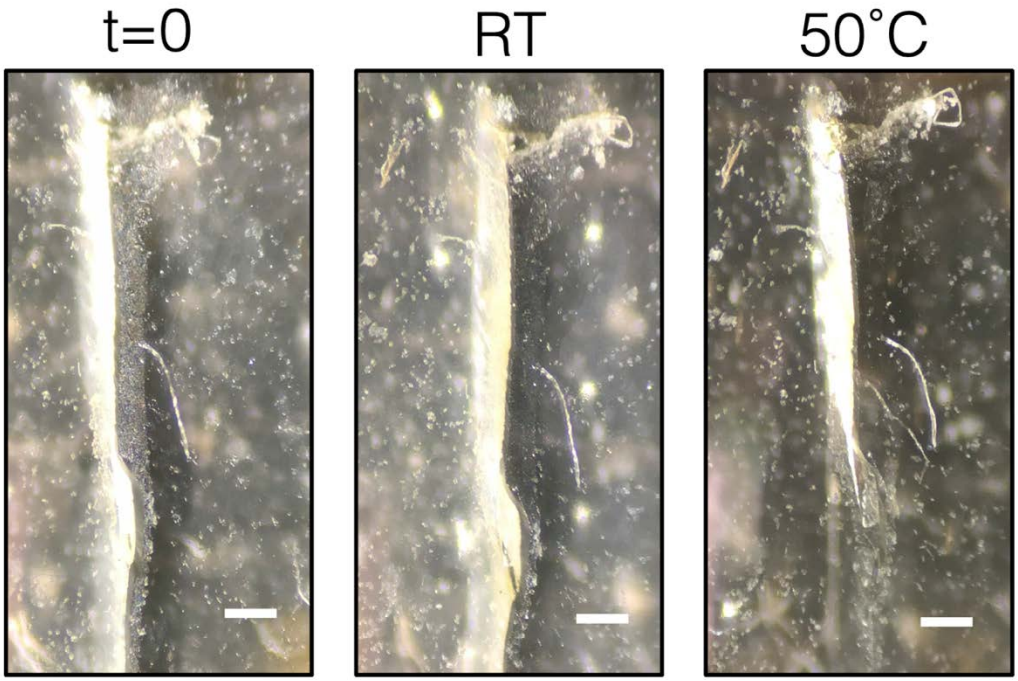

Figure S59. Self-healing optical images of the control latex with added UPy-Brush-5. The healing conditions were 24 hours at room temperature, and 24 hours at 50˚C. The scale bar represents 250 μm.

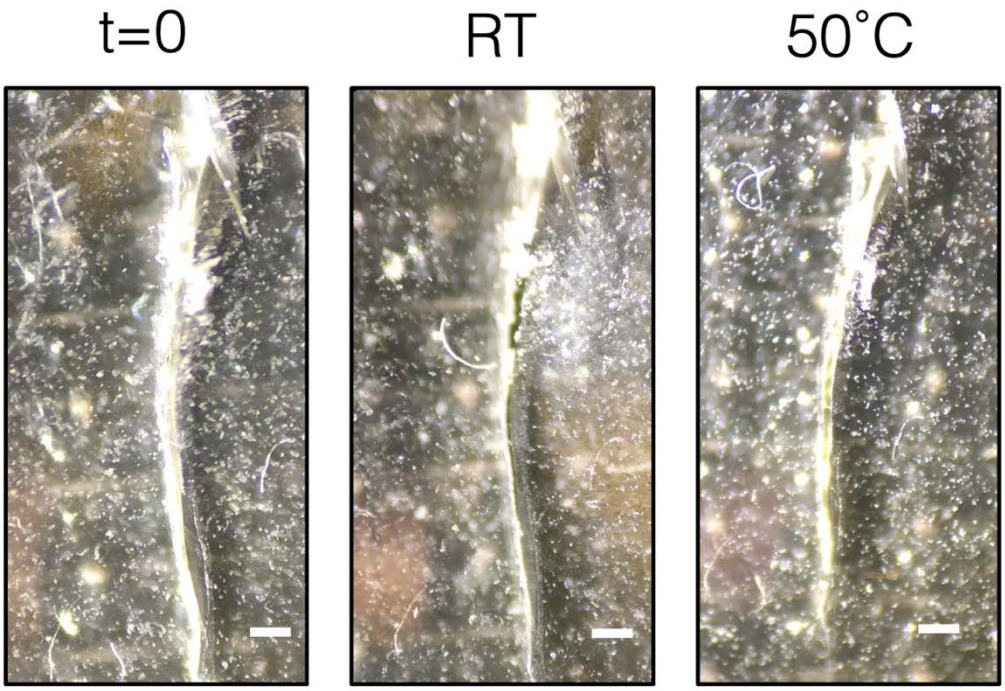

Figure S60. Self-healing optical images of the control latex with added UPy-Brush-20. The healing conditions were 24 hours at room temperature, and 24 hours at 50˚C. The scale bar represents 250 μm.

Strain recovery

Self-healing efficiency was calculated by comparing the strain-at-break (ε) between an undamaged coating and a damaged coating allowed to self-heal under certain conditions. Shown below are the raw values for the strain recovery of each UPy-Brush coating (UPy brush crosslinker + UPy-2 Latex) across three independent experiments. These values were compared to three control coatings, C1, C2 and C3, described in Chapter 3. No self-healing was observed for either C1 or C2, and the raw data for C3 is shown in Chapter 2's SI.

	Uncut	**RT**		**50˚C**	
	ε (%)	*ε (%)*	*Healing (%)*	*ε (%)*	*Healing (%)*
	67.8	20.6	30.3	54.9	80.9
	62.6	15.9	25.4	45.8	73.1
	66.2	19.6	29.6	51.8	78.2
Mean	65.5	18.7	28.4	50.8	77.4
σ	2.66	2.47	2.65	4.62	3.96

Figure S61. A table of the strain-at-break (ε) and the strain recovery (self-healing) (%) of the UPy-2 coating with added UPy-Brush-5 crosslinker at a UPy-mol ratio of 1:1 is shown for three independent experiments. The mean and standard deviation (σ) values are also shown at the bottom of the table. The healing conditions were 24 hours at temperatures of RT and 50˚C. Self-healing was calculated by comparing the strain-at-break of the healed coatings with the undamaged coating.

	Uncut	RT		50˚C	
	ε (%)	*ε (%)*	*Healing (%)*	*ε (%)*	*Healing (%)*
	82.8	30.4	36.7	60.9	73.5
	88.8	37.2	41.8	70.8	79.7
	87.8	30.0	34.1	68.3	77.8
Mean	86.4	32.5	37.5	66.7	77.0
σ	3.21	4.04	3.92	5.14	3.17

Figure S62. A table of the strain-at-break (ε) and the strain recovery (self-healing) (%) of the UPy-2 coating with added UPy-Brush-10 crosslinker at a UPy-mol ratio of 1:1 is shown for three independent experiments. The mean and standard deviation (σ) values are also shown at the bottom of the table. The healing conditions were 24 hours at temperatures of RT and 50˚C. Self-healing was calculated by comparing the strain-at-break of the healed coatings with the undamaged coating.

	Uncut	RT		50˚C	
	ε (%)	*ε (%)*	*Healing (%)*	*ε (%)*	*Healing (%)*
	100.0	23.7	23.7	80.1	80.1
	108.1	26.3	24.3	85.4	79.0
	94.2	21.6	22.9	73.5	78.0
Mean	100.8	23.9	23.6	79.7	79
σ	6.98	2.35	0.7	5.96	1.05

Figure S63. A table of the strain-at-break (ε) and the strain recovery (self-healing) (%) of the UPy-2 coating with added UPy-Brush-20 crosslinker at a UPy-mol ratio of 1:1 is shown for three independent experiments. The mean and standard deviation (σ) values are also shown at the bottom of the table. The healing conditions were 24 hours at temperatures of RT and

50˚C. Self-healing was calculated by comparing the strain-at-break of the healed coatings with the undamaged coating.

a)

Time (h)	0	1	24	48
Mean	0.7	1.0	3.4	7.1
SD	0.08	0.3	1.6	1.7
Mean	0.5	0.8	1.5	5.1
SD	0.14	0.08	0.14	—

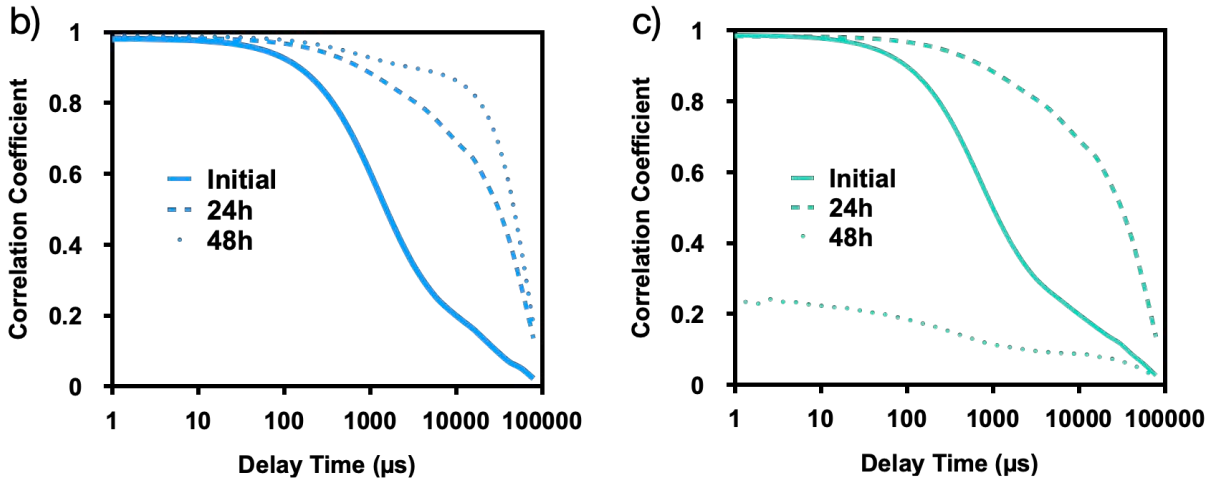

Figure S64. DLS analysis of UPy-XL-4 in an aqueous environment over 48 hours. a) A table showing the average dispersity and standard deviation (SD) of the UPy-XL-4 in de-ionized water over 48 hours (blue), and that solution diluted 1:100 (green). b) The correlation functions of UPy-XL-4 in de ionized water over 48 hours. c) The correlation functions of UPy-XL-4 (dilution 1:100) in de ionized water over 48 hours.

Control	UPy-Brush-5	UPy-Brush-10	UPy-Brush-20
H	B	B	2B
H	B	B	B
H	B	B	B

Figure S65. The surface hardness of each UPy-Brush coating was measured via the pencil hardness test. The hardness results are shown above for 3 separate measurements.

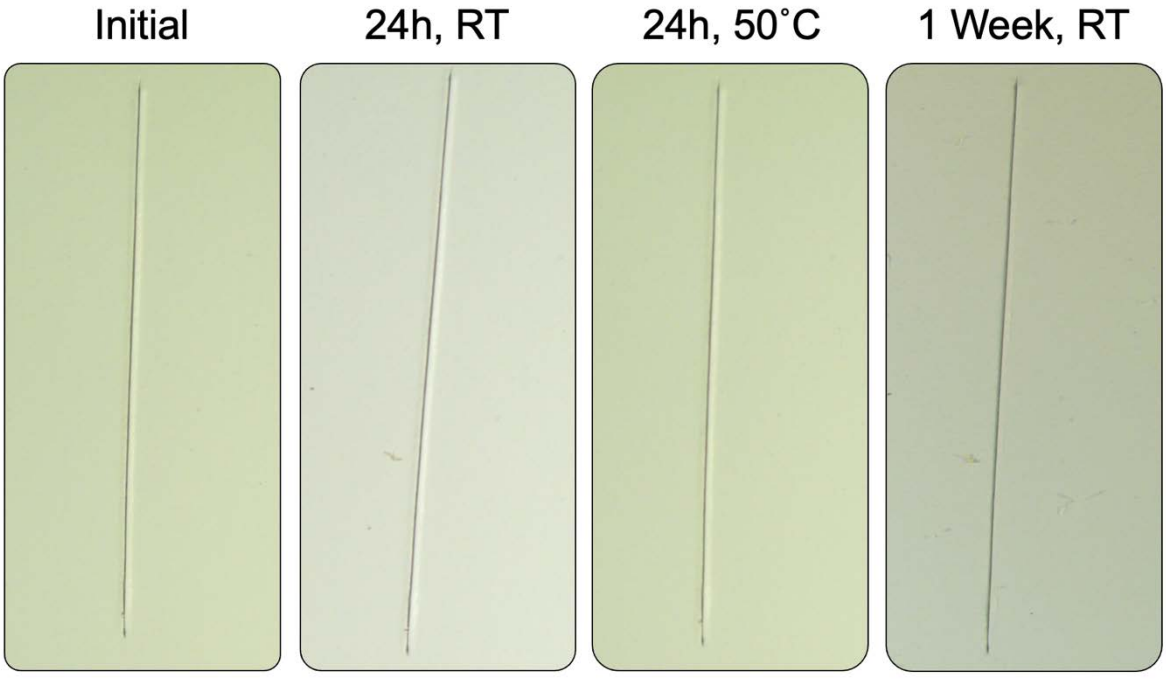

Figure S66. Optical microscope images of the UPy-Paint applied to a metal substrate and cut with a razor. The paint was left to heal at room temperature over 24 hours and 1 week, and at 50˚C over 24 hours.

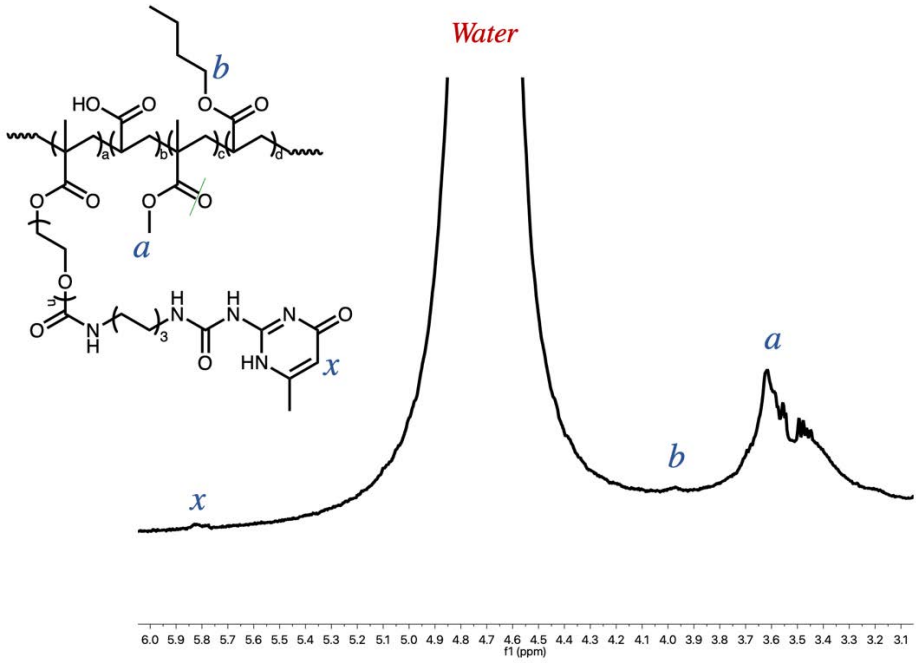

Figure S67. ^{1}H NMR spectrum of the UPy-2 latex in deuterium oxide (heavy water). The surface of the particle is shown, with only MMA (peak *a*) and the UPy monomer (peak *x*) present on the surface.

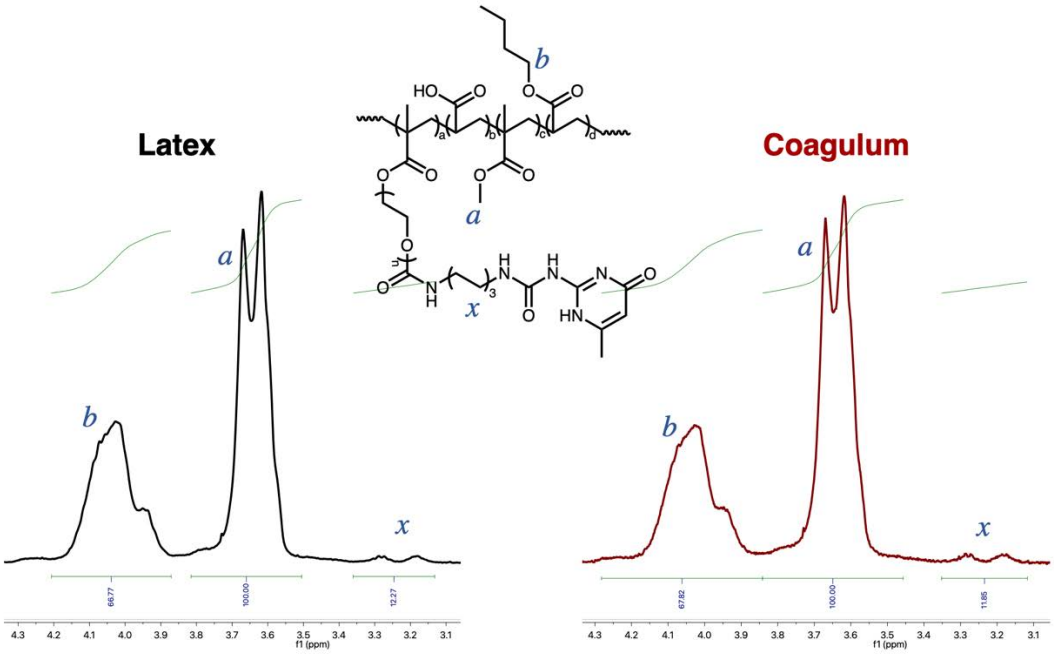

Figure S68. ^{1}H NMR spectra of the UPy-2 coating (black) and its coagulum (red). In both cases, the peak *x*, corresponding to UPy-2, is present in both spectra. Integration shows that the coagulum was not UPy rich, and was comprised of the same polymer as the latex.